JOHANNES GUTENBERG UNIVERSITÄT MAINZ

JG|U

Effective Field Theories for Physics Beyond the Standard Model

Dissertation

zur Erlangung des Grades „Doktor der Naturwissenschaften“
am Fachbereich Physik, Mathematik und Informatik
der Johannes Gutenberg-Universität in Mainz

Stefan Baumgart
geb. Alte

geb. in Hannover
Mainz, den 31. Januar 2020

Abstract

Under the assumption that the mass scale M of physics beyond the Standard Model (BSM) is far above the electroweak scale v, effective field theories (EFTs) are the suitable method for a consistent separation of the physical processes at these disparate mass scales. We construct EFT frameworks for the generic description of physics BSM - covering the two relevant cases that particles of the BSM sector can or can not be produced on-shell at the Large Hadron Collider (LHC) or a future collider.
In the first scenario we focus on the case where a new heavy resonance S with mass $M_S \gg v$ is discovered at a collider. We assume that the BSM sector contains further yet undiscovered particles with masses of order $M \sim M_S$. We discuss the case where S is a scalar Standard-Model (SM) gauge singlet and formulate an EFT to describe the decays of S into SM particles. We demonstrate that for a consistent separation of the mass scales M and v the appropriate operators in the EFT are non-local Soft-Collinear-Effective-Theory (SCET) operators rather than higher-dimensional local operators. We construct the effective Lagrangian up to the next-to-next-to-leading order in the power-counting parameter $\lambda \sim v/M$ and consider the renormalisation-group (RG) equations which allow the resummation of large logarithms of M/v. Our approach provides a template for the construction of analogous EFTs which are suited to describe resonances of different charges and spin. We illustrate our framework in two examples. In the first example we demonstrate that our EFT applies also in the case of the double hierarchy $v \ll M_S \ll M$. In the second example we consider a BSM model, where S and heavy, vector-like fermions are added to the SM. We perform the matching of the BSM model to the EFT and show that resummation yields sizeable effects in phenomenologically relevant decay channels.
In the second scenario we consider the case where the mass scale M of the BSM model is above the energy reach of the collider. We apply the Standard-Model Effective Theory (SMEFT) in collider studies for the processes dijet- and dilepton production. We derive bounds on the contributing Wilson coefficients and on the mass scale M. For the first time in analyses of this type we employ a consistent expansion in the EFT series in powers of $1/M^2$. We truncate our signal predictions for the cross sections at order $1/M^2$ and introduce a theory uncertainty to model the terms of order $1/M^4$. In our analysis we allow for multiple SMEFT operators to contribute at a time. We identify and bound two distinct linear combinations of Wilson coefficients in both studies. The bounds arising in our approach are generically weaker than the overly stringent bounds obtained in previous studies without appropriate theory uncertainties. The method developed in this work can be applied to further processes and the bounds obtained in our approach may serve as an important input for future global fits in the SMEFT framework.
The two frameworks developed and applied in this thesis provide a toolbox for the consistent EFT description of BSM physics in the cases described above.

Overview of Publications

This thesis is based on work published during the time of the author's PhD project. This chapter provides an overview of these publications and specifies the contribution of the author to the respective research project.

[1] S. Alte, M. König and M. Neubert, *Effective Field Theory after a New-Physics Discovery*, *JHEP* **08** (2018) 095 [1806.01278]:

In this work we construct an EFT framework - the SCET_{BSM} - for the case where a new heavy scalar with a mass far above the electroweak scale is discovered at a collider under the assumption that additional unobserved particles of the BSM sector with similar masses exist.

All authors contributed to the collection of the relevant SCET ingredients in Section 3.2, and to the construction of the SCET_{BSM} Lagrangian and the calculation of the decay rates in Sections 3.3 and 3.4. Matthias Neubert extracted some of the RG equations in Sections 3.5.1 and 3.5.2 from the literature and earlier calculations. The RG equations for the Wilson coefficients $\boldsymbol{C}^{(1)}_{Q_L\bar{q}_R\,\phi}$, $\boldsymbol{C}^{(2)}_{Q_L\bar{q}_R\,\phi}$ and $\boldsymbol{C}_{Q_L\bar{q}_R}$ in equations (3.79), (3.80) and (3.82) include the operator mixing and were derived independently by all authors. The resummation effects discussed in Section 3.5.3 were studied by all authors. The analysis of the SCET_{BSM} approach in Section 3.6 for the case of a double hierarchy $M \gg M_S \gg v$ was performed by all authors with the exception of the RG equations in Section 3.6.1, which were mainly obtained by Matthias Neubert.

For the calculations the author used the program `Mathematica` with the packages `Feyncalc` [2,3], `RunDec` [4] and `HypExp` [5,6]. For the publication the author created Figure 3.1 with `JaxoDraw` [7, 8] and Matthias König made Figures 3.2 to 3.7. All authors contributed to the text.

[9] S. Alte, M. König and M. Neubert, *Effective Theory for a Heavy Scalar Coupled to the SM via Vector-Like Quarks*, *Eur. Phys. J.* **C79** (2019) 352 [1902.04593]:

We illustrate the SCET_{BSM} approach by matching a concrete BSM model, where a scalar and additional vector-like fermions are added to the SM, to the EFT. We compute the Wilson coefficients and discuss the impact of resummation on the relevant decay channels.

All authors performed the computations underlying the whole work. For these calculations, the author used the program `Mathematica` with the packages `Feyncalc` [2, 3], `RunDec` [4] and `HypExp` [5, 6]. For the publication Matthias König created the figures and all authors contributed to the text.

[10] S. Alte, M. König and W. Shepherd, *Consistent Searches for SMEFT Effects in Non-Resonant Dijet Events*, *JHEP* **01** (2018) 094 [`1711.07484`]:

In this work we develop a framework for the consistent application of the SMEFT in collider studies. We apply this framework to the process dijet production and derive bounds on the parameters of the SMEFT.

The author generated the pseudodata underlying the whole collider analysis. The author implemented the SMEFT operators in `FeynRules` [11], generated partonic Monte-Carlo pseudodata with `MadGraph` [12], employed `PYTHIA` [13] for showering and simulated the detector effects with `Delphes` [14]. Based on these pseudodata Matthias König and the author performed the statistical analysis and derived the bounds on the SMEFT parameters with advice from William Shepherd. Matthias König and the author computed the analytic cross sections. For the whole analysis after the generation of the pseudodata, the author used `Mathematica` with the packages `Feyncalc` [2, 3], `RunDec` [4] and `ManeParse` [15].

For the publication, Matthias König created the figures and all authors contributed to the text. The figures shown in this thesis were produced by the author.

[16] S. Alte, M. König and W. Shepherd, *Consistent Searches for SMEFT Effects in Non-Resonant Dilepton Events*, *accepted for publication in JHEP* (2019) [`1812.07575`]:

In two collider studies we search for SMEFT effects in data for dilepton production taken at the LHC and the Tevatron. We apply the framework developed in [10] and derive bounds on the parameters of the SMEFT contributing to this process.

The author performed the Monte-Carlo simulations for both collider studies by generating partonic pseudodata with `MadGraph` [12]. The author used the `SMEFTsim` package [17, 18] for the contributing SMEFT operators. With advice from William Shepherd, Matthias König and the author derived the bounds in the statistical analysis based on the pseudodata. Matthias König and the author computed the analytic cross sections. For the analysis the author used the same programs as stated for the previous project [10]. In addition the author applied the `Mathematica` interface of the `Cuba` library [19] for the numerical integration over the parton distribution functions in the calculation of the hadronic cross sections.

Matthias König created the figures for the publication and all authors contributed

to the text. The figures shown in this thesis were produced by the author.

The author composed the following proceedings discussing the work of the four authors after his talk on ICHEP 2016:

[20] S. Alte, Y. Grossman, M. König and M. Neubert, *Exclusive Radiative Decays of Z Bosons in QCD Factorization*, *PoS* **ICHEP2016** (2016) 618 [1703.07242].

The following paper which contains partly work from the author's master project was finished and published during the time of the author's PhD project, but is not discussed in this thesis:

[21] S. Alte, M. König and M. Neubert, *Exclusive Weak Radiative Higgs Decays in the Standard Model and Beyond*, *JHEP* **12** (2016) 037 [1609.06310].

Notations and Conventions

In the following we collect the notations and conventions employed in the whole thesis. We use natural units where the speed of light c and the reduced Planck constant $\hbar$ fulfill

$$c = \hbar = 1\,.$$

Unless explicitly stated otherwise, we denote Lorentz indices with values 0,1,2,3 by greek letters. We employ the following convention for the metric tensor:

$$g^{\mu\nu} = g_{\mu\nu} = \begin{pmatrix} 1 & 0 & 0 & 0 \\ 0 & -1 & 0 & 0 \\ 0 & 0 & -1 & 0 \\ 0 & 0 & 0 & -1 \end{pmatrix}\,.$$

For the Levi-Civita tensor $\epsilon^{\mu\nu\alpha\beta}$ we use the convention $\epsilon_{0123} = -1$. The gamma matrices are denoted as γ^μ with the defining anticommutator

$$\{\gamma^\mu, \gamma^\nu\} = \gamma^\mu\gamma^\nu + \gamma^\nu\gamma^\mu = 2\,g^{\mu\nu}\,,$$

and the fifth gamma matrix is defined as $\gamma^5 = i\gamma^0\gamma^1\gamma^2\gamma^3$. Moreover, we use the quantity $\sigma^{\mu\nu} = \frac{i}{2}[\gamma^\mu, \gamma^\nu]$ with the commutator $[\gamma^\mu, \gamma^\nu] = \gamma^\mu\gamma^\nu - \gamma^\nu\gamma^\mu$. We employ the Feynman slash notation $\not{a} = \gamma^\mu a_\mu$ for a generic four-vector a_μ. Unless stated otherwise, we sum over repeated indices. For a generic Dirac spinor ψ we employ the definition $\bar{\psi} = \psi^\dagger\gamma^0$.
We denote the unitary group and the special unitary group of degree n by U(n) and SU(n), respectively. The structure constants of the non-abelian groups are defined by the relations $[T^a, T^b] = i\,f^{abc}\,T^c$ with $T^a = \lambda^a/2$ for SU(3), where λ^a is a Gell-Mann matrix, and by the relation $[\tau^i, \tau^j] = i\,\epsilon^{ijk}\,\tau^k$ with $\tau^i = \sigma^i/2$ for SU(2), where σ^i is a Pauli matrix. Unless stated otherwise, the indices in the adjoint representation of SU(3) are $a, b, c \in \{1, 2, \ldots, 8\}$ and indices in the adjoint representation of SU(2) are $i, j, k \in \{1, 2, 3\}$. The antisymmetric tensor in two and three dimensions is defined by $\epsilon^{123} = +1$ and $\epsilon^{12} = +1$.
Concerning loop calculations we use dimensional regularisation in $D = 4 - 2\epsilon$ dimensions and the $\overline{\text{MS}}$ scale $\mu_{\overline{\text{MS}}} = \mu\frac{e^{\gamma/2}}{\sqrt{4\pi}}$, where μ is the renormalisation scale and γ the Euler-Mascheroni constant.

List of Abbreviations

BSM	beyond the Standard Model.
ChPT	chiral perturbation theory.
CL	confidence level.
CP	charge conjugation and parity.
EFT	effective field theory.
EWSB	electroweak symmetry breaking.
HEFT	Higgs-Effective Field Theory.
HQET	Heavy-Quark Effective Theory.
IR	infrared.
LEP	Large Electron-Positron Collider.
LHC	Large Hadron Collider.
LO	leading order.
MC	Monte-Carlo.
MFV	minimal flavour violation.
NLO	next-to-leading order.
NNLO	next-to-next-to-leading order.
NP	new physics.
NRQCD	Non-Relativistic QCD.
PDF	parton distribution function.
QCD	Quantum Chromodynamics.
QED	Quantum Electrodynamics.
QFT	quantum field theory.
RG	renormalisation-group.
SCET	Soft-Collinear Effective Theory.
SM	Standard Model.

SMEFT	Standard-Model Effective Theory.
SSB	spontaneous symmetry breaking.
UV	ultraviolet.
VEV	vacuum expectation value.
VLQ	vector-like quark.

Contents

1 Introduction

The eagerness of mankind to understand the inner properties of matter exists at least since as early as 600 B.C. More than 2500 years lie between the philosophical concept of "atomism" and the discovery of the Higgs boson at a gigantic particle collider - the Large Hadron Collider (LHC) at CERN - in 2012 [22, 23]. The discovery of the Higgs boson - predicted already in the 1960s [24–29] - marks the end of the experimental searches for particles predicted by the Standard Model (SM). The time after the achievement of this great milestone is at least as exciting as it is uncertain. On the one hand, the SM provides a very successfull explanation of a plethora of phenomena and the discovery of the Higgs boson manifests another experimental confirmation of SM predictions. On the other hand, the SM does not account for gravity and further important experimental observations such as dark matter and neutrino oscillations. A vast variety of models beyond the Standard Model (BSM) addresses different shortcomings of the SM, such as for example supersymmetry, models with extra dimensions or models with compositeness. However, as for today concrete experimental evidence for these models is absent. In fact, the current bounds on the mass scales of various BSM models arising from searches at the LHC typically already lie in the TeV range. Many experimental anomalies such as the famous 750 GeV diphoton excess [30,31] turned out to be statistical fluctuations. The future will show whether the current anomalies observed in flavour observables [32–36] point to any specific extension of the SM.
In the current situation, where concrete evidence for BSM models is absent at the energies probed at the LHC, it is natural to assume that the mass scale M of these models lies well above the electroweak scale $v \approx 246$ GeV, i.e. $v \ll M$. The energy at the LHC might or might not be sufficient to produce the particles of the BSM sector on shell. In this thesis, we consider both of these options. If the energy reach of the LHC is sufficient and a new particle is discovered, it is very likely that further particles of a whole new BSM sector with similar masses exist. In this case and in the case where the energy at the collider is not sufficient for the on-shell production, it is crucial to develop consistent theoretical methods for the separation of the different mass scales.
Effective field theories (EFTs) provide the appropriate tools for this task. In a setting with one high energy scale - in our case the mass scale M - and one low energy scale - in our case v - an EFT framework allows a systematic separation of the physical processes relevant at the corresponding energy scale. Physical quantities are expanded in terms of the ratio v/M of both energy scales and large logarithms of the inverse scale ratio M/v emerging in perturbative calculations are resummed by renormalisation-group (RG) methods. The EFT framework allows one to study effects of BSM models with a minimum amount of well-defined assumptions regarding the underlying symmetries and the field content at the low energy scale. In this sense, the EFT is often referred to as being "model-

independent" as opposed to "ultraviolet (UV)-complete" models featuring the definition of the full particle content and the symmetries at the high energy scale.
In the first scenario [1, 9] we consider the case where a scalar, SM gauge singlet S with mass $M_S \gg v$ and width $\Gamma_S \ll M_S$ is discovered in a resonance search at the LHC or a future collider. Furthermore, we assume that other particles of the BSM sector with similar masses $M \sim M_S$ exist, but are not discovered. This scenario is completely analogous to many of the numerous explanations for the alleged 750 GeV diphoton resonance [30, 31]. In fact, approximately 500 publications emerged on the arXiv. In many of these publications a local effective Lagrangian containing operators with mass dimension five is employed to describe the coupling of the hypothetical resonance to photons. An example for a dimension-five operator inducing the decay of S into two photons is $\frac{1}{M} S F_{\mu\nu} F^{\mu\nu}$, where F denotes the field strength tensor of the photon and where we explicitly included the suppression by one power of the BSM scale M. However, the truncation of the local EFT expansion at the dimension-five level is not justified in general. To illustrate the problematic issue we add derivatives and consider the dimension-seven operator $\frac{1}{M^3} S \left(\partial_\alpha F_{\mu\nu}\right) \left(\partial^\alpha F^{\mu\nu}\right)$ which is suppressed by three powers of M at the Lagrangian level. However, the contribution of this operator to amplitudes for the decays of S is not necessarily suppressed since the derivatives can give rise to powers of $M_S \sim M$ in the numerator. While the diphoton excess made history as a statistical fluctuation rather than a spectacular discovery [37, 38], the fundamental question of how to describe the results in a consistent EFT approach remains.
In this work we provide an answer to this question and construct a consistent EFT tailored for the scenario described above. Our EFT approach achieves a consistent separation of the physics at the mass scales v and M. To this end we employ methods from Soft-Collinear Effective Theory (SCET) [39–42] and correspondingly name our EFT "SCET_{BSM}". We construct the Lagrangian to describe the decays of S into SM particles up to the next-to-next-to-leading order (NNLO) in the power-counting parameter $\lambda \sim v/M$, perform the resummation of large logarithms of the ratio M/v using the relevant RG equations and demonstrate the power of our theory by applying it in the context of a UV-complete model where S and heavy, vector-like fermions are added to the SM.
In the second scenario [10, 16] we focus on the case where the mass scale M of the BSM model is above the reach of the LHC, in addition to our underlying assumption $M \gg v$. In this case the Standard-Model Effective Theory (SMEFT) provides the suitable EFT framework to study BSM effects in collider studies. In the SMEFT the SM Lagrangian is systematically supplemented by local operators with mass dimensions larger than four. These higher-dimensional operators are built from SM fields and enter the SMEFT Lagrangian with corresponding dimensionless Wilson coefficients C and appropriate inverse powers of M. In particular, the dimension-six Lagrangian contains the suppression factor $1/M^2$ and the dimension-eight Lagrangian contains $1/M^4$. A large number of collider studies exists placing bounds on the Wilson coefficients of the dimension-six Lagrangian (see, e.g. [43–57] for different sets of dimension-six operators) and on the scale M. In this work we focus in particular on dijet production and dilepton production, where relevant previous studies include [58–60]. A huge number of SMEFT collider studies shares

a common, highly problematic feature concerning the consistency in the expansion of physical quantities in terms of the power-counting parameter $1/M$. The problematic aspect of these studies is that the Lagrangian and thus also the amplitude is truncated at the dimension-six level. However, the analysis is based on cross sections which contain the squared amplitude. In terms of the SMEFT power counting, the interference of the dimension-eight amplitude with the SM amplitude is of exactly the same importance as the squared dimension-six amplitude, yet it is neglected in these analyses. In addition to that, a SMEFT analysis at a hadron collider such as the LHC is complicated already at the level of the squared dimension-six amplitude. The reason is that the contribution to scattering processes arising from four-fermion operators grows with the partonic collision energy, which is not fixed between different events at a hadron collider. For events where the collision energy is close to the mass scale M, the SMEFT expansion breaks down. One approach to avoid this breakdown is to artificially remove events with partonic collision energies larger than M from the analysis (see, e.g [61–64]). However, this approach fails to quantify how reliable the influence of an event with a collision energy below but very close to M is in the statistical analysis. A final shortcoming of existing SMEFT collider studies concerns the number of operators considered. In many analyses only one operator is switched on at a time to derive bounds on the SMEFT parameters. This treatment gives rise to artificially strong bounds since cancellations between contributions from different operators are not taken into account.

In this work we develop a framework to resolve all these issues. We truncate the signal prediction for the cross sections at order $1/M^2$ in the power counting, i.e. at the level of the interference of the dimension-six amplitude with the SM amplitude. To account for the higher-order corrections in the SMEFT power counting we introduce a theory uncertainty which models the contributions at order $1/M^4$. The theory uncertainty contains the neglected squared dimension-six piece as well as an estimate for the contribution from the interference of the dimension-eight amplitude with the SM amplitude. To illustrate our approach we perform collider studies exploiting LHC and Tevatron data for dijet and dilepton production. We identify the relevant linear combinations of contributing operators and derive bounds on the Wilson coefficients and on the scale M.

This thesis is structured as follows: In Chapter 2 we provide a concise introduction to the theoretical background with a particular focus on the SM of particle physics, effective theories, the SMEFT and the SCET. In Chapter 3 we construct the SCET_{BSM} Lagrangian for the decays of the resonance S into SM particles up to the NNLO in power counting. Furthermore, we discuss the relevant RG evolution equations and extend our approach to the case where $M \gg M_S$ instead of $M \sim M_S$. In Chapter 4 we consider the matching of a UV-complete model, where the SM is supplemented by the scalar S and by heavy, vector-like fermions, to the SCET_{BSM} and discuss the effects of resummation for phenomenological studies. In Chapter 5 we discuss the consistency requirements for SMEFT analyses, develop our framework, and perform collider studies for dijet and dilepton production which give rise to bounds on a variety of SMEFT parameters. We draw our conclusions in Chapter 6.

2 Theoretical Foundations

In this chapter we provide the theoretical foundations for the studies presented in later chapters. We assume background knowledge about quantum field theory (QFT) and group theory. Some pedagogical introductions to these topics are [65–71]. In Section 2.1 we briefly summarise the SM of particle physics based on [67, 71–74]. Following [74–78] we discuss EFTs in Section 2.2. The two specific EFTs applied in this work, namely the SMEFT and the SCET, are introduced in Section 2.3 based on [74] and in Section 2.4 following [77, 79, 80], respectively.

2.1 The Standard Model

Our understanding of the fundamental particles and their interactions is collected in the SM of particle physics. The SM is the result of the fruitful interplay of theory and experiment. Many of the most important theoretical frameworks were already developed in the 1960s. A non-exhaustive selection of the relevant concepts contains the development of non-abelian gauge theories by Yang and Mills [81], the Goldstone theorem [82] concerning the spontaneous breaking of symmetries proven by Goldstone, Weinberg and Salam [83] and the mechanism explaining how the masses of the SM fields arise, commonly referred to by the "Higgs mechanism", developed by Higgs and others [24–29]. Further milestones in the development of the SM are the quark model invented by Gell-Mann and Zweig [84], the concept of asymptotic freedom developed by Gross, Wilczek and Politzer [85, 86] and the proof that spontaneously broken gauge theories are renormalisable from 't Hooft and Veltman [87, 88]. On the experimental side the discovery of the Higgs boson at CERN in 2012 [22, 23] is one of the numerous major achievements.
Mathematically the SM is a QFT. It exhibits a gauge symmetry with the underlying gauge group

$$\mathrm{SU}_c(3) \times \mathrm{SU}_W(2) \times \mathrm{U}_Y(1)\,, \tag{2.1}$$

where the subscripts indicate the charges associated with the gauge groups, namely colour c, weak isospin W and hypercharge Y. The particles are represented by quantum fields transforming under different representations of the gauge group (2.1) and the Lorentz group. The spin of a particle is related to the corresponding representation of the Lorentz group. The SM field content consists of the gauge fields with spin 1, the fermion fields with spin 1/2 and the Higgs field with spin 0. In Table 2.1 we provide an overview of the fermion fields and the Higgs field with the representation under the $\mathrm{SU}_c(3)$ gauge group (second column), the representation under the $\mathrm{SU}_W(2)$ gauge group (third column) and the hypercharge (fourth column). The fermion fields are represented by chiral projections

Field	$\mathrm{SU}_c(3)$	$\mathrm{SU}_W(2)$	$\mathrm{U}_Y(1)$
ϕ	**1**	**2**	$\frac{1}{2}$
$Q_L^p \in \left\{ \begin{pmatrix} u_L \\ d_L \end{pmatrix}, \begin{pmatrix} c_L \\ s_L \end{pmatrix}, \begin{pmatrix} t_L \\ b_L \end{pmatrix} \right\}$	**3**	**2**	$\frac{1}{6}$
$u_R^p \in \{u_R, c_R, t_R\}$	**3**	**1**	$\frac{2}{3}$
$d_R^p \in \{d_R, s_R, b_R\}$	**3**	**1**	$-\frac{1}{3}$
$L_L^p \in \left\{ \begin{pmatrix} \nu_L^e \\ e_L \end{pmatrix}, \begin{pmatrix} \nu_L^\mu \\ \mu_L \end{pmatrix}, \begin{pmatrix} \nu_L^\tau \\ \tau_L \end{pmatrix} \right\}$	**1**	**2**	$-\frac{1}{2}$
$e_R^p \in \{e_R, \mu_R, \tau_R\}$	**1**	**1**	-1

Table 2.1: Higgs field and fermion fields in the SM with the corresponding representation with respect to the gauge groups $\mathrm{SU}_c(3)$ (second column) and $\mathrm{SU}_W(2)$ (third column). The charges under $\mathrm{U}_Y(1)$ transformations are provided in the fourth column. The index $p \in \{1, 2, 3\}$ indicates the generation of the respective fermion. The fermion fields are projections of Dirac spinors on the left- and right-handed chiral components.

of Dirac spinors. For a generic Dirac spinor ψ we define the left-handed projection as $\psi_L = \frac{1-\gamma_5}{2}\psi$ and the right-handed projection as $\psi_R = \frac{1+\gamma_5}{2}\psi$. We note that fermion fields of different chirality transform differently under the SM gauge group. Furthermore, there exist three different generations of fermions, i. e. $p \in \{1, 2, 3\}$ in Table 2.1. In general we use the indices p, r, s, t as generation indices. The quarks are up quarks u, down quarks d, strange quarks s, charm quarks c, bottom quarks b and top quarks t. The leptons are electrons e, muons μ and tau leptons τ with the corresponding neutrinos ν^e, ν^μ and ν^τ.
The Lagrangian of the SM respects both Lorentz and gauge symmetry. It can be decomposed according to

$$\mathcal{L}_{\mathrm{SM}} = \mathcal{L}_{\mathrm{GB}} + \mathcal{L}_{\mathrm{F}} + \mathcal{L}_{\mathrm{H}} + \mathcal{L}_{\mathrm{Y}} + \mathcal{L}_{\mathrm{GF}} + \mathcal{L}_{\mathrm{FP}} \,. \tag{2.2}$$

The piece containing the kinetic terms for the gauge bosons is

$$\mathcal{L}_{\mathrm{GB}} = -\frac{1}{4} G^a_{\mu\nu} G^{\mu\nu,a} - \frac{1}{4} W^i_{\mu\nu} W^{\mu\nu,i} - \frac{1}{4} B_{\mu\nu} B^{\mu\nu} \,. \tag{2.3}$$

The field strength tensors are

$$G^a_{\mu\nu} = \partial_\mu G^a_\nu - \partial_\nu G^a_\mu + g_S \, f^{abc} \, G^b_\mu G^c_\nu \,, \tag{2.4}$$

$$W^i_{\mu\nu} = \partial_\mu W^i_\nu - \partial_\nu W^i_\mu + g \, \epsilon^{ijk} \, W^j_\mu W^k_\nu \,, \tag{2.5}$$

$$B_{\mu\nu} = \partial_\mu B_\nu - \partial_\nu B_\mu \,, \tag{2.6}$$

where the gauge fields of $\mathrm{SU}_c(3)$ - the gluon fields - are G^a_μ, the gauge fields of $\mathrm{SU}_W(2)$ are W^i_μ and the gauge field of $\mathrm{U}_Y(1)$ is B_μ. The corresponding gauge couplings are g_S, g

and g'. We furthermore define the strong coupling $\alpha_S = g_S^2/(4\pi)$ and the fine-structure constant $\alpha = e^2/(4\pi)$, where e is the elementary charge related to the gauge couplings by the weak mixing angle θ_W as $e = g \sin\theta_W$. The Lagrangian containing the kinetic terms for the fermions is

$$\mathcal{L}_{\mathrm{F}} = \sum_{\psi \in \mathrm{SM}} i\bar{\psi}\, \not{D}\, \psi\,, \tag{2.7}$$

where the sum includes the fermion fields presented in Table 2.1. The definition of the covariant derivative D_μ depends on the field it acts on. For the case where a generic field ψ transforms as $(\mathbf{3}, \mathbf{2}, Y)$ under the SM gauge group in the notation of Table 2.1, the covariant derivative is

$$D_\mu \psi = \left(\partial_\mu - i\, g_S\, G_\mu^a\, \frac{\lambda^a}{2} - i\, g\, W_\mu^i\, \frac{\sigma^i}{2} - i\, g'\, B_\mu\, Y \right) \psi\,. \tag{2.8}$$

The cases where ψ transforms as a singlet under a non-abelian gauge group is obtained by omitting the term containing the corresponding gauge field in equation (2.8). The piece of the Lagrangian $\mathcal{L}_{\mathrm{SM}}$ containing the kinetic term and the potential of the Higgs field is

$$\mathcal{L}_{\mathrm{H}} = (D_\mu \phi)^\dagger\, (D^\mu \phi) + \mu^2 \phi^\dagger \phi - \lambda \left(\phi^\dagger \phi \right)^2\,, \tag{2.9}$$

where μ^2 is the squared mass parameter and λ denotes the quartic Higgs coupling. Requiring the stability of the Higgs vacuum the quartic coupling needs to fulfill $\lambda > 0$. The piece of the Lagrangian coupling the fermions to the Higgs doublet is

$$\mathcal{L}_{\mathrm{Y}} = -Y_l^{pr}\, \bar{L}_L^p\, \phi\, l_R^r - Y_d^{pr}\, \bar{Q}_L^p\, \phi\, d_R^r - Y_u^{pr}\, \bar{Q}_L^p\, \tilde{\phi}\, u_R^r + \mathrm{h.c.}\,, \tag{2.10}$$

where Y_l^{pr}, Y_u^{pr} and Y_d^{pr} are the entries of the complex matrices $\boldsymbol{Y}_l$, $\boldsymbol{Y}_u$ and $\boldsymbol{Y}_d$, and h.c. denotes the hermitian conjugate. The conjugate of the Higgs doublet is defined as $\tilde{\phi} = i\sigma_2\, \phi^*$. The remaining pieces of the SM Lagrangian $\mathcal{L}_{\mathrm{GF}}$ and $\mathcal{L}_{\mathrm{FP}}$ arise in the process of quantising the gauge fields. They contain the gauge-fixing terms and the Faddeev-Popov ghosts [89]. Both pieces are not important for the discussion in this work.

There exist no explicit mass terms for the fermions and the gauge bosons in the Lagrangian $\mathcal{L}_{\mathrm{SM}}$ due to gauge and Lorentz symmetry. The masses are generated in the spontaneous symmetry breaking (SSB) of the $\mathrm{SU}_W(2) \times \mathrm{U}_Y(1)$ symmetry to the $\mathrm{U}_Q(1)$ symmetry of electromagnetism, where the electric charge Q is the associated quantum number [24–29]. The relation between the electric charge and the quantum numbers in the unbroken phase is $Q = T^3 + Y$, where T^3 is the third component of the weak isospin such that $T^3 = 1/2$ for the upper component of an $\mathrm{SU}_W(2)$ doublet and $T^3 = -1/2$ for the lower component. We refer to this symmetry-breaking process by electroweak symmetry breaking (EWSB). A necessary condition for EWSB is that the squared mass parameter μ^2 in the Higgs Lagrangian (2.9) is positive. The excitations of the Higgs

doublet around the ground state give rise to the physical Higgs boson. Concretely, we parameterise the Higgs doublet as

$$\phi(x) = \frac{1}{\sqrt{2}} \begin{pmatrix} -i\sqrt{2}\varphi^+(x) \\ v + h(x) + i\varphi^3(x) \end{pmatrix} , \tag{2.11}$$

where the scalar fields φ^+ and φ^3 are the Goldstone bosons arising in the EWSB according to the Goldstone theorem [82]. The physical Higgs boson is h and the vacuum expectation value (VEV) is denoted by v. The mass terms for the gauge bosons in the broken phase, the W and the Z boson, are generated from the kinetic term in the Higgs Lagrangian (2.9). The relevant relations at tree level are

$$v^2 = \frac{\mu^2}{\lambda} , \quad m_h^2 = 2\mu^2 , \quad \lambda = \frac{g^2}{8}\frac{m_h^2}{m_W^2} , \quad m_W = \frac{1}{2} g v , \quad m_Z = \frac{m_W}{\cos\theta_W} , \tag{2.12}$$

where m_h, m_W and m_Z are the masses of the Higgs boson, the W boson and the Z boson. The mass terms for the fermions arise in the EWSB from the Yukawa Lagrangian (2.10). In the broken phase the diagonalisation of the mass matrices in generation space is achieved by the transformations $f_L \to \boldsymbol{U}_{f_L} f_L$ and $f_R \to \boldsymbol{W}_{f_R} f_R$, where $f \in \{u, d, e\}$. In the context of these transformations we use u, d, e as a short-hand notation for the vectors in generation space. Concretely, the vector u corresponds to $(u, c, t)^T$, the vector d denotes $(d, s, b)^T$ and the vector e represents $(e, \mu, \tau)^T$. The unitary matrices $\boldsymbol{U}_{f_L}$ and $\boldsymbol{W}_{f_R}$ are chosen such that the matrices $\boldsymbol{U}_{e_L}^\dagger \boldsymbol{Y}_l \boldsymbol{W}_{e_R}$, $\boldsymbol{U}_{d_L}^\dagger \boldsymbol{Y}_d \boldsymbol{W}_{d_R}$ and $\boldsymbol{U}_{u_L}^\dagger \boldsymbol{Y}_u \boldsymbol{W}_{u_R}$ are diagonal.

The SM provides a very successful explanation of the phenomena observed up to energies currently probed at the LHC. However, there exist phenomena which are not captured by the SM such as dark matter [90–92], neutrino masses [93–97] and baryogenesis [98, 99]. Moreover, the SM does not incorporate gravity as an interaction. Finally, there are also concerns addressing the SM as a theory itself such as the hierarchy problem (see for example appendix A in [78] for a pedagogical explanation). These aspects make it necessary to develop theories beyond the SM referred to as physics BSM or new physics (NP). EFTs are a powerful tool for both physics within and beyond the SM.

2.2 Effective Field Theories

For the details about EFTs not covered in this section we refer the reader to a collection of review articles and lectures [77, 78, 100–107].

We illustrate the general notion of an effective theory by the following words from Howard Georgi [75]:

> *To do physics amid this remarkable richness, it is convenient to be able to isolate a set of phenomena from all the rest, so that we can describe it without having to understand everything. Fortunately, this is often possible. We can divide the parameter space of the world into different regions, in each of which*

> *there is a different appropriate description of the important physics. Such an appropriate description of the important physics is an "effective theory".*

The world we live in contains a vast amount of phenomena at disparate scales of energy, length and time. A concrete example is the difference in the time scales set by the age of the universe, $\sim 10^{17}$ s [92], and the lifetime of the top quark, $\sim 10^{-24}$ s [108]. In the construction of an effective theory the *important* physical processes at the scale of interest are *isolated* and an *appropriate* theory for those processes is developed. For the description of a process involving two disparate scales one constructs the effective theory by expanding physical quantities in the ratio of the scales. The leading term in this expansion corresponds to the limit where the small scale is set to zero and the large scale is set to infinity.
A familiar example is the description of motions with velocities v which we regularly encounter in our everyday life. These velocities are much smaller than the speed of light c. Thus, Newton's laws of motion [109] provide a valid approximate description of these motions and it is usually not necessary to include effects of the special theory of relativity [110]. The expansion parameter in this example is the ratio of velocities v/c. We motivate the necessity for effective quantum field theories or EFTs within fundamental particle physics by noting that even within the SM the mass scales of the particles range from the upper limit of the neutrino masses $\sim$ eV [108] up to the mass of the top quark $\sim 10^{11}$ eV [108].
In the following we illustrate the construction of an EFT in more detail. Under the assumption that there exists one fundamental mass scale M the EFT provides an approximate description for processes at energies E much smaller than M. The notion of "decoupling" formalised by theorems such as the one from Appelquist and Carrazone [111] describes the effect of heavy states, i. e. states with masses of order M, on processes with energies of order E at the perturbative level. In a simplified version decoupling theorems state that a Feynman diagram containing loops with internal heavy states is suppressed with respect to the diagram with no heavy states by some powers of the small scale ratio E/M. In the concrete construction of the EFT Lagrangian in the path-integral approach the integration over the Fourier modes of the fields with frequencies of order M is performed, a step commonly referred to as "integrating out" the high-frequency modes. We refer the reader to section 2 in [77] for further details about the construction of the effective Lagrangian. In the end, the general structure of the effective Lagrangian is

$$\mathcal{L}_{\text{eff}} = \sum_i g_i \, Q_i \,, \tag{2.13}$$

where the sum includes all the local operators Q_i built from the light fields. The operators are required to respect the symmetries of the theory. The couplings of the EFT g_i encode the information about the physics at energy scales of order M. We rewrite these couplings as

$$g_i = C_i \, M^{-\gamma_i} \,, \tag{2.14}$$

where the dimensionless quantities C_i are referred to as the Wilson coefficients. Working in four dimensions and denoting the mass dimensions of the effective operators by $[Q_i]$, it follows from a dimensional analysis that $\gamma_i = [Q_i]-4$. We apply the concept of naturalness in the sense of 't Hooft [112] and assume $C_i \sim 1$ for the Wilson coefficients. According to 't Hooft the couplings of the effective theory measured in appropriate units of the relevant mass scale, i. e. the Wilson coefficients C_i, should only deviate decisively from ~ 1 if there is a mechanism explaining this deviation. An example for such a mechanism is the case where setting a Wilson coefficient to zero increases the symmetry of the Lagrangian. In this case a Wilson coefficient much smaller than ~ 1 is still considered to be natural. For further details about the concept of naturalness we refer the reader to the review article [113]. Using dimensional analysis we expect the contribution of an operator Q_i to a dimensionless observable for a process at an energy $E \ll M$ to scale as

$$C_i \left(\frac{E}{M}\right)^{\gamma_i} . \tag{2.15}$$

The SM Lagrangian discussed in the last section contains one operator with $\gamma_i < 0$ - the Higgs mass operator - and operators with $\gamma_i = 0$. The contribution of these operators in the limit of low energies $E \to 0$ grows for the case $\gamma_i < 0$ and is constant for $\gamma_i = 0$. In this sense the SM can be viewed as an effective low-energy description of a more fundamental theory. We focus on the case $\gamma_i > 0$ in the following since it is the most relevant one for our later analysis[1]. Due to the assumption $E/M \ll 1$ the contribution of an operator is the more suppressed the higher the mass dimension of the operator is. As a consequence, one can truncate the sum in the effective Lagrangian (2.13) at a fixed order in the series in E/M depending on the desired precision of the calculation. However, it is crucial to estimate the effect of higher-order contributions in this series in concrete applications. As a summary of the decoupling EFT approach we point out that the separation of the physics at the low energy scale E and the high energy scale M is achieved as follows: the information about the physics at the UV energy scale M is encoded in the Wilson coefficients C_i whereas the physics at the infrared (IR) energy scale E is determined from low-energy matrix elements of the operators Q_i. Examples for decoupling EFTs are the effective Lagrangian for light-by-light scattering at energies much smaller than the mass of the electron [114] and the Fermi theory of the weak interactions at energies much smaller than the mass of the W boson [115]. In this work we focus on the SMEFT where the SM is viewed as an effective low-energy theory of some yet unknown UV theory. We discuss details of the SMEFT in Section 2.3.

The operators in the effective Lagrangian (2.13) are local operators. However, there exist EFTs where the effective Lagrangian contains non-local operators. Such non-local operators arise in particular in effective theories where different components of the four-momenta of the particles exhibit different scaling properties with respect to the scale ratio. In contrast to that one assigns a scaling to the square of the four-momenta in

[1] We intentionally refrain from assigning the misleading terms "relevant", "irrelevant" and "marginal" to the different cases for γ_i.

the local EFT discussed above. A prominent example for an EFT with non-local operators is the SCET [39–42] applied in this thesis. Originally, SCET was developed as an EFT for processes in Quantum Chromodynamics (QCD). We discuss details of SCET in Section 2.4 in particular explaining how non-local operators arise.

The SCET in its original formulation for QCD processes represents the concept of a top-down EFT where the UV-complete theory is known. Even though the UV-complete theory is known it is still useful and in many cases crucial to employ an EFT framework. In the calculation the EFT allows to employ the techniques and tools suitable to describe the physics at the corresponding energy scale. As an example, in many applications of EFTs to QCD processes the low energy scale lies in the non-perturbative regime of QCD whereas the theory is perturbative at the high energy scale. A further advantage of using an EFT is the resummation of large logarithms which we explain in more detail below. The Wilson coefficients in the top-down EFT approach can be calculated in a matching calculation. In this matching calculation one requires the EFT and the full theory to give rise to the same S-matrix elements at a certain scale referred to as the matching scale. Prominent examples for top-down EFTs are the Heavy-Quark Effective Theory (HQET) (see e. g. the review [116]) and the Non-Relativistic QCD (NRQCD) [117, 118]. These two EFTs provide low-energy descriptions of QCD suited for different applications.

As opposed to the top-down EFT approach the SMEFT is an example for a bottom-up EFT. The bottom-up approach is useful either when the UV-complete theory is not known or when the matching of the UV-complete theory to the EFT is difficult or not possible at all. In the bottom-up approach one constructs the most general Lagrangian containing the fields of the EFT at a certain order in the EFT power counting imposing the relevant symmetries on the operators in the Lagrangian. The couplings in the effective Lagrangian can be extracted from measuring suitable observables to the precision needed at the order in the power counting. The SMEFT is a bottom-up EFT since the UV-completion of the SM is not yet known. In this case the EFT allows a consistent interpretation of experimental results with a minimum amount of assumptions. Another example for a bottom-up EFT is chiral perturbation theory (ChPT) (see e. g. the reviews [119, 120]) developed to describe QCD below the scale of hadronisation. Although the UV-complete theory is known in this case it is not clear how the matching to QCD can be performed since QCD is not perturbative at the low energy scale where the degrees of freedom are bound states of baryons and mesons compared to the quarks and gluons in QCD.

As a final aspect of this discussion we elaborate on one main advantage of using an EFT framework, namely the ability to systematically account for large logarithms emerging in computations beyond tree level. We focus on a two-scale problem with one high energy scale M and one low energy scale $m \ll M$. In this setting a typical one-loop QCD diagram gives rise to terms of the form $\frac{\alpha_S}{4\pi} \ln\left(\frac{M^2}{m^2}\right)$ and in general powers of this term arise from Feynman diagrams beyond the one-loop level. Since by assumption $M \gg m$ the perturbative expansion in powers of α_S breaks down if $\frac{\alpha_S}{4\pi} \ln\left(\frac{M^2}{m^2}\right) \sim 1$. In an EFT approach to this two-scale problem employing dimensional regularisation the full-theory result is split up into the Wilson coefficients containing logarithms of the ratio M/μ

and operator matrix elements containing logarithms of the ratio m/μ, where μ denotes the mass scale introduced in dimensional regularisation. Thus, large logarithms do not arise if one evaluates the Wilson coefficients at the high scale, i.e. $\mu = M$, and the operator matrix elements at the low scale, i.e. $\mu = m$. The fact that large logarithms are absent if both quantities are evaluated at the suitable energy scales represents the general notion of EFTs discussed above, namely a systematic separation of the physical processes at disparate energy scales. However, it is still necessary to either express the Wilson coefficient at the high scale in terms of the Wilson coefficient at the low scale or - analogously - express the operator matrix elements at the low scale in terms of the operator matrix elements at the high scale. This is achieved by solving the relevant RG equation. A typical RG equation for a Wilson coefficient C exhibits the form

$$\mu \frac{d}{d\mu} C(\mu) = \left[\gamma_0 \frac{\alpha_S}{4\pi} + \mathcal{O}\left(\alpha_S^2\right) \right] C(\mu)\,, \tag{2.16}$$

where γ_0 is referred to as the anomalous dimension. Employing the one-loop running of the strong coupling,

$$\mu \frac{d}{d\mu} \alpha_S(\mu) = -2\beta_0 \frac{\alpha_S^2}{4\pi} + \mathcal{O}\left(\alpha_S^3\right)\,, \tag{2.17}$$

the general solution of the RG equation (2.16) is

$$C(\mu) = \left[\frac{\alpha_S(\mu)}{\alpha_S(\mu_0)} \right]^{-\frac{\gamma_0}{2\beta_0}} C(\mu_0) = \left[\sum_{j=0}^{\infty} \frac{a_j(\beta_0, \gamma_0)}{j!} \left(\frac{\alpha_S(\mu)}{4\pi} \ln\left(\frac{\mu^2}{\mu_0^2} \right) \right)^j \right] C(\mu_0)\,. \tag{2.18}$$

The second equality in this equation is the expansion in powers of the strong coupling, where the series coefficients a_j are functions of the coefficients β_0 and γ_0. We explicitly observe that applying this solution to the problem discussed above, i.e. identifying $\mu = M$ and $\mu_0 = m$, sums up the infinite tower of terms $\frac{\alpha_S}{4\pi} \ln\left(\frac{M^2}{m^2}\right)$.

2.3 The Standard-Model Effective Theory

We discussed in Section 2.1 the need for physics BSM. The bottom-up EFT approach presented in Section 2.2 allows a view of the SM as an EFT of some yet unkown UV-complete theory. Two different approaches exist in this context, namely the SMEFT and the Higgs-Effective Field Theory (HEFT). The main difference between the SMEFT and the HEFT lies in the assumptions applied in the scalar sector of the theory. In the HEFT the Higgs-like particle discovered at CERN [22, 23] is identified with a gauge-singlet scalar and thus not part of the $\mathrm{SU}_W(2)$ doublet ϕ as it is the case in both the SM and the SMEFT. As a gauge-singlet this field exhibits general couplings to the other SM fields. In the HEFT the Goldstone bosons of EWSB are treated in analogy to the pions in chiral symmetry breaking in ChPT. The HEFT was developed as a consistent EFT in [121–138] where we refer the reader to for further details.

The SMEFT is a decoupling EFT as described in Section 2.2. The light degrees of freedom are the SM states specified in Table 2.1, the EFT series is an expansion in powers of $1/M$, where M denotes the mass scale of NP[2], and the symmetries imposed are the SM gauge symmetry and Lorentz symmetry. These assumptions lead to the SMEFT Lagrangian

$$\mathcal{L}_{\text{SMEFT}} = \mathcal{L}_{\text{SM}} + \mathcal{L}^{(5)} + \mathcal{L}^{(6)} + \mathcal{L}^{(7)} + \mathcal{L}^{(8)} + \dots \,, \tag{2.19}$$

where the different pieces correspond to terms of different order in $1/M$. The leading term is the SM Lagrangian $\mathcal{L}_{\text{SM}}$. The couplings in $\mathcal{L}_{\text{SM}}$ receive corrections from the higher-dimensional operators in the pieces $\mathcal{L}^{(i)}$, where $i > 4$. These pieces have the structure

$$\mathcal{L}^{(i)} = \sum_{j=1}^{N_i} \frac{C_j^{(i)}}{M^{i-4}} Q_j^{(i)} \,, \tag{2.20}$$

where the Wilson coefficients are denoted by $C_j^{(i)}$ and the sum includes the complete set of N_i non-redundant operators Q_j with the mass dimension $[Q_j] = i$.
Such a set of non-redundant operators defines an operator basis. Two operators are redundant if they can be related to each other for example by applying the equations of motion, Fierz identites, integration by parts or field redefinitions. As an example we consider the dimension-six operator $Q_{2G} = (D^\mu G_{\mu\nu})^a (D^\rho G_\rho{}^\nu)^a$ from the set of operators considered in [56] in the conventions of [57], where $(D_\mu G_{\nu\alpha})^a = \partial_\mu G^a_{\nu\alpha} - g_S f^{abc} G^b_\mu G^c_{\nu\alpha}$. Applying the classical equations of motion one finds [57]

$$(D^\mu G_{\mu\nu})^a = g_S \left(\bar{Q}_L \gamma_\nu T^a Q_L + \bar{u}_R \gamma_\nu T^a u_R + \bar{d}_R \gamma_\nu T^a d_R \right) + \mathcal{O}\left(\frac{1}{M}\right) \,, \tag{2.21}$$

where a sum over the generations is implied on the right-hand side of the equation. Two important points are worth to note. First, we observe that the operator Q_{2G} can be mapped onto four-fermion operators by applying the equations of motion. Second, this mapping receives contributions suppressed by $1/M$. These corrections imply that a change of the operator basis at the dimension-six level in general gives rise to changes beyond the dimension-six Lagrangian.
In the following we discuss the different pieces of the SMEFT Lagrangian (2.19). Omitting to count the different combinations of flavour indices and the hermitian conjugate, there exists one operator in the dimension-five Lagrangian $\mathcal{L}^{(5)}$. This operator [139] in the convention of [57] is

$$Q_{\nu\nu} = \left(\tilde{\phi}^\dagger L_L^p \right)^T C \left(\tilde{\phi}^\dagger L_L^r \right) \,, \tag{2.22}$$

where C is the charge-conjugation operator. In general we omit the flavour indices on the operators and in particular write $Q_{\nu\nu}$ instead of $Q_{\nu\nu}^{pr}$. While this operator is irrelevant for the applications discussed in this work it is crucial in the context of neutrinos.

[2] Within the SMEFT community the scale M is widely referred to as Λ.

$\left(\bar{R}R\right)\left(\bar{R}R\right)$		$\left(\bar{L}L\right)\left(\bar{R}R\right)$	
Q_{ee}	$(\bar{e}_p\gamma_\mu e_r)\,(\bar{e}_s\gamma^\mu e_t)$	Q_{Le}	$\left(\bar{L}_p\gamma_\mu L_r\right)(\bar{e}_s\gamma^\mu e_t)$
Q_{uu}	$(\bar{u}_p\gamma_\mu u_r)\,(\bar{u}_s\gamma^\mu u_t)$	Q_{Lu}	$\left(\bar{L}_p\gamma_\mu L_r\right)(\bar{u}_s\gamma^\mu u_t)$
Q_{dd}	$\left(\bar{d}_p\gamma_\mu d_r\right)\left(\bar{d}_s\gamma^\mu d_t\right)$	Q_{Ld}	$\left(\bar{L}_p\gamma_\mu L_r\right)\left(\bar{d}_s\gamma^\mu d_t\right)$
Q_{eu}	$(\bar{e}_p\gamma_\mu e_r)\,(\bar{u}_s\gamma^\mu u_t)$	Q_{Qe}	$\left(\bar{Q}_p\gamma_\mu Q_r\right)(\bar{e}_s\gamma^\mu e_t)$
Q_{ed}	$(\bar{e}_p\gamma_\mu e_r)\left(\bar{d}_s\gamma^\mu d_t\right)$	$Q_{Qu}^{(1)}$	$\left(\bar{Q}_p\gamma_\mu Q_r\right)(\bar{u}_s\gamma^\mu u_t)$
$Q_{ud}^{(1)}$	$(\bar{u}_p\gamma_\mu u_r)\left(\bar{d}_s\gamma^\mu d_t\right)$	$Q_{Qu}^{(8)}$	$\left(\bar{Q}_p\gamma_\mu T^a Q_r\right)(\bar{u}_s\gamma^\mu T^a u_t)$
$Q_{ud}^{(8)}$	$(\bar{u}_p\gamma_\mu T^a u_r)\left(\bar{d}_s\gamma^\mu T^a d_t\right)$	$Q_{Qd}^{(1)}$	$\left(\bar{Q}_p\gamma_\mu Q_r\right)\left(\bar{d}_s\gamma^\mu d_t\right)$
		$Q_{Qd}^{(8)}$	$\left(\bar{Q}_p\gamma_\mu T^a Q_r\right)\left(\bar{d}_s\gamma^\mu T^a d_t\right)$
$\left(\bar{L}R\right)\left(\bar{R}L\right)$ and $\left(\bar{L}R\right)\left(\bar{L}R\right)$		$\left(\bar{L}L\right)\left(\bar{L}L\right)$	
Q_{LedQ}	$\left(\bar{L}_p^j e_r\right)\left(\bar{d}_s Q_t^j\right)$	Q_{LL}	$\left(\bar{L}_p\gamma_\mu L_r\right)\left(\bar{L}_s\gamma^\mu L_t\right)$
$Q_{QuQd}^{(1)}$	$\left(\bar{Q}_p^j u_r\right)\epsilon_{jk}\left(\bar{Q}_s^k d_t\right)$	$Q_{QQ}^{(1)}$	$\left(\bar{Q}_p\gamma_\mu Q_r\right)\left(\bar{Q}_s\gamma^\mu Q_t\right)$
$Q_{QuQd}^{(8)}$	$\left(\bar{Q}_p^j T^a u_r\right)\epsilon_{jk}\left(\bar{Q}_s^k T^a d_t\right)$	$Q_{QQ}^{(3)}$	$\left(\bar{Q}_p\gamma_\mu \tau^i Q_r\right)\left(\bar{Q}_s\gamma^\mu \tau^i Q_t\right)$
$Q_{LeQu}^{(1)}$	$\left(\bar{L}_p^j e_r\right)\epsilon_{jk}\left(\bar{Q}_s^k u_t\right)$	$Q_{LQ}^{(1)}$	$\left(\bar{L}_p\gamma_\mu L_r\right)\left(\bar{Q}_s\gamma^\mu Q_t\right)$
$Q_{LeQu}^{(3)}$	$\left(\bar{L}_p^j\sigma_{\mu\nu} e_r\right)\epsilon_{jk}\left(\bar{Q}_s^k\sigma^{\mu\nu} u_t\right)$	$Q_{LQ}^{(3)}$	$\left(\bar{L}_p\gamma_\mu \tau^i L_r\right)\left(\bar{Q}_s\gamma^\mu \tau^i Q_t\right)$

Table 2.2: Baryon-number-conserving four-fermion operators in the SMEFT Lagrangian in the basis of [57]. We omit to write the chirality labels. The operators are classified into four different classes according to their chirality structure. These classes are only right-handed fields (upper left list), only left-handed fields (lower right list) and two different types of left- and right-handed mixed operators (upper right and lower left lists).

After symmetry breaking the operator $Q_{\nu\nu}$ generates neutrino masses and mixings. As discussed in Section 2.1 neutrino masses are a phenomenon observed in nature which is not captured by the SM Lagrangian.

A large amount of phenomenological studies employing different sets of dimension-six operators exist (for example [43–56]). The first consistent reduction of dimension-six operators to an operator basis was achieved in [57]. We use this basis, commonly referred to as the "Warsaw basis", in this thesis. Focussing on the baryon-number-conserving operators, there exist ten classes of dimension-six operators in [57]. We collect the four-fermion operators in Table 2.2. We omit the chirality labels of the fields which are as specified in Table 2.1. In Table 2.2 the indices j and k are indices in the fundamental representation of $\mathrm{SU}_W(2)$. There exist four classes of four-fermion operators classified

according to the chirality structure of the fermion fields. These classes correspond to only right-handed fields (upper left list), only left-handed fields (lower right list) and two different types of left- and right-handed combinations (upper right and lower left lists) differing in the way the $\mathrm{SU}_W(2)$ indices are contracted. Omitting to count different flavour combinations the total number of four-fermion operators is 25. In addition to these four-fermion operators there exist 34 non-four fermion operators classified in six classes. The complete list of these operators is not relevant for the analyses in this thesis and we refer the reader to table 2 in [57]. Together there exist 59 operators under our assumptions if the operators are flavour universal. The RG evolution of these operators is studied in [140–142].
For the dimension-seven Lagrangian $\mathcal{L}^{(7)}$ an operator bases exists [143,144]. Furthermore, tools to count the number of non-redundant operators and to construct bases at even higher order exist [145–149].

2.4 The Soft-Collinear Effective Theory

A typical process suited to be described in terms of SCET contains particles where some components of their four-momenta p^μ are of the order of the high energy scale M whereas the invariant masses are small, i.e. $p^2 \ll M^2$. Originally, SCET was developed for decays of B mesons into final states with light mesons [39–42,150,151]. The high energy scale in these processes is determined by the mass of the decaying B meson and thus of the order of the b-quark mass m_b. The low energy scale is set by the masses of the light mesons and thus of the order of the QCD scale Λ_{QCD}. As a result, the expansion parameter of the SCET in these applications is $\lambda = \Lambda_{\mathrm{QCD}}/m_b$. Beyond these original applications, SCET methods were applied to a vast variety of processes, also including electroweak processes (see e.g. [152–154]). For an overview we refer the reader to chapter 9 in [79].
Before we discuss the construction of a SCET Lagrangian we introduce suitable coordinates. As indicated in the last paragraph we focus on a process where some components of the three-momenta of light particles are of the order of the large energy scale. We define a set of k three-vectors $\boldsymbol{n}_i$ with $|\boldsymbol{n}_i| = 1$ and $i \in \{1, \ldots, k\}$ by taking the three-momenta of the particles and neglecting the components which are not of the order of the large scale. These directions are the jets-defining directions. Using the three-vectors $\boldsymbol{n}_i$ we define four-vectors $n_i^\mu = (1, \boldsymbol{n}_i)$ and $\bar{n}_i^\mu = (1, -\boldsymbol{n}_i)$ such that $n_i \cdot \bar{n}_i = 2$ and decompose a general four-vector p^μ according to

$$p^\mu = \bar{n}_i \cdot p \, \frac{n_i^\mu}{2} + n_i \cdot p \, \frac{\bar{n}_i^\mu}{2} + p_\perp^\mu \,. \tag{2.23}$$

The four-vector $p_\perp^\mu$ contains the components from the plane perpendicular to n_i^μ and $\bar{n}_i^\mu$. A typical choice for one jet direction, i.e. $k = 1$, is $n_1^\mu = (1, 0, 0, -1)$ and $\bar{n}_1^\mu = (1, 0, 0, 1)$. In this case the perpendicular piece of the four-vector $p^\mu = (p_0, p_1, p_2, p_3)$ is $p_\perp^\mu = (0, p_1, p_2, 0)$. To discuss the scaling properties of p^μ with respect to the power-counting parameter λ we represent p^μ by the components in the decomposition (2.23) as $(n_i \cdot p, \bar{n}_i \cdot p, |p_\perp|)$.

The first step in the construction of a SCET for a given process is to identify the relevant momentum modes and their scaling properties with respect to λ. The momentum modes which are integrated out in the construction of the SCET Lagrangian are the hard modes with scaling $\sim M\,(1,1,1)$, where M denotes the large energy scale as above. In a typical setting there furthermore exist n_i-collinear momentum modes with scaling $\sim M\,(\lambda^2,1,\lambda)$ such that one component in the decomposition (2.23) is large. Momentum modes where the three pieces in (2.23) are suppressed by powers of λ but exhibit equal scaling properties are the soft modes with scaling $\sim M\,(\lambda,\lambda,\lambda)$ and the ultra-soft modes with scaling $\sim M\,(\lambda^2,\lambda^2,\lambda^2)$. Especially in the context of factorisation proofs so-called Glauber gluons with momenta scaling $\sim M\,(\lambda^2,\lambda^2,\lambda)$ play an important role (see, e.g. [155, 156]). For a comprehensive overview about the SCET approach to Glauber gluons we refer the reader to [157]. To conclude this paragraph about the different momentum scalings we note that in general one distinguishes two different classes of SCET applications. In a SCET_I setting the particles where the three terms in (2.23) exhibit the same scaling have a virtuality different from the virtuality of the n_i-collinear particles whereas both have the same virtuality in a SCET_II setting.
To illustrate the construction of the SCET Lagrangian we consider an example setting where the relevant momentum modes are hard, n_1-collinear, n_2-collinear and ultra-soft. The full-theory fields are split up into four pieces corresponding to the different momentum regions. Concretely, a full-theory quark field ψ is split up according to $\psi \to \psi_h + \psi_{n_1} + \psi_{n_2} + \psi_{us}$. The hard mode ψ_h is integrated out in the construction of the low-energy Lagrangian while the n_1-collinear mode ψ_{n_1}, the n_2-collinear mode ψ_{n_2} and the ultra-soft mode ψ_{us} constitute the degrees of freedom in the EFT Lagrangian. The scaling of these different components with respect to λ follows from suitable two-point correlation functions. The Dirac spinors ψ_{n_i} contain two components with different scaling. One splits up $\psi_{n_i} = \xi_{n_i} + \eta_{n_i}$, where the two components are defined by the projections $\xi_{n_i} = (\not{n}_i\not{\bar{n}}_i/4)\,\psi_{n_i}$ and $\eta_{n_i} = (\not{\bar{n}}_i\not{n}_i/4)\,\psi_{n_i}$. To derive the scaling of the component ξ_{n_i} we consider

$$\begin{aligned}\langle 0|T\left\{\xi_{n_i}(x)\bar{\xi}_{n_i}(0)\right\}|0\rangle &= \frac{\not{n}_i\not{\bar{n}}_i}{4}\,\langle 0|T\left\{\psi_{n_i}(x)\bar{\psi}_{n_i}(0)\right\}|0\rangle\,\frac{\not{\bar{n}}_i\not{n}_i}{4}\\ &= \int\frac{d^4p}{(2\pi)^4}\frac{i}{p^2+i\epsilon}\,e^{-ip\cdot x}\,\frac{\not{n}_i\not{\bar{n}}_i}{4}\,\not{p}\,\frac{\not{\bar{n}}_i\not{n}_i}{4}\\ &\sim \lambda^4\frac{1}{\lambda^2} = \lambda^2\,,\end{aligned} \tag{2.24}$$

where T denotes the time-ordered product. To arrive at the scaling in the last line of (2.24) we note that $p^2 \sim \lambda^2$ and $\not{p} \sim (\bar{n}_i\cdot p)\not{n}_i$ with $\bar{n}_i\cdot p \sim 1$ for n_i-collinear fields. The scaling relations presented in the construction of the SCET_BSM Lagrangian in Chapter 3 follow in analogy to the procedure presented here.
The scaling properties of the fields allow one to construct the SCET Lagrangian at some order in power counting. The most general set of operators is built - taking the relevant symmetries into account - from the field components in the EFT Lagrangian. For each operator a Wilson coefficient is introduced containing the information about the physics at

the high energy scale. As a special feature of the SCET the EFT operators are in general non local. In the following we explain how these non-localities arise. For a n_i-collinear momentum p the component $\bar{n}_i \cdot p$ scales as λ^0 and is thus unsuppressed. It follows that also the corresponding component of the derivative acting on a general n_i-collinear field is unsuppressed, i. e. $(\bar{n}_i \cdot \partial)\ \psi_{n_i} \sim \lambda^0$. Thus, in principle an infinite amount of these derivatives needs to be included for each n_i-collinear field in the Lagrangian giving rise to an infinite amount of operators with appropriate Wilson coefficients. However, it is more convenient to map the infinite amount of derivatives to non-localities of the fields. For that purpose we expand a general n_i-collinear SCET field ψ_{n_i} as

$$\psi_{n_i}(x + t\,\bar{n}_i) = \sum_{j=0}^{\infty} \frac{t^j}{j!}\ (\bar{n}_i \cdot \partial)^j\ \psi_{n_i}(x)\,, \tag{2.25}$$

where t parameterises the position along the light-like direction $\bar{n}_i$. Including a Wilson coefficient C_j for each term in the series yields

$$\sum_{j=0}^{\infty} \frac{C_j}{j!}\ (\bar{n}_i \cdot \partial)^j\ \psi_{n_i}(x) = \int dt\, C(t)\, \psi_{n_i}(x + t\,\bar{n}_i)\,, \tag{2.26}$$

where we introduce the Wilson-coefficient function C with the moments $C_j = \int dt\, C(t)\, t^j$. Including non-local operators, one carefully needs to restore the invariance of the Lagrangian under gauge transformations. One approach is to first construct a non-local operator and to restore gauge invariance by including Wilson lines as gauge links afterwards. Alternatively, one uses so-called gauge-covariant building blocks containing the Wilson lines in the first place and builds the operators from these building blocks. We pursue the latter option, define the relevant quantities in Section 3.2 and perform the construction of the SCET Lagrangian in Sections 3.3 and 3.4.
The Feynman rules for the SCET are derived from the SCET Lagrangian in analogy to the derivation of the SM Feynman rules from the SM Lagrangian. At the level of Feynman diagrams there exists a one-to-one correspondence between diagrams containing the low-energy modes from the SCET Lagrangian and diagrams in the full theory expanded in certain momentum regions. This correspondence is referred to by the "strategy of region" [158,159]. The strategy-of-region approach is a useful tool to identify the relevant degrees of freedom in the SCET construction. As a concrete example we refer the reader to a discussion of the Sudakov form factor as provided for example in section 3 of [80].
Concerning the RG equations it is a special feature of SCET that these are in general more complicated compared to the example we considered in equation (2.16) in Section 2.2. Concretely, the presence of Sudkov double logarithms gives rise to logarithms of the scale ratio in the anomalous dimensions. A typical RG equation for a two-scale problem similar to the one discussed in Section 2.2 exhibits the form

$$\mu \frac{d}{d\mu} C(\mu) = \left[\gamma_{\text{cusp}}(\alpha_S) \ln\left(\frac{M^2}{m^2}\right) + \gamma_V(\alpha_S)\right] C(\mu)\,, \tag{2.27}$$

where γ_{cusp} is the "cusp anomalous dimension". The solution of this RG equation resums the Sudakov logarithms. This resummation of Sudakov logarithms is one of the main advantages of the SCET. We discuss the solutions of RG equations of the form (2.27) in our concrete applications in Chapter 3.

3 Effective Field Theory After a New-Physics Discovery

3.1 Introduction

Following the discovery of a new heavy particle with mass far above the electroweak scale, understanding its properties will be a crucial task for both theorists and experimenters. In many well-motivated extensions of the SM, such as models based on supersymmetry, compositeness, or extra dimensions, one expects that the first new particle to be discovered is one member of a larger sector of particles with similar masses, characterised by a scale $M \gg v$. Barring any further discoveries, the most general approach to studying the new particle's properties – via its decays into SM particles and its production rates – would be to embed it into an EFT formalism. The purpose of this work is to show how this can be done consistently.

While no new particles have yet been discovered at the LHC, the high-luminosity run still offers a significant discovery potential for new heavy resonances, for which the mass reach extends out to about 6 TeV (see e.g. [160, 161]). An energy upgrade to 27 TeV or a future 100 TeV collider could extend this reach significantly. The phantom 750 GeV diphoton resonance, for which preliminary evidence was reported by the ATLAS and CMS collaborations in late 2015 [30, 31], provides a concrete example with which to illustrate the motivation for our work. Hundreds of phenomenological papers have been written in response to these hints. In most of them, the authors have assumed the existence of a neutral spin-0 boson S with mass $M_S \approx 750\,\text{GeV}$ and constructed the most general EFT Lagrangian at dimension-five order, in which S is coupled to SM fields. The underlying assumption is that these dimension-five operators arise from integrating out additional heavy particles. However, in the vast majority of models addressing the diphoton resonance these other particles had masses of the same order, governed by a scale $M \sim M_S \gtrsim 1\,\text{TeV}$. In such a situation, it is evident that a conventional EFT approach cannot be employed in a systematic way to study the on-shell decay and production rates of the new particle. The naive assumption that amplitudes of the dimension-five Lagrangian scale like v^n/M, where $v \approx 246\,\text{GeV}$ is the electroweak scale, is invalid in this case. The reason is that EFT matrix elements scale with powers of the mass parameters present in the theory, which now are v and M_S. For $M_S \sim M \gg v$, higher-dimensional operators can be unsuppressed with respect to lower-dimensional ones, since their con-

tributions can scale with $(M_S/M)^{2n} = \mathcal{O}(1)$ relative to the dimension-five contributions. Factors of M_S^2 in the numerator can arise, e.g., from operators containing extra derivatives or longitudinally polarised gauge fields. Thus, infinite towers of EFT operators would need to be retained to include all terms of a given order in v/M_S – a task that is usually impracticable. Also, a conventional EFT would not allow one to resum large logarithms of the scale ratio M_S/v.

A successful theoretical framework to address this situation will have to accomplish the following tasks: i) it must be flexible enough to retain the full dependence on the two NP scales: the mass M_S of the heavy resonance that has been discovered, and the mass scale M characterising the other particles belonging to the new sector; ii) it must allow for a consistent separation of the contributions arising from the scales M_S and v, and in particular it must provide the tools to resum large (double) logarithms of the scale ratio M_S/v using RG equations. Note that with $M_S \sim$ few TeV these logarithms can be very large, e.g. $\alpha_S \ln^2(M_S^2/m_t^2) \sim 5$ for $M_S = 5\,\text{TeV}$, and hence resummation is obligatory, even for electroweak radiative corrections.

The situation encountered here is similar to the case of B-meson decays to final states containing light mesons. A systematic heavy-quark expansion of the corresponding decay amplitudes in the small ratio Λ_{QCD}/m_b is made complicated by the fact that the light final-state particles carry energies $E_i = \mathcal{O}(m_b)$ that scale with the heavy-quark mass. This obstacle was overcome with the QCD factorisation approach developed in [162–164] and the construction of SCET [39–42]. In the present work, we use established SCET technology to derive a consistent EFT that can be employed to study the decays of a new heavy particle S into SM particles. The decay amplitudes are systematically expanded in powers of the ratio $\lambda = v/M_S \ll 1$. The scale M_S enters via the large energies and momenta carried by the light SM particles in the final state. While SCET was developed for QCD processes originally, generalisations to electroweak processes have been discussed in [152–154]. In several aspects our approach follows the line of reasoning laid out in these papers. However, we go significantly further by developing the SCET approach beyond the leading order in the power expansion, where several new and subtle issues arise. For example, there is a non-trivial mixing of operators at leading and subleading order, which gives rise to a novel source of large double logarithms, which we resum. We shall refer to the EFT we develop as "SCET beyond the SM" (SCET_{BSM}).

We stress that our effective theory is not meant as an alternative to the EFT extension of the SM referred to as SMEFT [43,45,46,57,139] (see [74] for a recent review). SMEFT parameterises NP effects from heavy virtual particles in a model-independent way by extending the SM through local, higher-dimensional operators built out of SM fields. Assuming there are no light new particles beyond the SM, it provides the appropriate EFT framework for studying indirect hints of NP. SCET_{BSM}, on the other hand, is constructed to describe the decays of a new on-shell heavy resonance into SM particles. In our treatment we will assume that the new resonance is narrow ($\Gamma_S/M_S \ll 1$), such that its width can be neglected when constructing the effective theory. If S decays primarily into SM particles, our results obtained for the various decay widths show a posteriori that this assumption is justified.

The construction of the SCET_{BSM} Lagrangian is process dependent. In this paper we will develop a general toolbox, which allows for a simple, systematic and intuitive construction of the relevant effective Lagrangians for BSM practitioners, even if they are not experts on SCET. For simplicity, we assume that S has spin-0 and is a gauge singlet under the SM. After reviewing some basic aspects of SCET in Section 3.2, we construct in Sections 3.3 and 3.4 the relevant effective Lagrangians for all two-body decays of S into SM particles, and for all three-body decay processes involving a fermion pair in the final state. The extension to new particles with spin $S = 1/2$ or 1, or particles which carry SM quantum numbers, is straightforward. However, if S is a member of an $\text{SU}_W(2)$ multiplet, then a gauge-invariant EFT can only be built in terms of the entire multiplet.
In the conventional EFT approach, the decay amplitudes of S into pairs of SM particles receive contributions from operators of dimension $D = 5$ (in the case of $S \to Zh$ these contributions start at one-loop order), but nevertheless these amplitudes have different scaling properties with $\lambda = v/M_S$, namely (see e.g. [165, 166])

$$\begin{aligned} \mathcal{M}(S \to hh) &= \mathcal{O}(\lambda^0)\,, & \mathcal{M}(S \to VV) &= \mathcal{O}(\lambda^0)\,, \\ \mathcal{M}(S \to f\bar{f}) &= \mathcal{O}(\lambda)\,, & \mathcal{M}(S \to Zh) &= \mathcal{O}(\lambda^2)\,, \end{aligned} \tag{3.1}$$

where V represents a gauge boson (massive or massless) and f a fermion. As mentioned earlier, for $M_S \sim M$ an infinite tower of higher-dimensional operators with $D \geq 7$ can give rise to unsuppressed corrections to these amplitudes. For example, the operators

$$\frac{1}{M}\, S B_{\mu\nu} B^{\mu\nu} \quad \text{and} \quad \frac{1}{M^3}\, S\, (\partial_\alpha B_{\mu\nu})(\partial^\alpha B^{\mu\nu})\,, \tag{3.2}$$

where $B^{\mu\nu}$ denotes the field strength associated with hypercharge, contribute terms of order M_S^2/M and M_S^4/M^3 to the $S \to \gamma\gamma$ amplitude, respectively. In the case of the decay $S \to Zh$, the scaling $\mathcal{M}(S \to Zh) \propto v^2/M$ derived in [166] arose from apparently accidental cancellations of terms scaling like M_S^2/M among different diagrams, and it is thus well motivated to ask whether higher-dimensional operators induce larger contributions scaling like $M_S^{2n}/M^{2n-1} = \mathcal{O}(\lambda^0)$.
In the present work, we derive the scaling laws (3.1) from first principles and show that they remain valid even in the case where the two scales M and M_S are of the same order. To this end, we construct the relevant SCET_{BSM} Lagrangians up to NNLO in λ. The finite sets of non-local SCET operators arising at each order in the λ expansion accounts for infinite towers of local EFT operators. The scaling properties of the operators in SCET translate directly into the scalings of the various decay amplitudes. The complete information about the UV completion of the theory, i.e. about the yet unknown particles with masses of order $M \sim M_S$ and their interactions, is contained in the Wilson coefficients of the effective Lagrangian. In Section 3.5 we show how by solving RG equations one can resum the large (double) logarithms of the scale ratio M_S/v. While most of our discussion focusses on the interesting case where $M \sim M_S$ are two scales of the same order, we discuss in Section 3.6 scenarios in which there is a double hierarchy, such that $M \gg M_S \gg v$. In this case a conventional EFT framework can be used to identify the

leading terms in an expansion in powers of M_S/M, while the SCET_{BSM} is needed to organise in a systematic way the expansion in $\lambda = v/M_S$ and resum large logarithms of this scale ratio. We derive model-independent expressions for the Wilson coefficients in the SCET_{BSM} Lagrangian in terms of the parameters of the local EFT including operators up to dimension five. In Section 3.7 we present our conclusions along with an outlook on future work.

3.2 Basic Elements of SCET

Our goal in this work is to develop a consistent EFT for the analysis of the on-shell decays of a hypothetical new, heavy spin-0 boson S (with mass $M_S \gg v$) into SM particles. For simplicity we assume that S is a singlet under the SM gauge group. We also allow for the existence of other heavy particles with similar masses $M \sim M_S$, which have not yet been discovered. They are integrated out and thus do not appear as degrees of freedom in the effective Lagrangian. As we will show, the appropriate EFT is intrinsically non-local and consists of operators defined in SCET. Nevertheless, the theory is well defined and can be constructed following a set of simple rules. As our desire is to elucidate the main ideas of our proposal and to present the construction of the SCET_{BSM} Lagrangian in the most simple and transparent way, we will be brief on some technicalities, which are familiar to SCET practitioners but may look intimidating to others. Interested readers can find more details in the original papers [39–42] and in the review [79].

The intrinsic complication in constructing an EFT for the decays of a heavy particle S into light (or massless) particles is that the large mass M_S enters the low-energy theory as a parameter characterising the large energies $E_i \sim M_S$ of the final-state particles. This is different from conventional EFTs of the Wilsonian type, in which short-distance fluctuations of heavy virtual particles are integrated out from the generating functional of low-energy Green's functions. In SCET, the large energies carried by the light particles give rise to non-localities along the nearly light-like directions in which these particles travel.

In a given decay process of the heavy particle S, the final state contains jets-defining directions $\{\boldsymbol{n}_1, \ldots, \boldsymbol{n}_k\}$ of large energy flow. Each jet may consist of one or more collinear particles, which have energies much larger than their rest masses. For each jet direction $\boldsymbol{n}_i$, we define two light-like reference vectors $n_i^\mu = (1, \boldsymbol{n}_i)$ and $\bar{n}_i^\mu = (1, -\boldsymbol{n}_i)$, with $n_i \cdot \bar{n}_i = 2$. The four-momentum p of a particle in the jet can then be written as

$$p^\mu = \bar{n}_i \cdot p \, \frac{n_i^\mu}{2} + n_i \cdot p \, \frac{\bar{n}_i^\mu}{2} + p_\perp^\mu \,, \tag{3.3}$$

where $\bar{n}_i \cdot p = \mathcal{O}(M_S)$ is much larger than $n_i \cdot p = \mathcal{O}(m^2/M_S)$. The different components scale as

$$(n_i \cdot p, \bar{n}_i \cdot p, p_\perp) \sim M_S \, (\lambda^2, 1, \lambda) \,, \tag{3.4}$$

where $\lambda = v/M_S$ is the expansion parameter of the effective theory, and we assume that the masses of the light particles are set by the electroweak scale v. Particles whose

momenta scale in this way are referred to as "n_i-collinear particles". The particles inside a given jet can interact with each other according to the Feynman rules of SCET, which are equivalent to the usual Feynman rules of the SM [42]. However, an n_i-collinear particle cannot interact directly with an n_j-collinear particle contained in another jet.[1] The effective Lagrangian of SCET, from which one derives the Feynman rules, is discussed in the Appendix 3.8.

In SCET, n_i-collinear particles are described by effective fields referred to as "collinear building blocks" [151, 167]. They are composite fields invariant under so-called "n_i-collinear gauge transformations", which preserve the scaling of the particle momenta shown in (3.4). The building blocks are defined with the help of n_i-collinear Wilson lines [39–41] built out of the various gauge bosons associated with the SM gauge group. We define

$$\begin{aligned} W_{n_i}^{(G)}(x) &= P \exp\left[ig_S \int_{-\infty}^{0} ds\, \bar{n}_i \cdot G_{n_i}(x + s\bar{n}_i)\right], \\ W_{n_i}^{(W)}(x) &= P \exp\left[ig \int_{-\infty}^{0} ds\, \bar{n}_i \cdot W_{n_i}(x + s\bar{n}_i)\right], \\ W_{n_i}^{(B)}(x) &= P \exp\left[ig' Y \int_{-\infty}^{0} ds\, \bar{n}_i \cdot B_{n_i}(x + s\bar{n}_i)\right], \end{aligned} \tag{3.5}$$

where g_S, g and g' denote the gauge couplings of $\mathrm{SU}_c(3)$, $\mathrm{SU}_W(2)$ and $\mathrm{U}_Y(1)$, while $G_{n_i}^{\mu}(x) \equiv G_{n_i}^{\mu,a}(x)\, T^a$, $W_{n_i}^{\mu}(x) \equiv W_{n_i}^{\mu,j}(x)\, \tau^j$ and $B_{n_i}(x)$ denote the corresponding n_i-collinear gauge fields. They are defined such that their Fourier transforms only contain particle modes whose momenta satisfy the scaling in (3.4). The path-ordering symbol "P" is defined such that the gauge fields are ordered from left to right in order of decreasing s values. For a given SM field, the corresponding collinear Wilson line is obtained by the appropriate product of the objects defined in (3.5), where the hypercharge generator Y in the definition of $W_{n_i}^{(B)}$ is replaced by the hypercharge of the respective field. For example, the collinear Wilson lines for the scalar Higgs doublet and a right-handed up-quark field are

$$W_{n_i}(x) = W_{n_i}^{(W)}(x)\, W_{n_i}^{(B)}(x) \quad \text{and} \quad W_{n_i}(x) = W_{n_i}^{(G)}(x)\, W_{n_i}^{(B)}(x)\,, \tag{3.6}$$

where Y takes the values $\frac{1}{2}$ and $\frac{2}{3}$, respectively.

The n_i-collinear building blocks for the scalar Higgs doublet and the SM fermions are defined as

$$\begin{aligned} \Phi_{n_i}(x) &= W_{n_i}^{\dagger}(x)\, \phi(x)\,, \\ \mathcal{X}_{n_i}(x) &= \frac{\not{n}_i \bar{\not{n}}_i}{4}\, W_{n_i}^{\dagger}(x)\, \psi(x) \equiv P_{n_i} W_{n_i}^{\dagger}(x)\, \psi(x)\,, \end{aligned} \tag{3.7}$$

where the projection operator P_{n_i}, which is defined such that $\not{n}_i P_{n_i} = 0$ and $P_{n_i}^2 = P_{n_i}$, projects out the large components of the spinor of a highly energetic fermion. The n_i-collinear building blocks for the gauge bosons are defined as (for $A = G, W, B$) [151, 167]

[1] Such interactions can however be mediated by the exchange of ultra-soft particles, see Section 3.5.

$$\mathcal{A}^{\mu}_{n_i}(x) = W^{(A)\dagger}_{n_i}(x)\,[iD^{\mu}_{n_i}\,W^{(A)}_{n_i}(x)] = g_A\int_{-\infty}^{0} ds\,\bar{n}_{i\nu}\,[W^{(A)\dagger}_{n_i}A^{\nu\mu}_{n_i}\,W^{(A)}_{n_i}](x+s\bar{n}_i)\,, \quad (3.8)$$

where $iD^{\mu}_{n_i} = i\partial^{\mu} + g_A A^{\mu}_{n_i}$ denotes the collinear covariant derivative, g_A is the appropriate gauge coupling (which in the case $A = B$ includes the hypercharge generator, so $g_G \equiv g_S$, $g_W \equiv g$, and $g_B \equiv g'\,Y$), and $A^{\nu\mu}_{n_i}$ is the field-strength tensor associated with the collinear gauge field $A^{\mu}_{n_i}$. Note that for the hypercharge gauge field the Wilson lines cancel out in the last expression in (3.8), and hence one finds

$$\mathcal{B}^{\mu}_{n_i}(x) = g'\,Y\int_{-\infty}^{0} ds\,\bar{n}_{i\alpha}B^{\alpha\mu}_{n_i}(x+s\bar{n}_i)\,. \quad (3.9)$$

We will also use the expansions of the gauge-boson building blocks in the generators of the gauge groups, i.e.

$$\mathcal{G}^{\mu}_{n_i}(x) = \mathcal{G}^{\mu,a}_{n_i}(x)\,T^a\,, \qquad \mathcal{W}^{\mu}_{n_i}(x) = \mathcal{W}^{\mu,j}_{n_i}(x)\,\tau^j\,, \qquad \mathcal{B}^{\mu}_{n_i}(x) = Y\,\mathcal{B}^{\mu,a}_{n_i}(x)\,, \quad (3.10)$$

where in the latter case $a = 1$. The building blocks for the collinear fermion and gauge fields satisfy the constraints

$$\not{n}_i\,\mathcal{X}_{n_i}(x) = 0\,, \qquad \bar{n}_i\cdot\mathcal{A}_{n_i}(x) = 0\,. \quad (3.11)$$

The Wilson lines contain the longitudinal components $\bar{n}_i\cdot A_{n_i}$ of the gauge fields, while the gauge-invariant collinear fields $\mathcal{A}^{\mu}_{n_i}$ themselves have no such components. Because of the presence of the Wilson lines, the SCET fields can create or absorb particles along with an arbitrary number of (longitudinal) gauge bosons coupling to these particles and traveling in the same direction. In this sense the effective fields describe "jets" of collinear partons. Note that a different set of collinear fields (scalars, fermions and gauge fields) is introduced for each direction $\boldsymbol{n}_i$ of large energy flow.
The collinear building blocks have well-defined scaling properties with the expansion parameter λ. One finds [41, 42]

$$\Phi_{n_i} \sim \lambda\,, \qquad \mathcal{X}_{n_i} \sim \lambda\,, \qquad \mathcal{A}^{\mu}_{n_i\perp} \sim \lambda\,, \qquad n_i\cdot\mathcal{A}_{n_i} \sim \lambda^2\,. \quad (3.12)$$

In analogy with (3.3), the transverse gauge fields are defined as

$$\mathcal{A}^{\mu}_{n_i\perp} = \mathcal{A}^{\mu}_{n_i} - n_i\cdot\mathcal{A}_{n_i}\,\frac{\bar{n}^{\mu}_i}{2}\,, \quad (3.13)$$

where we have used that $\bar{n}_i\cdot\mathcal{A}_{n_i} = 0$.
It follows that operators containing N collinear fields (irrespective of their directions) have scaling dimension $d \geq N$ in λ, and adding more fields to an operator always increases its scaling dimension. This is how SCET can be employed to construct a consistent expansion in powers of λ. Operators in the effective Lagrangian can also contain derivatives acting on collinear fields, which produce collinear momenta when taking matrix elements of an

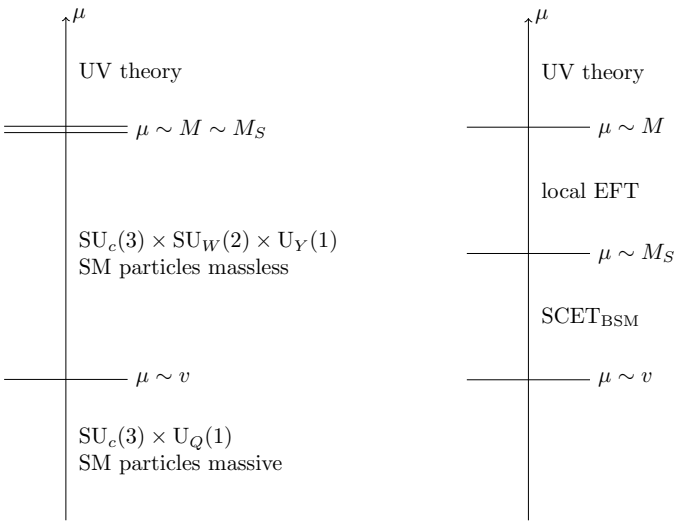

Figure 3.1: Schematic description of the construction of the SCET_{BSM} for the generic case $M \sim M_S$ (left), and for the case of a double hierarchy $M \gg M_S \gg v$ (right).

operator. There is no need to use covariant derivatives, since the building blocks are gauge invariant by themselves. From (3.4) it follows that one can add an arbitrary number of $i\bar{n}_i \cdot \partial$ derivatives acting on n_i-collinear fields, while $in_i \cdot \partial$ or $i\partial_\perp^\mu$ derivatives gives rise to additional power suppression. The freedom to introduce $i\bar{n}_i \cdot \partial$ derivatives at will implies that n_i-collinear fields can be delocalised along the $\bar{n}_i$ direction, and hence the operators appearing in the SCET Lagrangian are non-local. A first hint at this non-locality is the presence of the Wilson lines themselves, see (3.5).
The heavy particle S with four-velocity v should be represented in the effective theory by an effective field $S_v(x)\, e^{-iM_S v\cdot x}$, whose soft interactions are described by a "heavy-particle effective theory" constructed in analogy with heavy-quark effective theory [116,168–172]. Since in our case S is a gauge singlet and has no interactions, this step is unnecessary. It would become a relevant step if one constructs the effective theory for a resonance S that is charged under any of the SM gauge groups.

3.3 SCET_{BSM} for Two-Body Decays of S

We now have the tools to construct an EFT for the decays of a new heavy particle S with mass $M_S \gg v$ into SM particles. The basic construction of the SCET_{BSM} is illustrated in the left panel of Figure 3.1. It consists of the following steps:

1. At the NP scale $\mu \sim M_S \sim M$, the complete UV theory (which is unknown, of course) is matched onto an extension of SCET built out of the resonance S and

n_i-collinear SM fields. All heavy particles besides the resonance S, as well as "hard" quantum fluctuations with virtualities of order M_S, are integrated out in this step. Since the mass of S is much above the electroweak scale, its interactions can be described in terms of operators in the unbroken phase of the electroweak symmetry, preserving full $\mathrm{SU}_c(3) \times \mathrm{SU}_W(2) \times \mathrm{U}_Y(1)$ gauge invariance. If there is a hierarchy between the scales M and M_S (right panel of Figure 3.1), then the two scales are integrated out in two steps, see Section 3.6.

2. In the next step, the effective operators and their Wilson coefficients are evolved from the high-energy scale $\mu \sim M_S$ to the electroweak scale $\mu \sim v$. This is accomplished by solving the RG equations of the effective theory. In this process, the SM particles can be treated as massless. In the SCET community, this version of the effective theory is called $\mathrm{SCET_I}$. The relevant anomalous dimensions can be calculated using standard technology. Solving the RG equations resums large logarithms of the scale ratio M_S/v to all orders in perturbation theory.[2]

3. At the electroweak scale the symmetry is broken to $\mathrm{SU}_c(3) \times \mathrm{U}_Q(1)$, and mass effects from SM particles need to be taken into account. This is accomplished by introducing mass terms for the n_i-collinear fields. In loop calculations, it is also necessary to include so-called soft mass-mode fields with momentum scaling $(\lambda, \lambda, \lambda)$ [173–175]. This version of the effective theory is often referred to as $\mathrm{SCET_{II}}$. The presence of mass terms in loop calculations gives rise to the collinear anomaly [176]. The corresponding loop integrals require an additional analytic regulator beyond dimensional regularisation, which leads to the appearance of additional large logarithms in the matrix elements of the low-energy effective theory. It can be shown that these rapidity logarithms do not exponentiate and hence they do not spoil the resummation accomplished in step 2 [153, 176, 177].

4. If one is interested in processes involving particles much lighter than the weak scale, then at $\mu \approx v$ an additional matching step is required, in which the SM particles with weak-scale masses (the top quark, the Higgs boson, and the W and Z bosons) are integrated out. This theory is then evolved down to a scale μ characteristic to the process of interest, where the relevant operator matrix elements are evaluated.

Each n_i-collinear field in the $\mathrm{SCET_{BSM}}$ Lagrangian carries a collinear momentum in the corresponding direction $\boldsymbol{n}_i$ with a large net energy and thus must produce at least one n_i-collinear particle entering the final state. By momentum conservation, each operator in the $\mathrm{SCET_{BSM}}$ Lagrangian must contain at least two different types of collinear fields, representing particles moving in different directions. Because of EWSB, the effective theory also contains scalar fields carrying no four-momentum. These are represented by a constant field $\Phi_0 \sim \lambda$, which does not transform under collinear gauge transformations.

[2] Unlike in applications of SCET to hadronic decays of B mesons, there is no need to perform an additional matching at an intermediate "hard-collinear" scale $\mu \sim \sqrt{vM_S}$ [154]. The reason is simply that no such scale can be formed out of the physical momenta of the particles involved in the decay.

After EWSB one replaces

$$\Phi_0 \xrightarrow{\text{EWSB}} \frac{1}{\sqrt{2}} \begin{pmatrix} 0 \\ v \end{pmatrix}. \tag{3.14}$$

In this section we focus on the simplest, but phenomenologically most important case of two-body decays of the heavy resonance S. Then the vectors $\boldsymbol{n}_2 = -\boldsymbol{n}_1$ point in opposite directions, and therefore $n_2 = \bar{n}_1$ and $n_1 = \bar{n}_2$ for the light-like reference vectors. Since the choice of the direction of the reference vectors is arbitrary, all operators in the effective Lagrangian must be invariant under the exchange $n_1 \leftrightarrow n_2$.

3.3.1 Effective Lagrangian at $\mathcal{O}(\lambda^2)$

It is convenient to work in the rest frame of the decaying particle, in which the light final-state particles carry large energies $E_i = \mathcal{O}(M_S)$. Since the operators in the effective Lagrangian must contain at least one n_1-collinear and one n_2-collinear field, the power-counting rules in (3.12) imply that the leading operators have scaling dimension $d = 2$. While invariance under n_i-collinear gauge transformations is ensured by constructing the effective Lagrangian in terms of collinear building blocks, the operators must also be invariant under global gauge transformations, i.e. they must conserve the colour and electroweak charges. At $\mathcal{O}(\lambda^2)$, the only gauge-invariant operators are those containing either two scalar doublets or two transverse gauge fields. Considering the first possibility, we write the corresponding term in the effective Lagrangian as

$$\begin{aligned} \mathcal{L}_{\text{eff}} \ni \int ds\, dt\, \bar{C}_{\phi\phi}(s,t,M,\mu) \\ \times S(x) \big[\Phi_{n_1}^\dagger(x + s\bar{n}_1)\, \Phi_{n_2}(x + t\bar{n}_2) + \Phi_{n_2}^\dagger(x + t\bar{n}_2)\, \Phi_{n_1}(x + s\bar{n}_1)\big]\,, \end{aligned} \tag{3.15}$$

where we have taken into account that collinear field operators can be delocalised along the $\bar{n}_i$ directions, as discussed in Section 3.2. The position-space Wilson coefficient $\bar{C}_{\phi\phi}$ depends on the NP scale M via the masses of the yet unknown particles, which have been integrated out, and on the scale μ at which the effective operator is renormalised. It also depends on the coordinates s and t parameterising the non-locality of the operator with respect to the position of the field $S(x)$.
The large components $\bar{n}_i \cdot P_i$ of the total collinear momenta in each jet are fixed by external kinematics. We introduce momentum operators $\bar{n}_i \cdot \mathcal{P}_i$ to obtain these components from the quantum fields.[3] We can then use translational invariance to make the dependence on these components explicit. This gives

$$\mathcal{L}_{\text{eff}} \ni C_{\phi\phi}(\bar{n}_1 \cdot \mathcal{P}_1, \bar{n}_2 \cdot \mathcal{P}_2, M, \mu)\, S(x) \left[\Phi_{n_1}^\dagger(x)\, \Phi_{n_2}(x) + \Phi_{n_2}^\dagger(x)\, \Phi_{n_1}(x)\right], \tag{3.16}$$

where the Fourier-transformed Wilson coefficient is defined as

$$C_{\phi\phi}(\omega_1, \omega_2, M, \mu) = \int ds\, dt\, \bar{C}_{\phi\phi}(s,t,M,\mu)\, e^{is\omega_1}\, e^{it\omega_2}\,. \tag{3.17}$$

[3] In some formulations of SCET the collinear fields carry the large momentum components as labels, and the operators $\bar{n}_i \cdot \mathcal{P}_i$ are referred to as the "label operators" [41].

The dependence of the Wilson coefficient on its arguments is restricted by the fact that the Lagrangian must be invariant under the reparameterisation transformations $n_i^\mu \to \alpha_i\, n_i^\mu$, $\bar{n}_i^\mu \to \bar{n}_i^\mu/\alpha_i$ applied to the light-like reference vectors in each collinear sector [178]. It follows that $C_{\phi\phi}$ in (3.16) depends on its first two arguments only through the combination

$$\frac{n_1\cdot n_2}{2}\,\bar{n}_1\cdot\mathcal{P}_1\,\bar{n}_2\cdot\mathcal{P}_2 = \left(\frac{n_1}{2}\,\bar{n}_1\cdot\mathcal{P}_1 + \frac{n_2}{2}\,\bar{n}_2\cdot\mathcal{P}_2\right)^2 \simeq \mathcal{P}_S^2\,. \tag{3.18}$$

Here and below we use the symbol "$\simeq$" for equations valid at leading power in λ. For two-body decays, the total collinear momenta add up to the momentum of the decaying resonance S, and the operator $\mathcal{P}_S^2$ has eigenvalue M_S^2. With a slight abuse of notation, we thus write the corresponding contribution to the effective Lagrangian in the form

$$\mathcal{L}_{\rm eff} \ni M\, C_{\phi\phi}(M_S, M, \mu)\, O_{\phi\phi}(\mu)\,, \quad \text{with} \quad O_{\phi\phi} = S\,(\Phi^\dagger_{n_1}\Phi_{n_2} + \Phi^\dagger_{n_2}\Phi_{n_1})\,. \tag{3.19}$$

All fields are now evaluated at the same spacetime point. We have factored out the NP scale M in the final definition of the Wilson coefficient to ensure that the function $C_{\phi\phi}(M_S, M, \mu)$ is dimensionless. Contrary to a conventional EFT, in our approach the short-distance Wilson coefficients depend on all the relevant heavy scales in the problem (M_S and the mass scale M of yet undiscovered heavy particles), and this dependence can be arbitrarily complicated depending on the details of the underlying UV theory. In this way, the $\text{SCET}_{\rm BSM}$ Lagrangian accounts for infinite towers of local operators in the conventional EFT approach.

The remaining operators arising at $\mathcal{O}(\lambda^2)$ contain two transverse gauge fields. Their Lorentz indices can be contracted with the help of two rank-two tensors defined in the plane transverse to the vectors n_1 and n_2. We introduce the objects (with $\epsilon_{0123} = -1$)

$$g^\perp_{\mu\nu} = g_{\mu\nu} - \frac{n_{1\mu}n_{2\nu} + n_{2\mu}n_{1\nu}}{n_1\cdot n_2}\,, \qquad \epsilon^\perp_{\mu\nu} = \epsilon_{\mu\nu\alpha\beta}\,\frac{n_1^\alpha\, n_2^\beta}{n_1\cdot n_2}\,. \tag{3.20}$$

The latter definition is such that $\epsilon^\perp_{12} = 1$ if $n_1^\mu = (1,0,0,1)$ and $n_2^\mu = (1,0,0,-1)$. The complete effective Lagrangian can then be written in the form

$$\begin{aligned}\mathcal{L}^{(2)}_{\rm eff} &= M\, C_{\phi\phi}(M_S, M, \mu)\, O_{\phi\phi}(\mu) \\ &\quad + M \sum_{A=G,W,B} \Big[C_{AA}(M_S, M, \mu)\, O_{AA}(\mu) + \widetilde{C}_{AA}(M_S, M, \mu)\, \widetilde{O}_{AA}(\mu)\Big]\,,\end{aligned} \tag{3.21}$$

where (a summation over the group index a is understood for non-abelian fields)

$$\begin{aligned} O_{\phi\phi} &= S\,(\Phi^\dagger_{n_1}\Phi_{n_2} + \Phi^\dagger_{n_2}\Phi_{n_1})\,, \\ O_{AA} &= S\, g^\perp_{\mu\nu}\, \mathcal{A}^{\mu,a}_{n_1}\, \mathcal{A}^{\nu,a}_{n_2}\,, \\ \widetilde{O}_{AA} &= S\, \epsilon^\perp_{\mu\nu}\, \mathcal{A}^{\mu,a}_{n_1}\, \mathcal{A}^{\nu,a}_{n_2}\,. \end{aligned} \tag{3.22}$$

Note that $\epsilon^\perp_{\mu\nu}$ changes sign under $n_1 \leftrightarrow n_2$, and hence the last operator indeed has the correct symmetry properties. The first two operators in this list are even under a charge

conjugation and parity (CP) transformation whereas the third operator is odd (assuming that S does not transform under CP). Here and below we indicate CP-odd operators and their Wilson coefficients by a tilde.
The gauge fields contained in the Wilson lines entering the definitions of the gauge-invariant building blocks in (3.7) and (3.8) become important in loop calculations or in applications with multiple emissions of particles in the same jet direction. An exception is the Wilson line associated with the scalar doublet in (3.7), which after EWSB accounts for the longitudinal polarisation states of the two physical W bosons and the physical Z boson.
The SCET$_{\rm BSM}$ Lagrangian (3.21), which is valid for scales $\mu < M_S$, is constructed in the unbroken phase of the electroweak gauge symmetry, in which all particles other than the heavy resonance S can be treated as massless. As shown in Figure 3.1, at the electroweak scale $\mu \sim v$ this Lagrangian must be matched onto an effective Lagrangian constructed in the broken phase, where the residual gauge symmetry is $\mathrm{SU}_c(3) \times \mathrm{U}_Q(1)$ and where the SM particles acquire masses. While this matching is non-trivial at loop order (see e.g. [153, 154, 173–175]), at tree level one simply needs to transform the various fields to the mass basis. In particular, after EWSB the collinear building block representing the scalar doublet takes the form

$$\Phi_{n_i}(0) = \frac{1}{\sqrt{2}}\, W_{n_i}^\dagger(0) \begin{pmatrix} 0 \\ v + h_{n_i}(0) \end{pmatrix}, \tag{3.23}$$

where

$$W_{n_i}(0) = P \exp\left[\frac{ig}{2}\int_{-\infty}^0 ds \begin{pmatrix} \frac{c_w^2 - s_w^2}{c_w}\, \bar n_i \cdot Z_{n_i} + 2 s_w\, \bar n_i \cdot A_{n_i} & \sqrt{2}\, \bar n_i \cdot W_{n_i}^+ \\ \sqrt{2}\, \bar n_i \cdot W_{n_i}^- & -\frac{1}{c_w}\, \bar n_i \cdot Z_{n_i} \end{pmatrix} (s\bar n_i)\right]. \tag{3.24}$$

We have replaced the gauge fields $W^{\mu,j}$ and B^μ in terms of the mass eigenstates $W^\pm$, Z and A. Here $c_w = \cos\theta_W$ and $s_w = \sin\theta_W$ denote the cosine and sine of the weak mixing angle. It follows that

$$\begin{aligned} O_{\phi\phi} = {} & S(0)\, h_{n_1}(0)\, h_{n_2}(0) + m_Z^2 \int_{-\infty}^0 ds \int_{-\infty}^0 dt\, S(0)\, \bar n_1 \cdot Z_{n_1}(s\bar n_1)\, \bar n_2 \cdot Z_{n_2}(t\bar n_2) \\ & + m_W^2 \int_{-\infty}^0 ds \int_{-\infty}^0 dt\, S(0) \Big[\bar n_1 \cdot W_{n_1}^-(s\bar n_1)\, \bar n_2 \cdot W_{n_2}^+(t\bar n_2) + (+ \leftrightarrow -)\Big] + \dots, \end{aligned} \tag{3.25}$$

where the dots represent terms containing more than two collinear fields. Taking into account that external collinear Higgs and vector bosons have power counting λ^{-1}, it follows from (3.21) that the $S \to hh$ and $S \to VV$ decay amplitudes obey the scaling rules shown in (3.1). Note, however, that whereas these rules were obtained by considering dimension-five operators in the conventional EFT Lagrangian, the scaling relations derived in SCET are exact.
It is straightforward to evaluate the relevant two-body decay amplitudes and decay rates described by the effective Lagrangian (3.21). For the di-Higgs decay mode of S, we obtain

$$\mathcal{M}(S \to hh) = M\, C_{\phi\phi}\,, \qquad \Gamma(S \to hh) = \frac{M^2}{32\pi M_S}\,|C_{\phi\phi}|^2\,\sqrt{1-\frac{4m_h^2}{M_S^2}}\,, \tag{3.26}$$

where here and below we suppress the arguments of the Wilson coefficients.

The decay amplitudes involving two vector bosons in the final state can be expressed in terms of the general form-factor decomposition

$$\mathcal{M}(S \to V_1V_2) = M\Big[F_\perp^{V_1V_2}\,\varepsilon_{1\perp}^*\cdot\varepsilon_{2\perp}^* + \widetilde{F}_\perp^{V_1V_2}\,\epsilon_{\mu\nu}^\perp\,\varepsilon_{1\perp}^{*\mu}\,\varepsilon_{2\perp}^{*\nu} + F_\parallel^{V_1V_2}\,\frac{m_1m_2}{k_1\cdot k_2}\,\varepsilon_{1\parallel}^*\cdot\varepsilon_{2\parallel}^*\Big]\,, \tag{3.27}$$

where k_i^μ are the momenta of the outgoing bosons, m_i denote their masses, and $\varepsilon_i^\mu \equiv \varepsilon^\mu(k_i)$ are their polarisation vectors. The transverse and longitudinal projections of the polarisation vectors are defined as

$$\varepsilon_\perp^\mu(k_i) = \varepsilon^\mu(k_i) - \bar{n}_i\cdot\varepsilon(k_i)\,\frac{n_i^\mu}{2} - n_i\cdot\varepsilon(k_i)\,\frac{\bar{n}_i^\mu}{2}\,, \qquad \varepsilon_\parallel^\mu(k_i) = \varepsilon^\mu(k_i) - \varepsilon_\perp^\mu(k_i)\,. \tag{3.28}$$

The first two terms in (3.27) correspond to the perpendicular polarisation states of the two bosons, while the third term refers to the longitudinal polarisation states. The latter only arise for the massive vector bosons Z and W. The ratio $m_1m_2/(k_1{\cdot}k_2)$ factored out in the definition of the longitudinal form factor $F_\parallel^{VV}$ takes into account that the longitudinal polarisation vectors scale as $\varepsilon_{i\parallel}^\mu(k_i) \simeq k_i^\mu/m_i = \mathcal{O}(\lambda^{-1})$. Our definition ensures that all three form factors are of the same order in SCET power counting. The result (3.27) can also be written in the equivalent form

$$\begin{aligned}\mathcal{M}(S \to V_1V_2) = {}& MF_\perp^{V_1V_2}\left(\varepsilon_1^*\cdot\varepsilon_2^* - \frac{k_2\cdot\varepsilon_1^*\,k_1\cdot\varepsilon_2^*}{k_1\cdot k_2 - \frac{m_1^2\,m_2^2}{k_1\cdot k_2}}\right) + M\widetilde{F}_\perp^{V_1V_2}\,\frac{\epsilon_{\mu\nu\alpha\beta}\,k_1^\mu\,k_2^\nu\,\varepsilon_1^{*\alpha}\,\varepsilon_2^{*\beta}}{\left[(k_1\cdot k_2)^2 - m_1^2\,m_2^2\right]^{1/2}} \\ & + MF_\parallel^{V_1V_2}\,\frac{m_1m_2\,k_2\cdot\varepsilon_1^*\,k_1\cdot\varepsilon_2^*}{(k_1\cdot k_2)^2 - m_1^2\,m_2^2}\,,\end{aligned} \tag{3.29}$$

which is independent of the light-like reference vectors used in SCET.

To derive the tree-level expressions for the form factors from the effective Lagrangian (3.21), we use that the one-boson Feynman rule for the gauge-invariant SCET field $\mathcal{A}_{n_i\perp}^{\mu,a}$ yields $g_A\,\varepsilon_{i\perp}^{*\mu}(k_i)$, where g_A denotes the appropriate gauge coupling, while the Wilson-line terms in (3.25) produce the structure

$$\frac{\bar{n}_1\cdot\varepsilon_1^*}{\bar{n}_1\cdot k_1}\,\frac{\bar{n}_2\cdot\varepsilon_2^*}{\bar{n}_2\cdot k_2} = \frac{\varepsilon_{1\parallel}^*\cdot\varepsilon_{2\parallel}^*}{k_1\cdot k_2}\,. \tag{3.30}$$

We thus obtain the transverse form factors

$$\begin{aligned}
F_\perp^{gg} &= g_S^2\, C_{GG}\,, & \widetilde{F}_\perp^{gg} &= g_S^2\, \widetilde{C}_{GG}\,,\\
F_\perp^{\gamma\gamma} &= e^2\,(C_{WW}+C_{BB})\,, & \widetilde{F}_\perp^{\gamma\gamma} &= e^2(\widetilde{C}_{WW}+\widetilde{C}_{BB})\,,\\
F_\perp^{\gamma Z} &= e^2\left(\frac{c_w}{s_w}\,C_{WW}-\frac{s_w}{c_w}\,C_{BB}\right), & \widetilde{F}_\perp^{\gamma Z} &= e^2\left(\frac{c_w}{s_w}\,\widetilde{C}_{WW}-\frac{s_w}{c_w}\,\widetilde{C}_{BB}\right),\\
F_\perp^{ZZ} &= e^2\left(\frac{c_w^2}{s_w^2}\,C_{WW}+\frac{s_w^2}{c_w^2}\,C_{BB}\right), & \widetilde{F}_\perp^{ZZ} &= e^2\left(\frac{c_w^2}{s_w^2}\,\widetilde{C}_{WW}+\frac{s_w^2}{c_w^2}\,\widetilde{C}_{BB}\right),\\
F_\perp^{WW} &= \frac{e^2}{s_w^2}\,C_{WW}, & \widetilde{F}_\perp^{WW} &= \frac{e^2}{s_w^2}\,\widetilde{C}_{WW}\,,
\end{aligned} \tag{3.31}$$

while the longitudinal form factors are given by

$$F_\parallel^{ZZ} = -C_{\phi\phi}\,, \qquad F_\parallel^{WW} = -C_{\phi\phi}\,. \tag{3.32}$$

The fact that these form factors are given in terms of the Wilson coefficient of the operator containing two scalar fields is a nice expression of the Goldstone-boson equivalence theorem [179–181]. The remaining longitudinal form factors vanish.

From (3.27) we see that the $S \to V_1V_2$ decay amplitudes scale like M and hence are of $\mathcal{O}(\lambda^0)$ in SCET power counting. The corresponding decay rates can be obtained from the general expression

$$\Gamma(S\to V_1V_2) = S_{V_1V_2}\,\frac{M^2}{16\pi M_S}\,\lambda^{1/2}(x_1,x_2)\left[2\left(|F_\perp^{V_1V_2}|^2+|\widetilde{F}_\perp^{V_1V_2}|^2\right)+|F_\parallel^{V_1V_2}|^2\right], \tag{3.33}$$

where $x_i \equiv m_i^2/M_S^2$, and $\lambda(x,y) = (1-x-y)^2-4xy$. The factor $S_{V_1V_2}$ takes into account a symmetry factor $1/2$ for identical bosons and a colour factor $(N_c^2-1)=8$ for the digluon rate. By measuring the polarisations of the vector bosons it would be possible to separately probe the three form factors characterising each decay.

3.3.2 Effective Lagrangian at $\mathcal{O}(\lambda^3)$

The operators arising at subleading order in the expansion in λ contain fermion fields. We decompose Dirac matrices appearing in bilinears of the form $\bar{\mathcal{X}}_{n_1}\ldots\mathcal{X}_{n_2}$ as

$$\gamma^\mu = \frac{\not{n}_1}{n_1\cdot n_2}\,n_2^\mu + \frac{\not{n}_2}{n_1\cdot n_2}\,n_1^\mu + \gamma_\perp^\mu\,, \tag{3.34}$$

such that $n_{1\mu}\gamma_\perp^\mu = n_{2\mu}\gamma_\perp^\mu = 0$. Pulling out a factor $1/M$ to make the Wilson coefficients dimensionless, we find that the most general effective Lagrangian can be written in the

form

$$\begin{aligned}\mathcal{L}^{(3)}_{\text{eff}} = \frac{1}{M}\Bigg[& C^{ij}_{F_L\bar f_R}(M_S,M,\mu)\, O^{ij}_{F_L\bar f_R}(\mu) \\ & + \sum_{k=1,2}\int_0^1 du\, C^{(k)\,ij}_{F_L\bar f_R\,\phi}(u,M_S,M,\mu)\, O^{(k)\,ij}_{F_L\bar f_R\,\phi}(u,\mu) + \text{h.c.}\Bigg] \\ + \frac{1}{M}\sum_{A=G,W,B}\Bigg[& \int_0^1 du\, C^{ij}_{F_L\bar F_L A}(u,M_S,M,\mu)\, O^{ij}_{F_L\bar F_L A}(u,\mu) + (F_L\to f_R) + \text{h.c.}\Bigg],\end{aligned} \tag{3.35}$$

where we have defined the mixed-chirality operators

$$\begin{aligned} O^{ij}_{F_L\bar f_R}(\mu) &= S\,\bar{\mathcal{X}}^i_{L,n_1}\,\Phi_0\,\mathcal{X}^j_{R,n_2} + (n_1\leftrightarrow n_2)\,, \\ O^{(1)\,ij}_{F_L\bar f_R\,\phi}(u,\mu) &= S\,\bar{\mathcal{X}}^i_{L,n_1}\,\Phi^{(u)}_{n_1}\,\mathcal{X}^j_{R,n_2} + (n_1\leftrightarrow n_2)\,, \\ O^{(2)\,ij}_{F_L\bar f_R\,\phi}(u,\mu) &= S\,\bar{\mathcal{X}}^i_{L,n_1}\,\Phi^{(u)}_{n_2}\,\mathcal{X}^j_{R,n_2} + (n_1\leftrightarrow n_2)\,, \end{aligned} \tag{3.36}$$

and the same-chirality operators

$$\begin{aligned} O^{ij}_{F_L\bar F_L A}(u,\mu) &= S\,\bar{\mathcal{X}}^i_{L,n_1}\,\mathcal{A}^{\perp(u)}_{n_1}\,\mathcal{X}^j_{L,n_2} + (n_1\leftrightarrow n_2)\,, \\ O^{ij}_{f_R\bar f_R A}(u,\mu) &= S\,\bar{\mathcal{X}}^i_{R,n_1}\,\mathcal{A}^{\perp(u)}_{n_1}\,\mathcal{X}^j_{R,n_2} + (n_1\leftrightarrow n_2)\,. \end{aligned} \tag{3.37}$$

In (3.35) a sum over the flavour indices i,j is implied. We do not show colour and $\text{SU}_W(2)$ indices. The left-handed fermions F_L are $\text{SU}_W(2)$ doublets, while the right-handed fermions f_R are singlets. If the right-handed fermion field in (3.36) refers to an up-type quark, the scalar doublet Φ needs to be replaced by $\tilde\Phi$ with $\tilde\Phi_a = \epsilon_{ab}\,\Phi^*_b = (\phi_2^*, -\phi_1^*)^T$ to ensure gauge invariance. Our notation is such that, e.g., the coefficient $C^{ij}_{F_L\bar f_R}$ multiplies an operator which produces a left-handed fermion doublet F_L with generation index i and a right-handed anti-fermion $\bar f_R$ with generation index j. Note that, in general, the Wilson coefficients can be arbitrary complex matrices in generation space.

When SCET operators contain two or more collinear fields belonging to the same jet, the total collinear momentum P_i carried by the jet is shared by the various particles described by these fields. Each component field carries a positive fraction u_j of the large component $\bar n_i\cdot P_i$, such that $\sum_j u_j = 1$. The product of Wilson coefficients times operators then becomes generalised to a convolution in these variables. In our discussion above a single variable u appears, which refers to the longitudinal momentum fraction carried by the boson field. To see how it arises, consider the first operator in (3.37) as an example. Its contribution to the effective Lagrangian can be written in the form (leaving out flavour indices and omitting a second term with $n_1\leftrightarrow n_2$ for simplicity)

$$\begin{aligned} &\int dr\,ds\,dt\,\bar C_{F_L\bar F_L A}(r,s,t,M,\mu)\,S(x)\,\bar{\mathcal{X}}_{L,n_1}(x+s\bar n_1)\,\mathcal{A}^\perp_{n_1}(x+(r+s)\bar n_1)\,\mathcal{X}_{L,n_2}(x+t\bar n_2) \\ &= \int dr\, C_{F_L\bar F_L A}(r,\bar n_1\cdot\mathcal{P}_1,\bar n_2\cdot\mathcal{P}_2,M,\mu)\,S(x)\,\bar{\mathcal{X}}_{L,n_1}(x)\,\mathcal{A}^\perp_{n_1}(x+r\bar n_1)\,\mathcal{X}_{L,n_2}(x)\,, \end{aligned} \tag{3.38}$$

where the Wilson coefficient in the second step is defined in analogy with (3.17). To complete the switch to momentum space we take a Fourier transform of the Wilson coefficient with respect to r. This gives

$$\begin{aligned}&\int d\omega\, C_{F_L\bar{F}_L A}(\omega, \bar{n}_1\cdot\mathcal{P}_1, \bar{n}_2\cdot\mathcal{P}_2, M, \mu) \int \frac{dr}{2\pi}\, e^{-i\omega r}\, S(x)\, \bar{\mathcal{X}}_{L,n_1}(x)\, \mathcal{A}^\perp_{n_1}(x + r\bar{n}_1)\, \mathcal{X}_{L,n_2}(x)\\ &= \int d\omega\, C_{F_L\bar{F}_L A}(\omega, \bar{n}_1\cdot\mathcal{P}_1, \bar{n}_2\cdot\mathcal{P}_2, M, \mu)\, S(x)\, \bar{\mathcal{X}}_{L,n_1}(x) \Big[\delta(i\bar{n}_1\cdot\partial + \omega)\, \mathcal{A}^\perp_{n_1}(x)\Big]\, \mathcal{X}_{L,n_2}(x)\,.\end{aligned} \tag{3.39}$$

The δ-function ensures that the variable ω is set equal to the the large (outgoing) momentum component $\bar{n}_1\cdot p_A$ carried by n_1-collinear gauge field. Since this must be a fraction of the large component $\bar{n}_1\cdot P_1$ of the total collinear momentum, it is useful to replace $\omega = u\,\bar{n}_1\cdot\mathcal{P}_1$ in the final step. This yields

$$\begin{aligned}\int du\, C_{F_L\bar{F}_L A}(u\,\bar{n}_1\cdot\mathcal{P}_1, \bar{n}_1\cdot\mathcal{P}_1, \bar{n}_2\cdot\mathcal{P}_2, M, \mu)\, \delta\Big(u - \frac{\bar{n}_1\cdot\mathcal{P}_1^A}{\bar{n}_1\cdot\mathcal{P}_1}\Big)\\ \times S(x)\, \bar{\mathcal{X}}_{L,n_1}(x)\, \mathcal{A}^\perp_{n_1}(x)\, \mathcal{X}_{L,n_2}(x)\,.\end{aligned} \tag{3.40}$$

The operator $\bar{n}_1\cdot\mathcal{P}_1^A$ picks out the large momentum component carried by the gauge field, whereas $\bar{n}_1\cdot\mathcal{P}_1$ produces the large momentum component carried by all n_1-collinear fields together. Using reparameterisation invariance, the Wilson coefficient in this expression can be rewritten in the form $C_{F_L\bar{F}_L A}(u, M_S, M, \mu)$ shown in (3.35), where we also use the short-hand notation

$$S\, \bar{\mathcal{X}}^i_{L,n_1}\, \mathcal{A}^{\perp(u)}_{n_1}\, \mathcal{X}^j_{L,n_2} \equiv \delta\Big(u - \frac{\bar{n}_1\cdot\mathcal{P}_1^A}{\bar{n}_1\cdot\mathcal{P}_1}\Big)\, S(x)\, \bar{\mathcal{X}}_{L,n_1}(x)\, \mathcal{A}^\perp_{n_1}(x)\, \mathcal{X}_{L,n_2}(x)\,. \tag{3.41}$$

Several additional comments are in order. First, we do not include same-chirality operators in (3.37) in which instead of $\mathcal{A}^\perp_{n_1}$ there is a derivative $i\partial\!\!\!/_\perp$ acting on one of the collinear building blocks. These operators can be reduced to those in (3.35) using the equations of motion. For instance, one finds that

$$\begin{aligned}S\, \bar{\mathcal{X}}^i_{L,n_1} i\partial\!\!\!/_\perp \mathcal{X}^j_{L,n_2} + (n_1 \leftrightarrow n_2) &= (\boldsymbol{Y}_f)^{jk} \Big(O^{ik}_{F_L\bar{f}_R} + O^{(2)\,ik}_{F_L\bar{f}_R\,\phi}\Big) - \sum_r\, (O^{ji}_{F_L\bar{F}_L A_r})^\dagger\,,\\ S\, [\bar{\mathcal{X}}^i_{L,n_1}(-i\overleftarrow{\partial\!\!\!/}_\perp)\, \mathcal{X}^j_{L,n_2}] + (n_1 \leftrightarrow n_2) &= (\boldsymbol{Y}_f^*)^{ik} \Big[(O^{jk}_{F_L\bar{f}_R})^\dagger + (O^{(2)\,jk}_{F_L\bar{f}_R\,\phi})^\dagger\Big] - \sum_r\, O^{ij}_{F_L\bar{F}_L A_r}\,,\end{aligned} \tag{3.42}$$

where $\boldsymbol{Y}_f$ with $f = u, d, e$ are the SM Yukawa matrices (for quarks the expressions on the right-hand side must be summed over $f = u, d$), and the sums over r run over the different gauge bosons which couple to the fermion described by $\mathcal{X}_L$. Similar relations hold for the corresponding operators involving right-handed fields. Secondly, in addition to the operators in (3.37), one can construct operators in which the indices of the transverse objects $\mathcal{A}^\mu_{n_1\perp}$ and $\gamma^\nu_\perp$ are contracted using the $\epsilon^\perp_{\mu\nu}$ tensor defined in (3.20). However, these operators can be reduced to those in (3.37) using the identity (with $\gamma_5 = i\gamma^0\gamma^1\gamma^2\gamma^3$)

$$[\gamma^\perp_\mu, \gamma^\perp_\nu] = -i\epsilon^\perp_{\mu\nu}\, \frac{[n\!\!\!/_1, n\!\!\!/_2]}{n_1\cdot n_2}\, \gamma_5\,, \tag{3.43}$$

which holds in four spacetime dimensions [182].[4] From this relation it follows that

$$P_{n_1}^\dagger \epsilon_{\mu\nu}^\perp \gamma_\perp^\nu P_{n_2} = i P_{n_1}^\dagger \gamma_\mu^\perp \gamma_5 P_{n_2} \,. \tag{3.44}$$

Finally, we note that at $\mathcal{O}(\lambda^3)$ there do not appear operators containing two collinear fermion fields belonging to the same jet. These operators would need to include the bilinears (modulo $L \leftrightarrow R$)

$$\bar{\chi}_{L,n_1}^i \frac{\bar{n}\!\!\!/_1}{2} \chi_{L,n_1}^j = \mathcal{O}(\lambda^2) \qquad \text{or} \qquad \bar{\chi}_{L,n_1}^i \Phi_{n_i} \frac{\bar{n}\!\!\!/_1}{2} \gamma_\mu^\perp \chi_{R,n_1}^j = \mathcal{O}(\lambda^3) \,, \tag{3.45}$$

where $\gamma_\mu^\perp$ is now defined with respect to the plane spanned by the vectors n_1 and $\bar{n}_1$, and the subscript n_i on the scalar doublet could be 0, n_1 or n_2. In case of the first operator, the required n_2-collinear field could be $n_2\cdot\mathcal{A}_{n_2}$, $\Phi_{n_2}^\dagger\Phi_{n_2}$, $(\Phi_{n_2}^\dagger\Phi_{n_1}+\text{h.c.})$, or $(\Phi_{n_2}^\dagger\Phi_0+\text{h.c.})$, all of which are of $\mathcal{O}(\lambda^2)$. In the second case, the open Lorentz index must be contracted with $\mathcal{A}_{n_i\perp}^\mu$ or $\partial_\perp^\mu$, both of which count as $\mathcal{O}(\lambda)$. Hence, any such operator is at least of $\mathcal{O}(\lambda^4)$.

The effective Lagrangian (3.35) describes the two-body decays of S into a pair of SM fermions. Taking into account that external collinear fermions have power counting λ^{-1}, it follows that the $S \to f\bar{f}$ decay amplitudes obey the scaling rule shown in (3.1). At tree level, only the operator $O_{F_L\bar{f}_R}$ and its hermitian conjugate give non-zero contributions. After EWSB the fermion fields must be rotated from the weak to the mass basis, and in the process the Wilson coefficients in (3.35), which are matrices in generation space, are transformed as well. In matrix notation, we have e.g.

$$\boldsymbol{C}_{F_L\bar{f}_R} \to \boldsymbol{U}_{f_L}^\dagger \boldsymbol{C}_{F_L\bar{f}_R} \boldsymbol{W}_{f_R} \equiv \mathbf{C}_{f_L\bar{f}_R} \,, \tag{3.46}$$

where f_L (with a lower case) now refers to one of the two members of the left-handed doublet, and $\boldsymbol{U}_{f_L}$ and $\boldsymbol{W}_{f_R}$ with $f = u, d, e$ denote the rotation matrices transforming the left-handed and right handed fermions from the weak to the mass basis. In order not to clutter our notation too much, we use the same symbol but with a straight "C" instead of the slanted "C" for the Wilson coefficients in the mass basis. We then find the non-zero decay amplitudes

$$\begin{aligned}
\mathcal{M}(S \to f_{iL}\,\bar{f}_{jR}) &= \frac{v}{\sqrt{2}M}\, \mathrm{C}_{f_L\bar{f}_R}^{ij}\, \bar{u}_L(k_1) P_{n_1}^\dagger P_{n_2} v_R(k_2) = \frac{v}{\sqrt{2}}\,\frac{M_S}{M}\, \mathrm{C}_{f_L\bar{f}_R}^{ij}\, e^{i\varphi_{ij}} \,, \\
\mathcal{M}(S \to f_{iR}\,\bar{f}_{jL}) &= \frac{v}{\sqrt{2}\,M}\, \mathrm{C}_{f_L\bar{f}_R}^{ji\,*}\, \bar{u}_R(k_1) P_{n_1}^\dagger P_{n_2} v_L(k_2) = \frac{v}{\sqrt{2}}\,\frac{M_S}{M}\, \mathrm{C}_{f_L\bar{f}_R}^{ji\,*}\, e^{-i\varphi_{ji}} \,,
\end{aligned} \tag{3.47}$$

where i, j are flavour indices. Note that the products of two highly energetic fermion spinors give rise to the appearance of the hard scale M_S in the matrix elements of the

[4] In dimensional regularisation, so-called "evanescent" operators containing anti-symmetric products of more than two $\gamma_\perp^\mu$ matrices can appear at loop order. A regularisation scheme including the effects of these operators must be employed for higher-order calculations. This is the two-dimensional analogue, in the space of transverse directions, of the standard procedure employed in four dimensions [183,184].

SCET operators. The expressions on the right hold up to some complex phases, which depend on the phase conventions for the fermion fields. The corresponding decay rates are given by (with $x_i = m_i^2/M_S^2$)

$$\begin{aligned}\Gamma(S \to f_{iL}\,\bar{f}_{jR}) &= N_c^f\,\frac{v^2 M_S}{32\pi M^2}\,\lambda^{1/2}(x_i,x_j)\,\big|\mathrm{C}^{ij}_{f_L\bar{f}_R}\big|^2\,,\\ \Gamma(S \to f_{iR}\,\bar{f}_{jL}) &= N_c^f\,\frac{v^2 M_S}{32\pi M^2}\,\lambda^{1/2}(x_i,x_j)\,\big|\mathrm{C}^{ji}_{f_L\bar{f}_R}\big|^2\,,\end{aligned} \tag{3.48}$$

where N_c^f is a colour factor, which equals 3 for quarks and 1 for leptons. Beyond the Born approximation, the remaining operators in (3.35) also contribute to the decay rates. In Section 3.5 we will study the mixing of these operators under renormalisation.
In general, the couplings of S to fermions contain both CP-even and CP-odd terms. Let us decompose the various complex matrices of Wilson coefficients in the mass basis into their real and imaginary components, for example

$$\mathbf{C}_{f_L\bar{f}_R} \equiv \mathbf{K}_{f_L\bar{f}_R} + i\widetilde{\mathbf{K}}_{f_L\bar{f}_R}\,, \tag{3.49}$$

and likewise for $\mathbf{C}^{(i)}_{f_L\bar{f}_R\,\phi}$ and $\mathbf{C}_{f_L\bar{f}_R A}$. Under a CP transformation the effective Lagrangian (3.35) transforms into an analogous expression with all Wilson coefficients replaced by their complex conjugates. It follows that the terms involving the real parts of the coefficients ($\mathbf{K}_{f_L\bar{f}_R}$ etc.) are CP even, while those involving the imaginary parts ($\widetilde{\mathbf{K}}_{f_L\bar{f}_R}$ etc.) are CP odd.

3.3.3 Effective Lagrangian at $\mathcal{O}(\lambda^4)$

The only two-body decay of the heavy resonance S not yet accounted for is $S \to Zh$. Operators mediating this decay arise first at NNLO in the λ expansion. At this order a large number of new operators arise, but only a single operator contributes to the $S \to Zh$ decay amplitude at tree level. It reads

$$\begin{aligned}\mathcal{L}^{(4)}_{\text{eff}} &\ni \frac{\widetilde{C}_{\phi\phi\phi\phi}(M_S,M,\mu)}{M}\Big[iS\Big(\Phi^\dagger_{n_1}\Phi_0 - \Phi^\dagger_0\,\Phi_{n_1}\Big)\Big(\Phi^\dagger_{n_2}\Phi_0 + \Phi^\dagger_0\,\Phi_{n_2}\Big) + (n_1 \leftrightarrow n_2)\Big]\\ &= \frac{\widetilde{C}_{\phi\phi\phi\phi}(M_S,M,\mu)}{M}\,2iS\,\Big(\Phi^\dagger_{n_1}\Phi_0\,\Phi^\dagger_{n_2}\Phi_0 - \Phi^\dagger_0\,\Phi_{n_1}\,\Phi^\dagger_0\,\Phi_{n_2}\Big)\,.\end{aligned} \tag{3.50}$$

The tilde on the Wilson coefficient indicates that this operator is CP odd [166]. The corresponding decay amplitude is given by

$$\mathcal{M}(S \to Zh) = -i\widetilde{C}_{\phi\phi\phi\phi}\,\frac{v^2 m_Z}{M}\,\frac{\bar{n}_1\cdot\varepsilon^*_\parallel(k_1)}{\bar{n}_1\cdot k_1}\,. \tag{3.51}$$

It vanishes unless the Z boson is longitudinally polarised, in which case one finds

$$\mathcal{M}(S \to Z_\parallel h) = -i\widetilde{C}_{\phi\phi\phi\phi}\,\frac{v^2}{M}\,, \tag{3.52}$$

in accordance with (3.1). To derive this result, we have used the exact representation

$$\varepsilon_\parallel^\mu(k_1) = \frac{k_1\cdot k_2}{m_1\left[(k_1\cdot k_2)^2 - m_1^2\, m_2^2\right]^{1/2}}\left(k_1^\mu - \frac{m_1^2}{k_1\cdot k_2}\,k_2^\mu\right) \tag{3.53}$$

for the longitudinal polarisation vector. For the decay rate, we obtain (with $x_i = m_i^2/M_S^2$)

$$\Gamma(S\to Zh) = \frac{v^4}{16\pi M_S M^2}\,\lambda^{1/2}(x_Z,x_h)\,\left|\widetilde{C}_{\phi\phi\phi\phi}\right|^2. \tag{3.54}$$

The puzzling fact that the $S\to Zh$ decay amplitude scales like λ^2, whereas all other diboson amplitudes scale like λ^0, finds a natural explanation in our approach.
The complete list of the operators arising at $\mathcal{O}(\lambda^4)$ in the effective Lagrangian describing the two-body decays of the heavy resonance S is rather extensive. It includes operators containing S along with four scalar fields, four transverse gauge fields, two scalar fields and two transverse gauge fields, four fermion fields, two fermion fields and two scalar/transverse gauge fields, and two fermion fields and an ultra-soft gauge or scalar field. Moreover, in some of these operators a transverse gauge field can be replaced by a transverse derivative, or two transverse gauge fields can be replaced by a small component of a collinear gauge field or an ultra-soft gauge field. A complete classification of these operators is left for future work.

3.4 SCET$_{\mathsf{BSM}}$ for Three-Body Decays of S

The construction of the effective Lagrangian describing three-body decays of the heavy resonance S proceeds in analogy with Section 3.3. Generically, the three SM particles in the final state have momenta aligned with three different directions $\boldsymbol{n}_i$ with $i=1,2,3$, and hence the scalar products $k_i\cdot k_j = \mathcal{O}(M_S^2)$ are set by the mass scale of the decaying particle. The leading SCET operators involving three n_i-collinear fields are of $\mathcal{O}(\lambda^3)$ and contain fermion bilinears. The corresponding operators can be constructed as in Section 3.3.2. The purely bosonic three-body decays $S\to hhh$, $S\to hV_1V_2$ and $S\to V_1V_2V_3$ appear first at $\mathcal{O}(\lambda^4)$ in the SCET expansion. They will not be considered in detail here.
Without loss of generality, we choose the outgoing boson along the direction $\boldsymbol{n}_3$. Dirac matrices are still decomposed as shown in (3.34), where now $n_1\cdot n_2 = 1-\cos\phi_{12}$ with $\phi_{12} = \sphericalangle(\boldsymbol{n}_1,\boldsymbol{n}_2)$ is no longer equal to 2. We find

$$\begin{aligned}\mathcal{L}_{\text{eff}}^{(3)} &= \frac{1}{M}\left[D^{ij}_{F_L\bar f_R\,\phi}(\{m_{kl}^2\},M,\mu)\,Q^{ij}_{F_L\bar f_R\,\phi}(\mu) + \text{h.c.}\right]\\ &\quad+\frac{1}{M}\sum_{A=G,W,B}\Big[D^{ij}_{F_L\bar F_L A}(\{m_{kl}^2\},M,\mu)\,Q^{ij}_{F_L\bar F_L A}(\mu)\\ &\qquad\qquad + D^{ij}_{f_R\bar f_R A}(\{m_{kl}^2\},M,\mu)\,Q^{ij}_{f_R\bar f_R A}(\mu)\Big],\end{aligned} \tag{3.55}$$

with

$$\begin{aligned} Q^{ij}_{F_L\bar{f}_R\,\phi}(\mu) &= S\,\bar{\mathcal{X}}^i_{L,n_1}\Phi_{n_3}\mathcal{X}^j_{R,n_2} + (n_1 \leftrightarrow n_2)\,, \\ Q^{ij}_{F_L\bar{F}_L A}(\mu) &= S\,\bar{\mathcal{X}}^i_{L,n_1}\gamma^\perp_\mu \mathcal{A}^\mu_{n_3\perp}\,\mathcal{X}^j_{L,n_2} + (n_1 \leftrightarrow n_2)\,, \\ Q^{ij}_{f_R\bar{f}_R A}(\mu) &= S\,\bar{\mathcal{X}}^i_{R,n_1}\gamma^\perp_\mu \mathcal{A}^\mu_{n_3\perp}\,\mathcal{X}^j_{R,n_2} + (n_1 \leftrightarrow n_2)\,. \end{aligned} \tag{3.56}$$

Once again i, j are flavour indices. Note that the symbol $\perp$ on $\gamma^\perp_\mu$ means "perpendicular to the plane spanned by n_1 and n_2", see (3.34), while on the gauge field $\mathcal{A}^\mu_{n_3\perp}$ it means "perpendicular to the plane spanned by n_3 and $\bar{n}_3$", see (3.13). The contraction of these two objects gives rise to a non-trivial dependence on the light-like reference vectors of the three final-state particles, shown in relation (3.63) below.

We denote the Wilson coefficients by D and the operators by Q in order to distinguish them from the corresponding quantities in the Lagrangian for two-body decays shown in (3.35). If the right-handed fermion field in (3.56) refers to an up-type quark, the scalar doublet Φ_{n_3} needs to be replaced by $\tilde{\Phi}_{n_3}$ to ensure gauge invariance. The Wilson coefficients $\boldsymbol{D}_{F_L\bar{f}_R\,\phi}$ are arbitrary complex matrices in generation space, while $\boldsymbol{D}_{F_L\bar{F}_L A}$ and $\boldsymbol{D}_{f_R\bar{f}_R A}$ are hermitian matrices. As before, we will denote the corresponding coefficients after transformation to the mass basis with an unslanted symbol "D" (and use f_L instead of F_L to represent one of the two members of the weak doublet).

Note that there are no convolution integrals in (3.55), in contrast with (3.35). On the other hand, by a generalisation of the argument given before (3.18), the Wilson coefficients can now depend on the three invariants (with $k \neq l \in \{1,2,3\}$)

$$\frac{n_k\cdot n_l}{2}\,\bar{n}_k\cdot\mathcal{P}_k\,\bar{n}_l\cdot\mathcal{P}_l = \left(\frac{n_k}{2}\,\bar{n}_k\cdot\mathcal{P}_k + \frac{n_l}{2}\,\bar{n}_l\cdot\mathcal{P}_l\right)^2 \simeq (\mathcal{P}_k+\mathcal{P}_l)^2\,. \tag{3.57}$$

For a three-body decay, these invariants evaluate to the squared invariant masses m^2_{kl} of the different pairs of final-state particles, which are subject to the relation

$$m^2_{12}+m^2_{23}+m^2_{13} = M_S^2+m_1^2+m_2^2+m_3^2 \simeq M_S^2\,. \tag{3.58}$$

It is straightforward to derive from (3.55) the relevant tree-level expressions for the 3-body decay amplitudes of the heavy resonance S. Since both the Wilson coefficients and the matrix elements of the effective Lagrangian depend on the pair invariant masses squared, we can only compute the doubly differential decay rate, summed over polarisations of the vector boson where appropriate, in two of these variables (the so-called Dalitz-plot distribution) in a model-independent way.

We begin with the decay modes mediated by the opposite-chirality operators in (3.55), for which we obtain

$$\frac{d^2\Gamma(S\to f_{iL}\,\bar{f}_{jR}\,h)}{dm^2_{12}\,dm^2_{23}} = \frac{d^2\Gamma(S\to f_{iL}\,\bar{f}_{jR}\,Z)}{dm^2_{12}\,dm^2_{23}} = \frac{N_c^f}{512\pi^3 M_S^3}\,\frac{m^2_{12}}{M^2}\,\left|\mathrm{D}^{ij}_{f_L\bar{f}_R\,\phi}\right|^2, \tag{3.59}$$

and

$$\frac{d^2\Gamma(S\to f_{iL}\,\bar{f}_{jR}\,W^\pm)}{dm^2_{12}\,dm^2_{23}} = \frac{N_c^f}{256\pi^3 M_S^3}\,\frac{m^2_{12}}{M^2}\,\left|\mathrm{D}^{ij}_{f_L\bar{f}_R\,\phi}\right|^2, \tag{3.60}$$

Process	Colour/coupling factor	Coefficient
$S \to f_{iL}\,\bar{f}_{jL}\,\gamma$	$N_c^f\,\alpha$	$T_3^{f_L}\,\mathrm{D}^{ij}_{f_L\bar{f}_L W} + Y_{f_L}\mathrm{D}^{ij}_{f_L\bar{f}_L B}$
$S \to f_{iR}\,\bar{f}_{jR}\,\gamma$	$N_c^f\,\alpha$	$Y_{f_R}\mathrm{D}^{ij}_{f_R\bar{f}_R B}$
$S \to f_{iL}\,\bar{f}_{jL}\,Z$	$N_c^f\,\alpha$	$T_3^{f_L}\,\frac{c_w}{s_w}\,\mathrm{D}^{ij}_{f_L\bar{f}_L W} - \frac{s_w}{c_w}\,Y_{f_L}\mathrm{D}^{ij}_{f_L\bar{f}_L B}$
$S \to f_{iR}\,\bar{f}_{jR}\,Z$	$N_c^f\,\alpha$	$-\frac{s_w}{c_w}\,Y_{f_R}\mathrm{D}^{ij}_{f_R\bar{f}_R B}$
$S \to f_{iL}\,\bar{f}_{jL}\,W^\pm$	$N_c^f\,\alpha$	$\frac{1}{s_w}\,\mathrm{D}^{ij}_{f_L\bar{f}_L W}$
$S \to f_{iR}\,\bar{f}_{jR}\,W^\pm$	$N_c^f\,\alpha$	0
$S \to q_{iL}\,\bar{q}_{jL}\,g$	$N_c C_F \alpha_S$	$\mathrm{D}^{ij}_{f_L\bar{f}_L G}$
$S \to q_{iR}\,\bar{q}_{jR}\,g$	$N_c C_F \alpha_S$	$\mathrm{D}^{ij}_{f_R\bar{f}_R G}$

Table 3.1: Colour factors, gauge couplings and Wilson coefficients entering the expressions for the doubly differential decay rates for the three-body decays $S \to f_{iL}\,\bar{f}_{jL}\,V$ and $S \to f_{iR}\,\bar{f}_{jR}\,V$, all of which are given by a formula analogous to (3.62).

where as before $N_c^f = 3$ for quarks and 1 for leptons. Here $m_{12}^2 = m_{f\bar{f}}^2$ and $m_{23}^2 = m_{\bar{f}h}^2$ or $m_{\bar{f}V}^2$. Analogous expressions hold with $L \leftrightarrow R$ on the left-hand side and $i \leftrightarrow j$ on the right-hand side. To arrive at these results, we have used that

$$\frac{n_1\cdot n_2}{2}\,\bar{n}_1\cdot k_1\,\bar{n}_2\cdot k_2 \simeq 2k_1\cdot k_2 \simeq m_{12}^2\,. \tag{3.61}$$

Only the longitudinal polarisation state of the electroweak gauge bosons contributes to these rates.

From the same-chirality operators in (3.55) we obtain slightly more complicated expressions. Focussing on the case where a fermion pair is produced along with a photon, we find

$$\begin{aligned}
\frac{d^2\Gamma(S \to f_{iL}\,\bar{f}_{jL}\,\gamma)}{dm_{12}^2\,dm_{23}^2} &= \frac{N_c^f\,\alpha}{32\pi^2 M_S^3}\,\frac{m_{12}^2}{M^2}\,\frac{(m_{13}^2)^2+(m_{23}^2)^2}{(M_S^2-m_{12}^2)^2}\,\Big|T_3^{f_L}\,\mathrm{D}^{ij}_{f_L\bar{f}_L W} + Y_{f_L}\mathrm{D}^{ij}_{f_L\bar{f}_L B}\Big|^2\,,\\
\frac{d^2\Gamma(S \to f_{iR}\,\bar{f}_{jR}\,\gamma)}{dm_{12}^2\,dm_{23}^2} &= \frac{N_c^f\,\alpha}{32\pi^2 M_S^3}\,\frac{m_{12}^2}{M^2}\,\frac{(m_{13}^2)^2+(m_{23}^2)^2}{(M_S^2-m_{12}^2)^2}\,\Big|Y_{f_R}\mathrm{D}^{ij}_{f_R\bar{f}_R B}\Big|^2\,,
\end{aligned} \tag{3.62}$$

where $T_3^{f_L}$ denotes the weak isospin of the left-handed fermion, and Y_{f_L}, Y_{f_R} are the hypercharges of the fermions. Only the two transverse polarisation states of the vector bosons contribute to these rates. The squared decay amplitudes depend in a non-trivial way on the light-like reference vectors of the final-state mesons. We find that they involve the quantity

$$\frac{n_1\cdot n_3\,n_2\cdot\bar{n}_3 + n_2\cdot n_3\,n_1\cdot\bar{n}_3}{n_1\cdot n_2} \simeq 2\,\frac{(m_{13}^2)^2+(m_{23}^2)^2}{(M_S^2-m_{12}^2)^2}\,. \tag{3.63}$$

To derive this result, we have replaced $n_i\cdot\bar{n}_3 = 2n_i\cdot v - n_i\cdot n_3$, where v^μ is the four-velocity of the decaying resonance S. We have then multiplied all light-like vectors with

the corresponding energies (defined in the rest frame of S) to obtain $k_i^\mu \simeq E_i n_i^\mu$, and at the end eliminated the energies using that $m_{12}^2 = (k_1+k_2)^2 = (M_S v - k_3)^2 \simeq M_S^2 - 2M_S E_3$ etc. The decay rates for the production of fermion pairs along with other gauge bosons are given by analogous expressions with different charge and colour factors and involving different combinations of Wilson coefficients, as shown in Table 3.1.
Neglecting the masses of the final-state particles, the boundaries of the Dalitz plot are such that

$$0 < m_{12}^2 < M_S^2\,, \qquad 0 < m_{23}^2 < M_S^2 - m_{12}^2\,. \tag{3.64}$$

Since our results have been derived under the assumption that the invariant mass of each pair of final-state particles is of order M_S, strictly speaking they are not valid near the boundary of the Dalitz plot. On the other hand, since the boundary effect occurs in a power-suppressed region of phase space, one usually does not need to worry about this issue, unless the squared decay amplitude is singular near the boundary.
If the Wilson coefficients only depend on m_{12}^2 but not on m_{23}^2 and m_{13}^2 individually, the expressions in (3.59), (3.60) and (3.62) can be integrated over m_{23}^2 to obtain the distributions in the invariant mass of the fermion pair. We will show in Section 3.6 that this condition is satisfied (at least at tree level) in all models featuring a double hierarchy $M \gg M_S \gg v$. We quote the result for the interesting case of the decay $S \to t\bar{t}Z$. Summing over the different polarisation states of the fermions, and defining $x_{12} = m_{t\bar{t}}^2/M_S^2$, we find

$$\begin{aligned}\frac{d\Gamma(S\to t\bar{t}Z)}{dx_{12}} = \frac{N_c M_S^3}{512\pi^3 M^2}\, x_{12}(1-x_{12}) \Big\{ &\Big[\big|\mathrm{D}^{33}_{u_L\bar{u}_R\,\phi}(x_{12})\big|^2 + \big|\mathrm{D}^{33}_{u_R\bar{u}_L\phi}(x_{12})\big|^2\Big] \\ &+ \frac{32\pi\alpha}{3}\Big[\Big|\frac{c_w}{2s_w}\,\mathrm{D}^{33}_{u_L\bar{u}_L W}(x_{12}) - \frac{s_w}{6c_w}\,\mathrm{D}^{33}_{u_L\bar{u}_L B}(x_{12})\Big|^2 \\ &+ \Big|\frac{2s_w}{3c_w}\,\mathrm{D}^{33}_{u_R\bar{u}_R B}(x_{12})\Big|^2\Big]\Big\}.\end{aligned} \tag{3.65}$$

With the help of (3.59), (3.60) and Table 3.1, all other rates can be obtained from this expression by means of simple substitutions.

3.5 Evolution Equations for the Wilson Coefficients

Large logarithms of the scale ratio M_S/v can be systematically resummed to all orders in perturbation theory using our effective theory. The leading effects arise from Sudakov double logarithms related to the interplay of soft and collinear emissions of virtual particles. They are controlled by so-called cusp logarithms in the anomalous dimensions of SCET operators [39], which govern the scale dependence of the Wilson coefficients in the effective Lagrangian of $\mathrm{SCET}_{\mathrm{BSM}}$. The relevant anomalous dimensions are computed from the UV divergences of SCET operators and are independent of the masses of the SM particles. They can be most conveniently derived by setting all masses to zero and using off-shell external momenta as infrared regulators. The relevant version of the effective

theory is called SCET_I. It describes the interactions of n_i-collinear fields with so-called ultra-soft fields with momentum scaling $(\lambda^2, \lambda^2, \lambda^2)$ [41,42]. Note that the ultra-soft scale $\lambda^2 M_S \sim v^2/M_S$ lies parametrically below the characteristic scale v of the low-energy theory. This scale arises in intermediate steps of the calculation, but it drops out from the final expressions for the anomalous dimensions.[5]
The discussion in this section is considerably more technical than that in previous sections. The reader not interested in these technicalities may directly proceed with Section 3.6, noting however that there is a well-defined formalism which allows us to derive the evolution equations needed to resum large logarithms in the SCET_BSM.

3.5.1 Operators Containing a Single Field in Each Collinear Direction

The scale dependence of the Wilson coefficients of operators containing a single n_i-collinear field for each direction of large energy flow can be described by a universal anomalous dimension depending on scalar products formed out of the different collinear momenta $\{\underline{p}\} = \{p_1, \dots, p_n\}$ (strictly speaking the momenta p_i should be replaced by the corresponding label operators $\mathcal{P}_i$), such that [185]

$$\mu \frac{d}{d\mu} C(\{\underline{p}\}, \mu) = \Gamma(\{\underline{p}\}, \mu)\, C(\{\underline{p}\}, \mu)\,. \tag{3.66}$$

For the Wilson coefficients of operators containing at most three external particles, the all-order structure of the anomalous dimension is extremely simple: It contains so-called "dipole terms" for pairs of particles i and j, which involve logarithms of the kinematic invariants $s_{ij} = 2p_i \cdot p_j$ (with all momenta outgoing) and correlations of the two particles in the space of group generators, as well as single-particle terms for each field [185–188]. Moreover, using charge conservation, one can eliminate all group generators in terms of the eigenvalues of the quadratic Casimir operators $C_i \in \{C_F, C_A\}$ for particles transforming in the fundamental or the adjoint representation of the gauge group. The two-particle terms involve the universal cusp anomalous dimension for light-like Wilson loops [189]. Since the SM gauge group is a direct product of three simple groups G_r with $G_1 = \text{U}_Y(1)$, $G_2 = \text{SU}_W(2)$ and $G_3 = \text{SU}_c(3)$, the cusp terms involve a sum over the three group factors. The anomalous dimensions for two- and three-particle operators take the form

$$\begin{aligned}
\Gamma(\{p_1, p_2\}, \mu) &= \sum_r C_1^{(r)}\, \gamma_\text{cusp}^{(r)}\, \ln \frac{-s_{12} - i0}{\mu^2} + \sum_{i=1,2} \gamma^i\,, \\
\Gamma(\{p_1, p_2, p_3\}, \mu) &= \frac{1}{2} \sum_r \sum_{\pi(i,j,k)} \left(C_i^{(r)} + C_j^{(r)} - C_k^{(r)}\right) \gamma_\text{cusp}^{(r)}\, \ln \frac{-s_{ij} - i0}{\mu^2} + \sum_{i=1,2,3} \gamma^i\,,
\end{aligned} \tag{3.67}$$

[5] It would be possible to calculate the anomalous dimensions using the masses of the SM particles as infrared regulators. In this case the ultra-soft scale does not arise (except in graphs involving massless gauge-boson exchange), but the calculations are far more complicated due to the appearance of rapidity divergences, which require analytic regulators beyond dimensional regularisation [176, 177].

where $\pi(i,j,k)$ refers to the even permutations of $(1,2,3)$. For non-abelian $\mathrm{SU}(N)$ groups one has $C_F^{(r)} = (N^2-1)/(2N)$ and $C_A^{(r)} = N$. For the hypercharge group $G_1 = \mathrm{U}_Y(1)$ one sets $C_F^{(1)} = Y_i^2$ and $C_A^{(1)} = 0$, where Y_i denotes the hypercharge of the particle i. If a particle does not transform under a group G_r, then $C_i^{(r)}$ is set to zero.
The single-particle anomalous dimensions γ^i for fermions contain terms involving the SM Yukawa matrices, which multiply the Wilson coefficients in (3.66) from the left (for a field $\bar{\mathcal{X}}$ producing an outgoing fermion) or from the right (for a field $\mathcal{X}$ producing an outgoing anti-fermion).
From (3.67), it is straightforward to derive exact all-order relations for the anomalous dimensions governing the scale dependence of the Wilson coefficients of the two-jet operators in the effective Lagrangian (3.21) arising at $\mathcal{O}(\lambda^2)$ and for the three-jet operators in the effective Lagrangian (3.55) arising at $\mathcal{O}(\lambda^3)$. Omitting all arguments for simplicity, we obtain

$$\begin{aligned}
\Gamma_{\phi\phi} &= \left(\frac{1}{4}\,\gamma_{\text{cusp}}^{(1)} + \frac{3}{4}\,\gamma_{\text{cusp}}^{(2)}\right)\left(\ln\frac{M_S^2}{\mu^2} - i\pi\right) + 2\gamma^{\phi}\,, \\
\Gamma_{BB} &= \widetilde{\Gamma}_{BB} = 2\gamma^{B}\,, \\
\Gamma_{WW} &= \widetilde{\Gamma}_{WW} = 2\gamma_{\text{cusp}}^{(2)}\left(\ln\frac{M_S^2}{\mu^2} - i\pi\right) + 2\gamma^{W}\,, \\
\Gamma_{GG} &= \widetilde{\Gamma}_{GG} = 3\gamma_{\text{cusp}}^{(3)}\left(\ln\frac{M_S^2}{\mu^2} - i\pi\right) + 2\gamma^{G}\,,
\end{aligned} \tag{3.68}$$

and

$$\begin{aligned}
\Gamma^{Q}_{F_L\bar{f}_R\,\phi} &= \left[\frac{1}{2}\left(Y_{F_L}^2 + Y_{f_R}^2 - Y_{\phi}^2\right)\gamma_{\text{cusp}}^{(1)} + \delta_{fq}\,\frac{4}{3}\,\gamma_{\text{cusp}}^{(3)}\right]\left(\ln\frac{m_{12}^2}{\mu^2} - i\pi\right) \\
&\quad + \left[\frac{1}{2}\left(Y_{\phi}^2 + Y_{F_L}^2 - Y_{f_R}^2\right)\gamma_{\text{cusp}}^{(1)} + \frac{3}{4}\,\gamma_{\text{cusp}}^{(2)}\right]\left(\ln\frac{m_{13}^2}{\mu^2} - i\pi\right) \\
&\quad + \frac{1}{2}\left(Y_{\phi}^2 + Y_{f_R}^2 - Y_{F_L}^2\right)\gamma_{\text{cusp}}^{(1)}\left(\ln\frac{m_{23}^2}{\mu^2} - i\pi\right) + \gamma^{F_L} + \gamma^{\bar{f}_R} + \gamma^{\phi}\,, \\
\Gamma^{Q}_{f_R\bar{F}_L\phi} &= \Gamma^{Q}_{F_L\bar{f}_R\,\phi}(m_{13}^2 \leftrightarrow m_{23}^2, F_L \leftrightarrow f_R)\,, \\
\Gamma^{Q}_{F_L\bar{F}_L B} &= \left[Y_{F_L}^2\gamma_{\text{cusp}}^{(1)} + \frac{3}{4}\,\gamma_{\text{cusp}}^{(2)} + \delta_{fq}\,\frac{4}{3}\,\gamma_{\text{cusp}}^{(3)}\right]\left(\ln\frac{m_{12}^2}{\mu^2} - i\pi\right) + \gamma^{F_L} + \gamma^{\bar{F}_L} + \gamma^{B}\,, \\
\Gamma^{Q}_{F_L\bar{F}_L W} &= \left[Y_{F_L}^2\gamma_{\text{cusp}}^{(1)} - \frac{1}{4}\,\gamma_{\text{cusp}}^{(2)} + \delta_{fq}\,\frac{4}{3}\,\gamma_{\text{cusp}}^{(3)}\right]\left(\ln\frac{m_{12}^2}{\mu^2} - i\pi\right) \\
&\quad + \gamma_{\text{cusp}}^{(2)}\left(\ln\frac{m_{13}^2}{\mu^2} + \ln\frac{m_{23}^2}{\mu^2} - 2i\pi\right) + \gamma^{F_L} + \gamma^{\bar{F}_L} + \gamma^{W}\,, \\
\Gamma^{Q}_{Q_L\bar{Q}_L G} &= \left[Y_{Q_L}^2\gamma_{\text{cusp}}^{(1)} + \frac{3}{4}\,\gamma_{\text{cusp}}^{(2)} - \frac{1}{6}\,\gamma_{\text{cusp}}^{(3)}\right]\left(\ln\frac{m_{12}^2}{\mu^2} - i\pi\right) \\
&\quad + \frac{3}{2}\,\gamma_{\text{cusp}}^{(3)}\left(\ln\frac{m_{13}^2}{\mu^2} + \ln\frac{m_{23}^2}{\mu^2} - 2i\pi\right) + \gamma^{Q_L} + \gamma^{\bar{Q}_L} + \gamma^{G}\,,
\end{aligned} \tag{3.69}$$

$$\Gamma^Q_{f_R\bar{f}_R B} = \left[Y^2_{f_R}\gamma^{(1)}_{\text{cusp}} + \delta_{fq}\,\frac{4}{3}\,\gamma^{(3)}_{\text{cusp}}\right]\left(\ln\frac{m^2_{12}}{\mu^2} - i\pi\right) + \gamma^{f_R} + \gamma^{\bar{f}_R} + \gamma^B\,,$$
$$\Gamma^Q_{q_R\bar{q}_R G} = \left[Y^2_{q_R}\gamma^{(1)}_{\text{cusp}} - \frac{1}{6}\,\gamma^{(3)}_{\text{cusp}}\right]\left(\ln\frac{m^2_{12}}{\mu^2} - i\pi\right)$$
$$+ \frac{3}{2}\,\gamma^{(3)}_{\text{cusp}}\left(\ln\frac{m^2_{13}}{\mu^2} + \ln\frac{m^2_{23}}{\mu^2} - 2i\pi\right) + \gamma^{q_R} + \gamma^{\bar{q}_R} + \gamma^G\,,$$

where $\delta_{fq} = 1$ if the fermion is a quark and 0 otherwise. We have indicated the anomalous dimensions of the three-jet operators by a superscript "Q".
In general, the cusp anomalous dimensions $\gamma^{(r)}_{\text{cusp}}$ and the single-particle anomalous dimensions γ^i depend on the three gauge couplings $\alpha_1 = \alpha/c^2_w$, $\alpha_2 = \alpha/s^2_w$ and $\alpha_3 = \alpha_S$, the quartic scalar coupling, and the Yukawa couplings. Up to two-loop order, however, the cusp anomalous dimension for the gauge group G_r only depends on the corresponding coupling α_r. Explicitly, it is given by [189–191]

$$\gamma^{(r)}_{\text{cusp}} = \frac{\alpha_r}{\pi} + \left[\left(\frac{67}{36} - \frac{\pi^2}{12}\right)C^{(r)}_A - \sum_f \frac{5}{18}\,T^{(r)}_F d_f - \frac{1}{9}\,T^{(r)}_F d_\phi\right]\left(\frac{\alpha_r}{\pi}\right)^2 + \dots\,, \tag{3.70}$$

where $T^{(r)}_F = 1/2$ for the non-abelian groups ($r = 2, 3$) and $T^{(1)}_F = Y^2_i$ for the hypercharge group. The coefficients d_f and d_ϕ are the dimensions of the representations of the chiral fermions and the scalar doublet with respect to the other two gauge groups. The sum runs over the chiral fermion multiplets of the SM model, and we have used that there is a single complex scalar doublet.[6] Explicitly, one finds

$$\begin{aligned}
\gamma^{(1)}_{\text{cusp}} &= \frac{\alpha_1}{\pi} - \frac{17}{6}\left(\frac{\alpha_1}{\pi}\right)^2 + \dots\,,\\
\gamma^{(2)}_{\text{cusp}} &= \frac{\alpha_2}{\pi} + \left(2 - \frac{\pi^2}{6}\right)\left(\frac{\alpha_2}{\pi}\right)^2 + \dots\,,\\
\gamma^{(3)}_{\text{cusp}} &= \frac{\alpha_3}{\pi} + \left(\frac{47}{12} - \frac{\pi^2}{4}\right)\left(\frac{\alpha_3}{\pi}\right)^2 + \dots\,.
\end{aligned} \tag{3.71}$$

The three-loop coefficient of the cusp anomalous dimension is only known for a single gauge group and neglecting the contributions from the scalar Higgs doublet [193].
We will restrict our discussion here to a consistent resummation of Sudakov logarithms at leading logarithmic order. This requires the calculation of the cusp anomalous dimension to two-loop order, as given in (3.71), while the remaining anomalous dimensions are required with one-loop accuracy. For fermions and the scalar doublet, the one-loop

[6] In the same notation, the one-loop coefficient of the β function for a given gauge coupling reads [192]

$$\beta^{(r)}_0 = \frac{11}{3}\,C^{(r)}_A - \sum_f \frac{2}{3}\,T^{(r)}_F d_f - \frac{1}{3}\,T^{(r)}_F d_\phi\,.$$

coefficients from gauge interactions in units of α_r/π are $-3C_F^{(r)}/4$ [187] and $-C_F^{(r)}$ [152], respectively. The one-loop coefficients of the anomalous dimensions of the gauge fields vanish, since in contrast to [187] we have included the gauge couplings in the definitions of the n_i-collinear gauge fields in (3.8). Including also the contributions from the Yukawa interactions to the wave-function renormalisations of the fields, we obtain

$$\begin{aligned}
\gamma^{f_L} = \gamma^{\bar{f}_L} &= -Y_{f_L}^2\,\frac{\alpha_1}{4\pi} - \frac{9\alpha_2}{16\pi} - \delta_{fq}\,\frac{\alpha_3}{\pi} + \frac{1}{32\pi^2}\,\boldsymbol{Y}_f\boldsymbol{Y}_f^\dagger\,,\\
\gamma^{f_R} = \gamma^{\bar{f}_R} &= -Y_{f_R}^2\,\frac{\alpha_1}{4\pi} - \delta_{fq}\,\frac{\alpha_3}{\pi} + \frac{1}{32\pi^2}\,\boldsymbol{Y}_f^\dagger\boldsymbol{Y}_f\,,\\
\gamma^{\phi} &= -\frac{\alpha_1}{4\pi} - \frac{3\alpha_2}{4\pi} + \sum_f \frac{N_c^f y_f^2}{8\pi^2}\,,
\end{aligned} \tag{3.72}$$

where in the last expression the sum runs over the different fermion species, and y_f denotes the Yukawa coupling of the fermion f.

3.5.2 Two-Jet Operators at $\mathcal{O}(\lambda^3)$

For operators containing more than one n_i-collinear field in a given direction, the anomalous dimensions are more complicated than the simple expressions shown in (3.67). This concerns, in particular, the anomalous dimensions governing the scale dependence of the Wilson coefficients of the two-jet operators arising at $\mathcal{O}(\lambda^3)$ in the SCET_{BSM} Lagrangian, which we have defined in (3.36) and (3.37). Since these operators depend on a variable u (the fraction of the total collinear momentum carried by the boson field), the anomalous dimensions are distribution-valued functions. Also, there is a non-trivial mixing of these operators under renormalisation. Finally, we will find that some of the convolution integrals appearing in the evolution equations exhibit endpoint singularities at the boundary of the integration domain, which need to be treated with care. For simplicity, we will only explore the effects of QCD evolution here, leaving a more complete treatment to future work. We will thus assume that the fermion fields in the three-jet operators are quark fields.

The presence of the scalar doublet implies that, as far as QCD evolution is concerned, the mixed-chirality operators in (3.36) renormalise like two-jet operators, with anomalous dimensions given by (in this section we keep the dependence on the colour factors $C_F = 4/3$ and $C_A = 3$ explicit)

$$\begin{aligned}
\Gamma_{Q_L\bar{q}_R} &= C_F\,\gamma_{\text{cusp}}^{(3)}\left(\ln\frac{M_S^2}{\mu^2} - i\pi\right) + 2\gamma^q\,,\\
\Gamma_{Q_L\bar{q}_R\,\phi}^{(i)} &= C_F\,\gamma_{\text{cusp}}^{(3)}\left(\ln\frac{(1-u)M_S^2}{\mu^2} - i\pi\right) + 2\gamma^q\,; \quad i = 1,2\,,
\end{aligned} \tag{3.73}$$

where we have used that $\gamma^{Q_L} = \gamma^{q_R} \equiv \gamma^q = -3C_F\alpha_S/(4\pi) + \ldots$ under QCD evolution. The same is true for the same-chirality operators for which the gauge field belongs to

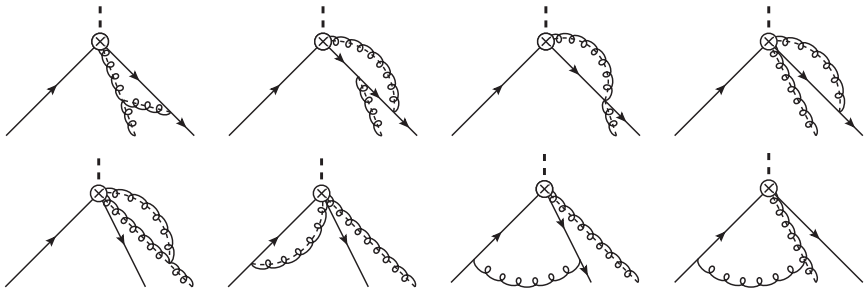

Figure 3.2: One-loop diagrams contributing to the anomalous dimension $\Gamma_{q\bar{q}G}$ in (3.75). The short dashed line represents the heavy scalar resonance S. Solid lines denote collinear quarks, curly lines with dashes denote collinear gluons, and simple curly lines represent ultra-soft gluons. Collinear fields moving along the same direction are drawn next to each other.

$\mathrm{SU}_W(2)$ or $\mathrm{U}_Y(1)$, i.e.

$$\Gamma_{Q_L\bar{Q}_LB} = \Gamma_{q_R\bar{q}_RB} = \Gamma_{Q_L\bar{Q}_LW} = \Gamma_{q_R\bar{q}_RW} = C_F\,\gamma^{(3)}_{\rm cusp}\left(\ln\frac{(1-u)M_S^2}{\mu^2} - i\pi\right) + 2\gamma^q\,. \quad (3.74)$$

When only QCD corrections are taken into account, the cusp anomalous dimension [193] and the anomalous dimension of the quark field [194, 195] are known to three-loop order. The same-chirality operators containing a gluon field exhibit a more interesting behavior. Due to the dependence of the operators $O_{Q_L\bar{Q}_LG}$ and $O_{q_R\bar{q}_RG}$ on the variable u, the anomalous dimension governing the multiplicative renormalisation of these operators is a distribution-valued function of two variables u and w. We find that the scale dependence of the corresponding Wilson coefficients is determined by the evolution equation (with $q = Q_L$ or q_R)

$$\mu\,\frac{d}{d\mu}\,\boldsymbol{C}_{q\bar{q}G}(u, M_S, M, \mu) = \int_0^1 dw\,\Gamma_{q\bar{q}G}(u, w, M_S, \mu)\,\boldsymbol{C}_{q\bar{q}G}(w, M_S, M, \mu)\,, \quad (3.75)$$

where here and below we use a boldface notation to indicate that the Wilson coefficients are matrices in generation space. The anomalous dimension $\Gamma_{q\bar{q}G}$ can be calculated in analogy with the derivation of the anomalous dimensions of the subleading SCET current operators arising in B-meson physics performed in [182, 196] (see [197] for related recent work). It is convenient to use the background-field gauge [198] for the external gluon, in which the combination $g_S\,G^{\mu,a}$ is not renormalised. Evaluating the UV divergences of the one-loop diagrams shown in Figure 3.2, supplemented by wave-function renormalisation, we obtain (with $\bar{u} \equiv 1-u$ and $\bar{w} \equiv 1-w$)

$$\begin{aligned}\Gamma_{q\bar{q}G}(u, w, M_S, \mu) = &\left[C_F\left(\ln\frac{\bar{u}M_S^2}{\mu^2} - i\pi - \frac{3}{2}\right) + \frac{C_A}{2}\left(\ln\frac{u}{\bar{u}} + 1\right)\right]\gamma^{(3)}_{\rm cusp}\,\delta(u-w)\\ &+ \bar{w}\Big[V_1(\bar{u}, \bar{w}) + V_2(\bar{u}, \bar{w})\Big] + \mathcal{O}(\alpha_S^2)\,.\end{aligned} \quad (3.76)$$

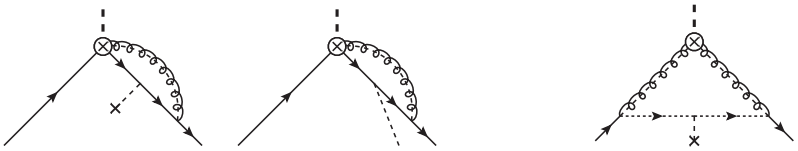

Figure 3.3: LEFT: One-loop diagram responsible for the mixing of the operators $O_{Q_L\bar{Q}_LG}$ and $O_{q_R\bar{q}_RG}$ into the three mixed-chirality operators in (3.36). A dashed line ended by a cross indicates a zero-momentum scalar field Φ_0, while a dashed line bending to the right shows a collinear scalar field. RIGHT: Mixing of the $\mathcal{O}(\lambda^2)$ operators O_{GG} and $\widetilde{O}_{GG}$ into the operator $O_{Q_L\bar{q}_R}$ by means of subleading interactions in the SCET Lagrangian. The dotted line represents an ultra-soft quark.

The logarithmic terms in the first line are exact to all orders in perturbation theory, whereas the remaining terms have been computed at one-loop order. The kernel functions V_i, which are symmetric in their arguments, have been computed first in [182]. At one-loop order one finds

$$\begin{aligned} V_1(\bar{u},\bar{w}) + V_2(\bar{u},\bar{w}) = -\frac{C_A}{2}\,\frac{\alpha_S}{\pi}\left\{\frac{1}{\bar{u}\bar{w}}\left[\bar{u}\,\frac{\theta(u-w)}{u-w} + \bar{w}\,\frac{\theta(w-u)}{w-u}\right]_+\right. \\ \left. + \left(\frac{w}{\bar{w}} - \frac{1}{u}\right)\theta(u-w) + \left(\frac{u}{\bar{u}} - \frac{1}{w}\right)\theta(w-u)\right\} \\ + \left(C_F - \frac{C_A}{2}\right)\frac{\alpha_S}{\pi}\left[\left(2 - \frac{\bar{u}\bar{w}}{uw}\right)\theta(u+w-1) + \frac{uw}{\bar{u}\bar{w}}\,\theta(1-u-w)\right], \end{aligned} \tag{3.77}$$

where for symmetric functions $g(u,w)$ the plus distribution is defined to act on test functions $f(w)$ as

$$\int_0^1 dw\,[g(u,w)]_+\,f(w) = \int_0^1 dw\,g(u,w)\,[f(w) - f(u)]\,. \tag{3.78}$$

Using arguments based on conformal symmetry, it was shown in [182] how the convolution in (3.75) can be diagonalised by expanding the Wilson coefficients in a suitable basis of Jacobi polynomials. This will be discussed in more detail elsewhere.

Next, we find that the operators $O_{Q_L\bar{Q}_LG}$ and $O_{q_R\bar{q}_RG}$ mix into the three mixed-chirality operators in (3.36). The diagram responsible for this mixing is shown on the left-hand side in Figure 3.3. The evolution equations for the Wilson coefficients of these operators

read

$$\begin{aligned}
\mu\,\frac{d}{d\mu}\,\boldsymbol{C}^{(1)}_{Q_L\bar{q}_R\,\phi}(u,\mu) &= \Gamma^{(1)}_{Q_L\bar{q}_R\,\phi}(u,\mu)\,\boldsymbol{C}^{(1)}_{Q_L\bar{q}_R\,\phi}(u,\mu) \\
&\quad + \int_0^1 dw\,\Gamma_{\rm mix}(u,w,\mu)\,\boldsymbol{Y}_q(\mu)\,\boldsymbol{C}_{q_R\bar{q}_R G}(w,\mu)\,, \\
\mu\,\frac{d}{d\mu}\,\boldsymbol{C}^{(2)}_{Q_L\bar{q}_R\,\phi}(u,\mu) &= \Gamma^{(2)}_{Q_L\bar{q}_R\,\phi}(u,\mu)\,\boldsymbol{C}^{(2)}_{Q_L\bar{q}_R\,\phi}(u,\mu) \\
&\quad + \int_0^1 dw\,\Gamma_{\rm mix}(u,w,\mu)\,\boldsymbol{C}^{\dagger}_{Q_L\bar{Q}_L G}(w,\mu)\,\boldsymbol{Y}_q(\mu)\,,
\end{aligned} \tag{3.79}$$

and (only if $C_{GG} = \widetilde{C}_{GG} = 0$!)

$$\begin{aligned}
\mu\,\frac{d}{d\mu}\,\boldsymbol{C}_{Q_L\bar{q}_R}(\mu) &= \Gamma_{Q_L\bar{q}_R}(\mu)\,\boldsymbol{C}_{Q_L\bar{q}_R}(\mu) \\
&\quad + \int_0^1 dw\,\Gamma_{\rm mix}(0,w,\mu)\,\Big[\boldsymbol{Y}_q(\mu)\,\boldsymbol{C}_{q_R\bar{q}_R G}(w,\mu) + \boldsymbol{C}^{\dagger}_{Q_L\bar{Q}_L G}(w,\mu)\,\boldsymbol{Y}_q(\mu)\Big]\,,
\end{aligned} \tag{3.80}$$

where we have defined the mixing kernel

$$\Gamma_{\rm mix}(u,w,\mu) = \frac{C_F\alpha_S(\mu)}{\pi}\,\frac{\theta(1-u-w)}{1-u} + \mathcal{O}(\alpha_S^2)\,. \tag{3.81}$$

The anomalous dimensions $\Gamma^{(i)}_{Q_L\bar{q}_R\,\phi}$ and $\Gamma_{Q_L\bar{q}_R}$ have been given in (3.73). For simplicity, we have omitted the dependence of the Wilson coefficients on the NP scales M_S and M, as well as the dependence of the anomalous dimensions on the scale M_S.
The evolution equation (3.80) needs to be modified if the Wilson coefficients $\boldsymbol{C}_{Q_L\bar{Q}_L G}$ and $\boldsymbol{C}_{q_R\bar{q}_R G}$ exhibit non-integrable singularities at the endpoint of the integration region. As we discuss in the Appendix, this happens whenever $C_{GG} \neq 0$ or $\widetilde{C}_{GG} \neq 0$. Hard matching contributions then produce poles in the Wilson coefficients located at $w = 1$,[7] whose residues are related to the coefficients C_{GG} and $\widetilde{C}_{GG}$. While at first sight the presence of these poles appears to give rise to endpoint-divergent integrals of the form $\int_0^1 dw\,\frac{1}{1-w}$ in (3.80), a careful treatment reveals that the form of the mixing kernel in (3.81) must be modified in this case. The dimensionally regularised loop integral produces an extra factor $\big(w(1-w)\big)^{-\epsilon}$, which regularises the singularities at $w = 1$ at the expense of introducing a $1/\epsilon^2$ pole. Next, for $C_{GG} \neq 0$ or $\widetilde{C}_{GG} \neq 0$ there is an additional contribution arising from the mixing of the operators in the $\mathcal{O}(\lambda^2)$ effective Lagrangian (3.35) into the $\mathcal{O}(\lambda^3)$ operator $O_{Q_L\bar{q}_R}$, which happens via subleading terms in the SCET Lagrangian connecting collinear fields with an ultra-soft quark field. The relevant diagram is shown on the right-hand side in Figure 3.3. The two effects conspire to produce an extra term in the evolution equation (3.80) proportional to a combination of C_{GG} and $\widetilde{C}_{GG}$ times a cusp logarithm. Details of this calculation are presented in the Appendix. The final

[7] In higher orders of perturbation theory, the poles can be multiplied by logarithms of $(1-w)$.

result for the corrected form of the evolution equation (3.80) reads

$$\begin{aligned}\mu\,\frac{d}{d\mu}\,\boldsymbol{C}_{Q_L\bar{q}_R}(\mu) &= \Gamma_{Q_L\bar{q}_R}(\mu)\,\boldsymbol{C}_{Q_L\bar{q}_R}(\mu)\\ &\quad+\frac{M^2}{M_S^2}\left[\gamma^{q\bar{q}}_{\rm cusp}\left(\ln\frac{M_S^2}{\mu^2}-i\pi\right)+\tilde{\gamma}_{q\bar{q}}\right]g_S^2(\mu)\left(C_{GG}(\mu)+i\widetilde{C}_{GG}(\mu)\right)\boldsymbol{Y}_q(\mu)\\ &\quad+\int_0^1 dw\,\Gamma_{\rm mix}(0,w,\mu)\left[\boldsymbol{Y}_q(\mu)\,\bar{\boldsymbol{C}}_{q_R\bar{q}_RG}(w,\mu)+\bar{\boldsymbol{C}}^\dagger_{Q_L\bar{Q}_LG}(w,\mu)\,\boldsymbol{Y}_q(\mu)\right],\end{aligned}\tag{3.82}$$

where

$$\gamma^{q\bar{q}}_{\rm cusp}=\frac{C_F\alpha_S(\mu)}{\pi}+\mathcal{O}(\alpha_S^2)\,,\qquad \tilde{\gamma}_{q\bar{q}}=\frac{C_F\alpha_S(\mu)}{\pi}+\mathcal{O}(\alpha_S^2)\,,\tag{3.83}$$

and the subtracted coefficients $\bar{\boldsymbol{C}}_{q\bar{q}G}(w,\mu)$ (with $q=Q_L$ or q_R) are obtained from the original ones by subtracting all terms of order $(1-w)^{-1}$ modulo logarithms. At lowest order in perturbation theory, we show in the Appendix that

$$\begin{aligned}\bar{\boldsymbol{C}}_{Q_L\bar{Q}_LG}(u,\mu)&=\boldsymbol{C}_{Q_L\bar{Q}_LG}(u,\mu)-\frac{M^2}{M_S^2}\,\frac{g_S^2(\mu)}{1-u}\left[C_{GG}(\mu)-i\widetilde{C}_{GG}(\mu)\right],\\ \bar{\boldsymbol{C}}_{q_R\bar{q}_RG}(u,\mu)&=\boldsymbol{C}_{q_R\bar{q}_RG}(u,\mu)-\frac{M^2}{M_S^2}\,\frac{g_S^2(\mu)}{1-u}\left[C_{GG}(\mu)+i\widetilde{C}_{GG}(\mu)\right].\end{aligned}\tag{3.84}$$

Note that the evolution equations (3.75) and (3.79) do not require similar modifications, because the factor $(1-w)$ in the second line of (3.76) and the $\theta(1-u-w)$ function in (3.81) eliminate the singularities at $w=1$.

The cusp anomalous dimension $\gamma^{q\bar{q}}_{\rm cusp}$ in (3.83) is a new object, which arises from the exchange of an ultra-soft quark between two collinear sectors. This is likely to be a new universal quantity, which arises in SCET applications beyond the leading power in the expansion parameter λ. The calculation of the two-loop coefficient of this quantity is an interesting open problem, to which we will return in future work.

3.5.3 Resummation of Large Logarithms

To illustrate the results derived above, we now perform the resummation of large logarithms of the scale ratio M_S/v for two representative cases, working consistently at leading logarithmic order. We focus on the examples $S\to 2$ jets and $S\to t\bar{t}+$ jet, where in both cases the jets are seeded by gluons (quark jets contribute at subleading power only). At tree level, the expression for the $S\to 2$ jets rate obtained from (3.33) reads

$$\Gamma(S\to 2\text{ jets})=\frac{M^2}{M_S}\,8\pi\alpha_S^2(\mu)\left(|C_{GG}(\mu)|^2+|\widetilde{C}_{GG}(\mu)|^2\right).\tag{3.85}$$

Likewise, the Dalitz distribution for the decay $S \to t\bar{t} + \text{jet}$ obtained from (3.62) reads

$$\begin{aligned}\frac{d^2\Gamma(S \to t\bar{t} + \text{jet})}{dx_{12}\, dx_{23}} = \frac{M_S^3}{M^2}\, \frac{\alpha_S(\mu)}{8\pi^2}\, \frac{x_{12}\,(x_{13}^2 + x_{23}^2)}{(1-x_{12})^2} \\ \times \left(\left| \mathrm{D}^{33}_{u_L \bar{u}_L G}(\{x_{ij}\}, \mu) \right|^2 + \left| \mathrm{D}^{33}_{u_R \bar{u}_R G}(\{x_{ij}\}, \mu) \right|^2 \right),\end{aligned} \tag{3.86}$$

where we have defined $x_{ij} = m_{ij}^2/M_S^2$ with $x_{12} + x_{23} + x_{13} = 1$. In the above relations we suppress the dependence of the Wilson coefficients on the NP scales M and M_S. The scales μ on the right-hand side of the equations should be chosen equal to a characteristic scale of the process. In the first case, this should be a scale associated with the definition of the jets, while in the second case the scale should be around the top-quark mass. We will now derive how the Wilson coefficients at these low scales can be computed, at leading logarithmic order, in terms of the Wilson coefficients at the high scale M_S. We will focus on QCD evolution only, since this will give rise to the largest effects.
The general solution of the RG equation (3.66) has been derived in [199, 200]. For the specific cases considered here, where the relevant anomalous dimensions are given by Γ_{GG} in (3.68) and $\Gamma^Q_{Q_L \bar{Q}_L G}$, $\Gamma^Q_{q_R \bar{q}_R G}$ in (3.69), we obtain at leading logarithmic order

$$C_{GG}(\mu) = \exp\left[\frac{6}{49}\, g(M_S, \mu) + \frac{6}{7}\, i\pi \ln r \right] C_{GG}(M_S)\,, \tag{3.87}$$

with the same relation connecting $\widetilde{C}_{GG}(\mu)$ with $\widetilde{C}_{GG}(M_S)$, and

$$\begin{aligned}\mathrm{D}^{33}_{u_A \bar{u}_A G}(\{x_{ij}\}, \mu) = \exp\left[\frac{17}{147}\, g(M_S, \mu) + \left(\frac{4}{7} + \frac{17}{21}\, i\pi \right) \ln r \right] \mathrm{D}^{33}_{u_A \bar{u}_A G}(\{x_{ij}\}, M_S) \\ \times (x_{12})^{\frac{1}{21} \ln r}\, (x_{23}\, x_{13})^{-\frac{3}{7} \ln r}\,,\end{aligned} \tag{3.88}$$

with $A = L, R$. We have defined the ratio $r = \alpha_S(\mu)/\alpha_S(M_S)$ and

$$g(M_S, \mu) = \frac{4\pi}{\alpha_S(M_S)} \left(1 - \frac{1}{r} - \ln r \right) + \left(\frac{251}{21} - \pi^2 \right) (1 - r + \ln r) + \frac{13}{7}\, \ln^2 r\,. \tag{3.89}$$

These expressions apply for six massless flavours of quarks, and they should thus not be evaluated below the scale of the top-quark mass $m_t \approx 173\,\text{GeV}$. For a scalar resonance of mass $M_S = 2\,\text{TeV}$, we find numerically

$$\begin{aligned}C_{GG}(m_t) &\approx (0.42 + 0.36\, i)\, C_{GG}(M_S)\,, \\ \mathrm{D}^{33}_{u_A \bar{u}_A G}(\{x_{ij}\}, m_t) &\approx (0.52 + 0.42\, i) \left(\frac{x_{12}^{1/9}}{x_{23}\, x_{13}} \right)^{0.11} \mathrm{D}^{33}_{u_A \bar{u}_A G}(\{x_{ij}\}, M_S)\,,\end{aligned} \tag{3.90}$$

indicating that evolution effects can be quite sizable. In the second case, these effects lead to an additional, non-trivial dependence on the kinematic variables x_{ij}.
The solution of the RG equations governing the evolution of the Wilson coefficients of the two-jet operators arising at $\mathcal{O}(\lambda^3)$, which we have derived in Section 3.5.2, is

more complicated. These equations can either be solved by numerical integration or by constructing a suitable complete set of basis functions which diagonalise the relevant anomalous-dimension kernels [182]. We leave a detailed discussion of these matters for future work.

3.6 SCET$_{\text{BSM}}$ for the Scale Hierarchy $M \gg M_S \gg v$

While our SCET$_{\text{BSM}}$ approach was designed to deal with the case where the masses of the heavy new resonance S and of other, yet undiscovered new particles are of the same order, it also applies to NP scenarios in which there is a double hierarchy, such that $M \gg M_S \gg v$. It is interesting to study this case in some detail, as it provides a nice test case with which to illustrate our method.

3.6.1 Effective Lagrangian Below the New-Physics Scale M

If the scale M characterising the NP lies much above the scale of the resonance S, the undiscovered heavy particles can be integrated out in a first step, see the right panel of Figure 3.1. This is the standard case of integrating out heavy virtual degrees of freedom, which are too massive to be produced as real particles. The effective Lagrangian obtained after this first step consists of local operators built out of S and SM fields. We can write

$$\mathcal{L}_{\text{eff}}(M > \mu > M_S) = \mathcal{L}_{\text{SM}} + \mathcal{L}_{\text{SMEFT}} + \mathcal{L}_S \,. \tag{3.91}$$

Here $\mathcal{L}_{\text{SMEFT}}$ is the EFT extension of the SM by higher-dimensional operators constructed out of SM fields only. Up to dimension-six order, the corresponding operators have been classified in [43, 45, 46, 57, 139]. $\mathcal{L}_S$ describes the interactions of S with itself and with SM fields. Up to dimension-five order, we write the most general expression for this Lagrangian in the form

$$\begin{aligned}
\mathcal{L}_S^{D\leq 5} = {} & \frac{1}{2}\,(\partial_\mu S)(\partial^\mu S) - V(S) - M\lambda_1\, S\,\phi^\dagger\phi - \frac{\lambda_2}{2}\,S^2\phi^\dagger\phi - \frac{\lambda_3}{6M}\,S^3\phi^\dagger\phi - \frac{\lambda_4}{M}\,S\left(\phi^\dagger\phi\right)^2 \\
& + \frac{c_{GG}}{M}\,\frac{\alpha_S}{4\pi}\,S\,G^a_{\mu\nu}G^{\mu\nu,a} + \frac{c_{WW}}{M}\,\frac{\alpha}{4\pi s_w^2}\,S\,W^i_{\mu\nu}W^{\mu\nu,i} + \frac{c_{BB}}{M}\,\frac{\alpha}{4\pi c_w^2}\,SB_{\mu\nu}B^{\mu\nu} \\
& + \frac{\tilde{c}_{GG}}{M}\,\frac{\alpha_S}{4\pi}\,S\,G^a_{\mu\nu}\tilde{G}^{\mu\nu,a} + \frac{\tilde{c}_{WW}}{M}\,\frac{\alpha}{4\pi s_w^2}\,S\,W^i_{\mu\nu}\tilde{W}^{\mu\nu,i} + \frac{\tilde{c}_{BB}}{M}\,\frac{\alpha}{4\pi c_w^2}\,SB_{\mu\nu}\tilde{B}^{\mu\nu} \\
& - \frac{1}{M}\left(S\,\bar{Q}_L\,\hat{\boldsymbol{Y}}_u\,\tilde{\phi}\,u_R + S\,\bar{Q}_L\,\hat{\boldsymbol{Y}}_d\,\phi\,d_R + S\,\bar{L}_L\,\hat{\boldsymbol{Y}}_e\,\phi\,e_R + \text{h.c.}\right).
\end{aligned} \tag{3.92}$$

Here $V(S)$ denotes the scalar potential, which in particular accounts for the mass M_S of the scalar resonance. $G^a_{\mu\nu}$, $W^i_{\mu\nu}$ and $B_{\mu\nu}$ denote the field strength tensors of $\text{SU}_c(3)$, $\text{SU}_W(2)$ and $\text{U}_Y(1)$, and $\tilde{G}^{\mu\nu,a} = \frac{1}{2}\,\epsilon^{\mu\nu\alpha\beta}\,G^a_{\alpha\beta}$ etc. are the dual field strengths. The quantities $\hat{\boldsymbol{Y}}_f$ with $f = u, d, e$ are arbitrary complex matrices in generation space. We have used the equations of motion for the SM fields and for the field S to eliminate redundant operators, such as $S\,\phi^\dagger D^2\phi$, $(\partial^\mu S)\,(\phi^\dagger i D_\mu\phi + \text{h.c.})$, $(\partial^\mu S)\,\bar{\psi}\gamma_\mu\psi$ (with an arbitrary chiral

fermion ψ), and $(\Box S)\,\phi^\dagger\phi$.[8] Note that the coupling $M\lambda_1$ of the Higgs-portal operator $S\,\phi^\dagger\phi$ is dimensionful and naturally of order M (i.e., it has a "hierarchy problem"). Our operator basis agrees with the one obtained in [201], where a complete operator basis was constructed up to dimension $D = 7$. Compared with [202], we have eliminated the redundant operator $S\,(\partial^\mu S)(\partial_\mu S)$.
It is straightforward to calculate the tree-level contributions to the $S \to hh$, $S \to VV$ and $S \to f\bar{f}$ decay amplitudes from the above effective Lagrangian and to reproduce the scaling relations shown in (3.1). The only non-trivial case concerns the $S \to Zh$ decay amplitude, for which the leading dimension-five contribution arises at one-loop order and was calculated in [166]. The first tree-level contribution to the $S \to Zh$ decay amplitude arises from the dimension-seven operator

$$\mathcal{L}_S^{D=7} \ni \frac{C_7}{M^3}\,(\partial^\mu S)\,(\phi^\dagger i D_\mu \phi + \text{h.c.})\,\phi^\dagger\phi\,. \tag{3.93}$$

This contribution is suppressed by three powers of the NP scale.

3.6.2 RG Evolution From the New-Physics Scale to the Scale M_S

Up to dimension-five order, the Wilson coefficients λ_i, c_{VV}, $\tilde{c}_{VV}$, and $\hat{\boldsymbol{Y}}_f$ in (3.92) evaluated at the NP scale $\mu_0 \sim M$ encode the complete information about the UV completion of the theory at higher scales.[9] After these coefficients have been fixed from a matching calculation in the context of a particular model, they can be evolved from the high scale $\mu_0 \sim M$ to the intermediate scale $\mu \sim M_S$ set by the mass of the resonance S (see the right panel in Figure 3.1). In this process, large logarithms of the scale ratio $M/M_S \gg 1$ are resummed. Since in our case S is a gauge singlet under the SM, the relevant anomalous dimensions are those of the corresponding SM operators without the field S. For simplicity, we will consider here only the effects related to QCD evolution.
At leading logarithmic order, only the Wilson coefficients $\hat{\boldsymbol{Y}}_f$ associated with quark fields change under scale variation, and we find (with $q = u, d$)

$$\hat{\boldsymbol{Y}}_q(\mu) = \left(\frac{\alpha_S(\mu)}{\alpha_S(\mu_0)}\right)^{3C_F/\beta_0} \hat{\boldsymbol{Y}}_q(\mu_0)\,, \tag{3.94}$$

where $\beta_0 = \frac{11}{3}\,C_A - \frac{2}{3}\,n_f$ is the first coefficient of the QCD β-function. All other Wilson coefficients are scale independent in this approximation. Beyond the leading order the evolution effects become more interesting. For the scale dependence of the coefficient

[8] The authors of [165] have used the equation of motion for the scalar Higgs doublet to eliminate the portal interaction $S\,\phi^\dagger\phi$ instead of the operator $S\,(D_\mu\phi)^\dagger(D^\mu\phi)$, which we have eliminated. This is not a suitable choice, because the portal interaction is a dimension-three operator, whose contribution is enhanced by two powers of the cutoff scale relative to the dimension-five operators in the effective Lagrangian.

[9] The Wilson coefficients of the Weinberg operators contained in $\mathcal{L}_{\text{SMEFT}}$ also enter at this order, but they do not play a role in our analysis.

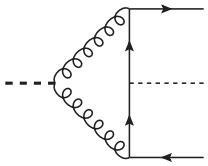

Figure 3.4: One-loop diagram responsible for the mixing of the Wilson coefficients c_{GG}, $\tilde{c}_{GG}$ and $\hat{\boldsymbol{Y}}_q$ described by (3.98).

$c_{GG}(\mu)$, which is renormalised multiplicatively, an exact solution can be written in terms of the QCD β-function [203, 204]. It reads

$$c_{GG}(\mu) = \frac{\beta(\alpha_S(\mu))/\alpha_S^2(\mu)}{\beta(\alpha_S(\mu_0))/\alpha_S^2(\mu_0)}\, c_{GG}(\mu_0) = \left[1 + \frac{\beta_1}{\beta_0}\,\frac{\alpha_S(\mu) - \alpha_S(\mu_0)}{4\pi} + \dots\right] c_{GG}(\mu_0)\,. \tag{3.95}$$

We write the perturbative expansions of the β-function in the form

$$\frac{\beta(\alpha_S)}{\alpha_S^2} = -\frac{1}{2\pi}\left(\beta_0 + \beta_1\,\frac{\alpha_S}{4\pi} + \dots\right), \tag{3.96}$$

where $\beta_1 = \frac{34}{3}\,C_A^2 - \frac{10}{3}\,C_A n_f - 2C_F n_f$. For the CP-odd coefficient $\tilde{c}_{GG}(\mu)$ no exact solution is available. At next-to-leading order (NLO), one obtains

$$\tilde{c}_{GG}(\mu) = \left[1 + \frac{(\gamma_J^s)_1}{\beta_0}\,\frac{\alpha_S(\mu) - \alpha_S(\mu_0)}{4\pi} + \dots\right] \tilde{c}_{GG}(\mu_0)\,. \tag{3.97}$$

Here $(\gamma_J^s)_1 = -6C_F n_f$ is the two-loop coefficient in the anomalous dimension of the flavour-singlet axial-vector current [205].
Starting at NLO, there is a non-trivial mixing of the Wilson coefficients c_{GG}, $\tilde{c}_{GG}$ and $\hat{\boldsymbol{Y}}_q$ under renormalisation, caused by the diagram shown in Figure 3.4. For the CP-even, flavour-diagonal coefficients, this effect was first studied in [206]. Including also flavour non-diagonal couplings and CP-odd coefficients, we find that the mixing is governed by the RG equation

$$\mu\,\frac{d}{d\mu}\,\hat{\boldsymbol{Y}}_q(\mu) = \gamma^y(\mu)\,\hat{\boldsymbol{Y}}_q(\mu) + \gamma^{qg}(\mu)\,\left[c_{GG}(\mu) - i\tilde{c}_{GG}(\mu)\right]\boldsymbol{Y}_q(\mu)\,, \tag{3.98}$$

where γ^y is the anomalous dimension of the SM Yukawa couplings, while γ^{qg} accounts for the mixing effects. The perturbative expansions of these objects read

$$\gamma^y(\alpha_S) = \gamma_0^y\,\frac{\alpha_S}{4\pi} + \gamma_1^y\left(\frac{\alpha_S}{4\pi}\right)^2 + \dots\,, \qquad \gamma^{qg}(\alpha_S) = \gamma_1^{qg}\left(\frac{\alpha_S}{4\pi}\right)^2 + \dots\,, \tag{3.99}$$

where $\gamma_0^y = -6C_F$, $\gamma_1^y = -3C_F^2 - \frac{97}{3}\,C_F C_A + \frac{20}{3}\,C_F T_F n_f$ [207], and $\gamma_1^{qg} = -24C_F$. At

NLO, the solution to the RG equation (3.98) takes the form

$$\hat{\boldsymbol{Y}}_q(\mu) = U_y(\mu,\mu_0)\left[\hat{\boldsymbol{Y}}_q(\mu_0) - \frac{\gamma_1^{qg}}{2\beta_0}\,\frac{\alpha_S(\mu)-\alpha_S(\mu_0)}{4\pi}\Big(c_{GG}(\mu_0) - i\tilde{c}_{GG}(\mu_0)\Big)\,\boldsymbol{Y}_q(\mu_0)\right], \tag{3.100}$$

where

$$U_y(\mu,\mu_0) = \left(\frac{\alpha_S(\mu)}{\alpha_S(\mu_0)}\right)^{-\frac{\gamma_0^y}{2\beta_0}}\left[1 - \frac{\gamma_1^y\beta_0 - \beta_1\gamma_0^y}{2\beta_0^2}\,\frac{\alpha_S(\mu)-\alpha_S(\mu_0)}{4\pi} + \dots\right]. \tag{3.101}$$

Relations (3.95), (3.97) and (3.100) describe the scale dependence of the Wilson coefficients between the NP scale $\mu_0 \sim M$ and the scale $\mu \sim M_S$.

3.6.3 Matching to SCET$_{\text{BSM}}$ at the Scale $\mu \sim M_S$

At the scale $\mu \sim M_S$, the effective Lagrangian (3.91) is matched onto the SCET$_{\text{BSM}}$ Lagrangians discussed in Section 3.3 and 3.4. The leading contributions arise from the operators of dimension up to five. They originate from the $D = 5$ operators contained in (3.92), or from the $D = 3$ Higgs-portal interaction $S\,\phi^\dagger\phi$ in combination with a $D = 6$ interaction from the effective Lagrangian $\mathcal{L}_{\text{SMEFT}}$. We will now derive the corresponding matching conditions at tree level. In this approximation, time-ordered products of $S\,\phi^\dagger\phi$ with operators of the SMEFT Lagrangian in the basis of [57] do not give rise to non-zero matching contributions.

Matching Coefficients at $\mathcal{O}(\lambda^2)$

We begin with the Wilson coefficients of the $\mathcal{O}(\lambda^2)$ SCET$_{\text{BSM}}$ operators in the effective Lagrangian (3.21), for which we obtain

$$\begin{aligned}
C_{\phi\phi}(M_S,M,\mu) &= -\lambda_1\,, \\
C_{GG}(M_S,M,\mu) &= -\frac{M_S^2}{M^2}\,\frac{c_{GG}}{8\pi^2}\,, & \widetilde{C}_{GG}(M_S,M,\mu) &= \frac{M_S^2}{M^2}\,\frac{\tilde{c}_{GG}}{8\pi^2}\,, \\
C_{WW}(M_S,M,\mu) &= -\frac{M_S^2}{M^2}\,\frac{c_{WW}}{8\pi^2}\,, & \widetilde{C}_{WW}(M_S,M,\mu) &= \frac{M_S^2}{M^2}\,\frac{\tilde{c}_{WW}}{8\pi^2}\,, \\
C_{BB}(M_S,M,\mu) &= -\frac{M_S^2}{M^2}\,\frac{c_{BB}}{8\pi^2}\,, & \widetilde{C}_{BB}(M_S,M,\mu) &= \frac{M_S^2}{M^2}\,\frac{\tilde{c}_{BB}}{8\pi^2}\,.
\end{aligned} \tag{3.102}$$

All scale-dependent quantities are evaluated at the matching scale $\mu \sim M_S$.

Matching Coefficients at $\mathcal{O}(\lambda^3)$

The matching conditions for the Wilson coefficients of the two-body $\mathcal{O}(\lambda^3)$ SCET$_{\text{BSM}}$ operators in the effective Lagrangian (3.35) follow by evaluating the tree-level Feynman

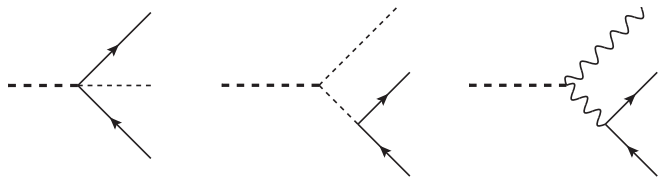

Figure 3.5: Diagrams contributing to the tree-level matching conditions for the Wilson coefficients of $\mathcal{O}(\lambda^3)$ operators. The first two graphs contribute the two terms in (3.103) and (3.106), while the third diagram generates the coefficients in (3.105) and (3.107).

diagrams shown in Figure 3.5. We write the results in terms of matrices in generation space. For the coefficients of the mixed-chirality operators, we obtain (with $f = u, d, e$)

$$\begin{aligned} \boldsymbol{C}_{F_L \bar{f}_R}(M_S, M, \mu) &= -\hat{\boldsymbol{Y}}_f - \frac{M^2 \lambda_1}{M_S^2}\, \boldsymbol{Y}_f \,, \\ \boldsymbol{C}^{(i)}_{F_L \bar{f}_R \phi}(u, M_S, M, \mu) &= -\hat{\boldsymbol{Y}}_f - \frac{M^2 \lambda_1}{(1-u) M_S^2}\, \boldsymbol{Y}_f \,; \quad i = 1, 2 \,. \end{aligned} \tag{3.103}$$

The matrices $\boldsymbol{Y}_f$ refer to the original Yukawa matrices of the SM. Several of the coefficients of the same-chirality operators vanish at tree level, namely

$$\begin{aligned} &\boldsymbol{C}_{L_L \bar{L}_L G}(u, M_S, M, \mu) = \boldsymbol{C}_{\ell_R \bar{\ell}_R G}(u, M_S, M, \mu) = \boldsymbol{0} \,, \\ &\boldsymbol{C}_{f_R \bar{f}_R W}(u, M_S, M, \mu) = \boldsymbol{0} \,. \end{aligned} \tag{3.104}$$

For the remaining coefficients, we find

$$\begin{aligned} \boldsymbol{C}_{Q_L \bar{Q}_L G}(u, M_S, M, \mu) &= -\frac{\alpha_S}{2\pi} \frac{u}{1-u} \left(c_{GG} + i\tilde{c}_{GG}\right) \boldsymbol{1} \,, \\ \boldsymbol{C}_{q_R \bar{q}_R G}(u, M_S, M, \mu) &= -\frac{\alpha_S}{2\pi} \frac{u}{1-u} \left(c_{GG} - i\tilde{c}_{GG}\right) \boldsymbol{1} \,, \\ \boldsymbol{C}_{F_L \bar{F}_L W}(u, M_S, M, \mu) &= -\frac{\alpha}{2\pi s_w^2} \frac{u}{1-u} \left(c_{WW} + i\tilde{c}_{WW}\right) \boldsymbol{1} \,, \\ \boldsymbol{C}_{F_L \bar{F}_L B}(u, M_S, M, \mu) &= -\frac{Y_{F_L} \alpha}{2\pi c_w^2} \frac{u}{1-u} \left(c_{BB} + i\tilde{c}_{BB}\right) \boldsymbol{1} \,, \\ \boldsymbol{C}_{f_R \bar{f}_R B}(u, M_S, M, \mu) &= -\frac{Y_{f_R} \alpha}{2\pi c_w^2} \frac{u}{1-u} \left(c_{BB} - i\tilde{c}_{BB}\right) \boldsymbol{1} \,, \end{aligned} \tag{3.105}$$

where Y_{F_L} and Y_{f_R} in the last two relations refer to the hypercharges of the fermions. Note that at tree level these coefficients are diagonal in flavour space. Once again, all scale-dependent quantities are evaluated at the matching scale $\mu \sim M_S$.
The matching conditions for the $\mathcal{O}(\lambda^3)$ operators governing three-body decays of the resonance S are given by similar expressions. In analogy with (3.103), we find

$$\boldsymbol{D}_{F_L \bar{f}_R \phi}(\{m_{kl}^2\}, M, \mu) = -\hat{\boldsymbol{Y}}_f - \frac{M^2 \lambda_1}{m_{12}^2}\, \boldsymbol{Y}_f \,. \tag{3.106}$$

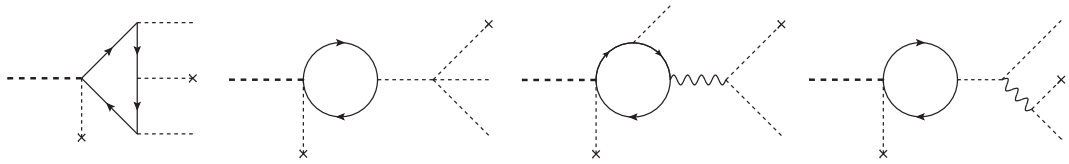

Figure 3.6: Representative one-loop diagrams contributing to the matching condition for the Wilson coefficients $\widetilde{C}_{\phi\phi\phi\phi}$ in (3.110). Dashed lines with a cross denote zero-momentum insertions of the scalar field φ_0^0. In the first and third graph one must sum over all possible attachments of the scalar lines on the fermion loop.

The coefficients $\boldsymbol{D}_{F_L\bar{F}_LA}$ and $\boldsymbol{D}_{f_R\bar{f}_RA}$ are given by expressions analogous to those in (3.105), with the replacement $u/(1-u) \to (M_S^2 - m_{12}^2)/m_{12}^2$; for example, we find

$$\boldsymbol{D}_{Q_L\bar{Q}_LG}(\{m_{kl}^2\}, M, \mu) = -\frac{\alpha_S}{2\pi}\,\frac{M_S^2 - m_{12}^2}{m_{12}^2}\,(c_{GG} + i\tilde{c}_{GG})\,\mathbf{1}\,. \tag{3.107}$$

Note that, as anticipated in Section 3.4, these results only depend on the invariant mass m_{12} of the fermion pair.
The explicit expressions for the Wilson coefficients in (3.103) and (3.105) confirm our general arguments presented in Section 3.5.2. The coefficients contain poles at $u = 1$, whose residues are determined in terms of the Wilson coefficients of the $\mathcal{O}(\lambda^2)$ operators given in (3.102).

Matching Coefficient $\widetilde{C}_{\phi\phi\phi\phi}$ at $\mathcal{O}(\lambda^4)$

The coefficient $\widetilde{C}_{\phi\phi\phi\phi}$ in the effective Lagrangian (3.50) receives matching contributions starting at one-loop order. Writing the scalar doublets in the form

$$\Phi_{n_i} = W_{n_i}^\dagger \begin{pmatrix} -i\varphi_{n_i}^+ \\ \frac{1}{\sqrt{2}}\left(\varphi_{n_i}^0 + i\varphi_{n_i}^3\right) \end{pmatrix}, \qquad \Phi_0 = \frac{1}{\sqrt{2}} \begin{pmatrix} 0 \\ \varphi_0^0 \end{pmatrix}, \tag{3.108}$$

where φ_0^0 denotes a zero-momentum boson, we find that

$$\mathcal{L}_{\text{eff}}^{(4)} \ni \frac{\widetilde{C}_{\phi\phi\phi\phi}(M_S, M, \mu)}{M}\, S \left(\varphi_0^0\right)^2 \left(\varphi_{n_1}^3 \varphi_{n_2}^0 + \varphi_{n_2}^3 \varphi_{n_1}^0\right) + \ldots, \tag{3.109}$$

where the dots represent contributions involving more than five fields. In order to determine $\widetilde{C}_{\phi\phi\phi\phi}$, we compute the four-particle decay amplitude $S \to \varphi^3(k_1)\,\varphi^0(k_2)\,\varphi^0(0)\,\varphi^0(0)$ with two zero-momentum particles in the final state, in both the full theory – defined by the Lagrangian (3.92) – and the effective theory. Treating all particles other than S as massless and performing the matching calculation with on-shell external states, all loop graphs in the effective theory are scaleless and hence vanish. In the full theory, the

one-loop diagrams shown in Figure 3.6 give rise to non-zero results. All other diagrams are scaleless. Note that the evaluation of the two graphs involving the B^μ and W_3^μ gauge bosons requires a regulator in order to avoid that the gauge-boson propagator becomes singular. We introduce an infinitesimal momentum q to the "zero-momentum" φ^0 boson coupling to the vector boson and take the limit $q \to 0$ after summing up all diagrams. In that way, we find in the $\overline{\text{MS}}$ subtraction scheme

$$\widetilde{C}_{\phi\phi\phi\phi}(M_S, M, \mu) = -\sum_{f=u,d,e} \frac{N_c^f T_3^{f_L}}{16\pi^2} \Bigg[\operatorname{Im}\operatorname{Tr}(\hat{\boldsymbol{Y}}_f \boldsymbol{Y}_f^\dagger \boldsymbol{Y}_f \boldsymbol{Y}_f^\dagger) \left(L^2 - 2i\pi L - \frac{7\pi^2}{6} \right) - \operatorname{Im}\operatorname{Tr}(\hat{\boldsymbol{Y}}_f \boldsymbol{Y}_f^\dagger) \left(4\lambda + \frac{e^2}{2 s_w^2 c_w^2} \right) (L - i\pi - 2) \Bigg] , \tag{3.110}$$

where λ denotes the quartic scalar coupling of the SM (not to be confused with our SCET expansion parameter), $T_3^{f_L}$ denotes the weak isospin of the left-handed fermions, and $L = \ln(M_S^2/\mu^2)$. The complex matrices $\hat{\boldsymbol{Y}}_f$ have been defined in (3.92), while $\boldsymbol{Y}_f$ are the Yukawa matrices of the SM. A simple result for the traces can be obtained by transforming the Yukawa matrices to the mass basis and defining $\left(\boldsymbol{U}_f^\dagger \hat{\boldsymbol{Y}}_f \boldsymbol{W}_f\right)_{ii} \equiv y_{f_i}(c_{f_i} + i\tilde{c}_{f_i})$, where y_{f_i} is the SM Yukawa coupling of the fermion f_i. This leads to

$$\widetilde{C}_{\phi\phi\phi\phi}(M_S, M, \mu) = -\sum_{f=u,d,e} \frac{N_c^f T_3^{f_L}}{16\pi^2} \sum_{i=1,2,3} \tilde{c}_{f_i} \Bigg[y_{f_i}^4 \left(L^2 - 2i\pi L - \frac{7\pi^2}{6} \right) - y_{f_i}^2 \left(4\lambda + \frac{e^2}{2 s_w^2 c_w^2} \right) (L - i\pi - 2) \Bigg] . \tag{3.111}$$

The dominant contribution is likely to arise from the top quark.
In [166], it was shown that a tree-level contribution to $\widetilde{C}_{\phi\phi\phi\phi}$ arises first from a dimension-seven operator in the effective Lagrangian obtained by integrating out the NP scale M, shown in (3.93). We find that the corresponding matching contribution reads

$$\delta\widetilde{C}_{\phi\phi\phi\phi} = -\frac{M_S^2}{2M^2}\, C_7 , \tag{3.112}$$

where C_7 itself is most likely suppressed by a loop factor. This contribution is parametrically suppressed compared with that in (3.110) by a factor $M_S^2/M^2 \ll 1$.

3.7 Conclusions

We have developed a theoretical framework to construct a consistent EFT for the on-shell decays into light SM particles of the first new heavy resonance beyond the SM that will be discovered at the LHC or elsewhere. Our approach is flexible enough to retain the full dependence on the mass M_S of the new resonance S and on the masses of other, yet undiscovered particles. It can thus deal with the important situation where the first

particle to be discovered is a member of a new sector characterised by a mass scale M. It provides a consistent separation between the electroweak scale $v \approx 246\,\text{GeV}$ and the NP scales M_S and M, irrespective of whether $M_S \sim M$ are of similar magnitude or if there is a double hierarchy $v \ll M_S \ll M$. Large double and single logarithms of scale ratios can be resummed to all orders in perturbation theory by solving RG evolution equations in the effective theory.

Our effective theory SCET_{BSM} is a variant of SCET, in which the effective Lagrangian is constructed out of gauge-invariant collinear building blocks for the particles of the SM along with a field representing the new heavy resonance S. We have worked out in detail the case where S is a spin-0 boson that is a singlet with respect to the SM gauge interactions. We have constructed the most general effective Lagrangian at leading, subleading, and partially subsubleading order in the expansion in $\lambda = v/M_S$. It describes all two-body decays of S into SM particles. We have also constructed the leading-order effective Lagrangian describing three-body decays of S. We have calculated the anomalous dimensions of the operators in the effective Lagrangian and derived the RG evolution equations for their Wilson coefficients. For the operators arising at next-to-leading order in λ several subtleties arise. These operators mix under renormalisation, and their anomalous dimensions are distribution-valued functions depending on the momentum fractions carried by different collinear field operators. The evolution equations involve a new cusp anomalous dimension originating from the exchange of an ultra-soft quark between two collinear sectors. There has recently been an increasing interest in applications of SCET beyond the leading power in λ [197, 208–216]. The results obtained in this paper are an important contribution to this rapidly developing field.

There are several extensions and refinements of our approach which are worth pursuing. The matrix elements of the SCET_{BSM} operators, which we have computed at tree level, should be calculated to one-loop order. These matrix elements contain large rapidity logarithms of the scale ratio M_S/v from the collinear anomaly, despite the fact that the hard scale M_S has been integrated out from the low-energy effective theory. Understanding the structure of these logarithms and showing that they do not spoil factorisation is an important ingredient of our approach. It will be important to complete the calculation of the one-loop anomalous dimensions of the two-jet operators arising at $\mathcal{O}(\lambda^3)$ in the SCET_{BSM} Lagrangian, which we have presented in Section 3.5.2, by including the contributions from electroweak and Yukawa interactions. Perhaps more importantly, the two-loop contribution to the cusp anomalous dimension $\gamma_{\text{cusp}}^{q\bar{q}}$ in (3.83) should be calculated. This quantity is associated with the exchange of an ultra-soft quark between two collinear fields moving along different directions. It is a crucial new ingredient for a consistent Sudakov resummation at subleading power in SCET. Finally, it would be interesting to provide a complete classification of the operators arising at $\mathcal{O}(\lambda^4)$ in the SCET_{BSM} Lagrangian, whose structure we have only sketched in Section 3.3.3.

Our work can be generalised in several ways. In particular, it would be interesting to extend it to other cases of new heavy resonances, which are well motivated theoretically. This includes various heavy leptoquarks or Z' bosons, which have been proposed to address some present anomalies in rare and semileptonic decays of B mesons [217–222]

(see [223] for a recent review). It also applies to heavy particles that can serve as mediators to the dark sector, generalising the hybrid EFT framework recently proposed in [224]. Finally, it would be interesting to calculate the Wilson coefficients in the SCET_{BSM} Lagrangian in some concrete NP models. Specifically, in future work we plan to illustrate our results in the context of an extension of the SM containing heavy, vector-like fermions. As our community eagerly awaits the discovery of new heavy particles, we have developed here a general EFT approach that allows one to describe the decays of such particles into SM particles in a model-independent way, systematically separating the NP scales from the scales of the SM, accounting for the full complexity of the (partially unknown) UV completion via Wilson coefficient functions and providing a framework for the resummation of large logarithms to all orders in perturbation theory.

Acknowledgments

The research of M.N. is supported by the Cluster of Excellence *Precision Physics, Fundamental Interactions and Structure of Matter* (PRISMA–EXC 1098) and grant 05H12UME of the German Federal Ministry for Education and Research (BMBF). S.A. gratefully acknowledges support from the DFG Research Training Group *Symmetry Breaking in Fundamental Interactions* (GRK 1581). The work of M.K. is supported by the Swiss National Science Foundation (SNF) under contract 200021-175940.

3.8 Appendix: Derivation of the Evolution Equation (3.82)

Effective Lagrangian of SCET

The leading-order SCET Lagrangian describing a massless, n-collinear fermion (of any chirality)

$$\xi_n(x) = \frac{\not{n}\bar{\not{n}}}{4}\,\psi(x) \tag{3.113}$$

interacting with a (abelian or non-abelian) gauge field A^μ reads [39, 42]

$$\mathcal{L}^{(0)}_{\xi,n}(x) = \bar{\xi}_n(x)\,\frac{\bar{\not{n}}}{2}\left(in\cdot D + i\not{D}_{\perp c}\,\frac{1}{i\bar{n}\cdot D_c}\,i\not{D}_{\perp c}\right)\xi_n(x) + \dots\,, \tag{3.114}$$

where the dots represent the effective Yang-Mills Lagrangian and gauge-fixing terms. The covariant collinear derivative is defined as

$$iD^\mu_c = i\partial^\mu + g_A\,A^\mu_n(x)\,, \tag{3.115}$$

where g_A denotes the relevant gauge coupling. The covariant derivative without a subscript "c" is defined as

$$in\cdot D = in\cdot\partial + g_A\,n\cdot A_n(x) + g_A\,n\cdot A_{us}(x_-)\,. \tag{3.116}$$

It includes the ultra-soft gauge field $n\cdot A_{us}$ in addition to the small component of the collinear gauge field $n\cdot A_n$, both of which have the same power counting ($\sim\lambda^2$). Note

that the ultra-soft gauge field is multipole-expanded and lives at position $x_- \equiv \frac{n}{2}\,\bar{n}\cdot x$. This ensures that only the relevant components $n\cdot p_{us}$ of ultra-soft momenta, which can compete with the corresponding small components $n\cdot p_n$ of collinear momenta, enter in the computation of Feynman diagrams. The Feynman rules of SCET follow from the Lagrangian (3.114) in the usual way.
At subleading order in the expansion in powers of λ new interaction vertices arise. The terms of $\mathcal{O}(\lambda)$ and $\mathcal{O}(\lambda^2)$ have been constructed in [42]. Of particular importance to our discussion below is the coupling of a collinear fermion to an ultra-soft fermion q_{us}, which enters at first order in λ. The relevant effective Lagrangian reads

$$\mathcal{L}^{(1)}_{\xi q,n} = \bar{\xi}_n(x)\, i\not{D}_{\perp c}\, W_n(x)\, q_{us}(x_-) + \text{h.c.}\,, \tag{3.117}$$

where W_n is the collinear Wilson line introduced in (3.5), and the ultra-soft quark field has power counting $q_{us}\sim\lambda^3$. The Lagrangians (3.114) and (3.117) can be written for any collinear sector of the theory.

Endpoint Singularities in Collinear Contributions

For NP models in which the Wilson coefficients of the leading SCET_{BSM} operators in (3.21) are non-zero, one can show on general grounds that the Wilson coefficients $\boldsymbol{C}^{(i)}_{F_L\bar{f}_R\,\phi}(u,\mu)$, $\boldsymbol{C}_{F_L\bar{F}_L A}(u,\mu)$, and $\boldsymbol{C}_{f_R\bar{f}_R A}(u,\mu)$ are singular in the limit $u\to 1$. The origin of these singularities can be understood as follows. When integrating out some heavy degrees of freedom generates the operators in (3.22), the same UV physics will also generate corresponding vertices in which one of the two outgoing collinear lines is replaced by a line carrying a hard momentum. Consider, for example, the vertex shown on the left-hand side in Figure 3.7 (a corresponding graph exists with n_1 and n_2 interchanged). If we denote the momentum of the n_1-collinear gluon by $k_1 = uP_1$, then the hard gluon carries momentum $k_2 = P_2 + (1-u)P_1$. The vertex function can then be written in the form

$$M\left[C_{GG}(u,M_S,M,\mu)\, g^{\perp}_{\alpha\beta} + \widetilde{C}_{GG}(u,M_S,M,\mu)\,\epsilon^{\perp}_{\alpha\beta}\right] g_S^2\,\delta_{ab}\,, \tag{3.118}$$

where the dependence on u enters through the invariants $2k_1\cdot k_2 = uM_S^2$ and $k_2^2 = (1-u)M_S^2$. Clearly, for $u\to 1$ we recover

$$\lim_{u\to 1} C_{GG}(u,M_S,M,\mu) = C_{GG}(M_S,M,\mu)\,, \tag{3.119}$$

and likewise for $\widetilde{C}_{GG}$, where C_{GG} and $\widetilde{C}_{GG}$ are the coefficients in the effective Lagrangian (3.21).[10] Consider now the diagram shown on the right-hand side in Figure 3.7, which yields the following hard matching contributions to the Wilson coefficients (omitting some

[10] Beyond tree level this relation is more complicated. The coefficient on the left-hand side can contain hard loop corrections $\sim(\mu^2/k_2^2)^{n\epsilon}$, which are absent in the coefficient on the right-hand side.

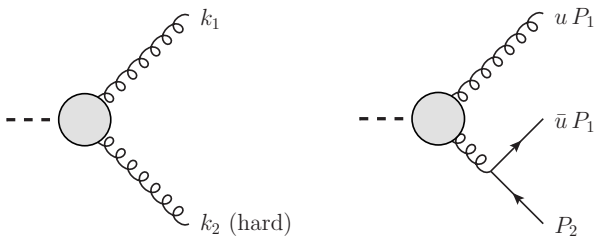

Figure 3.7: Vertex function connecting S with a collinear gluon and a hard gluon (left), and the corresponding hard matching contribution to the Wilson coefficients in (3.120) (right).

arguments):

$$\begin{aligned}\Delta\boldsymbol{C}_{Q_L\bar{Q}_LG}(u,\mu) &= \frac{M^2}{M_S^2}\,\frac{g_S^2(\mu)}{1-u}\left[C_{GG}(u,\mu) - i\widetilde{C}_{GG}(u,\mu)\right],\\ \Delta\boldsymbol{C}_{q_R\bar{q}_RG}(u,\mu) &= \frac{M^2}{M_S^2}\,\frac{g_S^2(\mu)}{1-u}\left[C_{GG}(u,\mu) + i\widetilde{C}_{GG}(u,\mu)\right].\end{aligned} \tag{3.120}$$

This produces poles at $u=1$, whose residues are given in terms of the coefficients C_{GG} and $\widetilde{C}_{GG}$ in the effective Lagrangian (3.21). At first sight, these give rise to endpoint-divergent integrals $\int_0^1 dw\,\frac{1}{1-w}$ when inserted into (3.80).
To see how these integrals are cured, we need to look at the relevant operator mixing contribution in more detail. Consider the one-loop contributions to the $S\to q_L^i(k_1)\bar{q}_R^j(k_2)\phi^*$ decay amplitude, where the scalar field carries zero momentum. We include multiplicative radiative corrections to the matrix element of the operator $O^{ij}_{Q_L\bar{q}_R}$ as well as the mixing contribution shown by the first diagram in Figure 3.3. Before renormalisation, i.e. written in terms of bare Wilson coefficients, we find

$$\begin{aligned}\mathcal{M}(S\to q_L^i\bar{q}_R^j\phi^*) = \frac{1}{M}\,&\Big\langle q_L^i\bar{q}_R^j\phi^*|O^{ij}_{Q_L\bar{q}_R}|S\Big\rangle_{\text{tree}}\\ &\times\left[Z^{-1}_{Q_L\bar{q}_R}\,C^{ij}_{Q_L\bar{q}_R} - \int_0^1 dw\,N_\epsilon(w)\left(\frac{\mu^2}{-k_1^2}\right)^{\epsilon} Y_q^{ik}\,C^{kj}_{q_R\bar{q}_RG}(w)\right.\\ &\left.- \int_0^1 dw\,N_\epsilon(w)\left(\frac{\mu^2}{-k_2^2}\right)^{\epsilon}\left(C^{\dagger}_{Q_L\bar{Q}_LG}(w)\right)^{ik} Y_q^{kj}\right],\end{aligned} \tag{3.121}$$

where (here and below we omit the "$-i0$" regulator in the arguments of the logarithms)

$$\begin{aligned}Z^{-1}_{Q_L\bar{q}_R} &= 1 + \frac{C_F\alpha_S}{\pi}\left[\frac{1}{2\epsilon^2} + \frac{1}{2\epsilon}\left(\ln\frac{\mu^2}{-M_S^2} + \frac{3}{2}\right)\right],\\ N_\epsilon(w) &= e^{\epsilon\gamma_E}\,\frac{C_F\alpha_S}{2\pi}\,(1-\epsilon)\,\Gamma(\epsilon)\,\big(w(1-w)\big)^{-\epsilon}.\end{aligned} \tag{3.122}$$

Naively expanding $N_\epsilon(w)$ as $N_\epsilon(w) = C_F\alpha_S/(2\pi\epsilon) +$"finite terms" reproduces the mixing terms shown in (3.80). However, in the presence of the poles at $u = 1$ in (3.120), such an expansion does not capture all the $1/\epsilon$ singularities. Let us split up the Wilson coefficients in two terms, such that

$$C^{ij}_{q_R\bar{q}_R G}(w) = \frac{M^2}{M_S^2}\,\frac{g_S^2}{1-w}\left(C_{GG} + i\widetilde{C}_{GG}\right)\delta^{ij} + \bar{C}^{ij}_{q_R\bar{q}_R G}(w)\,, \tag{3.123}$$

and similarly for $C^\dagger_{Q_L\bar{Q}_L G}(w)$. The subtracted coefficients $\bar{C}^{ij}_{q_R\bar{q}_R G}(w)$ and $\bar{C}^{ij}_{Q_L\bar{Q}_L G}(w)$ are integrable at $w = 1$. We then obtain from (3.121)

$$\begin{aligned}\mathcal{M}(S \to q_L^i \bar{q}_R^j \phi^*) = \frac{1}{M}\Bigg[& Z^{-1}_{Q_L\bar{q}_R}\, C^{ij}_{Q_L\bar{q}_R} \\ & - \frac{C_F\alpha_S}{2\pi\epsilon}\int_0^1 dw\left[Y_q^{ik}\,\bar{C}^{kj}_{q_R\bar{q}_R G}(w) + \left(\bar{C}^\dagger_{Q_L\bar{Q}_L G}(w)\right)^{ik} Y_q^{kj}\right] \\ & - \frac{C_F\alpha_S}{2\pi}\, e^{\epsilon\gamma_E}\,\Gamma(\epsilon)\,\frac{\Gamma(2-\epsilon)\,\Gamma(-\epsilon)}{\Gamma(1-2\epsilon)}\left[\left(\frac{\mu^2}{-k_1^2}\right)^\epsilon + \left(\frac{\mu^2}{-k_2^2}\right)^\epsilon\right] \\ & \times \frac{g_S^2 M^2}{M_S^2}\left(C_{GG} + i\widetilde{C}_{GG}\right) Y_q^{ij}\Bigg]\left\langle q_L^i \bar{q}_R^j \phi^* | O^{ij}_{Q_L\bar{q}_R} | S\right\rangle_{\text{tree}}.\end{aligned} \tag{3.124}$$

It follows that, in the $\overline{\text{MS}}$ subtraction scheme, the bare Wilson coefficient $C^{ij}_{Q_L\bar{q}_R}$ receives the counterterms

$$\begin{aligned}C^{ij}_{Q_L\bar{q}_R}\big|_{\text{ren}} = Z^{-1}_{Q_L\bar{q}_R}\, C^{ij}_{Q_L\bar{q}_R} & - \frac{C_F\alpha_S}{2\pi\epsilon}\int_0^1 dw\left[Y_q^{ik}\,\bar{C}^{kj}_{q_R\bar{q}_R G}(w) + \left(\bar{C}^\dagger_{Q_L\bar{Q}_L G}(w)\right)^{ik} Y_q^{kj}\right] \\ & + \frac{C_F\alpha_S}{2\pi}\left[\frac{2}{\epsilon^2} + \frac{1}{\epsilon}\left(\ln\frac{\mu^2}{-k_1^2} + \ln\frac{\mu^2}{-k_2^2} - 2\right)\right]\frac{g_S^2 M^2}{M_S^2}\left(C_{GG} + i\widetilde{C}_{GG}\right) Y_q^{ij}.\end{aligned} \tag{3.125}$$

The endpoint singularities are regularised in this expression and give rise to the double poles in $1/\epsilon$; however, the appearance of the collinear logarithms is worrisome, as it would indicate a sensitivity of the associated anomalous dimension to infrared scales.

Contribution From the Exchange of an Ultra-Soft Quark

This dependence is cancelled by the contribution from a loop diagram involving the exchange of an ultra-soft quark between the two collinear sectors, shown on the right-hand side in Figure 3.3. In this graph the Sgg vertex descents from the $\mathcal{O}(\lambda^2)$ effective Lagrangian (3.21). It is combined with two insertions of the subleading SCET Lagrangian (3.117), which couples a collinear fermion to a collinear gauge field and an ultra-soft quark. More accurately, the diagram arises from the subleading-power operator

$$T\left\{O_{GG}(x), i\int d^4y\,\mathcal{L}^{(1)}_{\xi q,n_1}(y), i\int d^4z\,\mathcal{L}^{(1)}_{\xi q,n_2}(z), i\int d^4w\,\mathcal{L}^{(-1)}_{\bar{q}\Phi q}(w)\right\}, \tag{3.126}$$

and similarly with $\widetilde{O}_{GG}$ instead of O_{GG}. The Lagrangian

$$\mathcal{L}^{(-1)}_{\bar{q}\Phi q} = -\left(\bar{q}_{us,L}\,\boldsymbol{Y}_q\,\Phi_0\,q_{us,R} + \text{h.c.}\right) \tag{3.127}$$

describes the coupling of ultra-soft quarks to the zero-momentum scalar field Φ_0. With $q_{us} \sim \lambda^3$ and $\Phi_0 \sim \lambda$, and taking into account that the ultra-soft measure scales as $d^4x_{us} \sim \lambda^{-8}$, it follows that this Lagrangian contributes terms of $\mathcal{O}(\lambda^{-1})$ to the action. This lifts the operator in (3.126) from the naive expectation $\mathcal{O}(\lambda^4)$ to $\mathcal{O}(\lambda^3)$.[11]
Evaluating the contribution of the operator (3.126) to the matrix element in (3.121), we obtain an extra contribution inside the bracket on the right-hand side of (3.124), which reads

$$-\frac{C_F\alpha_S}{2\pi}\,e^{\epsilon\gamma_E}\,(1-\epsilon)\,\Gamma(\epsilon)\,\frac{\pi}{\sin\pi\epsilon}\left(\frac{\mu^2(-M_S^2)}{(-k_1^2)(-k_2^2)}\right)^{\epsilon}\frac{g_S^2M^2}{M_S^2}\left(C_{GG}+i\widetilde{C}_{GG}\right)Y_q^{ij}\,. \tag{3.128}$$

This term has the effect of removing the collinear logarithms in expression (3.125) and replacing them by a logarithm of the hard scale. We thus obtain the final result

$$\begin{aligned} C^{ij}_{Q_L\bar{q}_R}\big|_{\text{ren}} = Z^{-1}_{Q_L\bar{q}_R}\,C^{ij}_{Q_L\bar{q}_R} &- \frac{C_F\alpha_S}{2\pi\epsilon}\int_0^1 dw\left[Y_q^{ik}\,\bar{C}^{kj}_{q_R\bar{q}_RG}(w) + \left(\bar{C}^{\dagger}_{Q_L\bar{Q}_LG}(w)\right)^{ik}Y_q^{kj}\right] \\ &+ \frac{C_F\alpha_S}{2\pi}\left[\frac{1}{\epsilon^2}+\frac{1}{\epsilon}\left(\ln\frac{\mu^2}{-M_S^2}-1\right)\right]\frac{g_S^2M^2}{M_S^2}\left(C_{GG}+i\widetilde{C}_{GG}\right)Y_q^{ij} \end{aligned} \tag{3.129}$$

for the counterterms. From this expression, it is straightforward to derive the RG evolution equation (3.82).

[11] One might worry that multiple insertions of the Lagrangian (3.127) can promote the operator to even lower order in λ. However, graphs with such multiple insertions do not produce UV poles and are scaleless when evaluated on shell. If we would introduce soft mass-mode fields instead of ultra-soft fields, then the coupling of the soft quark to the scalar doublet is a leading-power interaction, while the coupling of a soft quarks to a collinear quark and gluon in (3.117) appears at $\mathcal{O}(\lambda^{1/2})$. Also in this case the operator (3.126) is of $\mathcal{O}(\lambda^3)$.

4 Effective Theory for a Heavy Scalar Coupled to the SM via Vector-Like Quarks

4.1 Introduction

Following the discovery of a new particle with a mass far above the electroweak scale $v \approx 246\,\text{GeV}$, a program for studying its couplings to the SM would be of highest priority. In the likely situation where the new resonance is the first member of a richer sector of NP, the appropriate way to study its decay and production processes must rely on an EFT framework. The main reason is that other, yet undiscovered heavy particles can couple to both the SM and the new resonance S and hence affect its interactions. Secondly, the large scale hierarchy between the mass of the heavy resonance and the weak scale, which (roughly) sets the masses of the SM particles, introduces large Sudakov double logarithms in the calculation of decay rates and production cross sections, which must be resummed to all orders of perturbation theory. Finally, for the most interesting case where the mass of the new resonance is close to the masses M_i of yet undiscovered states, there is short-distance physics associated with both scales, which must be disentangled from the longer-distance physics associated with the electroweak scale.

We have shown in [1] that the appropriate EFT to deal with this scenario must be based on an effective Lagrangian built out of non-local light-ray operators defined in SCET [39–42]. Our theory called SCET_{BSM} provides a systematic expansion of the decay amplitudes of the new heavy particle in powers of $\lambda = v/M_S \ll 1$. For the case of a scalar resonance S transforming as a singlet under the SM gauge group, we have constructed the complete operator basis at leading and subleading order in the expansion, corresponding to operators of $\mathcal{O}(\lambda^2)$ and $\mathcal{O}(\lambda^3)$, respectively.

The leading-order effective Lagrangian for two-body decays of S consists of operators in which S is coupled to two effective bosonic fields, which describe so-called collinear particles moving along directions $\boldsymbol{n}_1$ and $\boldsymbol{n}_2$, which point back-to-back in the rest frame of the decaying resonance. One has [1]

$$\mathcal{L}^{(2)}_{\text{eff}} = M\, C_{\phi\phi}(M, M_S)\, O_{\phi\phi} + M \sum_A \Big[C_{AA}(M, M_S)\, O_{AA} + \widetilde{C}_{AA}(M, M_S)\, \widetilde{O}_{AA} \Big] . \tag{4.1}$$

Here M denotes the characteristic mass scale of unresolved new heavy particles. The sum extends over the three gauge groups of the SM: $A = B$ for $\text{U}_Y(1)$, $A = W$ for $\text{SU}_W(2)$,

and $A = G$ for $\mathrm{SU}_c(3)$. The relevant $\mathrm{SCET}_{\mathrm{BSM}}$ operators have the form (a summation over the group index a is understood for non-abelian fields)

$$\begin{aligned} O_{\phi\phi} &= S_v \left(\Phi^\dagger_{n_1} \Phi_{n_2} + \Phi^\dagger_{n_2} \Phi_{n_1}\right), \\ O_{AA} &= S_v \, g^\perp_{\mu\nu} \, \mathcal{A}^{\mu,a}_{n_1} \, \mathcal{A}^{\nu,a}_{n_2}, \\ \widetilde{O}_{AA} &= S_v \, \epsilon^\perp_{\mu\nu} \, \mathcal{A}^{\mu,a}_{n_1} \, \mathcal{A}^{\nu,a}_{n_2}. \end{aligned} \tag{4.2}$$

Here S_v is an effective field for the heavy resonance defined as in heavy-quark effective theory [116, 168, 169, 172], with v denoting its four-velocity. The reference vectors n_1 and n_2 indicate the directions of large momentum flow of the final-state particles. The effective fields consist of so-called "gauge covariant building blocks" [151, 167] Φ and $\mathcal{A}$ containing the Higgs doublet and the transversely polarised gauge fields, respectively, dressed up with Wilson lines in the appropriate representation of the gauge group. The Lorentz indices of the gauge fields can be contracted with either the symmetric tensor $g^\perp_{\mu\nu}$ or the antisymmetric tensor $\epsilon^\perp_{\mu\nu}$ defined in the plane orthogonal to n_1 and n_2. Note that the different fields in the operators in (4.2) interact only via soft quanta, since there is only a single collinear field in each sector; hard interactions with virtualities of order M_S^2 or M^2 are integrated out in the construction of the effective Lagrangian and are contained in the Wilson-coefficient functions.

Note the important fact that the Wilson coefficients in (4.1) depend on both, the mass M_S of the scalar resonance and the parameter M representing the typical mass scale of other, yet undiscovered heavy particles. As we shall see below, in this way our effective theory sums infinite towers of local operators in the conventional EFT approach. In some sense, the Wilson coefficients in our Lagrangian can be regarded as form factors depending on the large momentum transfers $q^2 = \mathcal{O}(M_S^2)$ flowing through Feynman diagrams, which can resolve the small non-localities corresponding to exchanges of the heavy vector-like quarks (VLQs).

At subleading order in power counting the operator basis contains five different types of operators, all of which consist of fermion bilinears along with a Higgs doublet or a gauge field, see Section 4.3. In Section 4.5 we study some aspects of the extension of the effective Lagrangian to $\mathcal{O}(\lambda^4)$, which is necessary to describe the two-body decay $S \to Zh$.

In this work, we illustrate the $\mathrm{SCET}_{\mathrm{BSM}}$ approach by considering a concrete extension of the SM featuring a heavy, gauge-singlet scalar field S along with three generations of heavy VLQs. Vector-like fermions play an important role in models of partial compositeness [225], as realized e.g. in composite-Higgs models (see e.g. [226–228]) and scenarios featuring a warped extra dimension [229–231]. Extensions of the SM featuring both vector-like fermions and a singlet scalar are among the popular simplified models for dark matter (see e.g. [232, 233]).

4.2 High-Energy Extension of the Standard Model

The benchmark model we explore in this paper is an extension of the SM by a real scalar S, transforming as a singlet under the SM gauge group, and (three generations of) a

VLQ doublet Ψ, transforming as $(\mathbf{3},\mathbf{2})_{1/6}$. Besides the Higgs portal, the VLQs mediate the renormalisable interactions between the SM and the new sector. We assume that the mass of the scalar and the masses of the VLQs are both much heavier than the electroweak scale $v \approx 246\,\text{GeV}$. The most general Lagrangian of our model is

$$\begin{aligned}\mathcal{L}_{\text{UV}} = \mathcal{L}_{\text{SM}} &+ \frac{1}{2}(\partial_\mu S)(\partial^\mu S) - \frac{M_S^2}{2}\,S^2 - \frac{\lambda_3}{3!}\,S^3 - \frac{\lambda_4}{4!}\,S^4 \\ &+ \bar\Psi(i\not{D} - \boldsymbol{M})\Psi - (\bar\Psi\tilde\phi\,\boldsymbol{G}_u u_R + \bar\Psi\phi\,\boldsymbol{G}_d d_R + \text{h.c.}) \\ &- \kappa_1 S\,\phi^\dagger\phi - \frac{\kappa_2}{2}\,S^2\phi^\dagger\phi \\ &- S\,\bar\Psi(\boldsymbol{X} - i\gamma_5\tilde{\boldsymbol{X}})\Psi - S\,(\bar\Psi\,\boldsymbol{V}_Q\,Q_L + \text{h.c.})\,.\end{aligned} \tag{4.3}$$

The second line contains the couplings of the VLQs to SM fields, where $\tilde\phi_a = \epsilon_{ab}\phi_b^*$. There is no need to include the gauge-invariant terms $\bar\Psi i\gamma_5\tilde{\boldsymbol{M}}\Psi - (\bar\Psi\,\boldsymbol{G}_Q Q_L + \text{h.c.})$, since they can be removed by unitary transformations of the quark fields. The terms in the third line contain the portal couplings of the heavy scalar to the Higgs field. Note that the couplings κ_1 and λ_3 have mass dimension 1. The interactions in the last line describe the couplings of S to the VLQs and SM quarks. We assume that the parameters λ_i in the scalar potential are chosen such that the scalar field S does not acquire a vacuum expectation value. For the same reason, we have omitted the tadpole term $\lambda_1 S$ from the potential.

Boldface symbols in (4.3) denote matrices in generation space. The matrices $\boldsymbol{G}_{u,d}$ and $\boldsymbol{V}_Q$ are arbitrary complex matrices, while $\boldsymbol{M}$, $\boldsymbol{X}$ and $\tilde{\boldsymbol{X}}$ are hermitian. Without loss of generality we work in the mass basis for the VLQs, where $\boldsymbol{M}$ is a real, positive diagonal matrix. For simplicity, we assume that the three mass eigenvalues are degenerate, i.e. $\boldsymbol{M} = M\,\mathbf{1}$. The common mass of the VLQs is then identified with the "new physics scale" M in (4.1).

Suppose that the heavy scalar S has been discovered, while the VLQs have not yet been observed experimentally. Our goal is to construct an EFT describing the interactions of S with SM particles. The appropriate EFT in such a scenario is the SCET$_{\text{BSM}}$ [1]. It would be straightforward to extend our analysis to the case of vector-like fermions with different quantum numbers. However, in order to keep the presentation as transparent as possible, we find it advantageous to consider the simplest case of a single type of VLQ.

4.3 Tree-level Matching Onto SCET$_{\text{BSM}}$

When the full theory in (4.3) is matched onto the SCET$_{\text{BSM}}$ two types of short-distance modes are integrated out: First, one removes virtual exchanges of the VLQs, which do not appear as external states in the EFT (since these particles are assumed to be yet undiscovered). In addition, one integrates out off-shell fluctuations of the SM fields as well as of the scalar field S carrying virtualities of order $q^2 \sim M_S^2$. While the first step is standard, the second step differentiates the SCET$_{\text{BSM}}$ approach from local EFTs such as the SMEFT [43, 45, 46, 57, 139].

4.3.1 Integrating out the Vector-Like Quarks

At tree level, the heavy VLQs can be integrated out by solving their classical equations of motion. This yields the "non-local effective Lagrangian"

$$\begin{aligned}\mathcal{L}_{\text{eff}} = \mathcal{L}_{\text{SM}} + \frac{1}{2}(\partial_\mu S)(\partial^\mu S) - \frac{M_S^2}{2}\,S^2 - \frac{\lambda_3}{3!}\,S^3 - \frac{\lambda_4}{4!}\,S^4 \\ - \kappa_1 S\,\phi^\dagger\phi - \frac{\kappa_2}{2}S^2\phi^\dagger\phi - \bar{F}\,\frac{1}{i\not{D} - M - S(\boldsymbol{X} - i\gamma_5\tilde{\boldsymbol{X}})}\,F\,,\end{aligned} \tag{4.4}$$

where

$$F = \tilde{\phi}\,\boldsymbol{G}_u u_R + \phi\,\boldsymbol{G}_d d_R + S\,\boldsymbol{V}_Q Q_L\,. \tag{4.5}$$

Note that the heavy scalar field S is still a propagating field at this stage, and indeed the last term in (4.4) contains couplings of SM fields to an arbitrary number of S fields. The terms of zeroth order in S read

$$\mathcal{L}_{\text{eff}}\big|_{S^0} = \mathcal{L}_{\text{SM}} + \bar{F}_0\,\frac{1}{M - i\not{D}}\,F_0\,, \tag{4.6}$$

where $F_0 = \tilde{\phi}\,\boldsymbol{G}_u u_R + \phi\,\boldsymbol{G}_d d_R$. Expanding the denominator in powers of covariant derivatives would generate an infinite set of higher-dimensional, gauge-invariant operators, which account for the virtual effects of heavy VLQs on the interactions among SM particles in the context of the SMEFT.
For our purposes the most relevant terms in (4.4) are those linear in S. They are

$$\begin{aligned}\mathcal{L}_{\text{eff}}\big|_{S^1} = -\kappa_1 S\,\phi^\dagger\phi + \left[S\,\bar{Q}_L\boldsymbol{V}_Q^\dagger\,\frac{1}{M - i\not{D}}\,F_0 + \text{h.c.}\right] \\ - \bar{F}_0\,\frac{1}{M - i\not{D}}\,S(\boldsymbol{X} - i\gamma_5\tilde{\boldsymbol{X}})\,\frac{1}{M - i\not{D}}\,F_0\,.\end{aligned} \tag{4.7}$$

In order to match this expression onto the SCET_{BSM} effective Lagrangian describing two-body decays of the heavy scalar S, we replace the SM fields by fields in the EFT. The relevant fields are the soft field S_v for the heavy resonance and collinear fields describing particle jets moving along light-like directions $n_1^\mu = (1, \boldsymbol{n}_1)$ and $n_2^\mu = (1, \boldsymbol{n}_2)$. The precise definitions of these fields, which include collinear Wilson lines, can be found in [1]. For the special case of the Higgs doublet, the low-energy theory also contains a soft field Φ_0 carrying no four-momentum. After EWSB this field is set to the Higgs vacuum expectation value. The relevant replacement rules are extremely simple:

$$\begin{aligned}\phi &\to \Phi_0 + \Phi_{n_1} + \Phi_{n_2} + \dots\,, \\ \psi &\to \psi_{n_1} + \psi_{n_2} + \dots\,, \\ gA^{\mu,a} &\to \mathcal{A}_{n_1}^{\mu,a} + \mathcal{A}_{n_2}^{\mu,a} + \dots\,.\end{aligned} \tag{4.8}$$

Here $\psi = Q_L, u_R, d_R$ denotes a generic SM quark field, while $A = B, W, G$ is a generic gauge field. The effective gauge fields in SCET_{BSM} include the gauge couplings in their

definition. The collinear quark and gauge fields are subject to the constraints $\not{n}_i\,\psi_{n_i} = 0$ and $\bar{n}_i{\cdot}\mathcal{A}^a_{n_i} = 0$, where $\bar{n}_i^\mu = (1, -\boldsymbol{n}_i)$. Note that the components $\bar{n}_i{\cdot}A^a$ of the gauge fields are contained in the Wilson lines of the effective theory. The collinear fields satisfy simple power-counting rules in the expansion parameter $\lambda = v/M_S$ of SCET$_{\rm BSM}$: the fields Φ_0, Φ_{n_i}, ψ_{n_i} and $\mathcal{A}^{\mu,a}_{\perp,n_i}$ are all of $\mathcal{O}(\lambda)$, whereas the longitudinal gauge fields $n_i\cdot\mathcal{A}^a_{\perp,n_i}$ are of $\mathcal{O}(\lambda^2)$. The subscript $\perp$ refers to the components of an n_i-collinear gauge field perpendicular to the four-vectors n_i^μ and $\bar{n}_i^\mu$. Derivatives acting on n_i-collinear fields can be decomposed into the components $\bar{n}_i\cdot\partial = \mathcal{O}(\lambda^0)$, $\partial_\perp^\mu = \mathcal{O}(\lambda)$ and $n_i\cdot\partial = \mathcal{O}(\lambda^2)$. The dots in (4.8) stand for soft fields, which are power-suppressed relative to the collinear fields and will play no role for our discussion.
It is now straightforward to extract from (4.7) the terms of leading order in the λ expansion. Obviously, the first term on the right-hand side generates the tree-level contribution

$$C_{\phi\phi} = -\frac{\kappa_1}{M} \tag{4.9}$$

to the Wilson coefficient of the scalar operator $O_{\phi\phi}$ in the SCET$_{\rm BSM}$ Lagrangian (4.1). After the introduction of SCET fields the quantity F_0 is of $\mathcal{O}(\lambda^2)$, while Q_L is of $\mathcal{O}(\lambda)$. Hence the leading terms in the Lagrangian originating from VLQ exchange are of $\mathcal{O}(\lambda^3)$ and arise from the term in brackets in the first line of (4.7). Since gauge fields in SCET$_{\rm BSM}$ are always power suppressed, we can expand the inverse-derivative operator sandwiched between spinor fields of opposite chirality in the form

$$\frac{1}{M - i\not{D}} \to \frac{M}{M^2 + \Box} + \mathcal{O}(\lambda)\,. \tag{4.10}$$

The Laplace operator in the denominators of these expressions must only be kept if the product of fields on which this operator acts has virtuality of order M_S^2. We thus obtain

$$\begin{aligned}\mathcal{L}_{\rm eff}\big|^{\lambda^3}_{S^1} = \frac{1}{M}\sum_{q=u,d}\Big[&S_v\,\bar{Q}_{L,n_1}\boldsymbol{V}_Q^\dagger\boldsymbol{G}_q(\Phi_0+\Phi_{n_2})q_{R,n_2}\\ &+ S_v\,\bar{Q}_{L,n_1}\boldsymbol{V}_Q^\dagger\boldsymbol{G}_q\,\frac{M^2}{M^2+\Box}\,\Phi_{n_1}q_{R,n_2} + \text{h.c.}\Big] + (n_1\leftrightarrow n_2)\,,\end{aligned} \tag{4.11}$$

where for $q = u$ the doublet Φ must be replaced by $\tilde{\Phi}$. The first graph in Figure 4.1 shows a diagram in the complete theory giving rise to these matching contributions.

4.3.2 Integrating out Off-Shell Fluctuations

If the portal coupling κ_1 in (4.3) is non-zero, then the second diagram shown in Figure 4.1 produces another tree-level matching contribution, in which the propagator for the Higgs doublet carries a virtuality of order $q^2 \sim M_S^2$. The corresponding contribution to the effective Lagrangian can be written in the form

$$\Delta\mathcal{L}_{\rm eff}\big|^{\lambda^3}_{S^1} = \sum_{q=u,d}\kappa_1 S_v(\Phi_0^a + \Phi_{n_1}^a + \Phi_{n_2}^a)\frac{1}{\Box}\,\bar{Q}^a_{L,n_1}\boldsymbol{Y}_q\,q_{R,n_2} + \text{h.c.} + (n_1\leftrightarrow n_2)\,, \tag{4.12}$$

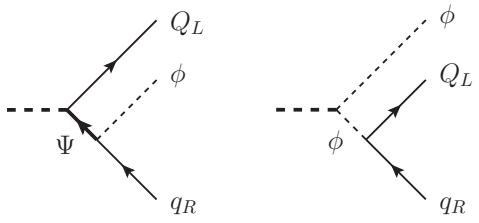

Figure 4.1: Tree-level diagrams giving rise to the effective Lagrangians (4.11) (left) and (4.12) (right). Thick lines denote S and the VLQs, whereas the thin lines represent SM particles.

where the inverse Laplace operator arises from the Higgs propagator. The sum of (4.11) and (4.12) gives the complete tree-level effective Lagrangian at $\mathcal{O}(\lambda^3)$.

4.3.3 Wilson Coefficients

The complete basis of SCET_{BSM} operators at $\mathcal{O}(\lambda^3)$ has been constructed in [1]. The effective Lagrangian at this order can be written in the form (summed over i, j)

$$\begin{aligned}\mathcal{L}^{(3)}_{\text{eff}} = \frac{1}{M}\sum_{q=u,d}\Bigg[&C^{ij}_{Q_L\bar{q}_R}(M,M_S)\,O^{ij}_{Q_L\bar{q}_R} \\ &+\sum_{k=1,2}\int_0^1 du\, C^{(k)\,ij}_{Q_L\bar{q}_R\,\phi}(u,M,M_S)\,O^{(k)\,ij}_{Q_L\bar{q}_R\,\phi}(u) + \text{h.c.}\Bigg] \\ +\frac{1}{M}\sum_A\Bigg[&\int_0^1 du\, C^{ij}_{Q_L\bar{Q}_L A}(u,M,M_S)\,O^{ij}_{Q_L\bar{Q}_L A}(u) + (Q_L\to q_R) + \text{h.c.}\Bigg],\end{aligned} \tag{4.13}$$

where the sum in the last lines runs over the three gauge fields $A = B, W, G$. For simplicity we consider operators containing quark fields only. We have defined the mixed-chirality operators

$$\begin{aligned}O^{ij}_{Q_L\bar{q}_R} &= S_v\,\bar{Q}^i_{L,n_1}\Phi_0\,q^j_{R,n_2} + (n_1\leftrightarrow n_2)\,,\\ O^{(1)\,ij}_{Q_L\bar{q}_R\,\phi}(u) &= S_v\,\bar{Q}^i_{L,n_1}\Phi^{(u)}_{n_1}\,q^j_{R,n_2} + (n_1\leftrightarrow n_2)\,,\\ O^{(2)\,ij}_{Q_L\bar{q}_R\,\phi}(u) &= S_v\,\bar{Q}^i_{L,n_1}\Phi^{(u)}_{n_2}\,q^j_{R,n_2} + (n_1\leftrightarrow n_2)\,,\end{aligned} \tag{4.14}$$

and the same-chirality operators

$$\begin{aligned}O^{ij}_{Q_L\bar{Q}_L A}(u) &= S_v\,\bar{Q}^i_{L,n_1}\,\mathcal{A}^{\perp(u)}_{n_1}\,Q^j_{L,n_2} + (n_1\leftrightarrow n_2)\,,\\ O^{ij}_{q_R\bar{q}_R A}(u) &= S_v\,\bar{q}^i_{R,n_1}\,\mathcal{A}^{\perp(u)}_{n_1}\,q^j_{R,n_2} + (n_1\leftrightarrow n_2)\,,\end{aligned} \tag{4.15}$$

where i, j are generation indices. When an operator contains more than two collinear fields describing particles moving in the same direction, the total collinear momentum

carried by this jet is split up among the fields. Our convention is that in each operator the bosonic field carries the longitudinal momentum fraction $u \in [0,1]$, while the fermionic field carries momentum fraction $(1-u)$. From (4.11) and (4.12), we obtain for the tree-level matching conditions in matrix notation (with $q = u, d$)

$$\begin{aligned}
\boldsymbol{C}_{Q_L \bar{q}_R} &= \boldsymbol{V}_Q^\dagger \boldsymbol{G}_q - \frac{\kappa_1}{M} \frac{\boldsymbol{Y}_q}{\xi}\,, \\
\boldsymbol{C}^{(1)}_{Q_L \bar{q}_R \phi} &= \frac{\boldsymbol{V}_Q^\dagger \boldsymbol{G}_q}{1 - \xi u - i\epsilon} - \frac{\kappa_1}{M} \frac{\boldsymbol{Y}_q}{\xi(1-u) + i\epsilon}\,, \\
\boldsymbol{C}^{(2)}_{Q_L \bar{q}_R \phi} &= \boldsymbol{V}_Q^\dagger \boldsymbol{G}_q - \frac{\kappa_1}{M} \frac{\boldsymbol{Y}_q}{\xi(1-u) + i\epsilon}\,, \\
\boldsymbol{C}_{Q_L \bar{Q}_L A} &= \boldsymbol{C}_{q_R \bar{q}_R A} = 0\,; \quad A = B, W, G\,,
\end{aligned} \tag{4.16}$$

where we have defined $\xi = M_S^2/M^2$. The $i\epsilon$ prescriptions are those from the Feynman propagators. Note that κ_1 is naturally of order M. The parameter ξ governs the ratio of the mass of the heavy scalar resonance, which we assume has been discovered, and the mass of the VLQs, which we assume have not yet been discovered. This ratio is in principle arbitrary, but in many realistic models is expected to be of $\mathcal{O}(1)$. The fact that SCET_{BSM} correctly captures the dependence on both mass parameters is a unique feature of this EFT [1].

Analogous operators containing lepton fields also exist, and indeed they can be generated at tree level in our model via the Higgs portal interaction proportional to κ_1. However, the corresponding Wilson coefficients are strongly suppressed by the leptonic Yukawa couplings.

The coefficients in (4.16) are given in the weak basis. After EWSB, these coefficients should be transformed to the mass basis of the SM quarks. This transformation diagonalises the Yukawa matrices $\boldsymbol{Y}_q$, while $\boldsymbol{V}_Q^\dagger \boldsymbol{G}_q \to \boldsymbol{U}_{q_L}^\dagger \boldsymbol{V}_Q^\dagger \boldsymbol{G}_q \boldsymbol{W}_{q_R}$, where $\boldsymbol{U}_{q_L}$ and $\boldsymbol{W}_{q_R}$ with $q = u, d$ denote the rotation matrices transforming the left-handed and right-handed quark fields from the weak to the mass basis.

4.4 One-Loop Matching

With the exception of $O_{\phi\phi}$, the bosonic operators in the SCET_{BSM} Lagrangian receive matching corrections starting at one-loop order. We now discuss the calculation of these corrections for the Wilson coefficients of the leading operators of $\mathcal{O}(\lambda^2)$ in (4.1). The relevant Feynman diagrams are shown in Figure 4.2. The first graph contains a loop of VLQs, while the remaining diagrams feature loops with off-shell Higgs doublets. To perform the matching in the simplest possible way, we calculate these diagrams setting all SM masses to zero. Then loop graphs in the EFT are scaleless and vanish, and hence the Wilson coefficients are given directly in terms of the diagrams shown in the figure.

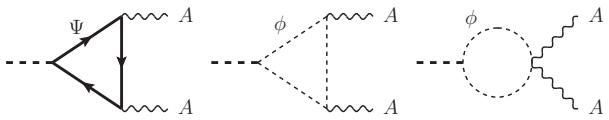

Figure 4.2: One-loop diagrams contributing to the Wilson coefficients C_{AA} and $\widetilde{C}_{AA}$ in (4.1). We do not show crossed graphs, in which the two boson lines are exchanged. Loops graphs involving SM fermions do not arise at leading order in λ.

We find (with $A = B, W, G$)

$$\begin{aligned} C_{AA} &= \frac{d_A}{\pi^2}\,\mathrm{Tr}(\boldsymbol{X})\left[\frac{4-\xi}{\xi}\,g^2(\xi)-1\right]+\frac{d'_A}{4\pi^2}\,\frac{\kappa_1}{M}\,, \\ \widetilde{C}_{AA} &= \frac{d_A}{\pi^2}\,\mathrm{Tr}(\tilde{\boldsymbol{X}})\,g^2(\xi)\,, \end{aligned} \tag{4.17}$$

where $\xi = M_S^2/M^2$ as above, and the group-theory factors d_A are given by

$$\begin{aligned} &d_B = N_c Y_\psi^2 = \frac{1}{12}\,, \quad d_W = \frac{T_F N_c}{2} = \frac{3}{4}\,, \quad d_G = T_F = \frac{1}{2}\,, \\ &d'_B = Y_\phi^2 = \frac{1}{4}\,, \qquad d'_W = \frac{T_F}{2} = \frac{1}{4}\,, \qquad d'_G = 0\,. \end{aligned} \tag{4.18}$$

The relevant loop function reads

$$g(\xi) = \begin{cases} \arcsin\dfrac{\sqrt{\xi}}{2}\,; & \xi \le 4\,, \\[2ex] \dfrac{i}{2}\ln\dfrac{1+\sqrt{1-4/\xi}}{1-\sqrt{1-4/\xi}}+\dfrac{\pi}{2}\,; & \xi \ge 4\,. \end{cases} \tag{4.19}$$

The ξ-dependent contributions arise from integrating out the VLQs, while the term proportional to the Higgs-portal coupling κ_1 is obtained by integrating out loops of virtual Higgs doublets carrying virtualities of order M_S^2, in analogy with the discussion in the previous section.

It is instructive to study the ξ-dependent terms in (4.17) in more detail. Focussing on the case of $\widetilde{C}_{AA}$ for concreteness, and assuming that $M_S^2 < 4M^2$, we can expand the Wilson coefficient in powers of the ratio $\xi = M_S^2/M^2$, finding

$$\widetilde{C}_{AA} = \frac{d_A}{2\pi^2}\,\mathrm{Tr}(\tilde{\boldsymbol{X}})\sum_{k=1}^{\infty}\frac{\Gamma\left(\frac{1}{2}\right)\Gamma(k)}{k\,\Gamma\left(\frac{1}{2}+k\right)}\left(\frac{M_S^2}{4M^2}\right)^k. \tag{4.20}$$

The first term in the sum gives a contribution to (4.1) which corresponds to the local dimension-five operator $SF_{\mu\nu}\widetilde{F}^{\mu\nu}$, the second term corresponds to local dimension-seven

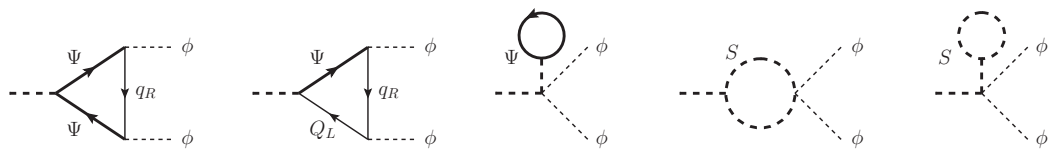

Figure 4.3: One-loop diagrams contributing to the coefficient $C^{(1)}_{\phi\phi}$ in (4.21).

operators such as $S(\partial_\alpha F_{\mu\nu})(\partial^\alpha \widetilde{F}^{\mu\nu})$ or $(\Box S)F_{\mu\nu}\widetilde{F}^{\mu\nu}$, the third term corresponds to local dimension-nine operators, and so on. Our SCET_{BSM} approach thus sums up an infinite tower of local operators. In an extension of the SMEFT consisting of local operators built out of SM field and the field S (see e.g. [165, 201]), one would typically only include the leading dimension-five operators. In realistic scenarios where $M_S \sim M$, however, all contributions are of the same order.

The one-loop matching calculation for the coefficient $C_{\phi\phi}$ in (4.1) is more involved. We write the result in the form

$$C_{\phi\phi} = -\frac{\kappa_1}{M}\,(1+\delta_{\kappa_1}) + C^{(1)}_{\phi\phi}\,. \tag{4.21}$$

The quantity δ_{κ_1} contains the loop corrections to the tree-level result in (4.9), while $C^{(1)}_{\phi\phi}$ contains contributions to the Wilson coefficient involving couplings other than κ_1. The relevant diagrams for the latter terms are shown in Figure 4.3. We obtain

$$\begin{aligned} C^{(1)}_{\phi\phi} &= \frac{N_c}{8\pi^2}\,\text{Tr}\big[\boldsymbol{X}(\boldsymbol{G}_u\boldsymbol{G}_u^\dagger + \boldsymbol{G}_d\boldsymbol{G}_d^\dagger)\big]\left[2\ln\frac{M^2}{\mu^2} - 3 + 2\sqrt{\frac{4-\xi}{\xi}}\,g(\xi) + \frac{4}{\xi}\,g^2(\xi)\right] \\ &\quad + \frac{N_c}{8\pi^2}\,\text{Re}\,\text{Tr}\big[\boldsymbol{V}_Q(\boldsymbol{Y}_u\boldsymbol{G}_u^\dagger + \boldsymbol{Y}_d\boldsymbol{G}_d^\dagger)\big]\left[2\ln\frac{M^2}{\mu^2} - 3 - \frac{1-\xi}{\xi}\ln(1-\xi-i\epsilon)\right] \\ &\quad - \frac{N_c\kappa_2}{2\pi^2\xi}\,\text{Tr}(\boldsymbol{X})\left(\ln\frac{M^2}{\mu^2} - 1\right) - \frac{\kappa_2\lambda_3}{32\pi^2 M}\left(\frac{\pi}{\sqrt{3}} - 1\right). \end{aligned} \tag{4.22}$$

The calculation of δ_{κ_1} is discussed in Appendix 4.8. Unlike the results shown in (4.17), these expressions contain an explicit dependence on the renormalisation scale μ, at which the operators and Wilson coefficients are defined (in the $\overline{\text{MS}}$ scheme). The matching results presented here refer to a scale $\mu \sim M$, at which they do not contain any large logarithms; the evolution to lower scales will be discussed later in Section 4.6. The scale dependence of the coefficient $C^{(1)}_{\phi\phi}$ must be compensated by the scale dependence of the portal coupling κ_1 in (4.21).

4.5 One-Loop Matching for $S \to Zh$

There is one potential two-body decay of a heavy scalar resonance S that cannot be described using the operators arising at leading and subleading order in SCET power

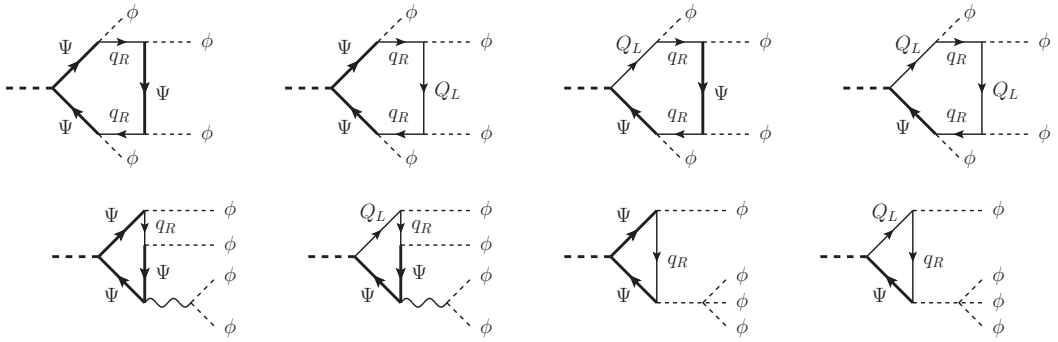

Figure 4.4: Example diagrams contributing to the matching of the Wilson coefficient $\widetilde{C}_{\phi\phi\phi\phi}$.

counting. This is the mode $S \to Zh$, where the Z boson is longitudinally polarised. Only the CP-odd component of the scalar can decay to this final state, which makes this channel interesting to study the CP properties of a new scalar resonance [166, 234]. The following discussion is significantly more technical than that in the previous two sections and can be skipped in a first reading.

The relevant $\mathcal{O}(\lambda^4)$ operators in the SCET_{BSM} Lagrangian mediating the $S \to Zh$ decay can be written in the form [1]

$$\mathcal{L}^{(4)}_{\text{eff}} = \frac{\widetilde{C}_{\phi\phi\phi\phi}(M, M_S)}{M}\, 2iS_v\Big(\Phi^\dagger_{n_1}\Phi_0\,\Phi^\dagger_{n_2}\Phi_0 - \text{h.c.}\Big) + \dots\,, \tag{4.23}$$

where the dots stand for fermionic operators, which contribute to the decay amplitude at one-loop order. The operator written out explicitly gives the tree-level contribution

$$\mathcal{M}(S \to Z_\parallel h)\big|_{\text{tree}} = -i\widetilde{C}_{\phi\phi\phi\phi}\,\frac{v^2}{M}\,. \tag{4.24}$$

Since in the VLQ model we consider the Wilson coefficient $\widetilde{C}_{\phi\phi\phi\phi}$ is generated starting at one-loop order, it will be necessary to include other loop-suppressed effects for consistency (see below).

Representative one-loop diagrams contributing to the matching coefficient $\widetilde{C}_{\phi\phi\phi\phi}$ are shown in Figure 4.4. Evaluating the relevant graphs in the $\overline{\text{MS}}$ scheme, we obtain after a lengthy calculation

$$\begin{aligned}\widetilde{C}_{\phi\phi\phi\phi} = -\frac{N_c}{16\pi^2\xi}\sum_{q=u,d} 2T_3^q \Big\{ &\text{Tr}\big(\tilde{\boldsymbol{X}}\boldsymbol{G}_q\boldsymbol{Y}_q^\dagger\boldsymbol{Y}_q\boldsymbol{G}_q^\dagger\big)\Big[-L_M\Big(\xi+(1-\xi)\ln(1-\xi)\Big)+f_1(\xi)\Big] \\ &+\text{Tr}\big(\tilde{\boldsymbol{X}}\boldsymbol{G}_q\boldsymbol{G}_q^\dagger\boldsymbol{G}_q\boldsymbol{G}_q^\dagger\big)\,f_2(\xi) + \text{Tr}\big(\tilde{\boldsymbol{X}}\boldsymbol{G}_q\boldsymbol{G}_q^\dagger\big)\Big[(g^2+g'^2)\,f_3(\xi)+\lambda_H\,f_4(\xi)\Big]\end{aligned}$$

$$
\begin{aligned}
&+ \operatorname{Im}\operatorname{Tr}(\boldsymbol{G}_q^\dagger \boldsymbol{V}_Q \boldsymbol{Y}_q \boldsymbol{Y}_q^\dagger \boldsymbol{Y}_q) \left[\frac{\xi}{2} L_S^2 - L_M\Big(\xi + (1+\xi)\ln(1-\xi)\Big) + f_5(\xi)\right] \\
&+ \operatorname{Im}\operatorname{Tr}(\boldsymbol{G}_q^\dagger \boldsymbol{V}_Q \boldsymbol{Y}_q \boldsymbol{G}_q^\dagger \boldsymbol{G}_q) \left[\xi\,(L_S - L_M)\ln(1+\xi) + f_6(\xi)\right] \\
&+ \operatorname{Im}\operatorname{Tr}(\boldsymbol{G}_q^\dagger \boldsymbol{V}_Q \boldsymbol{Y}_q) \left[(g^2 + g'^2)\Big[- L_M\Big(1 + \frac{4-3\xi}{4\xi}\ln(1-\xi)\Big)\right. \\
&\qquad\qquad \left. - \frac{\xi}{4}(L_S - L_M) + f_7(\xi)\Big] \right. \\
&\qquad \left. + \lambda_H \Big[2 L_M \ln(1-\xi) - 2\xi\,(L_S - L_M) + f_8(\xi)\Big]\right] \Bigg\} \\
&- \frac{N_c}{16\pi^2 \xi} \sum_{q=u,d} Q_q\, g'^2 \Bigg\{ \operatorname{Tr}(\tilde{\boldsymbol{X}} \boldsymbol{G}_q \boldsymbol{G}_q^\dagger) \left[L_M \left(\frac{2-\xi}{2} + \frac{1-\xi}{\xi}\ln(1-\xi)\right) + f_9(\xi)\right] \\
&+ \operatorname{Im}\operatorname{Tr}(\boldsymbol{G}_q^\dagger \boldsymbol{V}_Q \boldsymbol{Y}_q) \left[L_M \left(\frac{6-\xi}{2} + \frac{3-2\xi}{\xi}\ln(1-\xi)\right) + f_{10}(\xi)\right] \Bigg\} .
\end{aligned}
\tag{4.25}
$$

Here $T_3^u = \frac{1}{2}$ and $T_3^d = -\frac{1}{2}$ are the weak isospins of up- and down-type quarks, Q_q denote the quark electric charges in units of e, λ_H is the quartic coupling of the Higgs field, and g, g' are the gauge couplings of $\mathrm{SU}_W(2)$ and $\mathrm{U}_Y(1)$. The logarithms $L_M = \ln(M^2/\mu^2)$ and $L_S = \ln(M_S^2/\mu^2) - i\pi$ contain the dependence on the factorisation scale μ, and we have defined the functions $f_i(\xi)$ collected in Appendix 4.9. For $\xi > 1$, the above expressions must be analytically continued using the prescription $\xi \to \xi + i\epsilon$. In the limit where $\xi \ll 1$, corresponding to $M_S^2 \ll M^2$, the result (4.25) can be expanded in powers of ξ. We find that the leading terms of $\mathcal{O}(\xi^0)$ agree with eq. (6.20) in [1], where we had defined the matrices $\hat{\boldsymbol{Y}}_q = \boldsymbol{G}_q^\dagger \boldsymbol{V}_Q$. Moreover, the terms linear in ξ are consistent with eq. (24) in [234].

An interesting feature of the result (4.25) is the rather complicated dependence of the terms involving the factorisation scale μ, which are contained in the logarithms L_M and L_S, on the mass ratio $\xi = M_S^2/M^2$. In conventional EFT applications the coefficients of the μ-dependent terms in Wilson coefficients and operator matrix elements are functions of the coupling constants of the theory, but they do not depend in a non-trivial way on the masses of heavy particles that have been integrated out. The reason is that the μ-dependence must cancel between Wilson coefficients and matrix elements, and the low-energy theory does not know about the masses of the heavy particles.

In the present case, the μ-dependence of the contribution to the $S \to Zh$ decay amplitude entering via the Wilson coefficient $\widetilde{C}_{\phi\phi\phi\phi}$ in (4.25) is cancelled by the scale dependence of one-loop matrix elements of operators involving fermion pairs, which are induced by tree-level matching at $\mathcal{O}(\lambda^4)$. Indeed, since in our model $\widetilde{C}_{\phi\phi\phi\phi}$ arises at one-loop order, the one-loop matrix elements of other $\mathcal{O}(\lambda^4)$ operators, which appear already at tree level, must be included for consistency. The relevant terms can be extracted from (4.7). For the purpose of illustration we consider the last operator in this result, which contains

the flavour matrices $\boldsymbol{X}$ and $\tilde{\boldsymbol{X}}$. At $\mathcal{O}(\lambda^4)$, it gives rise to the structure

$$\begin{aligned}\mathcal{L}_{\text{eff}}\big|_{S^1}^{\lambda^4} \ni -\frac{1}{M}\sum_{q=u,d}\Big[&\bar{q}_{R,n_1}\Phi_0^\dagger\, S_v\, \boldsymbol{G}_q^\dagger(\boldsymbol{X}-i\gamma_5\tilde{\boldsymbol{X}})\boldsymbol{G}_q \\ &\times\frac{1}{M^2+\Box}\, i\not{\partial}\,\Phi_{n_2}\, q_{R,n_1} + \text{h.c.}\Big] + (n_1\leftrightarrow n_2)\,.\end{aligned} \tag{4.26}$$

For $q = u$ the doublet Φ must be replaced by $\tilde{\Phi}$. We only need to consider operators where both fermions are described by collinear fields moving along the same direction, since later we need to take matrix elements where the fermion pair is converted into a collinear Higgs or Z boson. Between the collinear spinors only the $n_1\cdot\partial$ component of the derivative survives, and hence the derivative gives zero when acting on the fermions. We now define the following set of SCET_{BSM} hermitian operators (here and below we abbreviate $\bar{u}\equiv 1-u$):

$$\begin{aligned}O^{(\pm)\,ij}_{q_R\bar{q}_R\phi\phi}(u) &= S_v\left[\bar{q}^{(u)\,i}_{R,n_1}\not{n}_1\, q^{(\bar{u})\,j}_{R,n_1} \mp \bar{q}^{(\bar{u})\,i}_{R,n_1}\not{n}_1\, q^{(u)\,j}_{R,n_1}\right]\left(\Phi^\dagger_{n_2}\Phi_0 \pm \Phi_0^\dagger\Phi_{n_2}\right),\\ \widetilde{O}^{(\pm)\,ij}_{q_R\bar{q}_R\phi\phi}(u) &= iS_v\left[\bar{q}^{(u)\,i}_{R,n_1}\not{n}_1\, q^{(\bar{u})\,j}_{R,n_1} \pm \bar{q}^{(\bar{u})\,i}_{R,n_1}\not{n}_1\, q^{(u)\,j}_{R,n_1}\right]\left(\Phi^\dagger_{n_2}\Phi_0 \pm \Phi_0^\dagger\Phi_{n_2}\right).\end{aligned} \tag{4.27}$$

Here u denotes the fraction of the total n_1-collinear momentum carried by the final-state quark. The operators shown in the first line are CP even, while those in the second line are CP odd. Writing the relevant terms in the Lagrangian in the form

$$\begin{aligned}\mathcal{L}^{(4)}_{\text{eff}} \ni \frac{1}{M^2}\sum_{q=u,d}\int_0^1 du\,\Big[&C^{(\pm)\,ij}_{q_R\bar{q}_R\phi\phi}(M,M_S,u)\, O^{(\pm)\,ij}_{q_R\bar{q}_R\phi\phi}(u) \\ &+ \widetilde{C}^{(\pm)\,ij}_{q_R\bar{q}_R\phi\phi}(M,M_S,u)\,\widetilde{O}^{(\pm)\,ij}_{q_R\bar{q}_R\phi\phi}(u)\Big],\end{aligned} \tag{4.28}$$

we obtain the Wilson coefficients (in matrix notation)

$$\begin{aligned}\boldsymbol{C}^{(+)}_{q_R\bar{q}_R\phi\phi}(u,M,M_S) &= \frac{M_S}{2M}\,\frac{\boldsymbol{G}_q^\dagger\boldsymbol{X}\boldsymbol{G}_q}{1-\xi\bar{u}}\,,\\ \boldsymbol{C}^{(-)}_{q_R\bar{q}_R\phi\phi}(u,M,M_S) &= \frac{M_S}{2M}\,2T_3^q\,\frac{\boldsymbol{G}_q^\dagger\boldsymbol{X}\boldsymbol{G}_q}{1-\xi\bar{u}}\,,\\ \widetilde{\boldsymbol{C}}^{(+)}_{q_R\bar{q}_R\phi\phi}(u,M,M_S) &= \frac{M_S}{2M}\,\frac{\boldsymbol{G}_q^\dagger\tilde{\boldsymbol{X}}\boldsymbol{G}_q}{1-\xi\bar{u}}\,,\\ \widetilde{\boldsymbol{C}}^{(-)}_{q_R\bar{q}_R\phi\phi}(u,M,M_S) &= \frac{M_S}{2M}\,2T_3^q\,\frac{\boldsymbol{G}_q^\dagger\tilde{\boldsymbol{X}}\boldsymbol{G}_q}{1-\xi\bar{u}}\,.\end{aligned} \tag{4.29}$$

The factors $2T_3^q$ arise because for $q = u$ the operators involve the scalar doublets $\tilde{\Phi}$ rather than Φ.

The CP-odd operators in (4.27) contribute at one-loop order to the $S \to Zh$ decay amplitude via the diagrams shown in Figure 4.5. Working in the fermion mass basis, we

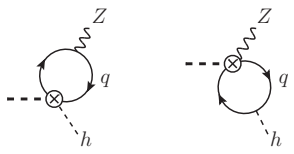

Figure 4.5: One-loop contributions of the operators $\widetilde{O}^{(+)\,ij}_{q_R\bar{q}_R\phi\phi}$ (left) and $\widetilde{O}^{(-)\,ij}_{q_R\bar{q}_R\phi\phi}$ (right) to the $S \to Zh$ decay amplitude.

find in the $\overline{\text{MS}}$ scheme

$$\begin{aligned} i\,\langle Z_\parallel h|\,\widetilde{O}^{(+)\,ij}_{q_R\bar{q}_R\phi\phi}(u)\,|S\rangle &= \frac{\delta^{ij}N_c}{8\pi^2}\,v^2 M_S(y_q^2\,T_3^q - Q_q g'^{\,2} u\bar{u})\ln\frac{\mu^2}{m_q^2 - u\bar{u}m_Z^2 - i\epsilon}\,, \\ i\,\langle Z_\parallel h|\,\widetilde{O}^{(-)\,ij}_{q_R\bar{q}_R\phi\phi}(u)\,|S\rangle &= \frac{\delta^{ij}N_c}{16\pi^2}\,v^2 M_S\,y_q^2\,(u-\bar{u})\ln\frac{\mu^2}{m_q^2 - u\bar{u}m_h^2 - i\epsilon}\,. \end{aligned} \tag{4.30}$$

Multiplying these expressions with the corresponding Wilson coefficients in (4.29) and integrating the result over u we obtain the contribution to the $S \to Zh$ decay amplitude, which must be added to the one in (4.24).

Here we are mainly concerned with the cancellation of the μ-dependent terms in the final expression for the decay amplitude. Note that the scale-dependent terms in (4.30) have simple coefficients involving coupling constants and some factors of v and M_S needed for dimensional reasons. The non-trivial dependence on the mass ratio ξ arises when these matrix elements are multiplied by the corresponding Wilson coefficients and integrated over the variable u. To display our results we use the Z-boson mass in the denominator of the corresponding logarithms, and we omit the remaining terms that are scale independent and free of large logarithms. Combining the contributions in (4.24) and (4.30), we find

$$\begin{aligned} \langle Z_\parallel h|\,\mathcal{L}^{(4)}_{\text{eff}}\,|S\rangle = -i\widetilde{C}_{\phi\phi\phi\phi}\,\frac{v^2}{M} \\ - i\,\frac{N_c}{16\pi^2\xi}\,\frac{v^2}{M}\sum_{q=u,d}\Big\{2T_3^q\,\text{Tr}\big(\tilde{\boldsymbol{X}}\boldsymbol{G}_q\boldsymbol{Y}_q^\dagger\boldsymbol{Y}_q\boldsymbol{G}_q^\dagger\big)\ln\frac{\mu^2}{m_Z^2}\Big(\xi + (1-\xi)\ln(1-\xi)\Big) \\ - Q_q\,g'^{\,2}\,\text{Tr}\big(\tilde{\boldsymbol{X}}\boldsymbol{G}_q\boldsymbol{G}_q^\dagger\big)\ln\frac{\mu^2}{m_Z^2}\Big(\frac{2-\xi}{2} + \frac{1-\xi}{\xi}\ln(1-\xi)\Big) \\ + \text{terms involving } \boldsymbol{V}_Q\Big\} \\ + \text{scale-independent terms}\,. \end{aligned} \tag{4.31}$$

We have transformed the expressions (4.30) back to the weak basis by replacing $y_q^2\,\delta_{ij} \to (\boldsymbol{Y}_q^\dagger\boldsymbol{Y}_q)_{ij}$. Inspection of (4.25) shows that the μ-dependent terms indeed cancel out in this result.

4.6 Resummation of Large Logarithms

SCET_{BSM} offers a systematic framework for expanding the decay amplitudes for the heavy resonance S into SM particles in powers of v/M_S and resumming large logarithms of this scale ratio. As before, we assume that the scales M and M_S are of similar magnitude. Since the rates are affected by Sudakov double logarithms, resummation is important even in cases where the logarithms arise from electroweak interactions [152–154]. These logarithms suppress the decay rates and hence should be taken into account when deriving bounds on the masses and couplings of hypothetical new heavy particles. We now illustrate this point by focussing on a few important two-body decay modes of a heavy scalar resonance S.

For the purposes of illustration, we assume $M_S = 2\,\text{TeV}$ and $M = 2.5\,\text{TeV}$ for the masses of S and of the VLQs, respectively. We calculate the Wilson coefficients in the effective Lagrangians (4.1) and (4.13) at the high scale $\mu = M$ and evolve them down to a characteristic scale for the process of interest. This evolution is governed by RG equations derived in [1]. As long as the characteristic scale is of the order of the weak scale, it is appropriate to include all SM particles in the anomalous dimensions and β-functions of the EFT. A consistent approximation is obtained by including the leading terms in the matching coefficients at the high scale and using two-loop approximations for the cusp anomalous dimension and β-functions as well as one-loop approximations for all other anomalous dimensions in the evolution to low energies (see below).

4.6.1 $S \to 2$ Jets Decay

At lowest order in perturbation theory the process $S \to 2\,\text{jets}$ proceeds primarily via the decay $S \to gg$, whose rate is enhanced by a factor M_S^2/v^2 relative to the $S \to q\bar{q}$ decay rate. Also, in many models the latter rate is suppressed by the light quark masses. We thus obtain $\Gamma(S \to 2\,\text{jets}) \approx \Gamma(S \to gg)$ with

$$\Gamma(S \to gg) = \frac{M^2}{M_S}\, 8\pi\alpha_S^2(\mu_j)\left(|C_{GG}(\mu_j)|^2 + |\widetilde{C}_{GG}(\mu_j)|^2\right). \tag{4.32}$$

Here μ_j is the characteristic scale inherent in the definition of the jets, such as an upper bound on the jet invariant mass. At the high matching scale $\mu_h = M$ the relevant Wilson coefficients have been given in (4.17). The two coefficients obey the same RG equation [1]

$$\mu\,\frac{d}{d\mu}\,C_{GG}(\mu) = \left[3\gamma_{\text{cusp}}^{(3)}\left(\ln\frac{M_S^2}{\mu^2} - i\pi\right) + 2\gamma^G\right] C_{GG}(\mu)\,. \tag{4.33}$$

Note the important fact that for Sudakov problems the anomalous dimensions themselves contain a (so-called "cusp") logarithm, and that they have non-zero imaginary parts. At leading logarithmic order, we need $\gamma_{\text{cusp}}^{(3)}$ to two-loop and γ^G to one-loop order. The relevant expressions are

$$\gamma_{\text{cusp}}^{(3)} = \frac{\alpha_S}{\pi} + \left(\frac{47}{12} - \frac{\pi^2}{4}\right)\left(\frac{\alpha_S}{\pi}\right)^2 + \mathcal{O}(\alpha_S^3)\,, \tag{4.34}$$

and $\gamma^G = 0 + \mathcal{O}(\alpha_S^2)$. Solving the RG equation, we find

$$C_{GG}(\mu)/C_{GG}(M) = \widetilde{C}_{GG}(\mu)/\widetilde{C}_{GG}(M) = U_{GG}(\mu, M)\,, \tag{4.35}$$

where [199, 200]

$$U_{GG}(\mu, M) = \exp\left[\frac{6}{49}\, g(\mu, M) + \frac{6}{7}\,(i\pi - \ln\xi)\ln r\right], \tag{4.36}$$

with $r = \alpha_S(\mu)/\alpha_S(M)$ and

$$g(\mu, M) = -\frac{4\pi}{\alpha_S(M)}\left(\frac{1}{r} - 1 + \ln r\right) - \left(\frac{251}{21} - \pi^2\right)(r - 1 - \ln r) + \frac{13}{7}\,\ln^2 r\,. \tag{4.37}$$

An analogous relation holds for $\widetilde{C}_{GG}$. If we assume that the characteristic jet scale is $\mu_j = 100\,\text{GeV}$, then

$$U_{GG}(\mu_j, M) \approx 0.38\, e^{0.98i}\,. \tag{4.38}$$

The decay rate in (4.32) is suppressed by the factor $|U_{GG}(\mu_j, M)|^2 \approx 0.147$. Not including these resummation effects would vastly overestimate the decay rate.

4.6.2 $S \to t\bar{t}$ Decay

The largest two-body decay rate into quark-antiquark final states is likely to be that into top quarks. At leading order in perturbation theory the corresponding decay rate is given by

$$\Gamma(S \to t\bar{t}) = \frac{3}{16\pi}\,\frac{v^2 M_S}{M^2}\,\sqrt{1 - \frac{4m_t^2}{M_S^2}}\,\left|\left(\mathbf{C}_{Q_L\bar{u}_R}\right)_{33}(m_t)\right|^2. \tag{4.39}$$

At the high matching scale $\mu_h = M$ the coefficient $\boldsymbol{C}_{Q_L\bar{u}_R}$ has been given in (4.16). The related coefficient $\mathbf{C}_{Q_L\bar{u}_R}$ (with a straight letter "C") is obtained by transforming this expression to the quark mass basis. Including only QCD effects, it obeys the RG equation [1]

$$\mu\,\frac{d}{d\mu}\,\mathbf{C}_{Q_L\bar{u}_R}(\mu) = \left[\frac{4}{3}\gamma^{(3)}_{\text{cusp}}\left(\ln\frac{M_S^2}{\mu^2} - i\pi\right) + 2\gamma^q\right]\mathbf{C}_{Q_L\bar{u}_R}(\mu)\,, \tag{4.40}$$

where $\gamma^q = -\alpha_S/\pi + \mathcal{O}(\alpha_S^2)$. Solving this equation, we obtain

$$\mathbf{C}_{Q_L\bar{u}_R}(\mu) = U_{q\bar{q}}(\mu, M)\,\mathbf{C}_{Q_L\bar{u}_R}(M)\,, \tag{4.41}$$

with

$$U_{q\bar{q}}(\mu, M) = \exp\left[\frac{8}{147}\, g(\mu, M) + \frac{8}{21}\left(i\pi + \frac{3}{2} - \ln\xi\right)\ln r\right]. \tag{4.42}$$

Evolving the coefficient down to the scale of the top-quark mass, we find

$$U_{q\bar{q}}(m_t, M) \approx 0.90\, e^{0.31i}\,. \tag{4.43}$$

The decay rate in (4.39) is suppressed by the factor $|U_{q\bar{q}}(m_t, M)|^2 \approx 0.81$. In this case, resummation effects have a more modest impact on the decay rate.

4.6.3 $S \to \gamma\gamma$ Decay

It is instructive to also consider an example where only electroweak Sudakov logarithms contribute. The diphoton decay mode has a very similar structure as the $S \to gg$ mode discussed above. At leading order in perturbation theory the decay rate is given by

$$\Gamma(S \to \gamma\gamma) = \frac{M^2}{M_S}\,\pi\alpha^2\Big(|C_{WW}(m_W)+C_{BB}(m_W)|^2+|\widetilde{C}_{WW}(m_W)+\widetilde{C}_{BB}(m_W)|^2\Big)\,. \quad (4.44)$$

Here $\alpha \approx 1/137.036$ is the fine-structure constant. The Wilson coefficients need to be evolved down to the scale of electroweak symmetry breaking, which we identify with the mass of the W boson. Below the weak scale the running stops. At the high matching scale $\mu_h = M$ the relevant coefficients have been given in (4.17). The coefficients C_{WW} and $\widetilde{C}_{WW}$ obey the same RG equation [1]

$$\mu\,\frac{d}{d\mu}\,C_{WW}(\mu) = \left[2\gamma^{(2)}_{\rm cusp}\left(\ln\frac{M_S^2}{\mu^2} - i\pi\right) + 2\gamma^W\right] C_{WW}(\mu)\,. \quad (4.45)$$

The relevant cusp anomalous dimension is

$$\gamma^{(2)}_{\rm cusp} = \frac{\alpha_2}{\pi} + \left(2 - \frac{\pi^2}{6}\right)\left(\frac{\alpha_2}{\pi}\right)^2 + \dots\,, \quad (4.46)$$

whereas γ^W vanishes at one-loop order. Here $\alpha_2 = g^2/(4\pi)$ is the coupling constant of $\mathrm{SU}_W(2)$. The Wilson coefficients C_{BB} and $\widetilde{C}_{BB}$, on the other hand, are scale independent at leading logarithmic order. It follows that

$$C_{WW}(m_W) + C_{BB}(m_W) = U_{WW}(m_W, M)\,C_{WW}(M) + U_{BB}(m_W, M)\,C_{BB}(M) \quad (4.47)$$

and similarly for the other two coefficients in (4.44), where $U_{BB}(m_W, M) \approx 1$, while $U_{WW}(\mu, M)$ is given by an expression similar to (4.36), but with different numerical coefficients and with $\alpha_S(\mu)$ replaced by the coupling $\alpha_2(\mu)$. Numerically, we obtain

$$U_{WW}(m_W, M) \approx 0.80\,e^{0.23i}\,, \quad U_{BB}(m_W, M) \approx 1\,. \quad (4.48)$$

The impact of these resummation effects on the diphoton decay rate depends on the values of κ_1/M and $\mathrm{Tr}(\boldsymbol{X})$ in (4.17). In the limit where the term proportional to κ_1 can be neglected, the decay rate is suppressed by the factor $|0.9\,U_{WW}(m_W, M)+0.1|^2 \approx 0.67$. The resummation of electroweak Sudakov logarithms thus has a sizable impact on the rate.

4.6.4 $S \to hh$ Decay

As a final example we consider the decay mode $S \to hh$, whose rate is given by

$$\Gamma_{S\to hh} = \frac{M^2}{32\pi M_S}\sqrt{1 - \frac{4m_h^2}{M_S^2}}\,|C_{\phi\phi}(m_h)|^2\,. \quad (4.49)$$

The Wilson coefficient satisfies the RG equation [1]

$$\mu \frac{d}{d\mu} C_{\phi\phi}(\mu) = \left[\left(\frac{1}{4} \gamma^{(1)}_{\rm cusp} + \frac{3}{4} \gamma^{(2)}_{\rm cusp} \right) \left(\ln \frac{M_S^2}{\mu^2} - i\pi \right) + 2\gamma^\phi \right] C_{\phi\phi}(\mu) \,, \tag{4.50}$$

where

$$\begin{aligned} \gamma^{(1)}_{\rm cusp} &= \frac{\alpha_1}{\pi} - \frac{17}{6} \left(\frac{\alpha_1}{\pi} \right)^2 + \dots \,, \\ \gamma^\phi &= -\frac{\alpha_1}{4\pi} - \frac{3\alpha_2}{4\pi} + \frac{3y_t^2}{8\pi^2} + \dots \,, \end{aligned} \tag{4.51}$$

and $\gamma^{(2)}_{\rm cusp}$ has been given in (4.46). Here α_1 is the coupling constant of $\mathrm{U}_Y(1)$ (not rescaled by a factor 5/3). Since there are now three different couplings involved, it is easiest to integrate the RG equation (4.50) numerically, using the one-loop β-functions for the various couplings. Writing the solution in the form $C_{\phi\phi}(m_h) = U_{\phi\phi}(m_h, M)\, C_{\phi\phi}(M)$, we find

$$U_{\phi\phi}(m_h, M) \approx 0.79\, e^{0.08i} \,. \tag{4.52}$$

It follows that the di-Higgs decay rate is suppressed by the factor $|U_{\phi\phi}(m_h, M)|^2 \approx 0.62$, which is once again a significant correction.

4.7 Conclusions

When a new heavy resonance beyond the SM is discovered, it will be important to have an EFT description of its decay and production modes, in which the NP scale M is disentangled from the electroweak scale. This effective theory should be able to deal with the situation that the new state is a member of a larger sector of NP. In this paper we have illustrated the recently developed $\mathrm{SCET}_{\rm BSM}$ approach [1] to solve this problem in the context of an extension of the SM by a heavy scalar singlet S and a set of vector-like heavy quarks. We have performed the matching calculation for the Wilson coefficients in the effective Lagrangian both at tree level and including the leading one-loop corrections. These coefficients are in general non-trivial functions of the mass ratio $\xi = M_S^2/M^2$, where M_S is the mass of the scalar resonance while M sets the masses of the vector-like quarks. In this way, our effective theory resums an infinite tower of local operators in the conventional effective field-theory approach to describe the interactions of S with SM fields. For the special case of the decay $S \to Zh$, the Wilson coefficient of the relevant operator contains logarithms of the form $\ln(M_S^2/\mu^2)$ and $\ln(M^2/\mu^2)$ with coefficients that depend in a non-polynomial way on the ratio ξ. We have explained the origin of this effect and demonstrated how the scale dependence is cancelled in the effective theory.
The $\mathrm{SCET}_{\rm BSM}$ framework allows one to resum large Sudakov logarithms affecting the decay rates of S into SM particles. We have explicitly performed the resummation at leading logarithmic order for the decays $S \to 2\,\text{jets}$, $S \to t\bar{t}$, $S \to \gamma\gamma$ and $S \to hh$, finding that in all cases the decay rates are significantly reduced. It is important to take these resummation effects into account when placing bounds on the masses and couplings of

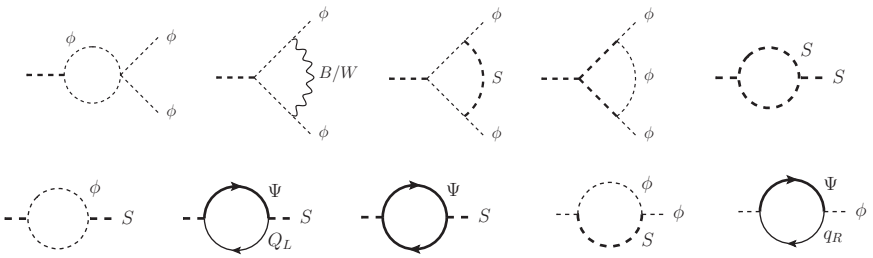

Figure 4.6: One-loop diagrams contributing to the parameter δ_{κ_1}. The graphs in the last two lines show the matching corrections to the wave-function renormalisation constants of the heavy resonance S and the Higgs scalar ϕ.

hypothetical new heavy particles. Possible avenues worthy to pursue in the future include extensions of our work to resonances of non-zero spin as well as particles that are not singlets under the SM gauge group. In this way, the SCET_{BSM} approach can be applied to collider searches for heavy particles proposed in many extensions of the SM.

4.8 Appendix I: Calculation of the Quantity δ_{κ_1}

Here we report our result for the one-loop coefficient δ_{κ_1} in (4.21). It receives contributions from the vertex-correction diagrams shown in the first line of Figure 4.6 as well as from hard matching corrections to the wave-function renormalisation constants of the scalar fields. We find

$$\begin{aligned}
\delta_{\kappa_1} = {} & \frac{3\lambda_H}{8\pi^2}\,(L_S-2) - \frac{3g^2+g'^2}{64\pi^2}\left(L_S^2 - L_S + 2 - \frac{\pi^2}{6}\right) \\
& + \frac{\kappa_1^2}{16\pi^2 M_S^2}\left(\frac{1}{2}+\frac{\pi^2}{12}+i\pi\ln 2\right) + \frac{\kappa_1\lambda_3}{16\pi^2 M_S^2}\,\frac{\pi^2}{9} \\
& - \frac{\lambda_3^2}{64\pi^2 M_S^2}\left(\frac{2\pi}{3\sqrt{3}}-1\right) + \frac{N_c}{8\pi^2}\,\text{Tr}(\boldsymbol{V}_Q^\dagger \boldsymbol{V}_Q)\left[L_M - 1 - \frac{1}{\xi} - \frac{1-\xi^2}{\xi^2}\ln(1-\xi)\right] \\
& + \frac{N_c}{8\pi^2}\,\text{Tr}(\boldsymbol{X}^2)\left[L_M - 1 - \frac{4}{\xi} + \frac{2(2+\xi)}{\xi}\sqrt{\frac{4-\xi}{\xi}}\,g(\xi)\right] \\
& + \frac{N_c}{8\pi^2}\,\text{Tr}(\tilde{\boldsymbol{X}}^2)\left[L_M - 1 + \frac{2(2-\xi)}{\sqrt{\xi(4-\xi)}}\,g(\xi)\right] \\
& + \frac{N_c}{8\pi^2}\,\text{Tr}(\boldsymbol{G}_u^\dagger \boldsymbol{G}_u + \boldsymbol{G}_d^\dagger \boldsymbol{G}_d)\left(L_M - \frac{1}{2}\right),
\end{aligned} \tag{4.53}$$

where $L_M = \ln(M^2/\mu^2)$ and $L_S = \ln(M_S^2/\mu^2) - i\pi$, and the function $g(\xi)$ has been given in (4.19).

4.9 Appendix II: Coefficient Functions $f_i(\xi)$

The explicit expressions for the functions $f_i(\xi)$ entering the result for $\widetilde{C}_{\phi\phi\phi\phi}$ in (4.25) are

$$
\begin{aligned}
f_1(\xi) &= \xi - (1-\xi)\ln^2(1-\xi) - (1-\xi)\,\mathrm{Li}_2(\xi) + 4\xi\, g^2(\xi),\\
f_2(\xi) &= -\xi + (1-\xi)\,\mathrm{Li}_2(\xi) + 2\xi\, g^2(\xi)\,,\\
f_3(\xi) &= -\frac{5-\xi}{4} - \frac{3-4\xi+\xi^2}{4\xi}\ln(1-\xi) + \frac{1}{2\xi}\,\mathrm{Li}_2(\xi) + \frac{1}{2}\sqrt{\xi(4-\xi)}\, g(\xi) - g^2(\xi)\,,\\
f_4(\xi) &= -2 + \xi - \frac{2(1-\xi)^2}{\xi}\ln(1-\xi) + 4\sqrt{\xi(4-\xi)}\, g(\xi) - 8g^2(\xi)\,,\\
f_5(\xi) &= \xi - (1+\xi)\ln^2(1-\xi) - (1+\xi)\,\mathrm{Li}_2(\xi) - \xi\,\frac{\pi^2}{12}\,,\\
f_6(\xi) &= -\xi + \xi\,\mathrm{Li}_2(-\xi) + (1+\xi)\,\mathrm{Li}_2(\xi)\,,\\
f_7(\xi) &= -\frac{5-\xi}{4} - \frac{3-2\xi-\xi^2}{4\xi}\ln(1-\xi) - \frac{4-3\xi}{4\xi}\ln^2(1-\xi) + \frac{2+5\xi}{4\xi}\,\mathrm{Li}_2(\xi)\,,\\
f_8(\xi) &= -2 + \xi - \frac{2(1-\xi^2)}{\xi}\ln(1-\xi) + 2\ln^2(1-\xi) + 2\,\mathrm{Li}_2(\xi)\,,\\
f_9(\xi) &= \frac{1-\xi}{\xi}\ln^2(1-\xi) - \mathrm{Li}_2(\xi)\,,\\
f_{10}(\xi) &= \frac{3-2\xi}{\xi}\ln^2(1-\xi) - 3\,\mathrm{Li}_2(\xi)\,.
\end{aligned}
\tag{4.54}
$$

5 Constraints on the Standard-Model Effective Theory

In this chapter we develop and apply a framework to derive bounds on the parameters of the SMEFT by comparing theoretical predictions with experimental data. Our approach addresses inconsistencies in current state-of-the-art collider analyses of this type. We discuss the three main inconsistencies and present our approach in Section 5.1. The application to different processes gives rise to bounds on a variety of SMEFT parameters. Concretely, we apply our approach to dijet production in Section 5.2 and to dilepton production in Section 5.3. The results presented in this chapter are published in [10] and [16].

5.1 Consistency Requirements for the Analyses

The first consistency requirement concerns the question whether to perform the SMEFT expansion in inverse powers of the NP scale M at the level of the amplitude or the squared amplitude. In this work we focus on processes where the leading order (LO) contribution arises from the SM piece $\mathcal{L}_{\text{SM}}$. We furthermore assume both baryon- and lepton-number conservation. It follows that contributions to the amplitude beyond the LO arise from operators with even mass dimension [235]. Thus, a generic amplitude including the NLO piece in the SMEFT expansion exhibits the form

$$\mathcal{A} = \mathcal{A}_{\text{SM}} + \frac{1}{M^2}\,\mathcal{A}_{\text{dim6}} + \dots\,, \tag{5.1}$$

where the terms $\mathcal{A}_{\text{SM}}$ and $\mathcal{A}_{\text{dim6}}$ are the LO and NLO pieces in the series expansion and the dots represent the terms of higher order which are not included. Squaring this expression we find

$$|\mathcal{A}|^2 = |\mathcal{A}_{\text{SM}}|^2 + \frac{1}{M^2}\,2\,\text{Re}\left[\mathcal{A}_{\text{SM}}^*\,\mathcal{A}_{\text{dim6}}\right] + \frac{1}{M^4}\,|\mathcal{A}_{\text{dim6}}|^2 + \dots\,. \tag{5.2}$$

Including the NNLO contribution from dimension-eight operators the amplitude is

$$\mathcal{A} = \mathcal{A}_{\text{SM}} + \frac{1}{M^2}\,\mathcal{A}_{\text{dim6}} + \frac{1}{M^4}\,\mathcal{A}_{\text{dim8}} + \dots\,, \tag{5.3}$$

where $\mathcal{A}_{\text{dim8}}$ denotes the NNLO contribution which is suppressed by four powers of the NP scale. Squaring this expression we find

$$|\mathcal{A}|^2 = |\mathcal{A}_{\text{SM}}|^2 + \frac{1}{M^2}\,2\,\text{Re}\left[\mathcal{A}_{\text{SM}}^*\,\mathcal{A}_{\text{dim6}}\right] + \frac{1}{M^4}\,\left(|\mathcal{A}_{\text{dim6}}|^2 + 2\,\text{Re}\left[\mathcal{A}_{\text{SM}}^*\,\mathcal{A}_{\text{dim8}}\right]\right) + \dots\,. \tag{5.4}$$

Comparing this square of the NNLO amplitude with the square of the NLO amplitude from equation (5.2) we observe that they differ by the interference piece of the NNLO amplitude with the LO amplitude, namely the term $\sim 2\,\mathrm{Re}\,[\mathcal{A}^*_{\mathrm{SM}}\,\mathcal{A}_{\mathrm{dim8}}]$ at order $1/M^4$. However, it is crucial to expand the squared amplitude rather than the amplitude to the desired order in power counting since the squared amplitude enters physical quantities such as cross sections and decay rates. This procedure is completely familiar from the treatment of other power series in perturbative QFT calculations. In a one-loop calculation in Quantum Electrodynamics (QED) divergencies at order α^2 emerge which are cancelled by the interference of the two-loop amplitude with the SM amplitude. A truncation at order α of the amplitude rather than the squared amplitude thus gives rise to divergent cross sections in this case. In the context of the SMEFT power series one problematic aspect of expanding the amplitude as in (5.1) and using equation (5.2) for the squared amplitude is that transformations between different bases of the dimension-six Lagrangian $\mathcal{L}^{(6)}$ in general induce changes in the pieces of the Lagrangian beyond the dimension-six level as discussed in Section 2.3. Including the term $\sim |\mathcal{A}_{\mathrm{dim6}}|^2$ while neglecting the term $\sim 2\,\mathrm{Re}\,[\mathcal{A}^*_{\mathrm{SM}}\,\mathcal{A}_{\mathrm{dim8}}]$ in the squared amplitude (5.4) at order $1/M^4$ may - depending on the considered process - thus result in a dependence of physical quantities on the choice of the operator basis for the Lagrangian piece $\mathcal{L}^{(6)}$.
Considering the squared amplitude in equation (5.4) there are two options for a consistent expansion of physical quantities. The first option is to work at the level of the dimension-six Lagrangian $\mathcal{L}^{(6)}$ truncating the squared amplitudes after the second term in equation (5.4). The alternative is to include contributions from both $\mathcal{L}^{(6)}$ and $\mathcal{L}^{(8)}$ and thus to truncate the expansion in equation (5.4) after the third term. In either approach it is crucial to take into account effects of higher-order in the expansion by introducing an appropriate theory uncertainty. The second approach exhibits two main disadvantages with respect to collider analyses. In a collider study the goal is to derive bounds on the Wilson coefficients and the scale M by fitting experimental data with theoretical predictions which include the SMEFT effects. In general, the number of contributing operators grows with the order in the expansion of $\mathcal{L}_{\mathrm{SMEFT}}$. Thus, adding effects from $\mathcal{L}^{(8)}$ on top of the effects from $\mathcal{L}^{(6)}$ increases the number of degrees of freedom in the fits. Furthermore, the theory predictions for cross sections contain both linear and quadratic terms in the dimension-six Wilson coefficients and terms linear in the Wilson coefficients of dimension-eight operators when effects of $\mathcal{L}^{(8)}$ are included. In contrast to that the theory predictions depend only linearly on the dimension-six Wilson coefficients when only the effect of $\mathcal{L}^{(6)}$ is included. These disadvantages make it much more challenging to constrain the parameter space in the approach where SMEFT effects up to and including dimension-eight operators are taken into account. Therefore, we truncate the series expansion in equation (5.4) after the second term for our signal prediction. We introduce a theory uncertainty scaling as $1/M^4$ to account for the third term. We provide the details about this theory uncertainty in the collider analyses in Sections 5.2 and 5.3.
The second consistency requirement concerns the main assumption about the SMEFT expansion, namely that contributions from higher-dimensional operators are suppressed with respect to contributions from operators of lower mass dimension. In this work we

consider processes at tree level where both Feynman diagrams with only SM vertices and Feynman diagrams with exactly one vertex arising from $\mathcal{L}^{(6)}$ contribute. It follows from a dimensional analysis that the diagrams with one vertex from $\mathcal{L}^{(6)}$ are suppressed by a factor s/M^2 relative to the diagrams with only SM vertices, where we assume four spacetime dimensions. The energy scale $\sqrt{s}$ represents the typical energy scale of the process such as the centre-of-mass energy. At the level of the squared amplitude the second term in equation (5.4) is suppressed by a factor s/M^2 with respect to the first term. Since the characteristic energy scale - the partonic centre-of-mass energy $\sqrt{s}$ - is not fixed at a hadron collider it is crucial to restrict any analysis to the regime where the SMEFT expansion is valid. This implies that for a particular collision event the criterion $s/M^2 \ll 1$ must hold. Established methods in practice are to remove events where $s > M^2$ from the analysis by hand [61–64]. While the implementation of this procedure in the analysis is straightforward, it corresponds to a physically not motivated theory uncertainty which is zero below the scale M and infinity above. In particular, there exists no measure of how reliable the influence of an event with an energy below but very close to M is in the analysis. As a major improvement of this method the theory uncertainty we introduce to the fit naturally removes the influence of the events where the condition is not fulfilled on the fit. The reason is that for increasing s the theory uncertainty grows as s^2/M^4 compared to the signal which only grows as s/M^2.
The third consistency requirement adresses the number of operators considered in an analysis. Deriving bounds on single Wilson coefficients while all other Wilson coefficients are set to zero is problematic because of two reasons. First, it is only possible in special cases to generate a single operator in a tree-level matching of a UV-complete model onto the SMEFT [236]. Second, one does not allow for cancellations between contributions from different operators. Hence, the bounds obtained with only one operator considered are artificially stringent. In our analysis we thus include all the operators which contribute under the specified assumptions and derive bounds on linear combinations of Wilson coefficients contributing to different observables.

5.2 Constraints From Dijet Production

Our focus in this analysis is the process of dijet production at the LHC. In dijet production, a partonic hard-scattering event produces energetic quarks or gluons. These quarks or gluons hadronise and form two energetic particle jets which are observed in the detectors. Extensive studies to constrain SMEFT parameters in dijet events exist [58, 59, 237–240]. In this work we focus on an analysis by the CMS collaboration [59].

5.2.1 Partonic Dijet Production in the Standard-Model Effective Theory

In our analysis we work at tree level and focus on QCD contributions in the SM piece. We collect a selection of tree-level diagrams for partonic processes relevant for dijet production in Figure 5.1. The first three diagrams are SM contributions, namely t-channel

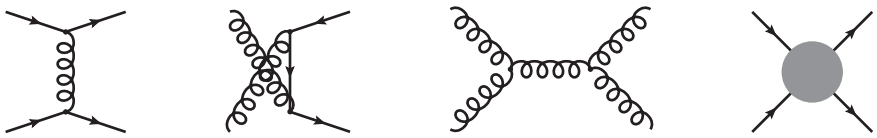

Figure 5.1: Partonic Feynman diagrams contributing to dijet production at tree level. The first three diagrams are SM contributions: t-channel quark scattering, u-channel gluon annihilation into quarks and s-channel gluon scattering. The fourth diagram represents a SMEFT contribution from a four-quark operator.

Q_{uu}	$(\bar{u}_p\gamma_\mu u_r)\,(\bar{u}_s\gamma^\mu u_t)$	$Q_{Qu}^{(8)}$	$\left(\bar{Q}_p\gamma_\mu T^a Q_r\right)(\bar{u}_s\gamma^\mu T^a u_t)$
Q_{dd}	$\left(\bar{d}_p\gamma_\mu d_r\right)\left(\bar{d}_s\gamma^\mu d_t\right)$	$Q_{Qd}^{(1)}$	$\left(\bar{Q}_p\gamma_\mu Q_r\right)\left(\bar{d}_s\gamma^\mu d_t\right)$
$Q_{ud}^{(1)}$	$(\bar{u}_p\gamma_\mu u_r)\left(\bar{d}_s\gamma^\mu d_t\right)$	$Q_{Qd}^{(8)}$	$\left(\bar{Q}_p\gamma_\mu T^a Q_r\right)\left(\bar{d}_s\gamma^\mu T^a d_t\right)$
$Q_{ud}^{(8)}$	$(\bar{u}_p\gamma_\mu T^a u_r)\left(\bar{d}_s\gamma^\mu T^a d_t\right)$	$Q_{QQ}^{(1)}$	$\left(\bar{Q}_p\gamma_\mu Q_r\right)\left(\bar{Q}_s\gamma^\mu Q_t\right)$
$Q_{Qu}^{(1)}$	$\left(\bar{Q}_p\gamma_\mu Q_r\right)(\bar{u}_s\gamma^\mu u_t)$	$Q_{QQ}^{(3)}$	$\left(\bar{Q}_p\gamma_\mu \tau^i Q_r\right)\left(\bar{Q}_s\gamma^\mu \tau^i Q_t\right)$

Table 5.1: Dimension-six four-fermion operators from the Warsaw basis contributing to dijet production at tree level under the assumption that the operators conserve baryon number, lepton number and CP.

quark scattering, u-channel gluon annihilation into quarks and s-channel gluon scattering. The fourth diagram is a SMEFT contribution arising from a four-quark operator. The Feynman diagrams for the partonic processes contributing to dijet production can be grouped into three categories: diagrams containing only quarks, diagrams containing both quarks and gluons and diagrams containing only gluons.

We assume that the contributing dimension-six operators conserve baryon number, lepton number and CP. From the 25 dimension-six four-fermion operators in Table 2.2 the ten operators collected in Table 5.1 contribute at the amplitude level under these assumptions. These operators are Q_{uu}, Q_{dd}, $Q_{ud}^{(1)}$ and $Q_{ud}^{(8)}$ from the $(\bar{R}R)(\bar{R}R)$ class, $Q_{Qu}^{(1)}$, $Q_{Qu}^{(8)}$, $Q_{Qd}^{(1)}$ and $Q_{Qd}^{(8)}$ from the $(\bar{L}L)(\bar{R}R)$ class and $Q_{QQ}^{(1)}$, $Q_{QQ}^{(3)}$ from the $(\bar{L}L)(\bar{L}L)$ class. For our analysis we assume that the Wilson coefficients of these operators exhibit the flavour structure $\delta_{pr}\delta_{st}$. A much more general flavour structure would introduce many more parameters to the fit and many of these parameters would be in conflict with bounds from flavour-physics analyses. A vast amount of studies translating experimental results from flavour physics into bounds on SMEFT parameters exist (see, e.g. [241] and references therein). Compared to the concept of minimal flavour violation (MFV) [242] our assumption about the flavour structure is slightly more stringent.

Calculating the squared partonic amplitude for dijet production at tree level we observe that the amplitude arising from the operators $Q_{ud}^{(1)}$, $Q_{Qu}^{(1)}$ and $Q_{Qd}^{(1)}$ does not interfere with the SM amplitude. These operators contain quark fields with distinct weak charges but the same colour charges. However, in the Feynman diagrams for the SM amplitude the

external quarks couple to gluons. The non-interference of the three operators arises from the fact that gluons couple quarks with the same weak charge but distinct colour charge. Thus, there are seven four-quark operators contributing to the cross section at NLO in the SMEFT expansion, namely Q_{uu}, Q_{dd}, $Q_{ud}^{(8)}$, $Q_{Qu}^{(8)}$, $Q_{Qd}^{(8)}$, $Q_{QQ}^{(1)}$ and $Q_{QQ}^{(3)}$.
Except for the four-fermion operators the following operator from the Warsaw basis contributes to the dijet amplitude by gluon scattering:

$$Q_G = f^{abc}\, G_\mu^{a,\nu} G_\nu^{b,\rho} G_\rho^{c,\mu}\,. \tag{5.5}$$

At the level of the squared amplitude the contribution from this operator does not interfere with the SM contribution since the helicity structure of the gluon fields differs between the two amplitudes [243, 244]. In more general terms the question wether a certain SMEFT operator gives rise to interference pieces with tree-level SM amplitudes is studied in [245] based on helicity arguments. For an analysis of the effects of the operator Q_G in three-jet events we refer the reader to [246].
We focus on the seven interfering four-quark operators in the following. To distinguish the SMEFT contribution from the SM contribution it is necessary to define suitable kinematic variables. Considering the partonic Feynman diagrams in Figure 5.1 we counterclockwise assign the two ingoing four-momenta p_1 and p_2 to the incoming partons and the two outgoing four-momenta p_3 and p_4 to the outgoing partons. We discussed in Section 5.1 that the effects of four-fermion operators in general grow with energy. Thus, it is reasonable to use the dijet invariant mass m_{jj} as one kinematic variable. Furthermore, we follow the CMS analysis in defining an angular variable χ. We demonstrate below the ability to distinguish SMEFT contributions from the SM in angular spectra. Concretely, the variables m_{jj} and χ are defined as

$$m_{jj} = \sqrt{(p_3 + p_4)^2}\,, \qquad \chi = e^{|y_3 - y_4|}\,. \tag{5.6}$$

The pseudorapidities of the final-state partons are $y_i = -\ln\left[\tan\left(\theta_i/2\right)\right]$, where $i \in \{3, 4\}$. The angles θ_i are the scattering angles with respect to the axis defined by the three-momentum piece of p_1. Defined as a difference of pseudorapidities the quantity χ is invariant with respect to boosts along this axis. It follows from four-momentum conservation that $\chi = e^{2|y_3|} = e^{2|y_4|}$ in the partonic analysis. We note that the value of χ ranges from $\chi = 1$ corresponding to the final-state parton being emitted at an angle of $\theta_3 = \pi/2$ to $\chi \to \infty$ in the limit of $\theta_3 \to 0$ or $\theta_3 \to \pi$.
To illustrate the discrimination power of distributions in the kinematic variables we consider the partonic process $u(p_1)\, d(p_2) \to u(p_3)\, d(p_4)$. The partonic cross section is shown in Figure 5.2 as a function of m_{jj} (left) and differential in χ (right). The distribution in m_{jj} is plotted in arbitrary units and the differential cross section in χ is normalised to the cross section in the range $\chi \in [1, 16]$. We show the SM cross section (blue, solid) and the interference contribution at order $1/M^2$ arising from the operators $Q_{QQ}^{(3)}$ (red, dashed) and $Q_{Qu}^{(8)}$ (black, dot-dashed). The interference distributions in the left panel coincide. We observe in the left panel that the relative importance of the interference cross section

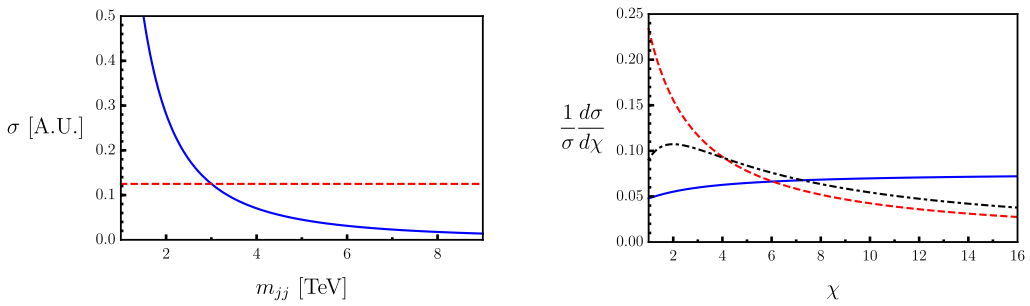

Figure 5.2: Cross section for the partonic process $u(p_1)\,d(p_2) \to u(p_3)\,d(p_4)$ as a function of m_{jj} in arbitrary units (left panel) and differential in the angular variable χ (right panel). The distributions in the right panel are normalised to the total cross section in the range $\chi \in [1, 16]$. Shown are the distributions for the SM (blue, solid) and the interference pieces arising from the operators $Q_{QQ}^{(3)}$ (red, dashed) and $Q_{Qu}^{(8)}$ (black, dot-dashed). The distributions for the two interference pieces in the left panel coincide.

compared with the SM cross section grows with the dijet invariant mass. Concerning the angular behaviour in the right panel we note that the SM distribution is flat with values between 0.05 for $\chi = 1$ and 0.07 for $\chi = 16$. Furthermore, the angular distribution of the interference piece from the operator $Q_{QQ}^{(3)}$ peaks at low values of χ reaching a value of 0.23 at $\chi = 1$ compared to the distribution from the operator $Q_{Qu}^{(8)}$ which is rather flat with values between 0.11 for $\chi = 2$ and 0.04 for $\chi = 16$. The two operators $Q_{QQ}^{(3)}$ and $Q_{Qu}^{(8)}$ are representatives for two classes of operators with distinct angular behaviour. The interference piece from operators in the first class peaks at small values of χ. These operators are $Q_{QQ}^{(1)}$, $Q_{QQ}^{(3)}$, Q_{uu}, Q_{dd} and $Q_{ud}^{(8)}$. The interference piece from operators in the second class exhibits a rather flat distribution in χ. The operators in this class are $Q_{Qu}^{(8)}$ and $Q_{Qd}^{(8)}$.

5.2.2 Analyses at the Detector Level

At the detector level the kinematic variables m_{jj} and χ are defined as in equation (5.6) with p_3 and p_4 now being the four-momenta of the two jets in the event which have the largest transverse momenta. These jets are referred to as the two hardest jets in the following.

The data taken by the CMS collaboration [59] corresponds to a centre-of-mass energy of 13 TeV and an integrated luminosity of 2.6 fb^{-1}. The data is reported binned in both the dijet invariant mass m_{jj} and the angular variable χ. The bin borders in m_{jj} are

$$m_{jj} \in \{1.9, 2.4, 3.0, 3.6, 4.2, 4.8, 13.0\}\ \text{TeV}\,. \tag{5.7}$$

Events selected for the analysis furthermore fulfill $\chi \in [1, 16]$. The concrete binning in χ

differs between the m_{jj} bins. A cut $|y_{\text{boost}}| < 1.11$ on the boost of the partonic centre-of-mass frame is applied, where $y_{\text{boost}} = (1/2)(y_3 + y_4)$. These criteria select events where the pseudorapitities and transverse momenta of the two hardest jets fulfill $|y_{3,4}| < 2.5$ and $p_{T_{3,4}} > 200$ GeV, respectively. Employing a modified-frequentist approach [247, 248], the CMS collaboration derives bounds on the parameters of the SMEFT by comparing the data with Monte-Carlo (MC) pseudodata. The pseudodata includes both QCD and electroweak corrections at the NLO. The factorisation and the renormalisation scales are set on an event-by-event basis to the average transverse momentum of the two hardest jets.
In our analysis we employ a chi-squared test to obtain bounds at the 95% confidence level (CL) by comparing the CMS data with MC pseudodata. For the generation of the pseudodata we implement the contributing SMEFT operators using `FeynRules` [11] (version 2.0). Working at the LO in QCD we generate partonic pseudodata using `MadGraph5` [12] (version 2.5.3) and employ the program `PYTHIA` [13] (version 6.4) for showering. As a detector simulation we use `DELPHES` [14] (version 3.4.0) with a default CMS detector setting. In our analysis we fix the factorisation and the renormalisation scale such that for partonic MC data the total cross section in one m_{jj} bin agrees with the cross section obtained when the scales are set on an event-by-event basis as in the CMS analysis. With this treatment we find better agreement of our LO simulation with the NLO pseudodata used by CMS.

5.2.3 Linear Combinations of Wilson Coefficients in Angular Spectra

Using our detector-level pseudodata we focus on the two linear combinations of Wilson coefficients in angular spectra discussed at the parton level in Section 5.2.1. For the interference cross section differential in the variable χ we find approximately the following linear combination with an angular spectrum peaking at small values of χ:

$$\left.\frac{d\sigma}{d\chi}\right|_{\text{central}} \propto -\left(C_{QQ}^{(1)} + 0.61\, C_{QQ}^{(3)} + 0.85\, C_{uu} + 0.15\, C_{dd} + 0.20\, C_{ud}^{(8)}\right) . \tag{5.8}$$

Analogously, we obtain the following dependence of the interference piece for the linear combination with a rather flat distribution in χ:

$$\left.\frac{d\sigma}{d\chi}\right|_{\text{flat}} \propto -\left(C_{Qu}^{(8)} + 0.45\, C_{Qd}^{(8)}\right) . \tag{5.9}$$

We normalised both linear combinations (5.8) and (5.9) to the dominant contribution which arises from the operators $Q_{QQ}^{(1)}$ in equation (5.8) and $Q_{Qu}^{(8)}$ in equation (5.9), respectively. The minus signs indicate that a positive Wilson coefficient corresponds to destructive interference whereas a negative Wilson coefficient corresponds to constructive interference with the SM contribution. The coefficients in front of the Wilson coefficients are approximate since they vary between the m_{jj} bins. This effect is caused by the different relative behaviour of the up- and down-type quark parton distribution functions (PDFs) under variation of the momentum fraction which corresponds to a variation of

	$C_{QQ}^{(3)}$	C_{uu}	C_{dd}	$C_{ud}^{(8)}$	$C_{Qd}^{(8)}$
Prefactor range	$[0.54, 0.67]$	$[0.78, 0.91]$	$[0.09, 0.22]$	$[0.14, 0.26]$	$[0.28, 0.64]$

Table 5.2: Range of the prefactor of the Wilson coefficients in the interference cross section for the "central" linear combination (5.8) and the "flat" linear combination (5.9). The linear combinations are normalised to the prefactor of $C_{QQ}^{(1)}$ in (5.8) and to the prefactor of $C_{Qu}^{(8)}$ in (5.9).

m_{jj}. To quantify this variation we show the range of the prefactors in Table 5.2. We note that the values quoted in equations (5.8) and (5.9) correspond to the mean of the lower and the upper border of these ranges. The operators Q_{dd}, $Q_{ud}^{(8)}$ and $Q_{Qd}^{(8)}$ exhibit the most pronounced differences in the prefactors between different m_{jj} bins. For these operators, the prefactors vary approximately by a factor two. In principle, these differences can be exploited to distinguish the contributions from different operators. We leave a detailed study of these effects for future work and derive bounds on the "central" linear combination of Wilson coefficients from (5.8) and the "flat" linear combination (5.9) in this work. Concretely, we use the operators with the dominant contributions, namely $Q_{QQ}^{(1)}$ and $Q_{Qu}^{(8)}$, as representatives of the linear combinations and switch off the other Wilson coefficients.

5.2.4 Reproduction of the CMS Analysis

Before we derive bounds employing our framework we first reproduce the analysis performed by the CMS collaboration. This comparison serves as an important validation step of our method.

In the CMS analysis the Wilson coefficients are fixed and bounds on the scale M are derived. One Wilson coefficient at a time is considered while the other Wilson coefficients are set to zero. The contributing operators are assumed to exhibit the diagonal flavour structure $\delta_{pr}\delta_{rs}\delta_{st}$ in the notation used in Section 5.2.1. Concerning the series expansion of the signal cross section in powers of $1/M^2$ the squared dimension-six piece is taken into account. This corresponds to truncating the expansion of the squared amplitude as in equation (5.2). The bounds are obtained by comparing the theory predictions with the data in angular distributions in χ in the three highest bins in the dijet invariant mass m_{jj}. The angular distributions are normalised to the total cross section in the corresponding m_{jj} bin.

Only in this reproduction step our procedure differs in a few aspects from the one discussed in Sections 5.2.1, 5.2.2 and 5.2.3 to adjust to the CMS analysis. We address these points in the following. We generate a separate set of pseudodata where the Wilson coefficients exhibit the flavour structure used by CMS. Moreover, we include the squared dimension-six piece in the signal cross section. Thus, the signal cross section exhibits the

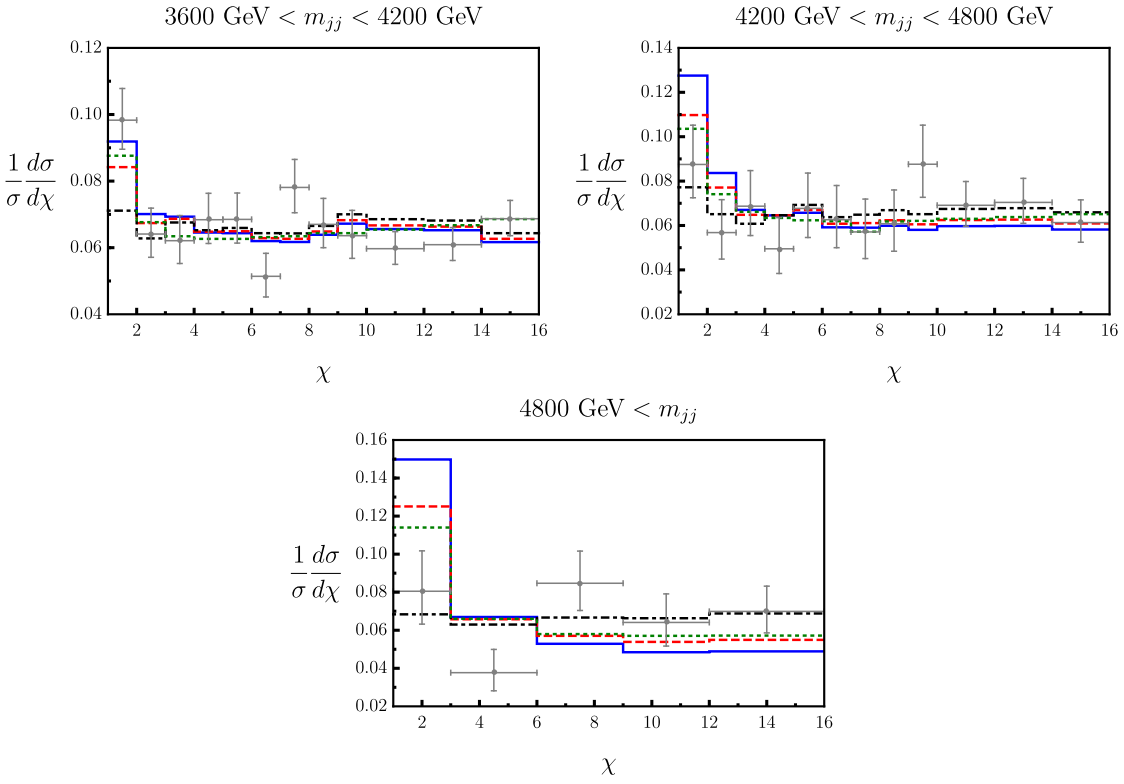

Figure 5.3: Dijet cross section differential in the angular variable χ normalised to the total cross section in the respective m_{jj} bin. We show the following predictions for the choice $M = 11$ TeV and $C_{QQ}^{(1)} = +2\pi$: the SM (black, dot-dashed), the signal including the dimension-six squared piece for $K = 1.0$ (blue, solid) and $K = 1.6$ (red, dashed) and the CMS signal prediction (green, dotted). The grey dots and uncertainty bars represent the data with statistical and systematic uncertainties added in quadrature.

form

$$\sigma|_{\text{signal}} = \sigma_{\text{SM}} + \frac{1}{M^2}\,\sigma_{\text{int}} + \frac{1}{M^4}\,\sigma_{\text{BSM}}\,, \tag{5.10}$$

where the different pieces arise from the three terms in the squared amplitude (5.2). As a validation we focus on the operator $Q_{QQ}^{(1)}$ for the two cases $C_{QQ}^{(1)} = \pm 2\pi$ and set the other Wilson coefficients to zero. To compare our LO prediction with the NLO prediction of CMS we introduce a rescaling factor $K \in [1.0, 1.6]$ for the SM cross section in every m_{jj} bin.

We present the normalised angular distributions in the three highest bins in m_{jj} in Figure 5.3, where we set $M = 11$ TeV and $C_{QQ}^{(1)} = +2\pi$. We show our SM prediction (black, dot-dashed), our signal predictions for $K = 1.0$ (blue, solid) and $K = 1.6$ (red, dashed)

Wilson coefficient	$C_{QQ}^{(1)} = +2\pi$	$C_{QQ}^{(1)} = -2\pi$
CMS	11.5	14.7
$K = 1.0$	12.1	15.2
$K = 1.3$	11.4	14.0
$K = 1.6$	11.0	13.2

Table 5.3: Lower bounds for the scale M in TeV obtained from normalised angular spectra in the three highest m_{jj} bins. The contribution of the operator $Q_{QQ}^{(1)}$ with Wilson coefficients $C_{QQ}^{(1)} = +2\pi$ (destructive interference, second column) and $C_{QQ}^{(1)} = -2\pi$ (constructive interference, third column) is considered. We show the bounds obtained by CMS (second row) and the bounds we find for three different choices for the K factors which rescale the SM distribution to account for higher-order effects (third - fifth row).

and the signal prediction from CMS (green, dotted). The CMS data with statistical and systematic uncertainties added in quadrature are represented by the grey dots and uncertainty bars. The bins in m_{jj} correspond to 3600 GeV $< m_{jj} <$ 4200 GeV (upper left plot), 4200 GeV $< m_{jj} <$ 4800 GeV (upper right plot) and 4800 GeV $< m_{jj}$ (lower plot). We note that in all three m_{jj} bins the deviation of the signal from the SM prediction is most pronounced in the lowest bin in χ. For example, for 4800 GeV $< m_{jj}$ and $K = 1.0$ ($K = 1.6$) the signal distribution is larger by approximately a factor of 2.1 (1.8) compared to the SM distribution in the lowest bin in χ. Although the case $C_{QQ}^{(1)} = +2\pi$ corresponds to destructive interference the signal prediction is larger in the lowest bin in χ compared to the SM distribution. This behaviour arises from the squared dimension-six contribution to the cross section.
Employing a chi-squared test by comparing our signal prediction with the data in the three highest m_{jj} bins we obtain the lower bounds for the scale M in TeV collected in Table 5.3. In the test the statistical and systematic uncertainties quoted by CMS are added in quadrature. We show the bounds for destructive interference with $C_{QQ}^{(1)} = +2\pi$ (second column) and for constructive interference with $C_{QQ}^{(1)} = -2\pi$ (third column) from CMS (second row) and for fixed K factors in the three m_{jj} bins of $K = 1.0$ (third row), $K = 1.3$ (fourth row) and $K = 1.6$ (fifth row). In general the lower bounds on M are larger for the case $C_{QQ}^{(1)} = -2\pi$ since the constructive interference causes the signal prediction to be pulled further away from the data compared to the destructive-interference case. For destructive interference the effect of the interference piece and the dimension-six squared piece cancel out at least to some extend. As an example we find the bound 12.1 TeV $< M$ for destructive interference and $K = 1.0$ compared to the bound 15.2 TeV $< M$ for constructive interference. Our bounds agree with the results from CMS at the level of approximately 5% for the case where we fix $K = 1.0$ in all three m_{jj} bins. Independently varying the values for K between the three m_{jj} bins we

find bounds differing from the CMS bounds by not more than approximately 10%. These differences most likely are caused by our different test procedure, by not including NLO predictions in our test, by the different treatment of both the renormalisation and the factorisation scale and by the different detector simulation.

5.2.5 Implementation of the Consistent Expansion

After the reproduction of the CMS analysis in the last section we apply the consistent SMEFT expansion as described in detail in Section 5.1 in this section and the following parts of the dijet analysis. Concretely, we truncate the signal prediction after the interference term such that the signal cross section exhibits the form

$$\sigma|_{\text{signal}} = \sigma_{\text{SM}} + \frac{1}{M^2}\,\sigma_{\text{int}}\,, \tag{5.11}$$

in contrast to the signal cross section (5.10) used in the last section. To account for the contribution of the dimension-six squared piece we introduce a theory uncertainty $\Delta\sigma_{\text{theo}}$ defined as

$$\Delta\sigma_{\text{theo}} = \frac{1}{M^4}\,\sigma_{\text{BSM}}\,. \tag{5.12}$$

We show the normalised angular distributions in Figure 5.4 for 4200 GeV $< m_{jj} <$ 4800 GeV (left) and 4800 GeV $< m_{jj}$ (right). The grey dots with uncertainty bars are the CMS data with statistical and systematic uncertainties added in quadrature and the blue solid line is the signal cross section as defined in (5.11). The blue shaded areas represent the uncertainties arising from the theory uncertainty (5.12). For this illustration we consider only the contribution from the operator $Q^{(1)}_{QQ}$ and use the parameters $K = 1.0$, $C^{(1)}_{QQ} = +2\pi$ and $M = 15$ TeV.
We note that the theory uncertainties in particular in the two lowest χ bins are sizeable. For 4200 GeV $< m_{jj} <$ 4800 GeV and $1 < \chi < 2$ the relative theory uncertainty amounts to approximately 60%. As discussed in the last section the lowest χ bins are the ones where the difference between the signal and the SM background is most pronounced when including the dimension-six squared piece in the signal. The distributions in Figure 5.4 show that the power to discriminate signal and background arising from these lowest χ bins is lost when excluding the squared-dimension six piece from the signal and including it as a theory uncertainty. In fact, the blue-shaded area indicating the theory uncertainty overlaps with the central values of the data in the two lowest χ bins for both m_{jj} bins. As a consequence, the ability to place a bound on the scale M by employing a chi-squared test it lost completey when including the theory uncertainty. Thus, it is necessary to design a new search in order to derive bounds on the SMEFT parameters.

5.2.6 Constraints from Unnormalised Angular Distributions

The analysis of normalised angular distributions exhibits the advantage that uncertainties cancel out to some extend in the normalisation. However, also the information about the

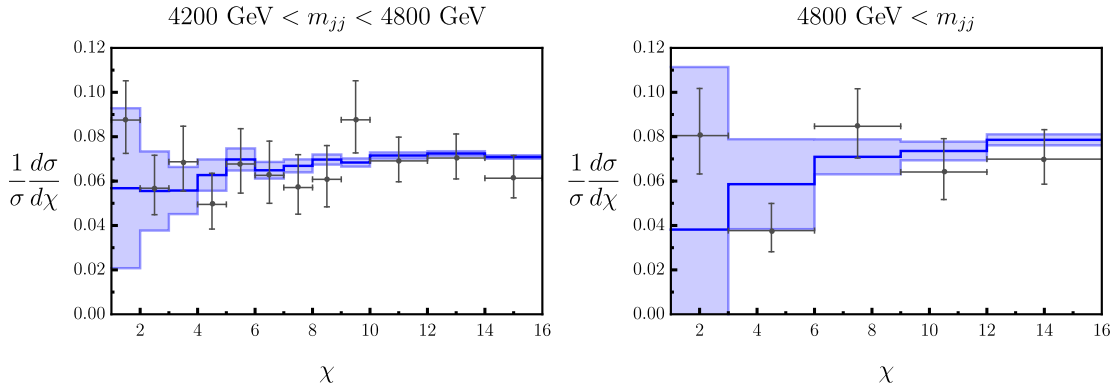

Figure 5.4: Dijet cross section differential in the angular variable χ normalised to the total cross section in the respective m_{jj} bin for 4200 GeV $< m_{jj} <$ 4800 GeV (left) and 4800 GeV $< m_{jj}$ (right). The signal prediction (blue solid line) arising from the operator $Q_{QQ}^{(1)}$ is truncated at the level of dimension-six interference. The parameters are fixed as $K = 1.0$, $C_{QQ}^{(1)} = +2\pi$ and $M = 15$ TeV. The blue shaded areas indicate the uncertainties arising from the dimension-six squared cross section. The grey dots with uncertainty bars represent the CMS data where the statistical and systematic uncertainties are added in quadrature.

total number of events is lost. Therefore, we study unnormalised angular distributions at different integrated luminosities in this section.

Compared to the previous two sections we do not only consider the contribution from the operator $Q_{QQ}^{(1)}$ but also take the operator $Q_{Qu}^{(8)}$ into account. We discussed in Section 5.2.3 that these two operators represent the two linear combinations of operators giving rise to distributions with distinct angular behaviour. The error budget in our analysis contains the statistical, the systematic and the theory error motivated in Section 5.1. We assume a Poisson uncertainty for the event number in every bin in χ as a statistical error. We rescale the systematic uncertainties reported by the CMS collaboration for the normalised distributions with the total number of events from our pseudodata to obtain the systematic error for our analysis. Since this assumption for the systematic error might underestimate the actual uncertainty we introduce an additional factor $R_{\text{syst}} \geq 1$ to rescale the systematic error. In our analysis we study how a variation of this factor effects the bounds. However, we note that by construction we do not assume any improvement of the the relative systematic error with increasing luminosity. Thus, even for the case $R_{\text{syst}} = 1$ our estimate for the systematic uncertainties is rather conservative. For the theory error we use the angular distributions of the squared dimension-six cross sections arising from the operators $Q_{QQ}^{(1)}$ and $Q_{Qu}^{(8)}$. These distributions correspond to the first term in the bracket in the squared amplitude (5.4). At this order the contributions of both operators do not interfere with each other. We do not work with a basis of dimension-eight operators but need to model the effect of the interference term between

the dimension-eight amplitude and the SM amplitude, i.e. the effect of the second term in the bracket in equation (5.4). We proceed as follows to capture both contributions at order $1/M^4$ in the cross section: first, we take the distributions for the operators $Q_{QQ}^{(1)}$ and $Q_{Qu}^{(8)}$ from the squared dimension-six term from our pseudodata. These distributions contain the square of the Wilson coefficients $C_{QQ}^{(1)}$ and $C_{Qu}^{(8)}$. We replace the squared Wilson coefficients by our model for the theory uncertainty according to $C_k^2 \to \Delta_{\text{theo},i}(C_k)$, where $k \in \{1,2\}$ and $i \in \{1,2\}$. The index $k = 1$ is a short-hand notation for $C_{QQ}^{(1)}$ and the index $k = 2$ represents $C_{Qu}^{(8)}$. The index i indicates the model for the theory uncertainty we consider. Our first model is[1]

$$\Delta_{\text{theo},1}(C_k) = \max\left\{C_k^2\,, g_S^2\, C_8\, \sqrt{N_8}\right\}\,. \tag{5.13}$$

The two arguments of the maximum function represent the first and the second term in the bracket in the squared amplitude (5.4). In particular, the second term models the interference of the amplitude arising from dimension-eight operators with the SM amplitude. The quantity N_8 parameterises the number of operators contributing at dimension eight with Wilson coefficients of typical size C_8. Moreover, we assume that the number of interfering dimension-eight operators grows as $\sqrt{N_8}$. The interference piece contains two powers of the strong coupling from the SM amplitude. In the theory uncertainty $\Delta_{\text{theo},1}$ we assume that one of the two contributions dominates in size and neglect the other one. In our second model we add both contributions in quadrature. This second model is[2]

$$\Delta_{\text{theo},2}(C_k) = \sqrt{C_k^4 + \left(g_S^2\, C_8\, \sqrt{N_8}\right)^2}\,. \tag{5.14}$$

In our analysis we fix the value for the size of the dimension-eight Wilson coefficients to $C_8 = 1/2 \sum_k |C_k|$. This choice prevents the dimension-eight Wilson coefficients to deviate sizably from the dimension-six Wilson coefficients. We do not fix the parameter N_8 but vary it in our analysis.

In Figure 5.5 we show the distribution of the event numbers differential in χ for the integrated luminosities $\mathcal{L}_{\text{int}} = 2.6\ \text{fb}^{-1}$ (left) and $\mathcal{L}_{\text{int}} = 50.0\ \text{fb}^{-1}$ (right) for 4.2 TeV $< m_{jj} <$ 4.8 TeV. The SM prediction is shown by the black dot-dashed line and the signal for $C_{QQ}^{(1)} = -2\pi$, $C_{Qu}^{(8)} = 0$ and $M = 11$ TeV is represented by the blue line. The blue-shaded region indicates the uncertainty where we added the statistical uncertainty, the systematic uncertainty with $R_{\text{syst}} = 1$ and the theory uncertainty in quadrature. For the illustration in Figure 5.5 and in general from here on we fix the K factors introduced to compare our LO result with the NLO results obtained from CMS to $K = 1.0$ in all bins in m_{jj}. In Figure 5.5 we observe that the statistical uncertainty plays an important

[1] Note that the factor g_S^2 differs from the published version [10] where g_S without a square is used. The square should be included since the SM amplitude contains g_S^2. This difference gives rise to small changes in the results since $g_S \approx 1$ in our application.

[2] See footnote 1.

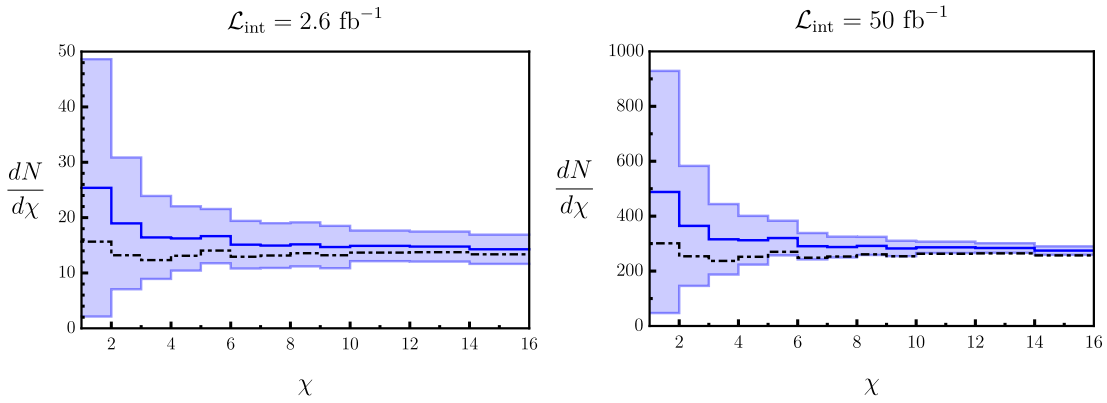

Figure 5.5: Event numbers differential in the angular variable χ for 4.2 TeV $< m_{jj} <$ 4.8 TeV for the integrated luminosities $\mathcal{L}_{\text{int}} = 2.6$ fb^{-1} (left) and $\mathcal{L}_{\text{int}} = 50.0$ fb^{-1} (right). We show the SM prediction (black, dot-dashed) and the signal (blue) for $C_{QQ}^{(1)} = -2\pi$, $C_{Qu}^{(8)} = 0$ and $M = 11$ TeV. The statistical, the systematic and the theory uncertainty are added in quadrature and represented by the blue-shaded area for $R_{\text{syst}} = 1$.

role for the analysis. While in the lowest bin in χ the relative uncertainty amounts to approximately 90% for both luminosities, it decreases for larger values of χ when increasing the luminosity. For example, the relative uncertainty in the fifth bin in χ decreases from approximately 30% for $\mathcal{L}_{\text{int}} = 2.6$ fb^{-1} to approximately 20% for $\mathcal{L}_{\text{int}} = 50$ fb^{-1}.

We derive the projections of bounds to different values of the integrated luminosity by employing our test on the angular spectra in the three highest m_{jj} bins. In our test we assume that the data exactly corresponds to the SM prediction. Omitting the renormalisation of the Wilson coefficients, the SMEFT effects enter our signal prediction by the ratios C_k/M^2. However, the dependence of the theory uncertainty on the parameters C_k and M as specified in equations (5.13) and (5.14) is more complicated. We distinguish two different cases in our analysis. In the first case - the "fixed-Wilson-coefficient case" - we fix the Wilson coefficient and derive bounds for the scale. In the second case - the "fixed-scale case" - we fix the scale and obtain bounds for the Wilson coefficients.

We present our results for the fixed-Wilson-coefficient case in the following. We fix the parameter $R_{\text{syst}} = 1$ and consider the Wilson coefficients $C_{QQ}^{(1)}, C_{Qu}^{(8)} \in \{0, \pm 1, \pm 2\pi, \pm 16\pi^2\}$. The exclusion plots for the case where only one of the two Wilson coefficients is non-zero are collected in Figure 5.6. The four plots show the cases $C_{QQ}^{(1)} = 1$ and $C_{Qu}^{(8)} = 0$ (upper left), $C_{QQ}^{(1)} = 0$ and $C_{Qu}^{(8)} = 1$ (upper right), $C_{QQ}^{(1)} = 2\pi$ and $C_{Qu}^{(8)} = 0$ (lower left) and $C_{QQ}^{(1)} = 0$ and $C_{Qu}^{(8)} = 2\pi$ (lower right). The excluded regions for the scale M are projected to different integrated luminosities. The regions bounded by the solid (dashed) lines arise when the theory uncertainty $\Delta_{\text{theo},1}$ ($\Delta_{\text{theo},2}$) is used. For the blue regions we

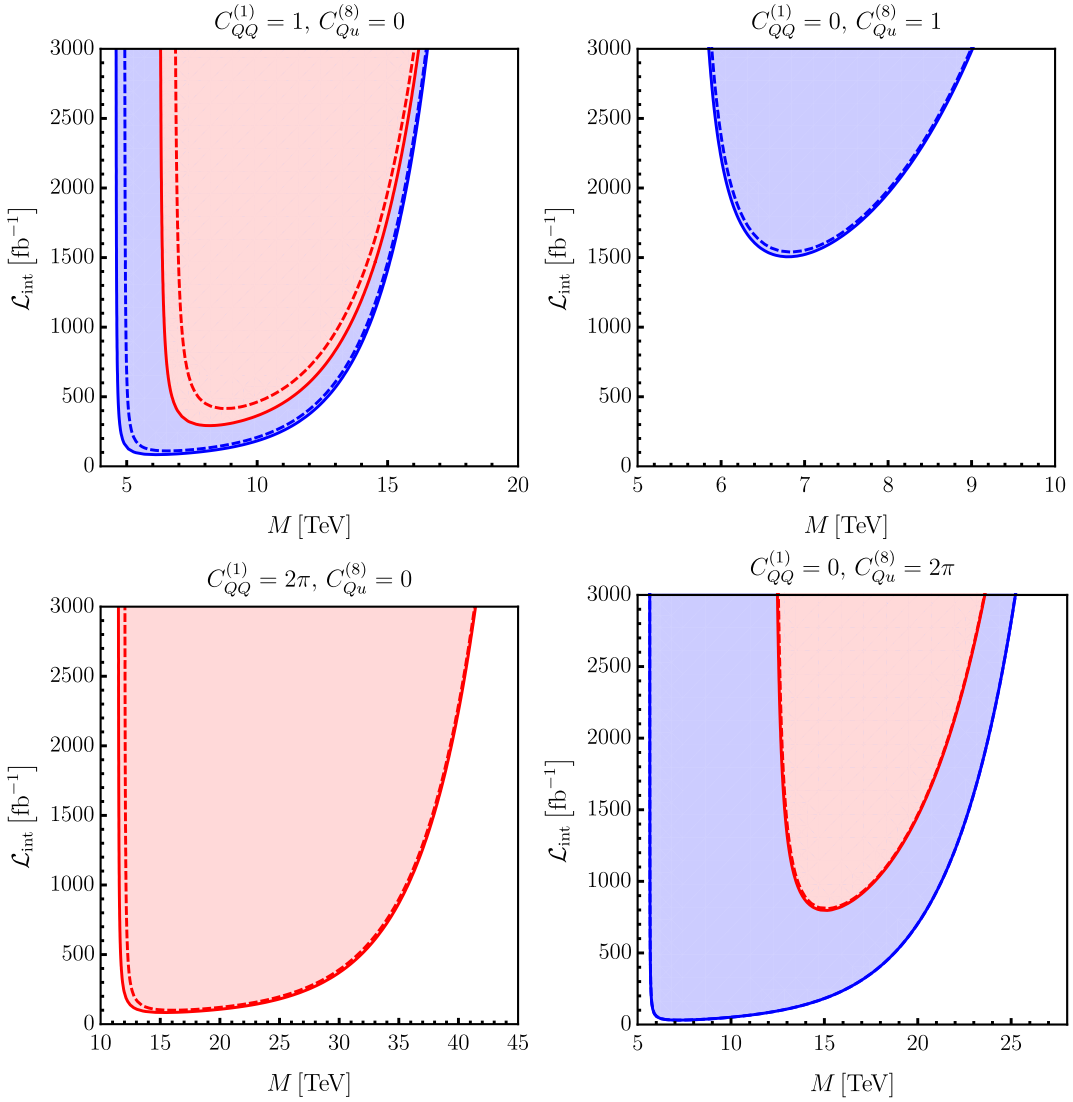

Figure 5.6: Excluded regions for the scale M in the fixed-Wilson-coefficient case for different values of $C_{QQ}^{(1)}$ and $C_{Qu}^{(8)}$, where only one Wilson coefficient is assumed to be non-zero. The bounded regions are projections to different integrated luminosities. The solid (dashed) lines indicate the excluded regions when the theory uncertainty $\Delta_{\text{theo},1}$ ($\Delta_{\text{theo},2}$) is used. The parameter N_8 is fixed to $N_8 = 1$ for the blue regions, to $N_8 = 10$ for the red regions in the upper left plot and to $N_8 = 25$ for the red regions in both lower plots. Note that no excluded region exists for $N_8 = 10$ in the upper right plot. Moreover, both blue lines coincide with the red solid line in the lower left plot and both blue and both red lines coincide in the lower right plot.

fix $N_8 = 1$ and for the red regions we use $N_8 = 10$ (upper left) or $N_8 = 25$ (lower left and lower right). As a general feature of all four considered cases we observe that a certain minimum integrated luminosity is necessary to obtain a bound at all. For example, a minimum integrated luminosity of approximately 1500 fb^{-1} is needed to obtain bounds on M for $C_{QQ}^{(1)} = 0$, $C_{Qu}^{(8)} = 1$ and $N_8 = 1$. This feature reflects the importance of the statistical uncertainty in our analysis. A second general feature of the four exlusion plots is that for a fixed integrated luminosity we do not only find a lower bound for M but rather an excluded region. For example, approximately the region 5 TeV $< M <$ 15 TeV is excluded at an integrated luminosity $\mathcal{L}_{\text{int}} = 1500$ fb^{-1} for $C_{QQ}^{(1)} = 1$ and $C_{Qu}^{(8)} = 0$ for $N_8 = 1$. Finding an excluded region rather than one lower bound on M is a difference to the state-of-the art analyses such as the one performed by the CMS collaboration. Our analysis does not exclude scales below some value since the SMEFT expansion breaks down at some scale for a fixed Wilson coefficient and decreasing values of M. In this limit the theory uncertainty grows as $1/M^4$ compared to the signal only growing as $1/M^2$. As a third general feature of the four cases shown in Figure 5.6 we observe that the excluded region shrinks both when using the theory uncertainty $\Delta_{\text{theo},2}$ instead of $\Delta_{\text{theo},1}$ and when increasing the parameter N_8. In both cases the theory uncertainty increases resulting in less stringent bounds on the scale M.
Comparing the case $C_{QQ}^{(1)} = 1$ and $C_{Qu}^{(8)} = 0$ with the case $C_{QQ}^{(1)} = 0$ and $C_{Qu}^{(8)} = 1$ we observe that the excluded region in the second case is much smaller. While bounds on M can be placed with integrated luminosities above approximately 100 fb^{-1} in the first case integrated luminosities above approximately 1500 fb^{-1} are necessary in the second case. The reason for the difference between these two cases is that the contribution from the operator $Q_{QQ}^{(1)}$ to the signal is larger than the one from the operator $Q_{Qu}^{(8)}$. For the cases where the absolute value of the Wilson coefficient is 2π the excluded region is larger compared to the case where the absolute value is 1. For example, for the case $C_{QQ}^{(1)} = 2\pi$ and $C_{Qu}^{(8)} = 0$ it is possible to exclude the approximate region 12 TeV $< M <$ 38 TeV for $\mathcal{L}_{\text{int}} = 1500$ fb^{-1} and $N_8 = 25$ whereas only the approximate region 9 TeV $< M <$ 13 TeV is excluded for the same integrated luminosity and the same value for N_8 in the case $C_{QQ}^{(1)} = 1$ and $C_{Qu}^{(8)} = 0$ (not shown in the plot).
We show our exclusion plots for the cases where both Wilson coefficients are non-zero in Figure 5.7. The cases we consider are $C_{QQ}^{(1)} = 1$ and $C_{Qu}^{(8)} = 1$ (upper left), $C_{QQ}^{(1)} = 1$ and $C_{Qu}^{(8)} = -1$ (upper right), $C_{QQ}^{(1)} = 2\pi$ and $C_{Qu}^{(8)} = -2\pi$ (lower left) and $C_{QQ}^{(1)} = 2\pi$ and $C_{Qu}^{(8)} = -2\pi$ (lower right). The differently marked regions are to be interpreted as in Figure 5.6 above. We first observe that the relative sign of both Wilson coefficients is important. For example, in the case $N_8 = 10$ there exists an excluded region for $C_{QQ}^{(1)} = 1$ and $C_{Qu}^{(8)} = 1$ whereas no bounds on M are obtained for $C_{QQ}^{(1)} = 1$ and $C_{Qu}^{(8)} = -1$. This difference is caused by cancellations in the signal between contributions from both operators for the case where the Wilson coefficients have opposite signs. While the relative sign between the two Wilson coefficients is important the absolute sign does not cause large differences in the bounds since we assume in the projections to higher integrated

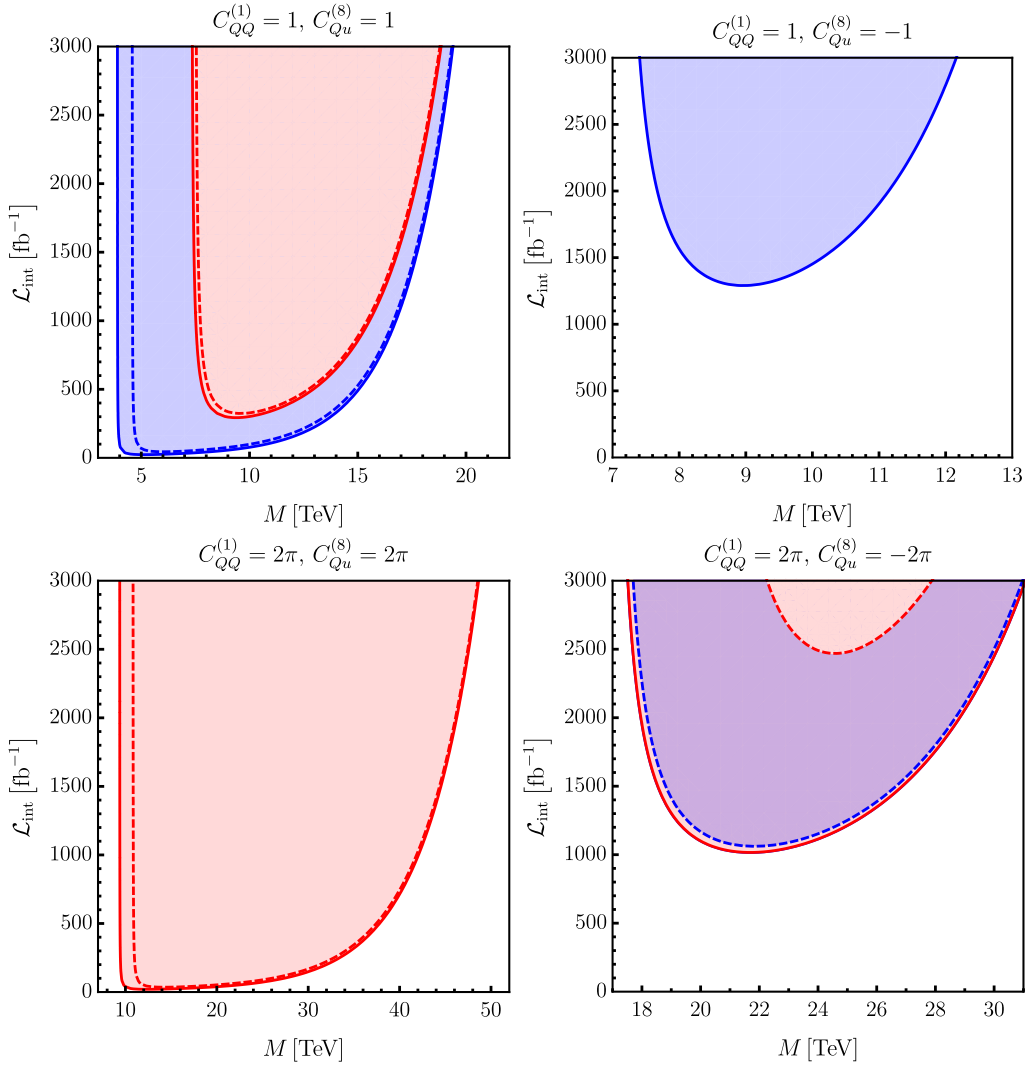

Figure 5.7: Excluded regions for the scale M in the fixed-Wilson-coefficient case for different values of $C_{QQ}^{(1)}$ and $C_{Qu}^{(8)}$, where both Wilson coefficients are assumed to be non-zero. The bounded regions are projections to different integrated luminosities. The solid (dashed) lines indicate the excluded regions when the theory uncertainty $\Delta_{\text{theo},1}$ ($\Delta_{\text{theo},2}$) is used. The parameter N_8 is fixed to $N_8 = 1$ for the blue regions, to $N_8 = 10$ for the red regions in the upper left plot and to $N_8 = 25$ for the red regions in both lower plots. Note that in the upper right plot no excluded regions exist for the theory uncertainty $\Delta_{\text{theo},1}$ with $N_8 = 10$ and for the theory uncertainty $\Delta_{\text{theo},2}$ for both $N_8 = 1$ and $N_8 = 10$. Moreover, both blue lines coincide with the red solid line in the lower left plot and both solid lines coincide in the lower right plot.

luminosities that the data is exactly our SM prediction. A different overall sign of the Wilson coefficients effects the bounds only due to small differences in the systematic uncertainties between the upper and the lower side of the data. The largest difference for the cases considered in Figure 5.6 and Figure 5.7 is less than 0.3 TeV in the bound on M for an integrated luminosity $\mathcal{L}_{\text{int}} = 3000$ fb^{-1} between switching the overall signs. We discuss the strongly-coupled case where we assume absolute values for the Wilson coefficients up to $16\pi^2$ next, focussing on an integrated luminosity of $\mathcal{L}_{\text{int}} = 1000$ fb^{-1}, the theory uncertainty $\Delta_{\text{theo},1}$ and $N_8 = 1$ for illustration. For the case $C_{QQ}^{(1)} = 16\pi^2$ and $C_{Qu}^{(8)} = 0$ our analysis yields approximately the excluded region 60 TeV $< M <$ 180 TeV. Analogously, we find the excluded regions 15 TeV $< M <$ 110 TeV for the case $C_{QQ}^{(1)} = 0$ and $C_{Qu}^{(8)} = 16\pi^2$ and the excluded region 50 TeV $< M <$ 210 TeV for $C_{QQ}^{(1)} = 16\pi^2$ and $C_{Qu}^{(8)} = 16\pi^2$. Comparing these three results we observe that the lower boundary of the excluded region for $C_{QQ}^{(1)} = 0$ and $C_{Qu}^{(8)} = 16\pi^2$ is much lower compared to the other two cases. The reason is that the contribution of the operator $Q_{QQ}^{(1)}$ to the theory uncertainty is larger compared to the one arising from $Q_{Qu}^{(8)}$. For the case $C_{QQ}^{(1)} = 0$ and $C_{Qu}^{(8)} = 16\pi^2$ the Wilson coefficient with value $16\pi^2$ enters the dominant contribution to the theory uncertainty only linearly through the variable C_8 defined below equation (5.14) in contrast to the other two cases where the Wilson coefficient of absolute value $16\pi^2$ enters quadratically.

In the discussion of the fixed-Wilson-coefficient case it remains to study the effect of the parameter R_{syst} rescaling the systematic uncertainty. We focus on the case $C_{Qu}^{(8)} = 0$ using the theory uncertainty $\Delta_{\text{theo},2}$ and the parameters $N_8 = 10$ and $\mathcal{L}_{\text{int}} = 3000$ fb^{-1}. We determine the largest integer value of R_{syst} where it is still possible to find an excluded region for M. For the Wilson coefficients $C_{QQ}^{(1)} = 1, 2\pi, 16\pi^2$ we find that these values are $R_{\text{syst}} = 3, 7, 7$. Thus, it is still possible to derive a bound on M when the systematic uncertainties are assumed to be seven times larger than our estimate for the case $C_{QQ}^{(1)} = 2\pi$.

We consider the fixed-scale case in the following. The projected exclusion regions are shown in Figure 5.8 for the scale $M = 10$ TeV and $R_{\text{syst}} = 1$. In the left plot we consider the integrated luminosity $\mathcal{L}_{\text{int}} = 300$ fb^{-1}. The regions bounded by the solid lines arise when the theory uncertainty $\Delta_{\text{theo},1}$ is used whereas the dashed lines bound the exclusion regions for the uncertainty $\Delta_{\text{theo},2}$. We distinguish the cases $N_8 = 1$ (blue regions) and $N_8 = 10$ (red regions). As a general feature we observe that two excluded regions exist which both exhibit a shape similar to an ellipse. In the limit of large absolute values for the Wilson coefficients no bounds are obtained since the theory uncertainty grows with the square of the Wilson coefficients compared to the signal which grows linear with the Wilson coefficients. The characteristic kinks arise for the case where the theory uncertainty $\Delta_{\text{theo},1}$ is used and are caused by the maximum function in equation (5.13). In analogy to the fixed-Wilson-coefficient case the excluded area decreases when either

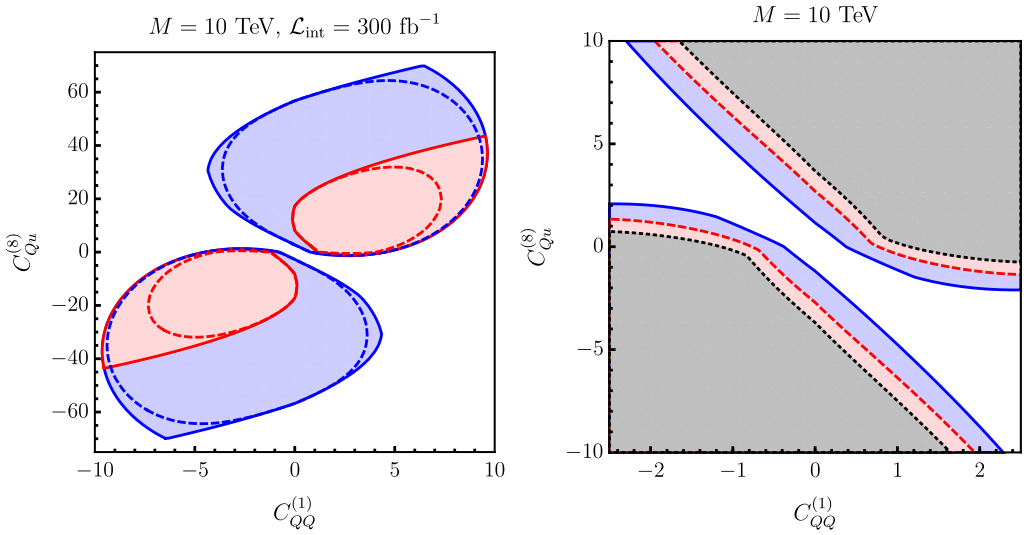

Figure 5.8: Excluded regions for the Wilson coefficients $C_{QQ}^{(1)}$ and $C_{Qu}^{(8)}$ for a fixed scale $M = 10$ TeV. In the left panel we consider the projection to the integrated luminosity $\mathcal{L}_{\text{int}} = 300$ fb^{-1}. The solid (dashed) line indicates the excluded region when the theory uncertainty $\Delta_{\text{theo},1}$ ($\Delta_{\text{theo},2}$) is used. We fix $N_8 = 1$ for the blue regions and $N_8 = 10$ for the red regions. In the right panel we use the theory uncertainty $\Delta_{\text{theo},1}$, fix $N_8 = 1$ and bound the excluded regions for integrated luminosities $\mathcal{L}_{\text{int}} = 150$, 300, 3000 fb^{-1} by the black-dotted, the red-dashed and the blue line.

N_8 is increased or when the theory uncertainty $\Delta_{\text{theo},2}$ is used instead of $\Delta_{\text{theo},1}$.
The right plot in Figure 5.8 shows the projected bounds using the theory uncertainty $\Delta_{\text{theo},1}$ and fixing $N_8 = 1$ for three different integrated luminosities. We consider the cases $\mathcal{L}_{\text{int}} = 150, 300, 3000$ fb^{-1} indicated by the black-dotted, the red-dashed and the blue line, respectively. These values correspond to the integrated luminosity by the end of Run 2, the integrated luminosity by the end of Run 3 and the integrated luminosity by the end of the high-luminosity run (see, e.g [249]). We observe that for fixed $C_{QQ}^{(1)} = -1$ the allowed range for $C_{Qu}^{(8)}$ shrinks from approximately $-0.2 < C_{Qu}^{(8)} < 7.5$ to approximately $1.1 < C_{Qu}^{(8)} < 4.7$ when increasing the luminosity from $\mathcal{L}_{\text{int}} = 150$ fb^{-1} to $\mathcal{L}_{\text{int}} = 3000$ fb^{-1}.

5.2.7 Constraints from Unnormalised Invariant-Mass Spectra

In the searches in the previous section we employed a two-dimensional binning in both the dijet invariant mass m_{jj} and the angular variable χ. In many of the considered scenarios a minimum amount of integrated luminosity is necessary to obtain bounds on the SMEFT parameters. As an alternative we perform searches where the data is binned in the dijet invariant mass m_{jj} only in this section. Concretely, we employ the binning from the CMS analysis specified in equation (5.7). Since we do not distinguish the different angular shapes we consider the contribution from the dominant operator $Q_{QQ}^{(1)}$ only and set $C_8 = \left|C_{QQ}^{(1)}\right|$ in the theory uncertainty. We add the systematic uncertainties reported by the CMS collaboration in the different χ bins in quadrature and rescale the results to the corresponding luminosity to obtain the systematic uncertainties for our analysis. We explicitly check the effect of adding the systematic uncertainties linearly. While the bounds weaken the analysis can still provide constraints on the SMEFT parameters. For the theory uncertainty $\Delta_{\text{theo},1}$ and the parameters $C_{QQ}^{(1)} = 1$, $N_8 = 1$ and $\mathcal{L}_{\text{int}} = 1000$ fb^{-1} the excluded region for M is 7 TeV $< M <$ 12 TeV for linearly added uncertainties compared to 5 TeV $< M <$ 18 TeV for the uncertainties added in quadrature.
Our projections for the bounds in the fixed-Wilson-coefficient case are collected in Figure 5.9. We use the theory uncertainty $\Delta_{\text{theo},1}$ and consider the cases $C_{QQ}^{(1)} = 1$ with $N_8 = 1$ in the left plot and $C_{QQ}^{(1)} = 2\pi$ with $N_8 = 25$ in the right plot. The blue regions arise from the searches in the dijet invariant mass spectrum. As a reference we include the bounds from the searches in angular spectra discussed in the last section by the black-dashed lines. It is important to note that compared to the searches in the angular spectra discussed in the last section less integrated luminosity is necessary to obtain bounds. Moreover, the region excluded at the same amount of luminosity extends to larger values of M. For example, for an integrated luminosity of 1000 fb^{-1} the largest scales excluded are approximately 18 TeV for $C_{QQ}^{(1)} = 1$ and 45 TeV for $C_{QQ}^{(1)} = 2\pi$ compared to 14 TeV and 36 TeV obtained from the searches in the angular spectra. At the lower boundary of the excluded region the searches in the angular spectra yield more stringent bounds compared to the searches in the dijet invariant mass spectrum. These differences are less than 1 TeV in both cases considered in Figure 5.9. In this regime

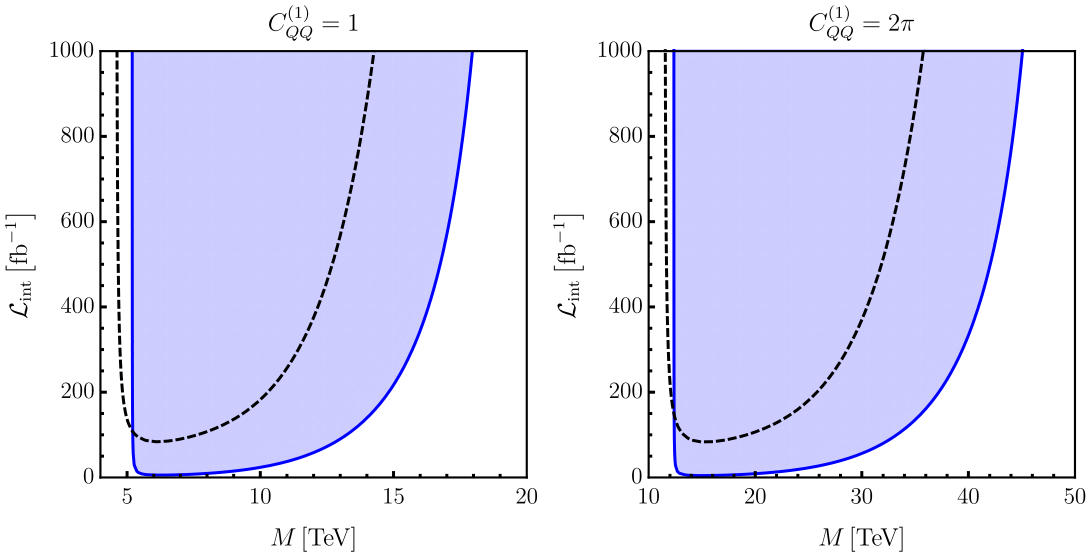

Figure 5.9: Excluded regions for the scale M in the fixed-Wilson-coefficient case for $C_{QQ}^{(1)} = 1$ (left) and $C_{QQ}^{(1)} = 2\pi$ (right). The bounded regions are projections to different integrated luminosities. We use the theory uncertainty $\Delta_{\text{theo},1}$ and fix $N_8 = 1$ in the left plot and $N_8 = 25$ in the right plot. The blue regions arise from the searches in the invariant mass spectra. For comparison we include the bounded regions obtained for the same parameters when applying the searches in the unnormalised angular spectra. These regions are indicated by the black-dashed lines.

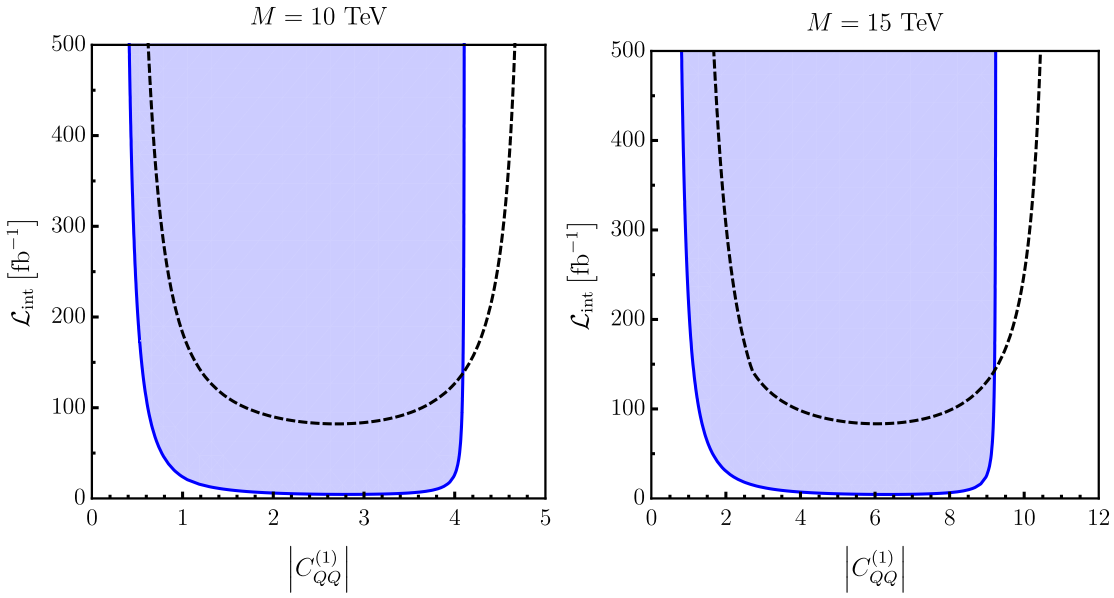

Figure 5.10: Excluded regions for the Wilson coefficient $C_{QQ}^{(1)}$ in the fixed-scale case for $M = 10$ TeV (left) and $M = 15$ TeV (right). The bounded regions are projections to different integrated luminosities. We use the theory uncertainty $\Delta_{\text{theo},1}$ and fix $N_8 = 1$. The blue regions arise from the searches in the invariant mass spectra. For comparison we include the excluded regions obtained for the same parameters when applying the searches in the unnormalised angular spectra. These regions are indicated by the black-dashed lines.

the theory uncertainty dominates compared to the statistical uncertainty. The theory uncertainty is reduced when considering dijet-invariant-mass spectra instead of angular spectra since the impact of the lowest bins in χ, where this uncertainty exhibits the largest values, is smeared out over all angular bins. However, along the same lines of reasoning the ability to distinguish signal and background is reduced. The behaviour we observe in Figure 5.9 arises from the interplay of these two effects. In an analysis where the full details about the experimental uncertainties are known one would design a combination of both searches to maximise the excluded region.

Our exclusion plots for the fixed-scale case are shown in Figure 5.10. Using the theory uncertainty $\Delta_{\text{theo},1}$ and the parameter $N_8 = 1$ we consider the cases $M = 10$ TeV (left) and $M = 15$ TeV (right). As in the discussion of the fixed-Wilson-coefficient case we include the bounds obtained from the searches in the angular spectra. The corresponding exclusion regions are indicated by the black-dashed lines. In analogy to the fixed-Wilson-coefficient case the bounded region extends to smaller absolute values of the Wilson coefficient for the searches in the dijet invariant mass spectrum compared to the case where the search is performed in the angular spectra. Moreover, the behaviour at the upper boundary of the excluded region, where the search in the angular spectra yields

more stringent bounds, corresponds to the behaviour at low scales in the fixed-Wilson coefficient case.
Finally, we comment on the sensitivity of our bounds to a rescaling of the systematic uncertainties with a factor R_{syst}. For both the fixed-Wilson-coefficient case and the fixed-scale case the bounds are quite sensitive to this parameter. For the fixed-Wilson-coefficient case with the parameters $\mathcal{L}_{\text{int}} = 1000\ \text{fb}^{-1}$, $C_{QQ}^{(1)} = 1$, $N_8 = 1$ and the theory uncertainty $\Delta_{\text{theo},1}$ the excluded region is 7 TeV $< M <$ 11 TeV for $R_{\text{syst}} = 3$ compared to 5 TeV $< M <$ 18 TeV for $R_{\text{syst}} = 1$. Increasing the systematic uncertainties to $R_{\text{syst}} = 4$ causes the excluded region to vanish completely.

5.3 Constraints From Dilepton Production

In this analysis we consider the process of dilepton production employing the framework developed in our study of dijet production in the last section. One main feature of the bounds we obtained in the dijet analysis is that in the fixed-Wilson-coefficient case scales smaller than a certain value are not excluded. Correspondingly, Wilson coefficients with an absolute value above a certain boundary are not excluded in the fixed-scale case. In this region of parameter space the SMEFT expansion breaks down which is taken into account by an appropriate theory uncertainty in our approach. We discussed in Section 5.1 that signal and theory uncertainty scale as s/M^2 and s^2/M^4, respectively. Thus, to derive bounds on the SMEFT for small values of M or large Wilson coefficients data obtained at lower centre-of-mass energies can be exploited. We do not only perform a study based on LHC results reported by the ATLAS collaboration [60] but also use results from the Tevatron reported by the CDF collaboration [250].

5.3.1 Partonic Dilepton Production in the Standard-Model Effective Theory

In our analysis we focus on tree-level Drell-Yan production [251] and in particular we consider the production of an electron and a positron. In the SM this process corresponds to the annihilation of a quark and an antiquark into an electron and a positron via the exchange of a photon or Z boson. Two classes of dimension-six SMEFT operators with different behaviour contribute. An example for an operator in the first class is

$$Q_{\phi L}^{(1)} = \left(\phi^\dagger \, i\overleftrightarrow{D}_\mu \, \phi\right) \left(\bar{L}_p \, \gamma^\mu \, L_r\right) . \tag{5.15}$$

In the process of EWSB the terms where both Higgs doublets are replaced by the VEV and gauge fields are taken from the covariant derivative modify the couplings of the Z boson to the leptons. The contribution of this operator to the dilepton cross section scales as v^2/M^2. Analyses of operators shifting the SM couplings exist from measurements at the Large Electron-Positron Collider (LEP) and further experiments [252–257]. The second class of operators are four-fermion operators familiar from the dijet analysis where we discussed in detail that the effect of these operators grows with energy. In this thesis we focus on the effect of four-fermion operators and leave a study of the operators

$Q_{LQ}^{(1)}$	$\left(\bar{L}_p\gamma_\mu L_r\right)\left(\bar{Q}_s\gamma^\mu Q_t\right)$	Q_{Lu}	$\left(\bar{L}_p\gamma_\mu L_r\right)\left(\bar{u}_s\gamma^\mu u_t\right)$
$Q_{LQ}^{(3)}$	$\left(\bar{L}_p\gamma_\mu\tau^i L_r\right)\left(\bar{Q}_s\gamma^\mu\tau^i Q_t\right)$	Q_{Ld}	$\left(\bar{L}_p\gamma_\mu L_r\right)\left(\bar{d}_s\gamma^\mu d_t\right)$
Q_{eu}	$\left(\bar{e}_p\gamma_\mu e_r\right)\left(\bar{u}_s\gamma^\mu u_t\right)$	Q_{Qe}	$\left(\bar{Q}_p\gamma_\mu Q_r\right)\left(\bar{e}_s\gamma^\mu e_t\right)$
Q_{ed}	$\left(\bar{e}_p\gamma_\mu e_r\right)\left(\bar{d}_s\gamma^\mu d_t\right)$		

Table 5.4: Dimension-six four-fermion operators from the Warsaw basis contributing to dilepton production at tree level under the assumption that the operators conserve baryon number, lepton number and CP.

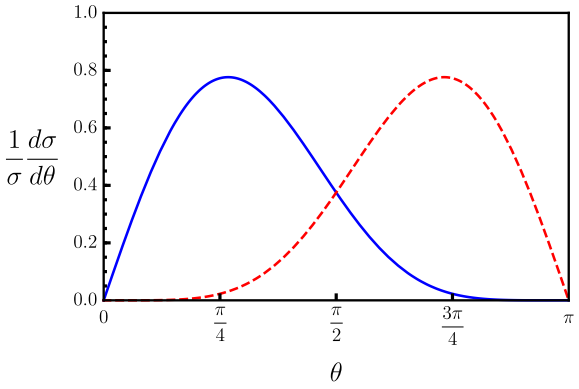

Figure 5.11: Cross section for the partonic process $u\bar{u} \to e^+e^-$ at order $1/M^2$ in the SMEFT expansion as a function of the partonic scattering angle θ. The distributions are normalised to the total cross section in the range $\theta \in [0, \pi]$. Shown are the distributions arising from the operators $Q_{LQ}^{(3)}$ (blue, solid) and Q_{Lu} (red, dashed).

shifting the SM couplings for future work. We collect the contributing four-fermion operators conserving baryon number, lepton number and CP in Table 5.4. We assume an unbroken flavour-symmetric $U(3)^5$ limit for the Lagrangian which corresponds to the flavour structure $\delta_{pr}\delta_{st}$ for the Wilson coefficients of the operators from Table 5.4 as explained for example in [17].

In analogy to our dijet study we exploit angular distributions to distinguish two different linear combinations of operators. The angular behaviour is defined by the scattering angle θ between the three-momentum of the electron and the three-momentum of the quark in the partonic centre-of-mass frame. As an illustration we consider the partonic cross section for the process $u\bar{u} \to e^+e^-$ at centre-of-mass energies much larger than the mass of the Z boson. We show the cross section differential in θ at order $1/M^2$ in the SMEFT expansion in Figure 5.11, where we consider the contribution from the operator $Q_{LQ}^{(3)}$ (blue, solid) and the operator Q_{Lu} (red, dashed). Both cross sections are normalised to the total cross section in the interval $\theta \in [0, \pi]$. We observe that

the distribution for the operator $Q_{LQ}^{(3)}$ peaks approximately at $\theta \approx \pi/4$ corresponding to forward scattering whereas the distribution for the operator Q_{Lu} peaks approximately at $\theta \approx 3\pi/4$ corresponding to backward scattering. In our searches we consider only the contributions from the operators $Q_{LQ}^{(3)}$ and Q_{Lu} which are both representatives for a class of operators with the same angular behaviour. The class of operators giving rise to forward scattering consists of $Q_{LQ}^{(3)}$, Q_{eu}, $Q_{LQ}^{(1)}$ and Q_{ed} and the class of operators for backward scattering contains Q_{Lu}, Q_{Qe} and Q_{Ld}.
At hadron colliders the direction of the incoming quark is not fixed since both the quark and the antiquark in the initial state exist as sea quarks in protons and antiprotons. However, the distribution of the momentum fractions as described by the PDFs is such that on average valence quarks carry a larger fraction of the hadron's momentum compared to sea quarks. At a proton-antiproton collider like the Tevatron it is thus reasonable to use the direction of the incoming proton as a reference for the direction of the incoming quark in a process at high energies. At the Tevatron we refer to an event where the electron has a pseudorapidity fulfilling $y_{e^-} > 0$ ($y_{e^-} < 0$) as forward (backward), where we assume that the beam axis is defined by the three-momentum of the proton. At a proton-proton collider like the LHC the situation is more subtle. On average the quark carries a larger fraction of the proton's momentum compared to the antiquark. Thus, the partonic centre-of-mass frame is on average boosted in the direction of the incoming quark. Therefore, an electron which is emitted in the forward direction in the partonic frame exhibits a larger absolute pseudorapidity in the laboratory frame. Hence, it is reasonable to define a forward (backward) event at the LHC to produce an electron and a positron where the pseudorapidities in the laboratory frame fulfill $|y_{e^-}| > |y_{e^+}|$ ($|y_{e^-}| < |y_{e^+}|$).

5.3.2 Strategy for the Searches and Technical Details

Similar to the dijet study we perform the searches in the total number of events and an angular variable both binned in the dilepton invariant mass m_{ll}. For the angular variable we use the asymmetry of the forward and backward events. Concretely, the total number of events N_{tot} and the asymmetry A_{FB} are defined as

$$N_{\text{tot}} = N_{\text{F}} + N_{\text{B}}\,, \qquad A_{\text{FB}} = \frac{N_{\text{F}} - N_{\text{B}}}{N_{\text{F}} + N_{\text{B}}}\,, \tag{5.16}$$

where N_{F} and N_{B} are the number of forward and backward events, respectively. As specified in the last section, the definition of a forward and a backward event depends on the collider which is considered. The analyses by ATLAS [60] and CDF [250] do not report the quantity A_{FB} for the whole range of dilepton invariant masses considered in our study. Thus, we perform the search in N_{tot} for recasts at the current integrated luminosity and include the searches in A_{FB} in projections to higher integrated luminosities.
In complete analogy to the dijet study we expand N_{tot} and A_{FB} in $1/M^2$, include the terms up to the order $1/M^2$ in the signal prediction and use the term at order $1/M^4$ to model the theory uncertainty. To obtain the theory uncertainty we sum the squared

dimension-six piece and two pieces - one for the forward bin and one for the backward bin - for the interference of the dimension-eight amplitude with the SM amplitude in quadrature. We use MC pseudodata simulated as specified below in the forward and the backward bin for the squared dimension-six piece. As a model for the dimension-eight interference pieces we symmetrise the results from the MC simulation for the squared dimension-six piece over the forward and the backward bin. In the result we substitute the squared Wilson coefficients according to

$$C_k^2 \to g^2\, C_8\, \sqrt{N_8}\,, \tag{5.17}$$

where $k \in \{1, 2\}$ with $k = 1$ being a short-hand notation for $C_{LQ}^{(3)}$ and $k = 2$ being a short-hand notation for C_{Lu}. Furthermore, $\sqrt{N_8}$ parameterises the number of dimension-eight operators giving rise to interference with the SM amplitude and we assume $C_8 = \max(1, |C_k|)$ to represent the size of the Wilson coefficients at dimension eight. Our model for the theory uncertainty takes account of the fact that the unkown interference pieces in the forward and the backward bin are independent. To obtain the total uncertainty we add the theory uncertainty, a Poisson uncertainty and a systematic uncertainty in quadrature. We provide details about the systematic uncertainty in the discussion of the corresponding analyses in Sections 5.3.3 and 5.3.4.
For our analysis we employ the `SMEFTsim` package [17, 18] for the contribution of the SMEFT operators. We generate MC pseudodata at LO using `MadGraph5` [12], where we fix the renormalisation and factorisation scales on an event-by-event basis to the sum of the transverse energies of the electron and the positron. As in the dijet analysis our bounds are derived at the 95% CL using a chi-squared test.

5.3.3 Searches at the Large Hadron Collider

The basis for our search are results reported by the ATLAS collaboration [60]. The data is taken at a centre-of-mass energy of 13 TeV and corresponds to an integrated luminosity of 36.1 fb^{-1}. We generate the MC pseudodata using the CT10 PDF [258] binned in seven bins in the dilepton invariant mass m_{ll} and in ten bins in the rapidities of the leptons. The bin borders are

$$m_{ll} \in \{0.4, 0.5, 0.7, 0.9, 1.2, 1.8, 3.0, 6.0\}\ \text{TeV}\,, \tag{5.18}$$

$$y_{e^-}, y_{e^+} \in \{-2.5, -2.0, -1.5, -1.0, -0.5, 0.0, 0.5, 1.0, 1.5, 2.0, 2.5\}\,. \tag{5.19}$$

The applied cuts select events where both pseudorapidities fulfill $2.47 > |y_{e^-,e^+}| > 1.52$ or $1.37 > |y_{e^-,e^+}|$ and where both transverse momenta are larger than 30 GeV. We assume that the systematic uncertainty on the asymmetry A_{FB} is negligible due to cancellations in the normalisation. For the total number of events N_{tot} we use the systematic uncertainty reported by ATLAS at an integrated luminosity of 36.1 fb^{-1}. For our projections to higher integrated luminosities we assume that these uncertainties decrease proportional to the square root of the integrated luminosity down to a minimum relative uncertainty of 2 %. To validate our procedure we compare our results for the SM pseudodata with

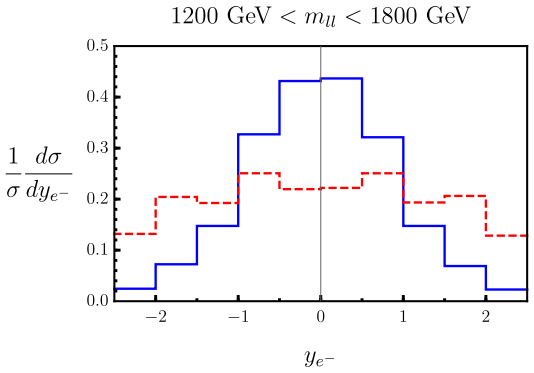

Figure 5.12: Cross section at order $1/M^2$ for 1200 GeV $< m_{ll} <$ 1800 GeV differential in the pseudorapidity y_{e^-} of the electron. Shown are the distributions arising from the operators Q_{Lu} (blue, solid) and $Q_{LQ}^{(3)}$ (red, dashed). Both distributions are normalised to the total cross section in the interval $y_{e^-} \in [-2.5, 2.5]$.

the corresponding predictions by the ATLAS collaboration from table 3 in [60]. The comparison yields a chi-squared value of 0.52.
To illustrate how the distinct angular behaviour discussed at the parton level in Section 5.3.1 is manifest in the pseudodata we show the two angular distributions of the cross section at order $1/M^2$ differential in the pseudorapidity of the electron in Figure 5.12. Shown is the cross section in the bin 1200 GeV $< m_{ll} <$ 1800 GeV normalised to the total cross section in the range $y_{e^-} \in [-2.5, 2.5]$ for the operator Q_{Lu} (blue, solid) and for the operator $Q_{LQ}^{(3)}$ (red, dashed). We note that the dips in the distribution for $Q_{LQ}^{(3)}$ in the two bins where $1.0 < |y_{e^-}| < 1.5$ originate from the cut specified above. As expected from the partonic discussion in Section 5.3.1 the electrons in the distribution for Q_{Lu} on average have pseudorapidities with smaller absolute values compared to the electrons in the distribution for the operator $Q_{LQ}^{(3)}$. The two linear combinations of Wilson coefficients represented by the distributions from $Q_{LQ}^{(3)}$ and Q_{Lu} in Figure 5.12 are

$$\left.\frac{d\sigma}{dy_{e^-}}\right|_{\text{forward}} \propto C_{LQ}^{(3)} - 0.48\, C_{eu} - 0.32\, C_{LQ}^{(1)} + 0.15\, C_{ed}\,, \tag{5.20}$$

$$\left.\frac{d\sigma}{dy_{e^-}}\right|_{\text{backward}} \propto -\left(C_{Lu} + 0.81\, C_{Qe} - 0.33\, C_{Ld}\right)\,, \tag{5.21}$$

where we normalised both linear combinations to the dominant Wilson coefficient and averaged the prefactors over all the m_{ll} bins. The overall signs in the linear combinations indicate that the case $C_{LQ}^{(3)} > 0$ corresponds to constructive interference and the case $C_{Lu} > 0$ corresponds to destructive interference. As in our dijet study the prefactors of the Wilson coefficients in equation (5.20) and (5.21) vary due to the different PDFs of up- and down-type quarks. We leave a detailed analysis of these effects for future work.

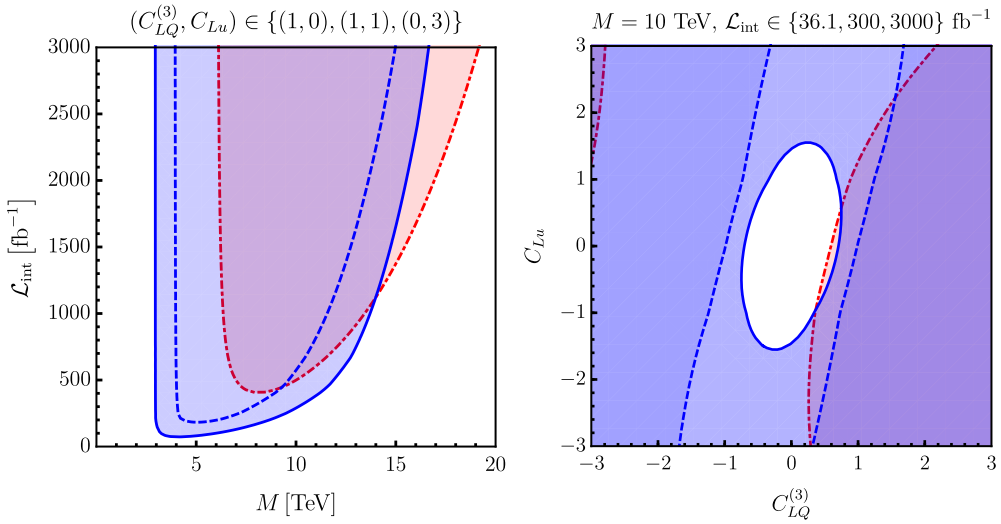

Figure 5.13: Excluded regions arising from the LHC searches for the scale M in the fixed-Wilson-coefficient case (left) and for the Wilson coefficients in the fixed-scale case (right). In the left plot projections to different integrated luminosities are shown for the Wilson coefficients $(C_{LQ}^{(3)}, C_{Lu}) = (1,0)$ (blue, solid), $(C_{LQ}^{(3)}, C_{Lu}) = (1,1)$ (blue, dashed) and $(C_{LQ}^{(3)}, C_{Lu}) = (0,3)$ (red, dot-dashed). In the right plot we fix $M = 10$ TeV and show the excluded regions for the integrated luminosities $\mathcal{L}_{\text{int}} = 36.1$ fb^{-1} (red, dot-dashed), $\mathcal{L}_{\text{int}} = 300$ fb^{-1} (blue, dashed) and $\mathcal{L}_{\text{int}} = 3000$ fb^{-1} (blue, solid). We fix $N_8 = 20$ in both plots.

We show the exclusion plots in Figure 5.13 for the fixed-Wilson-coefficient case (left) and the fixed-scale case (right). In the left plot we consider projections for the bounds to different integrated luminosities for the Wilson coefficients $(C_{LQ}^{(3)}, C_{Lu}) = (1,0)$ (blue, solid), $(C_{LQ}^{(3)}, C_{Lu}) = (1,1)$ (blue, dashed) and $(C_{LQ}^{(3)}, C_{Lu}) = (0,3)$ (red, dot-dashed). In the right plot we show the excluded regions for the integrated luminosities $\mathcal{L}_{\text{int}} = 36.1$ fb^{-1} (red, dot-dashed), $\mathcal{L}_{\text{int}} = 300$ fb^{-1} (blue, dashed) and $\mathcal{L}_{\text{int}} = 3000$ fb^{-1} (blue, solid) for the fixed scale $M = 10$ TeV. For both plots we fix the parameter $N_8 = 20$.

In the fixed-Wilson-coefficient case in the left plot in Figure 5.13 we observe the same characteristic shape of the excluded regions as in our dijet study. At an integrated luminosity of $\mathcal{L}_{\text{int}} = 3000$ fb^{-1} the excluded region is approximately 3 TeV $< M <$ 17 TeV in the case $(C_{LQ}^{(3)}, C_{Lu}) = (1,0)$ and 6 TeV $< M <$ 19 TeV in the case $(C_{LQ}^{(3)}, C_{Lu}) = (0,3)$. In the fixed-scale case in the right plot in Figure 5.13 we observe that a large fraction of the parameter space where $C_{LQ}^{(3)} > 0$ and $C_{Lu} < 0$ is excluded at the luminosity $\mathcal{L}_{\text{int}} = 36.1$ fb^{-1}. As an example, for $C_{Lu} = -1.5$ the region $C_{LQ}^{(3)} > 0.3$ in the plotted domain is excluded and analogously for $C_{LQ}^{(3)} = 1.5$ all negative values of C_{Lu} in the plotted

domain are excluded. The region where $C_{LQ}^{(3)} > 0$ and $C_{Lu} < 0$ is the domain where the total number of signal events is enhanced. We remind the reader that at this luminosity we only include the total number of events in the search since data for the asymmetry is not reported by the ATLAS collaboration in the full range of dilepton invariant masses m_{ll}. A further interesting feature of the exclusion plot for $\mathcal{L}_{\text{int}} = 36.1$ fb^{-1} is the flat direction in parameter space. In this region the effect of the two linear combinations cancels out in the total number of events. As a final remark concerning the excluded region for $\mathcal{L}_{\text{int}} = 36.1$ fb^{-1} we note that there exists a deficit of the data compared to the predicted number of events in the SM in the high m_{ll} bins. It is this deficit which causes that the excluded region is not symmetric under a change of signs in both Wilson coefficients. For the projections to higher integrated luminosities we assume that the data matches the SM exactly and include the asymmetry in the search. While the flat direction still exists at $\mathcal{L}_{\text{int}} = 300$ fb^{-1} due to the statistical uncertainty it vanishes approximately at $\mathcal{L}_{\text{int}} = 400$ fb^{-1} - a case which is not shown. Beyond this integrated luminosity the exluded region forms an approximate ellipse with the major axis being aligned along the direction of the cancellation between the two linear combinations in the total number of events. It is the inclusion of the asymmetry which provides the constraining power in this region of parameter space. In analogy to our dijet study we do not only find an upper boundary for the Wilson coefficients but also a lower one. For Wilson coefficients larger than this lower boundary the theory uncertainty is too large and no bounds are obtained in the search. Along the major axis of the ellipse this lower boundary is approximately $(C_{LQ}^{(3)}, C_{Lu}) \approx (\pm 2, \pm 11)$ at an integrated luminosity $\mathcal{L}_{\text{int}} = 3000$ fb^{-1}.

5.3.4 Searches at the Tevatron

Our searches at the Tevatron are based on data reported by the CDF collaboration [250]. The data corresponds to a centre-of-mass energy of 1.96 TeV and an integrated luminosity of $\mathcal{L}_{\text{int}} = 9.4$ fb^{-1}. We generate the MC pseudodata using the CTEQ5L PDF [259]. We consider the two different acceptance regions referred to as the "central-central" (CC) region and the "central-plug" region by the CDF collaboration. For our analysis we combine several of the m_{ll} bins used by CDF. Our bin borders for the binning in the dilepton invariant mass m_{ll} in the two regions are

$$\text{CC region:} \qquad m_{ll} \in \{130, 162, 203, 255, 320, 400\} \text{ GeV}\,, \tag{5.22}$$

$$\text{CP region:} \qquad m_{ll} \in \{130, 163, 205, 256, 321, 402\} \text{ GeV}\,. \tag{5.23}$$

Concerning the binning in the pseudorapidity we use the same bin borders as specified in equation (5.19) for the LHC study in the last section. The cuts applied in the CC region select events where one of the two transverse energies of the electron and the positron is larger than 15 GeV, one transverse energy is larger than 25 GeV and both pseudorapidities fulfill $0.05 < |y_{e^-,e^+}| < 1.05$. The cuts in the CP region select events where both transverse energies are larger than 20 GeV, one pseudorapidity fulfills $0.05 < |y_{e^-,e^+}| < 1.05$ and the other pseudorapidity fulfills $1.2 < |y_{e^-,e^+}| < 2.8$.

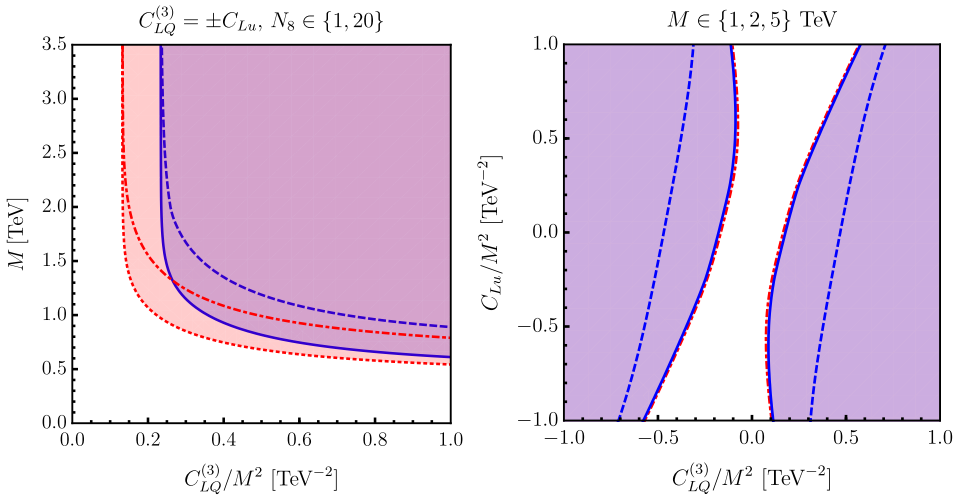

Figure 5.14: Excluded regions arising from the Tevatron searches. In the left plot we fix the Wilson coefficients to $C_{LQ}^{(3)} = -C_{Lu}$ with $N_8 = 1$ (red, dotted) and $N_8 = 20$ (red, dot-dashed) and to $C_{LQ}^{(3)} = +C_{Lu}$ with $N_8 = 1$ (blue, solid) and $N_8 = 20$ (blue, dashed). In the right plot we show the excluded regions in the fixed-scale case with $N_8 = 10$ for $M = 1$ TeV (blue, dashed), $M = 2$ TeV (blue, solid) and $M = 5$ TeV (red, dot-dashed). We normalise the Wilson coefficients in both plots to the square of the scale M.

To account for the misidentification of electrons in the detector we determine one correction factor for all the m_{ll} bins in each region by fitting our SM pseudodata to the SM prediction of the CDF collaboration. After the application of these efficiency factors we compare our SM pseudodata with the prediction of CDF as a validation. We find chi-squared values $\chi^2 \approx 5$ in the CC region and $\chi^2 \approx 2$ in the CP region. We apply the correction factors to the distributions of the signal and the theory uncertainty and perform the search by comparing our prediction to the data obtained by CDF. The asymmetry values are not reported over the full range of dilepton invariant masses and thus our search is based on the data binned in m_{ll} only. Concerning the systematic uncertainties we assume a relative uncertainty of 5% in our analysis.
We show our exclusion plots in Figure 5.14. In both plots we normalise the Wilson coefficients to the square of the scale M. Therefore, differences between curves for different values of M arise from an independent sensitivity of the search to the scale and the Wilson coefficients. In the left plot in Figure 5.14 we consider the cases $C_{LQ}^{(3)} = -C_{Lu}$ with $N_8 = 1$ (red, dotted) and $N_8 = 20$ (red, dot-dashed) and $C_{LQ}^{(3)} = +C_{Lu}$ with $N_8 = 1$ (blue, solid) and $N_8 = 20$ (blue, dashed). We observe that the lower boundary of the excluded region for scales above a certain value is independent of the scale. These scales are approximately 2.0 TeV for $N_8 = 1$ and 3.5 TeV for $N_8 = 20$. Below these scales the effects of dimension-eight interference in the theory uncertainty cause the search to

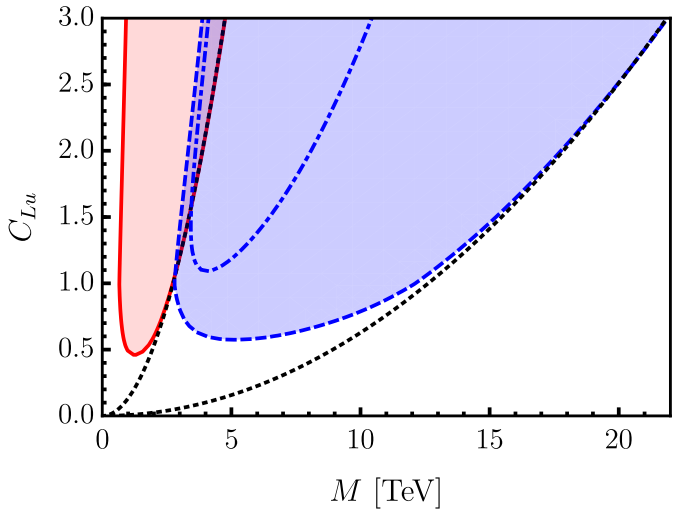

Figure 5.15: Excluded regions for $N_8 = 20$ and $C_{LQ}^{(3)} = -C_{Lu}$ from searches at the Tevatron (red, solid), the LHC with $\mathcal{L}_{\text{int}} = 36.1$ fb^{-1} (blue, dot-dashed) and the LHC with $\mathcal{L}_{\text{int}} = 300$ fb^{-1} (blue, dashed). The dotted black lines are parabolas $C_{Lu} = M^2/M'^2$, where the mass scale M' arises from fitting the boundaries of the excluded regions for the Tevatron analysis in the interval 2 TeV $< M <$ 5 TeV and for the LHC analysis with $\mathcal{L}_{\text{int}} = 300$ fb^{-1} in the interval 15 TeV $< M <$ 25 TeV. The black curves illustrate the case where the analysis does not contain an appropriate theory uncertainty and hence depends only on the ratio C_{Lu}/M^2.

be separately sensitive to the Wilson coefficient and the scale. In the right plot in Figure 5.14 we fix $N_8 = 10$ and consider the fixed-scale case for $M = 1$ TeV (blue, dashed), $M = 2$ TeV (blue, solid) and $M = 5$ TeV (red, dot-dashed). We note the flat direction in parameter space familiar from the LHC study in the last section. In the projections to higher integrated luminosities in the LHC analysis the inclusion of the asymmetry causes the flat direction to vanish. It is therefore interesting to study the effect of including the asymmetry in the search at the Tevatron and we strongly advocate to report the asymmetry over the full range of m_{ll} values. Concerning the excluded region outside the flat direction we find for $C_{Lu} = 0$ that values fulfilling approximately $|C_{LQ}^{(3)}| > 5.7\, M^2/\text{TeV}^2$ are not excluded due to the invalidity of the SMEFT expansion in this regime.

It is interesting to study the complimentarity of the two analyses we performed with data from different colliders. In Figure 5.15 we show a combination of excluded regions arising from our searches at the LHC and the Tevatron. We fix $N_8 = 20$, choose $C_{LQ}^{(3)} = -C_{Lu}$ and show the excluded region from the searches using Tevatron data (red, solid), the searches at the LHC for $\mathcal{L}_{\text{int}} = 36.1$ fb^{-1} (blue, dot-dashed) and the extrapolation of the LHC search to an integrated luminosity $\mathcal{L}_{\text{int}} = 300$ fb^{-1} (blue, dashed). For better

comparison we included the asymmetry in the search at the LHC for the integrated luminosity $\mathcal{L}_{\text{int}} = 36.1\ \text{fb}^{-1}$ and assume that the data matches the SM prediction. To illustrate the complimentarity of these searches we consider the Wilson coefficient $C_{Lu} = 2.0$ where the Tevatron search exludes approximately the scales $0.8\ \text{TeV} < M < 3.9\ \text{TeV}$, the LHC search with $\mathcal{L}_{\text{int}} = 36.1\ \text{fb}^{-1}$ excludes approximately the regime $3.6\ \text{TeV} < M < 8.0\ \text{TeV}$ and the LHC extrapolation to $\mathcal{L}_{\text{int}} = 300\ \text{fb}^{-1}$ excludes $3.3\ \text{TeV} < M < 17.8\ \text{TeV}$. These values illustrate that the analysis at the Tevatron probes a different region of the SMEFT parameter space at lower scales due to the lower centre-of-mass energy. An interesting future project is to study the bounds arising from LHC data taken at lower m_{ll} values compared to the dilepton invariant masses of the data used in our analysis. The dotted black lines in Figure 5.15 are fits to the boundaries of the excluded region for the Tevatron in the interval $2\ \text{TeV} < M < 5\ \text{TeV}$ and for the LHC analysis with $\mathcal{L}_{\text{int}} = 300\ \text{fb}^{-1}$ in the interval $15\ \text{TeV} < M < 25\ \text{TeV}$. The fit parameter is the mass scale M' in the parabola $C_{Lu} = M^2/M'^2$. These curves represent a hypothetical analysis where no theory uncertainty is included. The bounds in this case are functions of the ratio C_{Lu}/M^2. We find the mass scales $M' \approx 3\ \text{TeV}$ for the Tevatron analysis and $M' \approx 13\ \text{TeV}$ for the LHC analysis. The differences between the areas bounded by the black dotted lines and the red solid or the blue dashed lines clearly indicate that it is not reasonable to claim a single lower boundary for the scale M in a SMEFT collider analysis of this type.

6 Conclusions

In this thesis we have developed a broad set of EFT tools for the generic description of BSM physics. Under the assumption that the mass scale M of the BSM model is far above the electroweak scale v, i.e. $v \ll M$, we covered the two relevant cases that the BSM states can or can not be produced on shell at the LHC or a future collider.
In the first scenario we considered the case where a heavy, scalar resonance S with mass M_S and width $\Gamma_S \ll M_S$ is discovered at the LHC or a future collider via its decays into SM particles. We constructed an EFT - the SCET_{BSM} - under the assumption that S is only the first member of a whole BSM sector of particles with masses $M \sim M_S$ and demonstrated that it is straightforward to apply our theory also in the case of the double hierarchy $v \ll M_S \ll M$. We discussed the relevant RG evolution equations necessary for the resummation of large single and double logarithms of the scale ratios. As an illustration of our approach we performed the matching of a UV-complete model featuring the SM, the scalar S, and additional heavy, vector-like fermions to the SCET_{BSM}. In this context we computed the rates for the decays of S into SM particles and studied the impact of resummation on these rates.
The key results obtained in this work are the SCET_{BSM} Lagrangians at the LO, the NLO and partially the NNLO order in the power-counting parameter $\lambda \sim v/M$ for two-body decays of S in Section 3.3, and the LO Lagrangian relevant for three-body decays of S in Section 3.4. If particle physics faces a situation similar to the diphoton resonance in the future, the SCET_{BSM} Lagrangian allows a consistent description of the experimental observations in terms of an EFT. Concerning the behaviour of the SCET_{BSM} operators under renormalisation, the mixing of the subleading two-jet operators in equations (3.79), (3.80) and (3.82) is a further main result. The cusp anomalous dimension $\gamma^{q\bar{q}}_{\text{cusp}}$ contributing to this mixing arises from Feynman diagrams where an ultra-soft gluon is exchanged between two collinear quarks in different sectors. We expect $\gamma^{q\bar{q}}_{\text{cusp}}$ to be a generic quantity playing an important role in future applications of SCET beyond the leading power - a rather new field (see, e.g. [197, 208–216]). As a major result from our illustrative analysis, which features a UV-complete model with heavy, vector-like fermions, we highlight that the Wilson coefficients are, in general, complicated functions of the scale ratio $\xi = M_S^2/M^2$. A prominent example is the Wilson coefficient $\tilde{C}_{\phi\phi\phi\phi}$ in equation (4.25). We demonstrated in equation (4.20) that the dependence of the Wilson coefficients on ξ in the limit $\xi \ll 1$ corresponds to the contribution from an infinite tower of local operators. This result confirms the intuition built up in the introduction of this thesis, namely that the SCET_{BSM} approach captures the contribution from an infinite number of higher-dimensional local operators. Concerning phenomenological studies, one of our major results are the sizeable resummation effects in the rates for the decays $S \to 2$ jets, $S \to t\bar{t}$, $S \to \gamma\gamma$ and $S \to hh$ discussed in Section 4.6. In fact, the decay rates in our

scenario are suppressed by factors down to approximately 0.15 for the decay $S \to 2$ jets. There exist many avenues for future work concerning both the phenomenologically relevant aspects and the questions regarding the SCET_{BSM} as a theory itself. It is interesting to construct the relevant Lagrangian for resonances apart from a scalar SM gauge singlet such as Z' bosons or heavy leptoquarks. Once these Lagrangians are build, it will be possible - just as we did in our illustrative model - to match corresponding UV-complete models to the Lagrangian and to study the effects of resummation in this context. For all these steps our work may serve as a guideline. On the more theoretical side it is interesting to calculate the matrix elements of the SCET operators at the one-loop level. Depite being low-energy matrix elements in the EFT, logarithms of the scale ratio M_S/v contribute. In our case the hard scale M_S enters via the mass of the decaying resonance. It is important to show that this dependence does not spoil factorisation. Furthermore, it will be useful to include electroweak corrections in the one-loop anomalous dimensions and to compute the generic cusp anomalous dimension $\gamma^{q\bar{q}}_{\text{cusp}}$ at two-loop order.
In the second scenario we focused on the case where the mass scale M of the BSM model is too large for the on-shell production of the BSM states at a collider. In this scenario the SMEFT provides a suitable way to study BSM effects independent from a UV-complete model. The bounds obtained on SMEFT parameters in collider analyses can directly be translated into bounds on particular models via matching calculations. We discussed in detail why it is necessary to truncate the signal prediction in these SMEFT analyses at order $1/M^2$ in the power-counting and introduced a theory uncertainty taking account of the neglected terms at order $1/M^4$. We applied our method to dijet production at the LHC and to dilepton production at the LHC and the Tevatron. In our collider studies we derived bounds on the linear combinations of contributing Wilson coefficients and on the scale M.
The key result of our work is the framework described in Section 5.1, which allows a study of SMEFT effects in collider studies employing a consistent expansion in the EFT power series. Our approach is a major improvement of current state-of-the-art analyses, which are missing a reliable estimate of the size of power corrections in the EFT series. The bounds we derived differ in two main aspects from the results quoted by previous analyses: First, we find excluded regions for both the Wilson coefficients and the scale M rather than a single upper bound for the Wilson coefficient or a single lower bound for the scale M, respectively. The exclusion plots shown in Figure 5.6 and 5.10 are representative examples of these findings. In this regard our results agree with the intuition that an analysis at a fixed collision energy should not exclude very small scales or very large Wilson coefficients since the SMEFT expansion breaks down in this regime. Second, our bounds are considerably weaker compared to the ones obtained by state-of-the-art analyses where no theoretical uncertainty for higher-power EFT corrections is included. The most striking example in this context is our dijet study where we demonstrated in Section 5.2.5 that no bounds on the SMEFT parameters arise from established searches in normalised angular distributions when our consistent treatment of the EFT expansion is employed. As a solution to this problem we designed and performed searches in unnormalised distributions in Sections 5.2.6 and 5.2.7, and showed that the addi-

tional knowledge about the absolute number of events gives rise to bounds from these searches. Dijet production is among the most challenging processes for an EFT analysis at a hadron collider since dijet events naturally exhibit very high energies. Thus, our dijet study should be viewed as a proof of concept and we strongly advocate to employ our framework in future SMEFT collider studies. We considered dilepton production as a first application beyond dijet production. As a highlight of this analysis we demonstrated in Section 5.3.4 that data obtained at lower collision energies - in our case at the Tevatron - provide important exclusion limits in the regime where the scale M is small. A major result from both analyses are the linear combinations of Wilson coefficients contributing to the observables presented in equations (5.8), (5.9), (5.20) and (5.21).
The development of our framework and the first two applications in collider studies are at the starting point of a full program to bound SMEFT parameters employing a consistent EFT expansion. We leave it for future work to include NLO QCD and electroweak corrections in our analysis and to study the systematic uncertainties in full detail. Concerning the dilepton study an interesting future project is the analysis of the operators contributing via shifts of SM couplings. The application of our approach to further processes, such as top-quark production for example, will give rise to bounds on further parameters. The ultimate goal is a global picture of the parameter landscape of the SMEFT.
In conclusion, we developed and applied powerful EFTs tools tailored for the generic description of BSM physics in the two relevant cases where the BSM states are within or above the energy reach of the LHC or a future collider. We saw that EFTs are fascinating as theoretical models on their own, provide a parameterisation of BSM physics with a minimum amount of assumptions and can be applied in collider studies to translate experimental data into bounds on various BSM scenarios. While we do not know the nature of BSM physics, yet, we know that it is hidden somewhere out there. The tools discussed in this thesis provide a possible way to find it. It is high time for evidence of BSM physics to show up in experiments.

Bibliography

[1] S. Alte, M. König and M. Neubert, *Effective Field Theory after a New-Physics Discovery*, *JHEP* **08** (2018) 095 [1806.01278].

[2] R. Mertig, M. Böhm and A. Denner, *FEYN CALC: Computer algebraic calculation of Feynman amplitudes*, *Comput. Phys. Commun.* **64** (1991) 345.

[3] V. Shtabovenko, R. Mertig and F. Orellana, *New Developments in FeynCalc 9.0*, *Comput. Phys. Commun.* **207** (2016) 432 [1601.01167].

[4] K. G. Chetyrkin, J. H. Kühn and M. Steinhauser, *RunDec: A Mathematica package for running and decoupling of the strong coupling and quark masses*, *Comput. Phys. Commun.* **133** (2000) 43 [hep-ph/0004189].

[5] T. Huber and D. Maitre, *HypExp: A Mathematica package for expanding hypergeometric functions around integer-valued parameters*, *Comput. Phys. Commun.* **175** (2006) 122 [hep-ph/0507094].

[6] T. Huber and D. Maitre, *HypExp 2, Expanding Hypergeometric Functions about Half-Integer Parameters*, *Comput. Phys. Commun.* **178** (2008) 755 [0708.2443].

[7] D. Binosi and L. Theussl, *JaxoDraw: A Graphical user interface for drawing Feynman diagrams*, *Comput. Phys. Commun.* **161** (2004) 76 [hep-ph/0309015].

[8] D. Binosi, J. Collins, C. Kaufhold and L. Theussl, *JaxoDraw: A Graphical user interface for drawing Feynman diagrams. Version 2.0 release notes*, *Comput. Phys. Commun.* **180** (2009) 1709 [0811.4113].

[9] S. Alte, M. König and M. Neubert, *Effective Theory for a Heavy Scalar Coupled to the SM via Vector-Like Quarks*, *Eur. Phys. J.* **C79** (2019) 352 [1902.04593].

[10] S. Alte, M. König and W. Shepherd, *Consistent Searches for SMEFT Effects in Non-Resonant Dijet Events*, *JHEP* **01** (2018) 094 [1711.07484].

[11] A. Alloul, N. D. Christensen, C. Degrande, C. Duhr and B. Fuks, *FeynRules 2.0 - A complete toolbox for tree-level phenomenology*, *Comput. Phys. Commun.* **185** (2014) 2250 [1310.1921].

[12] J. Alwall, R. Frederix, S. Frixione, V. Hirschi, F. Maltoni, O. Mattelaer et al., *The automated computation of tree-level and next-to-leading order differential cross sections, and their matching to parton shower simulations*, *JHEP* **07** (2014) 079 [1405.0301].

[13] T. Sjostrand, S. Mrenna and P. Z. Skands, *PYTHIA 6.4 Physics and Manual*, *JHEP* **05** (2006) 026 [hep-ph/0603175].

[14] DELPHES 3 collaboration, *DELPHES 3, A modular framework for fast simulation of a generic collider experiment*, *JHEP* **02** (2014) 057 [1307.6346].

[15] D. B. Clark, E. Godat and F. I. Olness, *ManeParse : A Mathematica reader for Parton Distribution Functions*, *Comput. Phys. Commun.* **216** (2017) 126 [1605.08012].

[16] S. Alte, M. König and W. Shepherd, *Consistent Searches for SMEFT Effects in Non-Resonant Dilepton Events*, *accepted for publication in JHEP* (2019) [1812.07575].

[17] I. Brivio, Y. Jiang and M. Trott, *The SMEFTsim package, theory and tools*, *JHEP* **12** (2017) 070 [1709.06492].

[18] J. Aebischer et al., *WCxf: an exchange format for Wilson coefficients beyond the Standard Model*, *Comput. Phys. Commun.* **232** (2018) 71 [1712.05298].

[19] T. Hahn, *CUBA: A Library for multidimensional numerical integration*, *Comput. Phys. Commun.* **168** (2005) 78 [hep-ph/0404043].

[20] S. Alte, Y. Grossman, M. König and M. Neubert, *Exclusive Radiative Decays of Z Bosons in QCD Factorization*, *PoS* **ICHEP2016** (2016) 618 [1703.07242].

[21] S. Alte, M. König and M. Neubert, *Exclusive Weak Radiative Higgs Decays in the Standard Model and Beyond*, *JHEP* **12** (2016) 037 [1609.06310].

[22] ATLAS collaboration, *Observation of a new particle in the search for the Standard Model Higgs boson with the ATLAS detector at the LHC*, *Phys. Lett.* **B716** (2012) 1 [1207.7214].

[23] CMS collaboration, *Observation of a new boson at a mass of 125 GeV with the CMS experiment at the LHC*, *Phys. Lett.* **B716** (2012) 30 [1207.7235].

[24] P. W. Higgs, *Broken symmetries, massless particles and gauge fields*, *Phys. Lett.* **12** (1964) 132.

[25] P. W. Higgs, *Broken Symmetries and the Masses of Gauge Bosons*, *Phys. Rev. Lett.* **13** (1964) 508.

[26] P. W. Higgs, *Spontaneous Symmetry Breakdown without Massless Bosons*, *Phys. Rev.* **145** (1966) 1156.

[27] G. S. Guralnik, C. R. Hagen and T. W. B. Kibble, *Global Conservation Laws and Massless Particles*, *Phys. Rev. Lett.* **13** (1964) 585.

[28] F. Englert and R. Brout, *Broken Symmetry and the Mass of Gauge Vector Mesons*, *Phys. Rev. Lett.* **13** (1964) 321.

[29] P. W. Anderson, *Plasmons, Gauge Invariance, and Mass*, *Phys. Rev.* **130** (1963) 439.

[30] ATLAS collaboration, *Search for resonances in diphoton events at $\sqrt{s}$=13 TeV with the ATLAS detector*, *JHEP* **09** (2016) 001 [1606.03833].

[31] CMS collaboration, *Search for Resonant Production of High-Mass Photon Pairs in Proton-Proton Collisions at $\sqrt{s}$ =8 and 13 TeV*, *Phys. Rev. Lett.* **117** (2016) 051802 [1606.04093].

[32] BaBar collaboration, *Measurement of an Excess of $\bar{B} \to D^{(*)}\tau^-\bar{\nu}_\tau$ Decays and Implications for Charged Higgs Bosons*, *Phys. Rev.* **D88** (2013) 072012 [1303.0571].

[33] LHCb collaboration, *Measurement of the ratio of branching fractions $\mathcal{B}(\bar{B}^0 \to D^{*+}\tau^-\bar{\nu}_\tau)/\mathcal{B}(\bar{B}^0 \to D^{*+}\mu^-\bar{\nu}_\mu)$*, *Phys. Rev. Lett.* **115** (2015) 111803 [1506.08614].

[34] Belle collaboration, *Measurement of the τ lepton polarization and $R(D^*)$ in the decay $\bar{B} \to D^*\tau^-\bar{\nu}_\tau$*, *Phys. Rev. Lett.* **118** (2017) 211801 [1612.00529].

[35] LHCb collaboration, *Test of lepton universality using $B^+ \to K^+\ell^+\ell^-$ decays*, *Phys. Rev. Lett.* **113** (2014) 151601 [1406.6482].

[36] LHCb collaboration, *Test of lepton universality with $B^0 \to K^{*0}\ell^+\ell^-$ decays*, *JHEP* **08** (2017) 055 [1705.05802].

[37] ATLAS collaboration, *Search for new phenomena in high-mass diphoton final states using 37 fb^{-1} of proton–proton collisions collected at $\sqrt{s} = 13$ TeV with the ATLAS detector*, *Phys. Lett.* **B775** (2017) 105 [1707.04147].

[38] CMS collaboration, *Search for high-mass diphoton resonances in proton–proton collisions at 13 TeV and combination with 8 TeV search*, *Phys. Lett.* **B767** (2017) 147 [1609.02507].

[39] C. W. Bauer, S. Fleming, D. Pirjol and I. W. Stewart, *An Effective field theory for collinear and soft gluons: Heavy to light decays*, *Phys. Rev.* **D63** (2001) 114020 [hep-ph/0011336].

[40] C. W. Bauer and I. W. Stewart, *Invariant operators in collinear effective theory*, *Phys. Lett.* **B516** (2001) 134 [hep-ph/0107001].

[41] C. W. Bauer, D. Pirjol and I. W. Stewart, *Soft collinear factorization in effective field theory*, *Phys. Rev.* **D65** (2002) 054022 [hep-ph/0109045].

[42] M. Beneke, A. P. Chapovsky, M. Diehl and T. Feldmann, *Soft collinear effective theory and heavy to light currents beyond leading power*, *Nucl. Phys.* **B643** (2002) 431 [hep-ph/0206152].

[43] F. Wilczek and A. Zee, *Operator Analysis of Nucleon Decay*, *Phys. Rev. Lett.* **43** (1979) 1571.

[44] L. F. Abbott and M. B. Wise, *The Effective Hamiltonian for Nucleon Decay*, *Phys. Rev.* **D22** (1980) 2208.

[45] C. N. Leung, S. T. Love and S. Rao, *Low-Energy Manifestations of a New Interaction Scale: Operator Analysis*, *Z. Phys.* **C31** (1986) 433.

[46] W. Buchmüller and D. Wyler, *Effective Lagrangian Analysis of New Interactions and Flavor Conservation*, *Nucl. Phys.* **B268** (1986) 621.

[47] K. Hagiwara, S. Ishihara, R. Szalapski and D. Zeppenfeld, *Low-energy effects of new interactions in the electroweak boson sector*, *Phys. Rev.* **D48** (1993) 2182.

[48] C. Arzt, M. B. Einhorn and J. Wudka, *Patterns of deviation from the standard model*, *Nucl. Phys.* **B433** (1995) 41 [hep-ph/9405214].

[49] G. J. Gounaris, J. Layssac and F. M. Renard, *Testing the Higgs boson gluonic couplings at CERN LHC*, *Phys. Rev.* **D58** (1998) 075006 [hep-ph/9803422].

[50] V. Barger, T. Han, P. Langacker, B. McElrath and P. Zerwas, *Effects of genuine dimension-six Higgs operators*, *Phys. Rev.* **D67** (2003) 115001 [hep-ph/0301097].

[51] A. V. Manohar and M. B. Wise, *Modifications to the properties of the Higgs boson*, *Phys. Lett.* **B636** (2006) 107 [hep-ph/0601212].

[52] A. V. Manohar and M. B. Wise, *Flavor changing neutral currents, an extended scalar sector, and the Higgs production rate at the CERN LHC*, *Phys. Rev.* **D74** (2006) 035009 [hep-ph/0606172].

[53] G. F. Giudice, C. Grojean, A. Pomarol and R. Rattazzi, *The Strongly-Interacting Light Higgs*, *JHEP* **06** (2007) 045 [hep-ph/0703164].

[54] B. Grinstein and M. Trott, *A Higgs-Higgs bound state due to new physics at a TeV*, *Phys. Rev.* **D76** (2007) 073002 [0704.1505].

[55] J. A. Aguilar-Saavedra, *Effective four-fermion operators in top physics: A Roadmap*, *Nucl. Phys.* **B843** (2011) 638 [1008.3562].

[56] J. Elias-Miró, C. Grojean, R. S. Gupta and D. Marzocca, *Scaling and tuning of EW and Higgs observables*, *JHEP* **05** (2014) 019 [1312.2928].

[57] B. Grzadkowski, M. Iskrzynski, M. Misiak and J. Rosiek, *Dimension-Six Terms in the Standard Model Lagrangian*, *JHEP* **10** (2010) 085 [1008.4884].

[58] ATLAS collaboration, *Search for new phenomena in dijet mass and angular distributions from pp collisions at $\sqrt{s} = 13$ TeV with the ATLAS detector*, *Phys. Lett.* **B754** (2016) 302 [1512.01530].

[59] CMS collaboration, *Search for new physics with dijet angular distributions in proton-proton collisions at $\sqrt{s} = 13$ TeV*, *JHEP* **07** (2017) 013 [1703.09986].

[60] ATLAS collaboration, *Search for new high-mass phenomena in the dilepton final state using 36 fb^{-1} of proton-proton collision data at $\sqrt{s} = 13$ TeV with the ATLAS detector*, *JHEP* **10** (2017) 182 [1707.02424].

[61] C. Englert and M. Spannowsky, *Effective Theories and Measurements at Colliders*, *Phys. Lett.* **B740** (2015) 8 [1408.5147].

[62] R. Contino, A. Falkowski, F. Goertz, C. Grojean and F. Riva, *On the Validity of the Effective Field Theory Approach to SM Precision Tests*, *JHEP* **07** (2016) 144 [1604.06444].

[63] M. Farina, G. Panico, D. Pappadopulo, J. T. Ruderman, R. Torre and A. Wulzer, *Energy helps accuracy: electroweak precision tests at hadron colliders*, *Phys. Lett.* **B772** (2017) 210 [1609.08157].

[64] S. Alioli, M. Farina, D. Pappadopulo and J. T. Ruderman, *Precision Probes of QCD at High Energies*, *JHEP* **07** (2017) 097 [1706.03068].

[65] J. D. Bjorken and S. D. Drell, *Relativistic Quantum Mechanics*. McGraw-Hill, 1965.

[66] T. Cheng and L. Li, *Gauge theory of elementary particle physics*. Clarendon Press, 1984.

[67] M. E. Peskin and D. V. Schroeder, *An Introduction to Quantum Field Theory*. Westview Press, 1995.

[68] L. H. Ryder, *Quantum Field Theory*. Cambridge University Press, 1996.

[69] S. Weinberg, *The Quantum Theory of Fields*. Cambridge University Press, 2005.

[70] M. A. Srednicki, *Quantum Field Theory*. Cambridge University Press, 2007.

[71] M. D. Schwartz, *Quantum Field Theory and the Standard Model*. Cambridge University Press, 2014.

[72] S. Weinberg, *The Making of the standard model*, *Eur. Phys. J.* **C34** (2004) 5 [hep-ph/0401010].

[73] J. C. Romao and J. P. Silva, *A resource for signs and Feynman diagrams of the Standard Model*, *Int. J. Mod. Phys.* **A27** (2012) 1230025 [1209.6213].

[74] I. Brivio and M. Trott, *The Standard Model as an Effective Field Theory*, 1706.08945.

[75] H. Georgi, *Effective field theory*, *Ann. Rev. Nucl. Part. Sci.* **43** (1993) 209.

[76] G. Ecker, *The Standard model at low-energies*, *Czech. J. Phys.* **44** (1995) 405 [hep-ph/9309268].

[77] M. Neubert, *Effective field theory and heavy quark physics*, in *Physics in $D \geq 4$. Proceedings, Theoretical Advanced Study Institute in elementary particle physics, TASI 2004, Boulder, USA, June 6-July 2, 2004*, pp. 149–194, 2005, hep-ph/0512222.

[78] A. V. Manohar, *Introduction to Effective Field Theories*, in *Les Houches summer school: EFT in Particle Physics and Cosmology Les Houches, Chamonix Valley, France, July 3-28, 2017*, 2018, 1804.05863.

[79] T. Becher, A. Broggio and A. Ferroglia, *Introduction to Soft-Collinear Effective Theory*, *Lect. Notes Phys.* **896** (2015) pp.1 [1410.1892].

[80] T. Becher, *Les Houches Lectures on Soft-Collinear Effective Theory*, in *Les Houches summer school: EFT in Particle Physics and Cosmology Les Houches, Chamonix Valley, France, July 3-28, 2017*, 2018, 1803.04310.

[81] C.-N. Yang and R. L. Mills, *Conservation of Isotopic Spin and Isotopic Gauge Invariance*, *Phys. Rev.* **96** (1954) 191.

[82] J. Goldstone, *Field Theories with Superconductor Solutions*, *Nuovo Cim.* **19** (1961) 154.

[83] J. Goldstone, A. Salam and S. Weinberg, *Broken Symmetries*, *Phys. Rev.* **127** (1962) 965.

[84] M. Gell-Mann, *A Schematic Model of Baryons and Mesons*, *Phys. Lett.* **8** (1964) 214.

[85] D. J. Gross and F. Wilczek, *Ultraviolet Behavior of Nonabelian Gauge Theories*, *Phys. Rev. Lett.* **30** (1973) 1343.

[86] H. D. Politzer, *Reliable Perturbative Results for Strong Interactions?*, *Phys. Rev. Lett.* **30** (1973) 1346.

[87] G. 't Hooft and M. J. G. Veltman, *Regularization and Renormalization of Gauge Fields*, *Nucl. Phys.* **B44** (1972) 189.

[88] G. 't Hooft and M. J. G. Veltman, *Combinatorics of gauge fields*, *Nucl. Phys.* **B50** (1972) 318.

[89] L. D. Faddeev and V. N. Popov, *Feynman Diagrams for the Yang-Mills Field*, *Phys. Lett.* **B25** (1967) 29.

[90] F. Zwicky, *Die Rotverschiebung von extragalaktischen Nebeln*, *Helv. Phys. Acta* **6** (1933) 110.

[91] V. C. Rubin and W. K. Ford, Jr., *Rotation of the Andromeda Nebula from a Spectroscopic Survey of Emission Regions*, *Astrophys. J.* **159** (1970) 379.

[92] Planck collaboration, *Planck 2015 results. XIII. Cosmological parameters*, *Astron. Astrophys.* **594** (2016) A13 [1502.01589].

[93] J. N. Bahcall, *Solar neutrinos. I: Theoretical*, *Phys. Rev. Lett.* **12** (1964) 300.

[94] R. Davis, *Solar neutrinos. II: Experimental*, *Phys. Rev. Lett.* **12** (1964) 303.

[95] Super-Kamiokande collaboration, *Evidence for oscillation of atmospheric neutrinos*, *Phys. Rev. Lett.* **81** (1998) 1562 [hep-ex/9807003].

[96] SNO collaboration, *Measurement of the rate of $\nu_e + d \to p + p + e^-$ interactions produced by ^8B solar neutrinos at the Sudbury Neutrino Observatory*, *Phys. Rev. Lett.* **87** (2001) 071301 [nucl-ex/0106015].

[97] SNO collaboration, *Direct evidence for neutrino flavor transformation from neutral current interactions in the Sudbury Neutrino Observatory*, *Phys. Rev. Lett.* **89** (2002) 011301 [nucl-ex/0204008].

[98] V. A. Kuzmin, V. A. Rubakov and M. E. Shaposhnikov, *On the Anomalous Electroweak Baryon Number Nonconservation in the Early Universe*, *Phys. Lett.* **155B** (1985) 36.

[99] A. D. Sakharov, *Violation of CP Invariance, C asymmetry, and baryon asymmetry of the universe*, *Pisma Zh. Eksp. Teor. Fiz.* **5** (1967) 32.

[100] J. Polchinski, *Effective field theory and the Fermi surface*, in *Proceedings, Theoretical Advanced Study Institute (TASI 92): From Black Holes and Strings to Particles: Boulder, USA, June 1-26, 1992*, pp. 235–276, 1992, hep-th/9210046.

[101] A. J. Buras, *Weak Hamiltonian, CP violation and rare decays*, in *Probing the standard model of particle interactions. Proceedings, Summer School in Theoretical Physics, NATO Advanced Study Institute, 68th session, Les Houches, France, July 28-September 5, 1997. Pt. 1, 2*, pp. 281–539, 1998, hep-ph/9806471.

[102] A. Pich, *Effective field theory: Course*, in *Probing the standard model of particle interactions. Proceedings, Summer School in Theoretical Physics, NATO Advanced Study Institute, 68th session, Les Houches, France, July 28-September 5, 1997. Pt. 1, 2*, pp. 949–1049, 1998, hep-ph/9806303.

[103] I. Z. Rothstein, *TASI lectures on effective field theories*, 2003, hep-ph/0308266.

[104] D. B. Kaplan, *Five lectures on effective field theory*, 2005, nucl-th/0510023.

[105] C. P. Burgess, *Introduction to Effective Field Theory*, *Ann. Rev. Nucl. Part. Sci.* **57** (2007) 329 [hep-th/0701053].

[106] W. Skiba, *Effective Field Theory and Precision Electroweak Measurements*, in *Physics of the large and the small, TASI 09, proceedings of the Theoretical Advanced Study Institute in Elementary Particle Physics, Boulder, Colorado, USA, 1-26 June 2009*, pp. 5–70, 2011, 1006.2142.

[107] T. Cohen, *As Scales Become Separated: Lectures on Effective Field Theory*, 1903.03622.

[108] Particle Data Group collaboration, *Review of particle physics*, *Phys. Rev. D* **98** (2018) 030001.

[109] I. Newton, *Philosophiæ Naturalis Principia Mathematica*. 1687.

[110] A. Einstein, *On the electrodynamics of moving bodies*, *Annalen Phys.* **17** (1905) 891.

[111] T. Appelquist and J. Carazzone, *Infrared Singularities and Massive Fields*, *Phys. Rev.* **D11** (1975) 2856.

[112] G. 't Hooft, *Naturalness, chiral symmetry, and spontaneous chiral symmetry breaking*, *NATO Sci. Ser. B* **59** (1980) 135.

[113] G. F. Giudice, *Naturally Speaking: The Naturalness Criterion and Physics at the LHC*, 0801.2562.

[114] W. Heisenberg and H. Euler, *Folgerungen aus der Diracschen Theorie des Positrons*, *Z. Phys.* **98** (1936) 714 [physics/0605038].

[115] E. Fermi, *An attempt of a theory of beta radiation. 1.*, *Z. Phys.* **88** (1934) 161.

[116] M. Neubert, *Heavy quark symmetry*, *Phys. Rept.* **245** (1994) 259 [hep-ph/9306320].

[117] W. E. Caswell and G. P. Lepage, *Effective Lagrangians for Bound State Problems in QED, QCD, and Other Field Theories*, *Phys. Lett.* **167B** (1986) 437.

[118] G. T. Bodwin, E. Braaten and G. P. Lepage, *Rigorous QCD analysis of inclusive annihilation and production of heavy quarkonium*, *Phys. Rev.* **D51** (1995) 1125 [hep-ph/9407339].

[119] G. Ecker, *Chiral perturbation theory*, *Prog. Part. Nucl. Phys.* **35** (1995) 1 [hep-ph/9501357].

[120] S. Scherer, *Introduction to chiral perturbation theory*, *Adv. Nucl. Phys.* **27** (2003) 277 [hep-ph/0210398].

[121] F. Feruglio, *The Chiral approach to the electroweak interactions*, *Int. J. Mod. Phys.* **A8** (1993) 4937 [hep-ph/9301281].

[122] G. Buchalla and O. Catà, *Effective Theory of a Dynamically Broken Electroweak Standard Model at NLO*, *JHEP* **07** (2012) 101 [1203.6510].

[123] R. Alonso, M. B. Gavela, L. Merlo, S. Rigolin and J. Yepes, *The Effective Chiral Lagrangian for a Light Dynamical "Higgs Particle"*, *Phys. Lett.* **B722** (2013) 330 [1212.3305].

[124] R. Alonso, M. B. Gavela, L. Merlo, S. Rigolin and J. Yepes, *Flavor with a light dynamical "Higgs particle"*, *Phys. Rev.* **D87** (2013) 055019 [1212.3307].

[125] G. Buchalla, O. Catà and C. Krause, *Complete Electroweak Chiral Lagrangian with a Light Higgs at NLO*, *Nucl. Phys.* **B880** (2014) 552 [1307.5017].

[126] G. Buchalla, O. Catà and G. D'Ambrosio, *Nonstandard Higgs couplings from angular distributions in $h \to Z\ell^+\ell^-$*, *Eur. Phys. J.* **C74** (2014) 2798 [1310.2574].

[127] I. Brivio, T. Corbett, O. J. P. Éboli, M. B. Gavela, J. Gonzalez-Fraile, M. C. Gonzalez-Garcia et al., *Disentangling a dynamical Higgs*, *JHEP* **03** (2014) 024 [1311.1823].

[128] I. Brivio, O. J. P. Éboli, M. B. Gavela, M. C. Gonzalez-Garcia, L. Merlo and S. Rigolin, *Higgs ultraviolet softening*, *JHEP* **12** (2014) 004 [1405.5412].

[129] M. B. Gavela, J. Gonzalez-Fraile, M. C. Gonzalez-Garcia, L. Merlo, S. Rigolin and J. Yepes, *CP violation with a dynamical Higgs*, *JHEP* **10** (2014) 044 [1406.6367].

[130] M. B. Gavela, K. Kanshin, P. A. N. Machado and S. Saa, *On the renormalization of the electroweak chiral Lagrangian with a Higgs*, *JHEP* **03** (2015) 043 [1409.1571].

[131] R. Alonso, I. Brivio, B. Gavela, L. Merlo and S. Rigolin, *Sigma Decomposition*, *JHEP* **12** (2014) 034 [1409.1589].

[132] G. Buchalla, O. Catà, A. Celis and C. Krause, *Note on Anomalous Higgs-Boson Couplings in Effective Field Theory*, *Phys. Lett.* **B750** (2015) 298 [1504.01707].

[133] I. M. Hierro, L. Merlo and S. Rigolin, *Sigma Decomposition: The CP-Odd Lagrangian*, *JHEP* **04** (2016) 016 [1510.07899].

[134] G. Buchalla, O. Catà, A. Celis and C. Krause, *Fitting Higgs Data with Nonlinear Effective Theory*, *Eur. Phys. J.* **C76** (2016) 233 [1511.00988].

[135] I. Brivio, J. Gonzalez-Fraile, M. C. Gonzalez-Garcia and L. Merlo, *The complete HEFT Lagrangian after the LHC Run I*, *Eur. Phys. J.* **C76** (2016) 416 [1604.06801].

[136] M. B. Gavela, K. Kanshin, P. A. N. Machado and S. Saa, *The linear–non-linear frontier for the Goldstone Higgs*, *Eur. Phys. J.* **C76** (2016) 690 [1610.08083].

[137] L. Merlo, S. Saa and M. Sacristán-Barbero, *Baryon Non-Invariant Couplings in Higgs Effective Field Theory*, *Eur. Phys. J.* **C77** (2017) 185 [1612.04832].

[138] P. Hernandez-Leon and L. Merlo, *Distinguishing A Higgs-Like Dilaton Scenario With A Complete Bosonic Effective Field Theory Basis*, *Phys. Rev.* **D96** (2017) 075008 [1703.02064].

[139] S. Weinberg, *Baryon and Lepton Nonconserving Processes*, *Phys. Rev. Lett.* **43** (1979) 1566.

[140] E. E. Jenkins, A. V. Manohar and M. Trott, *Renormalization Group Evolution of the Standard Model Dimension Six Operators I: Formalism and λ Dependence*, *JHEP* **10** (2013) 087 [1308.2627].

[141] E. E. Jenkins, A. V. Manohar and M. Trott, *Renormalization Group Evolution of the Standard Model Dimension Six Operators II: Yukawa Dependence*, *JHEP* **01** (2014) 035 [1310.4838].

[142] R. Alonso, E. E. Jenkins, A. V. Manohar and M. Trott, *Renormalization Group Evolution of the Standard Model Dimension Six Operators III: Gauge Coupling Dependence and Phenomenology*, *JHEP* **04** (2014) 159 [1312.2014].

[143] L. Lehman, *Extending the Standard Model Effective Field Theory with the Complete Set of Dimension-7 Operators*, *Phys. Rev.* **D90** (2014) 125023 [1410.4193].

[144] Y. Liao and X.-D. Ma, *Renormalization Group Evolution of Dimension-seven Baryon- and Lepton-number-violating Operators*, *JHEP* **11** (2016) 043 [1607.07309].

[145] L. Lehman and A. Martin, *Low-derivative operators of the Standard Model effective field theory via Hilbert series methods*, *JHEP* **02** (2016) 081 [1510.00372].

[146] B. Henning, X. Lu, T. Melia and H. Murayama, *2, 84, 30, 993, 560, 15456, 11962, 261485, ...: Higher dimension operators in the SM EFT*, *JHEP* **08** (2017) 016 [1512.03433].

[147] L. Lehman and A. Martin, *Hilbert Series for Constructing Lagrangians: expanding the phenomenologist's toolbox*, *Phys. Rev.* **D91** (2015) 105014 [1503.07537].

[148] B. Henning, X. Lu, T. Melia and H. Murayama, *Hilbert series and operator bases with derivatives in effective field theories*, *Commun. Math. Phys.* **347** (2016) 363 [1507.07240].

[149] B. Henning, X. Lu, T. Melia and H. Murayama, *Operator bases, S-matrices, and their partition functions*, *JHEP* **10** (2017) 199 [1706.08520].

[150] C. W. Bauer, S. Fleming and M. E. Luke, *Summing Sudakov logarithms in $B \to X_s\gamma$ in effective field theory*, *Phys. Rev.* **D63** (2000) 014006 [hep-ph/0005275].

[151] R. J. Hill and M. Neubert, *Spectator interactions in soft collinear effective theory*, *Nucl. Phys.* **B657** (2003) 229 [hep-ph/0211018].

[152] J.-y. Chiu, F. Golf, R. Kelley and A. V. Manohar, *Electroweak Sudakov corrections using effective field theory*, *Phys. Rev. Lett.* **100** (2008) 021802 [0709.2377].

[153] J.-y. Chiu, F. Golf, R. Kelley and A. V. Manohar, *Electroweak Corrections in High Energy Processes using Effective Field Theory*, *Phys. Rev.* **D77** (2008) 053004 [0712.0396].

[154] J.-y. Chiu, R. Kelley and A. V. Manohar, *Electroweak Corrections using Effective Field Theory: Applications to the LHC*, *Phys. Rev.* **D78** (2008) 073006 [0806.1240].

[155] M. D. Schwartz, K. Yan and H. X. Zhu, *Collinear factorization violation and effective field theory*, *Phys. Rev.* **D96** (2017) 056005 [1703.08572].

[156] M. D. Schwartz, K. Yan and H. X. Zhu, *Factorization Violation and Scale Invariance*, *Phys. Rev.* **D97** (2018) 096017 [1801.01138].

[157] I. Z. Rothstein and I. W. Stewart, *An Effective Field Theory for Forward Scattering and Factorization Violation*, *JHEP* **08** (2016) 025 [1601.04695].

[158] M. Beneke and V. A. Smirnov, *Asymptotic expansion of Feynman integrals near threshold*, *Nucl. Phys.* **B522** (1998) 321 [hep-ph/9711391].

[159] V. A. Smirnov, *Applied asymptotic expansions in momenta and masses*, *Springer Tracts Mod. Phys.* **177** (2002) 1.

[160] CMS collaboration, *Projected Performance of an Upgraded CMS Detector at the LHC and HL-LHC: Contribution to the Snowmass Process*, in *Proceedings, 2013 Community Summer Study on the Future of U.S. Particle Physics: Snowmass on the Mississippi (CSS2013): Minneapolis, MN, USA, July 29-August 6, 2013*, 2013, 1307.7135.

[161] ATLAS collaboration, *Physics at a High-Luminosity LHC with ATLAS*, in *Proceedings, 2013 Community Summer Study on the Future of U.S. Particle Physics: Snowmass on the Mississippi (CSS2013): Minneapolis, MN, USA, July 29-August 6, 2013*, 2013, 1307.7292.

[162] M. Beneke, G. Buchalla, M. Neubert and C. T. Sachrajda, *QCD factorization for $B \to \pi\pi$ decays: Strong phases and CP violation in the heavy quark limit*, *Phys. Rev. Lett.* **83** (1999) 1914 [hep-ph/9905312].

[163] M. Beneke, G. Buchalla, M. Neubert and C. T. Sachrajda, *QCD factorization for exclusive, nonleptonic B meson decays: General arguments and the case of heavy light final states*, *Nucl. Phys.* **B591** (2000) 313 [hep-ph/0006124].

[164] M. Beneke, G. Buchalla, M. Neubert and C. T. Sachrajda, *QCD factorization in $B \to \pi K, \pi\pi$ decays and extraction of Wolfenstein parameters*, *Nucl. Phys.* **B606** (2001) 245 [hep-ph/0104110].

[165] R. Franceschini, G. F. Giudice, J. F. Kamenik, M. McCullough, A. Pomarol, R. Rattazzi et al., *What is the $\gamma\gamma$ resonance at 750 GeV?*, *JHEP* **03** (2016) 144 [1512.04933].

[166] M. Bauer, M. Neubert and A. Thamm, *Analyzing the CP Nature of a New Scalar Particle via $S \to Zh$ Decay*, *Phys. Rev. Lett.* **117** (2016) 181801 [1610.00009].

[167] C. W. Bauer, S. Fleming, D. Pirjol, I. Z. Rothstein and I. W. Stewart, *Hard scattering factorization from effective field theory*, *Phys. Rev.* **D66** (2002) 014017 [hep-ph/0202088].

[168] E. Eichten and B. R. Hill, *An Effective Field Theory for the Calculation of Matrix Elements Involving Heavy Quarks*, *Phys. Lett.* **B234** (1990) 511.

[169] H. Georgi, *An Effective Field Theory for Heavy Quarks at Low-energies*, *Phys. Lett.* **B240** (1990) 447.

[170] E. Eichten and B. R. Hill, *Static Effective Field Theory: 1/m Corrections*, *Phys. Lett.* **B243** (1990) 427.

[171] A. F. Falk, H. Georgi, B. Grinstein and M. B. Wise, *Heavy Meson Form-factors From QCD*, *Nucl. Phys.* **B343** (1990) 1.

[172] A. F. Falk, B. Grinstein and M. E. Luke, *Leading mass corrections to the heavy quark effective theory*, *Nucl. Phys.* **B357** (1991) 185.

[173] S. Fleming, A. H. Hoang, S. Mantry and I. W. Stewart, *Jets from massive unstable particles: Top-mass determination*, *Phys. Rev.* **D77** (2008) 074010 [hep-ph/0703207].

[174] S. Fleming, A. H. Hoang, S. Mantry and I. W. Stewart, *Top Jets in the Peak Region: Factorization Analysis with NLL Resummation*, *Phys. Rev.* **D77** (2008) 114003 [0711.2079].

[175] J.-y. Chiu, A. Fuhrer, A. H. Hoang, R. Kelley and A. V. Manohar, *Soft-Collinear Factorization and Zero-Bin Subtractions*, *Phys. Rev.* **D79** (2009) 053007 [0901.1332].

[176] T. Becher and M. Neubert, *Drell-Yan Production at Small q_T, Transverse Parton Distributions and the Collinear Anomaly*, *Eur. Phys. J.* **C71** (2011) 1665 [1007.4005].

[177] J.-y. Chiu, A. Jain, D. Neill and I. Z. Rothstein, *The Rapidity Renormalization Group*, *Phys. Rev. Lett.* **108** (2012) 151601 [1104.0881].

[178] A. V. Manohar, T. Mehen, D. Pirjol and I. W. Stewart, *Reparameterization invariance for collinear operators*, *Phys. Lett.* **B539** (2002) 59 [hep-ph/0204229].

[179] J. M. Cornwall, D. N. Levin and G. Tiktopoulos, *Derivation of Gauge Invariance from High-Energy Unitarity Bounds on the s Matrix*, *Phys. Rev.* **D10** (1974) 1145.

[180] C. E. Vayonakis, *Born Helicity Amplitudes and Cross-Sections in Nonabelian Gauge Theories*, *Lett. Nuovo Cim.* **17** (1976) 383.

[181] M. S. Chanowitz and M. K. Gaillard, *The TeV Physics of Strongly Interacting W's and Z's*, *Nucl. Phys.* **B261** (1985) 379.

[182] R. J. Hill, T. Becher, S. J. Lee and M. Neubert, *Sudakov resummation for subleading SCET currents and heavy-to-light form-factors*, *JHEP* **07** (2004) 081 [hep-ph/0404217].

[183] A. J. Buras and P. H. Weisz, *QCD Nonleading Corrections to Weak Decays in Dimensional Regularization and 't Hooft-Veltman Schemes*, *Nucl. Phys.* **B333** (1990) 66.

[184] M. J. Dugan and B. Grinstein, *On the vanishing of evanescent operators*, *Phys. Lett.* **B256** (1991) 239.

[185] T. Becher and M. Neubert, *Infrared singularities of scattering amplitudes in perturbative QCD*, *Phys. Rev. Lett.* **102** (2009) 162001 [0901.0722].

[186] E. Gardi and L. Magnea, *Factorization constraints for soft anomalous dimensions in QCD scattering amplitudes*, *JHEP* **03** (2009) 079 [0901.1091].

[187] T. Becher and M. Neubert, *On the Structure of Infrared Singularities of Gauge-Theory Amplitudes*, *JHEP* **06** (2009) 081 [0903.1126].

[188] L. J. Dixon, E. Gardi and L. Magnea, *On soft singularities at three loops and beyond*, *JHEP* **02** (2010) 081 [0910.3653].

[189] G. P. Korchemsky and A. V. Radyushkin, *Renormalization of the Wilson Loops Beyond the Leading Order*, *Nucl. Phys.* **B283** (1987) 342.

[190] I. A. Korchemskaya and G. P. Korchemsky, *On lightlike Wilson loops*, *Phys. Lett.* **B287** (1992) 169.

[191] B. Jantzen, J. H. Kuhn, A. A. Penin and V. A. Smirnov, *Two-loop electroweak logarithms in four-fermion processes at high energy*, *Nucl. Phys.* **B731** (2005) 188 [hep-ph/0509157].

[192] D. J. Gross and F. Wilczek, *Asymptotically Free Gauge Theories - I*, *Phys. Rev.* **D8** (1973) 3633.

[193] S. Moch, J. A. M. Vermaseren and A. Vogt, *The Three loop splitting functions in QCD: The Nonsinglet case*, *Nucl. Phys.* **B688** (2004) 101 [hep-ph/0403192].

[194] S. Moch, J. A. M. Vermaseren and A. Vogt, *The Quark form-factor at higher orders*, *JHEP* **08** (2005) 049 [hep-ph/0507039].

[195] T. Becher, M. Neubert and B. D. Pecjak, *Factorization and Momentum-Space Resummation in Deep-Inelastic Scattering*, *JHEP* **01** (2007) 076 [hep-ph/0607228].

[196] M. Beneke and D. Yang, *Heavy-to-light B meson form-factors at large recoil energy: Spectator-scattering corrections*, *Nucl. Phys.* **B736** (2006) 34 [hep-ph/0508250].

[197] M. Beneke, M. Garny, R. Szafron and J. Wang, *Anomalous dimension of subleading-power N-jet operators*, *JHEP* **03** (2018) 001 [1712.04416].

[198] L. F. Abbott, *The Background Field Method Beyond One Loop*, *Nucl. Phys.* **B185** (1981) 189.

[199] T. Becher and M. Neubert, *Threshold resummation in momentum space from effective field theory*, *Phys. Rev. Lett.* **97** (2006) 082001 [hep-ph/0605050].

[200] T. Becher, M. Neubert and G. Xu, *Dynamical Threshold Enhancement and Resummation in Drell-Yan Production*, *JHEP* **07** (2008) 030 [0710.0680].

[201] B. Gripaios and D. Sutherland, *An operator basis for the Standard Model with an added scalar singlet*, *JHEP* **08** (2016) 103 [1604.07365].

[202] R. Franceschini, G. F. Giudice, J. F. Kamenik, M. McCullough, F. Riva, A. Strumia et al., *Digamma, what next?*, *JHEP* **07** (2016) 150 [1604.06446].

[203] T. Inami, T. Kubota and Y. Okada, *Effective Gauge Theory and the Effect of Heavy Quarks in Higgs Boson Decays*, *Z. Phys.* **C18** (1983) 69.

[204] B. Grinstein and L. Randall, *The Renormalization of g^2*, *Phys. Lett.* **B217** (1989) 335.

[205] S. A. Larin, *The Renormalization of the axial anomaly in dimensional regularization*, *Phys. Lett.* **B303** (1993) 113 [hep-ph/9302240].

[206] J. C. Collins, A. Duncan and S. D. Joglekar, *Trace and Dilatation Anomalies in Gauge Theories*, *Phys. Rev.* **D16** (1977) 438.

[207] R. Tarrach, *The Pole Mass in Perturbative QCD*, *Nucl. Phys.* **B183** (1981) 384.

[208] D. Bonocore, E. Laenen, L. Magnea, L. Vernazza and C. D. White, *The method of regions and next-to-soft corrections in Drell–Yan production*, *Phys. Lett.* **B742** (2015) 375 [1410.6406].

[209] D. Bonocore, E. Laenen, L. Magnea, S. Melville, L. Vernazza and C. D. White, *A factorization approach to next-to-leading-power threshold logarithms*, *JHEP* **06** (2015) 008 [1503.05156].

[210] D. Bonocore, E. Laenen, L. Magnea, L. Vernazza and C. D. White, *Non-abelian factorisation for next-to-leading-power threshold logarithms*, *JHEP* **12** (2016) 121 [1610.06842].

[211] V. Del Duca, E. Laenen, L. Magnea, L. Vernazza and C. D. White, *Universality of next-to-leading power threshold effects for colourless final states in hadronic collisions*, *JHEP* **11** (2017) 057 [1706.04018].

[212] A. A. Penin, *High-Energy Limit of Quantum Electrodynamics beyond Sudakov Approximation*, *Phys. Lett.* **B745** (2015) 69 [1412.0671].

[213] T. Liu and A. A. Penin, *High-Energy Limit of QCD beyond the Sudakov Approximation*, *Phys. Rev. Lett.* **119** (2017) 262001 [1709.01092].

[214] I. Moult, L. Rothen, I. W. Stewart, F. J. Tackmann and H. X. Zhu, *Subleading Power Corrections for N-Jettiness Subtractions*, *Phys. Rev.* **D95** (2017) 074023 [1612.00450].

[215] R. Boughezal, X. Liu and F. Petriello, *Power Corrections in the N-jettiness Subtraction Scheme*, *JHEP* **03** (2017) 160 [1612.02911].

[216] I. Moult, I. W. Stewart, G. Vita and H. X. Zhu, *First Subleading Power Resummation for Event Shapes*, *JHEP* **08** (2018) 013 [1804.04665].

[217] W. Altmannshofer and D. M. Straub, *New Physics in $B \to K^* \mu\mu$?*, *Eur. Phys. J.* **C73** (2013) 2646 [1308.1501].

[218] G. Hiller and M. Schmaltz, *R_K and future $b \to s\ell\ell$ physics beyond the standard model opportunities*, *Phys. Rev.* **D90** (2014) 054014 [1408.1627].

[219] R. Alonso, B. Grinstein and J. Martin Camalich, *Lepton universality violation and lepton flavor conservation in B-meson decays*, *JHEP* **10** (2015) 184 [1505.05164].

[220] M. Freytsis, Z. Ligeti and J. T. Ruderman, *Flavor models for $\bar{B} \to D^{(*)}\tau\bar{\nu}$*, *Phys. Rev.* **D92** (2015) 054018 [1506.08896].

[221] M. Bauer and M. Neubert, *Minimal Leptoquark Explanation for the $R_{D^{(*)}}$, R_K , and $(g-2)_g$ Anomalies*, *Phys. Rev. Lett.* **116** (2016) 141802 [1511.01900].

[222] R. Barbieri, G. Isidori, A. Pattori and F. Senia, *Anomalies in B-decays and $U(2)$ flavour symmetry*, *Eur. Phys. J.* **C76** (2016) 67 [1512.01560].

[223] I. Doršner, S. Fajfer, A. Greljo, J. F. Kamenik and N. Košnik, *Physics of leptoquarks in precision experiments and at particle colliders*, *Phys. Rept.* **641** (2016) 1 [1603.04993].

[224] T. Alanne and F. Goertz, *Extended Dark Matter EFT*, 1712.07626.

[225] D. B. Kaplan, *Flavor at SSC energies: A New mechanism for dynamically generated fermion masses*, *Nucl. Phys.* **B365** (1991) 259.

[226] M. J. Dugan, H. Georgi and D. B. Kaplan, *Anatomy of a Composite Higgs Model*, *Nucl. Phys.* **B254** (1985) 299.

[227] K. Agashe, R. Contino and A. Pomarol, *The Minimal composite Higgs model*, *Nucl. Phys.* **B719** (2005) 165 [hep-ph/0412089].

[228] R. Contino, *The Higgs as a Composite Nambu-Goldstone Boson*, in *Physics of the large and the small, TASI 09, proceedings of the Theoretical Advanced Study Institute in Elementary Particle Physics, Boulder, Colorado, USA, 1-26 June 2009*, pp. 235–306, 2011, 1005.4269.

[229] L. Randall and R. Sundrum, *A Large mass hierarchy from a small extra dimension*, *Phys. Rev. Lett.* **83** (1999) 3370 [hep-ph/9905221].

[230] Y. Grossman and M. Neubert, *Neutrino masses and mixings in nonfactorizable geometry*, *Phys. Lett.* **B474** (2000) 361 [hep-ph/9912408].

[231] T. Gherghetta and A. Pomarol, *Bulk fields and supersymmetry in a slice of AdS*, *Nucl. Phys.* **B586** (2000) 141 [hep-ph/0003129].

[232] M. R. Buckley, D. Feld and D. Goncalves, *Scalar Simplified Models for Dark Matter*, *Phys. Rev.* **D91** (2015) 015017 [1410.6497].

[233] P. Harris, V. V. Khoze, M. Spannowsky and C. Williams, *Constraining Dark Sectors at Colliders: Beyond the Effective Theory Approach*, *Phys. Rev.* **D91** (2015) 055009 [1411.0535].

[234] M. Bauer, M. Neubert and A. Thamm, *The "forgotten" decay $S \to Z + h$ as a CP analyzer*, 1607.01016.

[235] C. Degrande, N. Greiner, W. Kilian, O. Mattelaer, H. Mebane, T. Stelzer et al., *Effective Field Theory: A Modern Approach to Anomalous Couplings*, *Annals Phys.* **335** (2013) 21 [1205.4231].

[236] Y. Jiang and M. Trott, *On the non-minimal character of the SMEFT*, *Phys. Lett.* **B770** (2017) 108 [1612.02040].

[237] ATLAS collaboration, *ATLAS search for new phenomena in dijet mass and angular distributions using pp collisions at $\sqrt{s} = 7$ TeV*, *JHEP* **01** (2013) 029 [1210.1718].

[238] ATLAS collaboration, *Search for New Phenomena in Dijet Angular Distributions in Proton-Proton Collisions at $\sqrt{s} = 8$ TeV Measured with the ATLAS Detector*, *Phys. Rev. Lett.* **114** (2015) 221802 [1504.00357].

[239] CMS collaboration, *Search for quark compositeness in dijet angular distributions from pp collisions at $\sqrt{s} = 7$ TeV*, *JHEP* **05** (2012) 055 [1202.5535].

[240] CMS collaboration, *Search for quark contact interactions and extra spatial dimensions using dijet angular distributions in proton–proton collisions at $\sqrt{s} = 8$ TeV*, *Phys. Lett.* **B746** (2015) 79 [1411.2646].

[241] T. Hurth, S. Renner and W. Shepherd, *Matching for FCNC effects in the flavour-symmetric SMEFT*, *JHEP* **06** (2019) 029 [1903.00500].

[242] G. D'Ambrosio, G. F. Giudice, G. Isidori and A. Strumia, *Minimal flavor violation: An Effective field theory approach*, *Nucl. Phys.* **B645** (2002) 155 [hep-ph/0207036].

[243] E. H. Simmons, *Dimension-six Gluon Operators as Probes of New Physics*, *Phys. Lett.* **B226** (1989) 132.

[244] E. H. Simmons, *Higher dimension gluon operators and hadronic scattering*, *Phys. Lett.* **B246** (1990) 471.

[245] A. Azatov, R. Contino, C. S. Machado and F. Riva, *Helicity selection rules and noninterference for BSM amplitudes*, *Phys. Rev.* **D95** (2017) 065014 [1607.05236].

[246] L. J. Dixon and Y. Shadmi, *Testing gluon selfinteractions in three jet events at hadron colliders*, *Nucl. Phys.* **B423** (1994) 3 [hep-ph/9312363].

[247] T. Junk, *Confidence level computation for combining searches with small statistics*, *Nucl. Instrum. Meth.* **A434** (1999) 435 [hep-ex/9902006].

[248] A. L. Read, *Presentation of search results: The CLs technique*, *J. Phys.* **G28** (2002) 2693.

[249] ATLAS collaboration, *Future Plans of the ATLAS Collaboration for the HL-LHC*, Tech. Rep. ATL-PHYS-PROC-2018-015, CERN, Geneva, March, 2018.

[250] CDF collaboration, *Measurement of* $\sin^2\theta_{eff}^{lept}$ *using* e^+e^- *pairs from* γ^*/Z *bosons produced in* $p\bar{p}$ *collisions at a center-of-momentum energy of 1.96 TeV*, *Phys. Rev.* **D93** (2016) 112016 [1605.02719].

[251] S. D. Drell and T.-M. Yan, *Massive Lepton Pair Production in Hadron-Hadron Collisions at High-Energies*, *Phys. Rev. Lett.* **25** (1970) 316.

[252] L. Berthier and M. Trott, *Towards consistent Electroweak Precision Data constraints in the SMEFT*, *JHEP* **05** (2015) 024 [1502.02570].

[253] L. Berthier and M. Trott, *Consistent constraints on the Standard Model Effective Field Theory*, *JHEP* **02** (2016) 069 [1508.05060].

[254] M. Bjørn and M. Trott, *Interpreting W mass measurements in the SMEFT*, *Phys. Lett.* **B762** (2016) 426 [1606.06502].

[255] L. Berthier, M. Bjørn and M. Trott, *Incorporating doubly resonant* $W^\pm$ *data in a global fit of SMEFT parameters to lift flat directions*, *JHEP* **09** (2016) 157 [1606.06693].

[256] J. Ellis, C. W. Murphy, V. Sanz and T. You, *Updated Global SMEFT Fit to Higgs, Diboson and Electroweak Data*, *JHEP* **06** (2018) 146 [1803.03252].

[257] E. da Silva Almeida, A. Alves, N. Rosa Agostinho, O. J. P. Éboli and M. C. Gonzalez–Garcia, *Electroweak Sector Under Scrutiny: A Combined Analysis of LHC and Electroweak Precision Data*, *Phys. Rev.* **D99** (2019) 033001 [1812.01009].

[258] H.-L. Lai, M. Guzzi, J. Huston, Z. Li, P. M. Nadolsky, J. Pumplin et al., *New parton distributions for collider physics*, *Phys. Rev.* **D82** (2010) 074024 [1007.2241].

[259] CTEQ collaboration, *Global QCD analysis of parton structure of the nucleon: CTEQ5 parton distributions*, *Eur. Phys. J.* **C12** (2000) 375 [hep-ph/9903282].

Colophon

This thesis was typeset with `LaTeX2e` using `BibTeX` with the style file from the *Journal of High Energy Physics*. The Feynman diagrams created by the author were drawn in `JaxoDraw` [7, 8]. The plots in Chapter 5 were created with `Mathematica` using the package `MaTeX`.